Dissertation

ADSORPTIVE DESLUPHURSATION OF DIESEL FUEL ON UNPROCESSED AMARULA (*SCLEROCARYA BIRREA*) WASTES OR SYNTHESIZED ACTIVATED CARBONS FROM BIOMASS WASTES

by

TSEPISO REGINA KABI

submitted in accordance with the requirements for

the degree of

MASTER OF TECHNOLOGY

in

CHEMICAL ENGINEERING

At the

Institute for the Development of Energy for African Sustainability

UNIVERSITY OF SOUTH AFRICA

SUPERVISOR: Professor Yali Yao

CO-SUPERVISORS: Professor Diane Hildebrandt & Professor Xinying Liu

Date: October 2020

DECLARATION

Name: __Tsepiso R. Kabi_____

Student
number:_____55264018_____

Degree: M-Tech   Chemical   Engineering
_____

Exact wording of the title of the dissertation as appearing on the electronic copy submitted for examination:

Adsorptive Desulphurization of Diesel Fuel on Unprocessed Amarula (*Sclerocarya birrea*) Waste or Synthesized Activated Carbons from Biomass Waste

Key Terms

Adsorptive Desulphurization. Diesel fuel. Dibenzothiophene. Biomass waste. Amarula. *Sclerocarya birrea*. Activated carbon. Gasification biochar. Reactor. Lignocellulose. Heteroatoms. Surface chemistry. Crystallinity. Therma stability. Morphology. Mesoporous. Microporous. Adsorption-Desorption mechanism. Kinetics. Isotherms. Thermodynamics. Pollution. Environment.

I declare that the above dissertation is my own work and that all the sources that I have used or quoted have been indicated and acknowledged by means of complete references.

I further declare that I submitted the dissertation to originality checking software and that it falls within the accepted requirements for originality.

I further declare that I have not previously submitted this work, or part of it, for examination at Unisa for another qualification or at any other higher education institution.

_____   _____30 October 2020

DEDICATIONS

This Dissertation is

Dedicated to

My Child Ntando Rorisang Kabi

ABSTRACT

Diesel fuel has been found to contain highly concentrated organo-sulphur compounds which have bad impact economically, environmentally, and health-wise. Adsorptive desulphurization (ADS) is one of the promising processes which are carried out under atmospheric conditions. Amarula (*Sclerocarya birrea*) waste biomass from the production plant of Amarula liqueur, was utilized as a low-cost adsorbent and as a source of synthesized activated carbon for reducing sulphur content in diesel fuel. The performance of gasification char (waste from syngas production) was also compared with Amarula shells waste biochar.

The Amarula wastes Biomass: fruit, seed, and shell waste were used as adsorbents to reduce the content of sulphur in dibenzothiophene model diesel fuel. The results showed that raw Amarula Shells (AmSh) waste had the highest adsorption efficiency as compared to Amarula seeds (AmSe) and fruit (AmWa) wastes. The effect of adsorption temperature revealed that the sorption is more favourable at room temperatures. The selected Amarula shell wastes showed that as the adsorbent quantity increases, the sorption efficiency also increases.

The three Amarula wastes biomass were processed to synthesise activated carbons (ACs) using pyrolysis, and then steam activation at 800 °C for 45 min. The adsorption efficiency of DBT in model diesel fuel was found to improve on Amarula wastes ACs with the order of AmShAC-ST > AmSeAC-ST > AmWaAC-ST. The effect of steam residence time on selected Amarula shell wastes biomass revealed that the desulphurization efficiency of DBT increased outstandingly with increased steam residence time. The AmShAC-ST produced at 90 min steam resident time reduced the highest content of DBT within 30 min.

The gasification chars from a down draft gasifier (DG) and a plasma gasifier (PG) were utilized for adsorption of DBT in model diesel fuel. The Algae biochar (ALGC-DGBC) was from gasification of Algae binder mixed with coal- fines in a down-draft gasifier. The Wood-DGBC was a waste product from wood pellets gasifier in a down-draft gassier, the Wood-PGBC was a by-product from Plasma gasification of wood pellets. These chars were able to reduce sulphur content in DBT model diesel fuel with Amarula shells biochar (AmShBC) being the best performer as compared to other chars. The KOH and steam were used as activating agents on biochar to improve their performance. The results showed that the gasification chars treated with the steam agent had a higher desulphurization efficiency of DBT than the ones treated with KOH agent. The desulphurisation efficiency trend: AmShBC-ACST > Wood-PGBC-ACST > Wood-DGBC-ACST > ALGC-DGBC-ACST was achieved for steam activation. In the contrary, for KOH/BC the trend was in the order of Wood-DGBC-KOH > Wood- PGBC-KOH > AmShBC-KOH > ALGC-DGBC-KOH, but with lower ADS efficiency values as compared to steam/BC.

Pseudo-second-order was found to be the best fit kinetic model on experimental data. While Langmuir isotherm was found to be a better fit as compared to Freundlich isotherm for both processed and unprocessed Amarula wastes biomass. Thermodynamic studies were carried out to determine the spontaneity of the adsorption of DBT on Amarula wastes adsorbents.

Qualitative analysis was carried out by techniques such as TGA, XRD, FESEM, TEM, BET and FTIR. The raw Amarula waste biomass had more O-functional groups as compared to their biochar and activated carbons. After thermal/steam activation of biomass, the micropores and mesopores were increased. This was concluded as the reason for improved desulphurisation efficiency of diesel fuel. The selected AmShAC-ST produced at 90 min steam residence time had increased mesopores and less micropores with a BET surface area of 1 194 m^2/g and the highest pore volume of 0.98 cm^3/g. On the other side, the gasification chars were found to have more micropores than mesopores. The ACs from KOH activation had less mesopores than the ACs from steam activation.

Therefore, the above desulphurization's data was found to contribute to the design of a small-scale adsorptive desulphurization plant for diesel fuel.

ACKNOWLEDGMENTS

I would like to acknowledge everyone who has contributed to my research journey both directly and indirectly. God Almighty, my family, friends, supervisors, and academics. This thesis would not have been a success without you. I would like to mention all of you one by one, but I would not finish you therefore I would like to mention these few:

1.   My child Ntando Rorisang Kabi for understanding and enduring the pain every time I had to leave you behind and come to further my studies. For the hardships you and I went through, but we still maintain mother to child good relationship. You are such a brave child. Continue being a kind respectful child you are. This is for you my boy, my 1st year university student of 2027....halaaaaaala….young engineer halaaaaa! 🥳.

2.   Kuwena mbokodo! My mother, Mrs Evelyn B Kabi for taking care of my child while I juggled with my career, for the love and support you gave me through thick and thin, where would I be without you mum. We may disagree on some matters, but you are the best mum in the whole world. This dissertation would not have been a success without your tremendous emotional support. The support and unconditional love you have for me and your grandson Ntando. Thank you for always being there for me when I feel like the world is shutting down on me. Thank you for your patience, your strength, and your love. Thank you for everything. Ngiyabonga Ntombi yakwa Mtshali, Hlabangani, Matshinga, Magalela, Umagwaza njenge ngonyama!!! Ngiyabonga mama.

3.   To my Father, Mr Francis N. Kabi for applauding me when I told you I have enrolled for masters. The excitement in your voice, the words of encouragement, you are my sanity, my strength, my voice of reason. Thank you for always telling me to remember GOD and to pray when the going gets tougher. Thank you, dad. Keyaleboha Motaung wa ha Moletsane, Letotoi le siya rumo. Yeo ereng ha aja ebe ha a hadimane, empa u adimana ntweng feela. Keyaleboha Ntate.

4.   To my lovely supervisor, Prof. Yali Yao; Thank you for choosing me to be your student. You must have seen something in me that I did not see in myself because I enjoyed this project to an extent that I felt I was destined to be a researcher and mostly to be your student. Your listening skills, humbleness, patience and most of all, your guidance during this journey has been so amazing. Thank you for academically trusting me, for allowing me to be me, to spread

my wings and to make my own mistakes and learn from them with your guidance. Thank you for making sure that you are available for me whenever I needed to talk to you either personally or academically.

5.   To Prof. Xinying Liu. Thank you for the words of courage. When I first came to IDEAS offices you said, "Research is not as easy as it sounds, things may not go as you wish, and there may be times when you would want to quit, and some people do quit. Therefore, you need to be sure you do research for the love of it, and choose research that interest you or something you have passion on..." And I said to myself, "I am ready for the challenge and I am not a quitter." Little did I know how tough things would be for me during my research and yes, there were some occasions when an evil voice would whisper words "quit this Tsepiso….quit now!!! "eish, but I would remember your words, "You need to have passion because things may not go your way...." Then I would pause, and remember, "I am Tsepiso Kabi and I am not a quitter… research is my thing! Then the following day, I would wake up more motivated and more vivacious than before. Thank you for always criticizing our work even though sometimes it hurts but your criticisms sharpened me because I would go back to my books and read even more harder.

6.   To Prof. Diane Hildebrandt. It was an honour to work under your wing. You had always been an inspirational to me. I used to read a lot about you before I enrolled. Little did I know that I would suddenly find you in UNISA and be under your research group! That was a "Wow". I so much wished to be close to you that when GOD made it happen unknowingly, I got so intimidated by you that every time I saw you coming my way, I would dodge you because I was so scared you would ask me some scientific/engineering problem and I would not be able to answer. Nevertheless, that fear motivated me to always get my story straight in terms of research. And it turned out you are such a wonderful person who even love kids... You are not just a leader but a mum to us and to me. Thank you for creating a warm environment to work at, particularly for women in research. The calmness in you even when we irritate you has shown me what it means to be a leader under difficult circumstances. Thank you for being a good listener and for always making sure your door is always open whenever we needed you. Thank you for your support both emotionally, personally, financially, and academically.

7.   To Prof Neil Coville. Thank you very much for allowing me to perform all my synthesis in your catalysis lab. You accepted me to work in your lab before you even knew who my supervisors were. That alone showed me that you have so much love for student's success no matter who they are or where they come from. I am so honoured and privileged to

have worked under you as a legend of scientific community. Thank you for making my synthesis work at Wits to be smooth and successful. Thank you for being you.

8. To Prof. Tondi Matambo. Thank you for always ensuring that safety protocols are followed in our Bio-Lab when caring out desulphurization experiments.

9. To Prof. Linda Jewell. Thank you for your endless support personally and in the department.

10. To Dr. Clayton Bhondayi. Thank you for listening to my academic problems and for being my first audience every time I am preparing for conference presentations. I must admit; you are a scary audience but very constructive. Thank you for always making time when I needed an extra eye.

11. Thank you Dr. Morena Xaba for proof-reading my work. It is not an easy task to do but your willingness and your enthusiasm on my research made it simpler and enjoyable to you hence you were so effective. Thank you.

12. Thanks to all IDEAS groups mainly catalysis group; Fischer–Tropsch (FT) and desulphurization group in UNISA and, to the CATMAT group in Wits for the good team spirit and weekly group meetings we had. They empowered not only me but everyone in the group.

13. To the IDEAS administrative staff; Alicia Bayi-Bayi and Genevieve Ngubane, thank you for your constant assistant you provided during my research journey.

14. Thank you to UNISA-IDEAS for funding and for NRF master block.

15. Thanks to Juliet Gillies, an English specialist from "writeskills" for double checking my English skills.

16. Last but not least. I would like to thank MYSELF for hard work and for enduring all the frustrations I came across with during this research. It was through my determination and desire to reach my end goal that I did not let the obstacles perish me. I would like to thank my MIND for keeping me going even when I felt lifeless. Empa tsena tsohle ha dia etsahala hobane kele ya bohlale hara babang mona lefatsheng. Tsohle tsena diphethahetsi hobane ke ne keitshitlehile ho wena Modimo waka. Wena Mbopi wa Mahodimo le Lefatshe. Wena o ileng watseba ka bophelo baka kesale ka popelong ya mme. God Almighty Lord, You are the one who gave me strength to survive it all. Thank you!!!

Presentations

1.   <u>Tsepiso Kabi</u>, Yali Yao, Diane Hildebrandt, Xinying Liu: Desulphurization of Model Diesel Fuel by adsorption on synthesized activated carbon from Amarula waste, biomass of Africa. **Catalysis Society of South Africa (CATSA)**, Kwa Maritane Bush Lodge, Rustenburg, North West Province, South Africa, 19-22nd November 2017. (Oral presentation).

2.   <u>Tsepiso Kabi</u>, Yali Yao, Diane Hildebrandt, Xinying Liu: Effect of activating agent on Synthesis of Amarula waste activated carbon for Desulphurization of Model Diesel Fuel. **International Workshop on Porous Materials and their Applications (IWPMA),** Council of Scientific and Industrial Research (CSIR), Casa Toscana, Lynnwood Manor, Pretoria, Gauteng Province, SA, 13-14th September 2018. (Oral presentation)

3.   <u>Tsepiso Kabi</u>, Yali Yao, Diane Hildebrandt, Xinying Liu, Neil Coville: Deep Desulphurization of Diesel Fuel by adsorption on activated carbon from Amarula wastes biomass. **Interdisciplinary Academy - College of Science, Engineering & Technology (CSET),** UNISA Science Campus, Johannesburg, Gauteng Province, SA, November 2018. (Poster presentation).

4.   <u>Tsepiso Kabi</u>, Yali Yao, Diane Hildebrandt, Xinying Liu, Neil Coville: Deep Desulphurization of Diesel Fuel by adsorption on activated carbon from Amarula wastes biomass. **Catalysis Society of South Africa (CATSA),** Legend Golf & Safari Resort, Limpopo Province, SA, 11-14th Nov 2018. (Poster presentation).

5.   <u>Tsepiso Kabi</u>, Yali Yao, Diane Hildebrandt, Xinying Liu, Neil Coville: Microscopy Analysis - Effect of Synthesis Temperature on Amarula shells waste activated carbon for Desulphurization of Diesel Fuel. **Microscopy Society of South Africa (MSSA) Workshop**, Science Stadium, University of Witwatersrand, Gauteng Province, SA, 3-5th December 2018. (Poster presentation).

6.   <u>Tsepiso Kabi</u>, Yali Yao, Diane Hildebrandt, Xinying Liu: Adsorption of Dibenzothiophene in Model Diesel Fuel using Amarula Wastes Biomass as a Low-Cost

Adsorbent. **US-Africa Forum on Nanotechnology Convergence for Sustainable Energy, Water and Environment**, Glenburn Lodge & Spa, Kromdraai Road, Muldersdrift, Johannesburg, Gauteng Province, SA. 11-15th August 2019. (Poster presentation)

7.   Tsepiso Kabi, Yali Yao, Diane Hildebrandt, Xinying Liu, Neil Coville: Deep Desulphurization of Dibenzothiophene in Model Diesel Fuel by adsorption on Amarula wastes as a low-cost adsorbent. **The 2nd International Symposium on Environment, Energy Science and Technology (ISEEST),** Mistry Hills Country Hotel & Conference Centre, Drift Boulevard, Muldersdrift, Johannesburg, Gauteng Province, SA. 18-21st August 2019. (Oral presentation).

8.   Tsepiso Kabi, Yali Yao, Diane Hildebrandt, Xinying Liu, Neil Coville: Gasification biochar as Potential Adsorbents for Adsorptive Desulphurization of Diesel Fuel. **Catalysis Society of South Africa (CATSA),** Club Mykonos, Langebaan, Cape Town, Western Cape Province, SA, 10-13th November 2019. (Poster presentation)

Publications and Awards

Publications

1.	Tsepiso Kabi, Yali Yao, Diane Hildebrandt, Xinying Liu.	Adsorption of Dibenzothiophene in model diesel by Amarula wastes biomass, a low-cost adsorbent. (Ready for submission).

2.	Tsepiso Kabi[a], Yali Yao[a], Diane Hildebrandt[a], Xinying Liu[a]. Neil J Coville[b].	Deep desulphurization of diesel fuel by steam processed Amarula wastes to activated carbons, as low-cost adsorbents. (Ready for submission).

3.	Tsepiso Kabi[a], Yali Yao[a], Diane Hildebrandt[a], Xinying Liu[a]. Neil J Coville[b]. Gasification biochar's as Potential Adsorbents for Adsorptive Desulphurization of Diesel Fuel. (Ready for submission).

Awards

1.	Best poster presentation: CSET- Interdisciplinary academy: November 2018
2.	Best poster presentation: Limpopo: CATSA 2018

Dissertation layout & Delimitation

Dissertation layout

The layout of this dissertation involves 7 chapters at which chapter 1 is about the background introduction, problem statements and objectives. Chapter 2 is about literature review. Chapter 3 is the summery of experiments. Chapter 5-6 is the research data at which chapter 4 fore cussed on raw biomass (Amarula fruit waste, Amarula seed wastes and Amarula shell wastes) as low-cost adsorbent for reducing sulphur content in diesel fuel, and its characterization before and after adsorption. Chapter 5 is the synthesis of activated carbons from three types of Amarula waste biomass and their application on organo-sulphur compounds in diesel fuel; it also involves studies on determining the effect of steam residence time during the activation process on selected Amarula shell waste AC and characterization of fresh activated carbons. Chapter 6 is about utilizing gasification char for desulphurization of diesel fuel and comparing their performance with selected Amarula shells biochar. Chapter 7 is the general conclusion.

Delimitation

This research was carried out in South Africa. The biomass studied was Amarula wastes from the production plant of Amarula liqueur. These wastes were collected from Limpopo province in Phalaborwa during their season between March and April. Amarula wastes from other provinces in South Africa or other countries were not part of this current study.

Table of Contents

Nomenclature & Abbreviations

A	Arrhenius constant
AC	Activated Carbon
Ads	Adsorbent or Adsorption
ADS	Adsorption Desulphurization
AmSh	Amarula shell wastes
AmSe	Amarula seed wastes
AmWa	Amarula fruit wastes
AmShAC	Amarula shell waste activated carbon
AmSeAC	Amarula seed waste activated carbon
AmWaAC	Amarula fruit waste activated carbon
AmShAC-ST	Amarula shell waste activated carbon from steam activation
AmSeAC-ST	Amarula seed waste activated carbon from steam activation
AmWaAC-ST	Amarula fruit waste activated carbon from Steam activation
AmSh-BC	Amarula shell biochar
AmShBC-ACST	AmSh-BC activated by steam agent
ALGC-DGBC	Algae-coal biochar from a Down-Draft Gasifier
ALGC-DGBC-ACST	ALGC-DGBC activated by steam agent
ASTM	American Society for testing and materials
BC	Biochar
BET	Branauer Emmett-Teller

BJH	Barret-Joyner-Halenda
C	Constant related to energy of adsorption
CAGR	Compound Annual Growth Rate
CATMAT	Catalysis and Materials
CATSA	Catalysis Society of South Africa
CSET	College of Science, Engineering and Technology
CSIR	Council of Science and Industrial Research
C_0	Initial concentration of sulphur (ppmw)
C_t	Concentration of sulphur at time t (ppmw)
C_e	Concentration of sulphur at equilibrium (ppmw)
Cu-Kα	Copper-X-ray energy frequency
DBT	Dibenzothiophene
DG	Down-Draft Gasifier
DTG	Derivative Thermogravimetry
Ea	Activation energy (KJ mol^{-1})
EDS	Energy Dispersive X-ray Spectroscopy
FESEM	Field Emission Scanning Electron Microscopy
Eff	Efficiency
Fig	Figure
FTIR	Fourier Transform Infrared
GAGR	Compound Annual Growth Rate
GC	Gas Chromatography
h	Initial rate in ddsorption

IDEAS	Institute of Development Energy African Sustainability
ISEET	International Symposium of Environment, Energy Science and Technology
IUPAC	International Union of Pure and Applied Chemistry
K_1	Rate constant of pseudo 1st order kinetic (min^{-1})
K_2	Rate constant of pseudo 2nd order kinetic
K_i	Rate constant of intraparticle diffusion
K_d	Distribution coefficient
K_L/b	Langmuir constant (mg/g)
K_F	Freundlich constant (mg/g)
KBr	Potassium Bromide
KOH	Potassium Hydroxide
KOH/BC	Potassium Hydroxide on Biochar
n	Freundlich constant related to adsorption intensity
PFPD	Pulse Flame Photometric Detector
PG	Plasma Gasifier
q_t	Adsorption capacity at time t (mg/g)
q_e	Adsorption capacity at equilibrium (mg/g)
$q_{e\ exp}$	Experimental equilibrium adsorption capacity (mg/g)
$q_{e\ calc}$	Calculated equilibrium adsorption capacity (mg/g)
q_m	Maximum adsorption capacity (mg/g)
r	Reaction rate of pseudo 1st order kinetic
r'	Reaction rate of pseudo 2nd order kinetic

R	Universal gas constant (J mol^{-1})
R^2	Correlation coefficient
Ramp	Ramping
rpm	Revolutions per minute
SEM	Scanning Electron Microscopy
ST	Steam
Sf	Separation factor
T	Absolute temperature (K)
Temp	Temperature
TEM	Transmission Electron Microscopy
TGA	Thermal Gravimetry Analysis
TPGC	Temperature Programme in Gas Chromatography
UNISA	University of South Africa
USA	United State of America
USD	United State Dollar
w$_{ads}$	Mass of adsorbent (g)
w$_{soln}$	Mass of solution-diesel fuel (g)
Wits	University of Witwatersrand
Wood- DGBC	Wood pellets biochar form a Down-Draft Gasifier
Wood-PGBC	Wood pellets biochar from a Plasma Gasifier
Wood- DGBC-ACST	Wood- DGBC activated by Steam agent
Wood-PGBC-ACST	Wood-PGBC activated by Steam agent
XRD	X-Ray Diffraction

[S]	Concentration of sulphur (ppmw)
ΔS	Entropy change (KJ/mol)
ΔH	Enthalpy change (KJ/mol)
ΔG	Gibbs free energy change (KJ/mol)

Standard Units and Mathematical Symbols

Å	angstrom (a metric unit of length equal to 10^{-10} m)
cm^3g/g	cubic centimetre per gram
g	grams
h	hour
KJ/mol	Kilojoules per moles
kV	kilovolts
L	litres
m	meters
m^2/g	meters squared per gram
mA	milliampere
mgS/g	milligrams of sulphur per gram
min	minutes
min^{-1}	per minute
ml	millilitre
mm	millimetre
m/v	mass by volume
nm	nanometre
ppb	parts per billion
ppm	parts per million
ppmw	parts per million weight
R	Rand

USD	United State Dollars
wt.	weight
μl	microliter
μm	micrometre
°C	degrees Celsius
%	percentage
±	plus, or minus sign
=	equals
≈	approximately
<	smaller than
>	greater than
≥	greater or equals to
≤	smaller or equals to
*	multiplication
/	division
Δ	delta
θ	Theta
δ	sigma
&	and
α	alpha
β	beta
γ	gamma

List of Figures

List of Tables

Chapter 1

Introduction

1.1 Background

1.1.1 Diesel fuel

Diesel fuel is a petrochemical substance that is distilled from crude oil. It has been found to contain sulphur compounds in high concentrations. These sulphur compounds have a negative economic, environmental and health impact. Sulphur compounds poison the fuel-processing and reforming catalysts; they also cause direct and indirect corrosion inside the system by damaging the linings of pipes, boilers and parts of engines [1],[2]. Sulphur dioxide emitted into the atmosphere causes acid rain, which pollutes the environment, compromising the lifespan of plants and animals [1]. Furthermore, long-term exposure to these sulphur compounds results in respiratory infections, cancer and eventually infertility in human beings [2]. For these reasons, and to avoid these detrimental effects, it is imperative to apply desulphurization processes to diesel fuels before their use as energy.

1.1.2 Desulphurization

Different methods of desulfurization [2],[3] are being applied to reduce sulphur compounds in diesel fuel in order to comply with the relevant regulations. Some of these methods are hydrogen desulfurization (HDS), bio-desulphurization (BDS), oxidative desulphurization (ODS) and adsorption desulphurization (ADS) [2],[3]. Unfortunately, some of these desulphurization methods, such as HDS, require many processing operations that require higher temperatures and pressure. Even though HDS is the main desulphurization method being globally used in petroleum refineries, it does not lead to friendly economics. As a result, some of the other methods listed above are sometimes preferred. It is for these reasons that this study has chosen the use of ADS. Furthermore, it mostly favours small-scale operations, and less energy is required to carry out the process, which is run at atmospheric conditions. Another

1

advantage of this process is that it removes larger sulphur compounds without the use of hydrogen, which is very expensive compared to HDS. ADS do not need to further use expensive solvents and oxidants or even degrading enzymes, as its the case with ODS and BDS. Despite all the benefits of ADS, it is limited to removing organo-sulphur compounds present in diesel fuel selectively.

1.1.3 Adsorbents

A variety of adsorbents have been employed for adsorption desulphurization. These include zeolites, activated carbons (AC), metal-organic-frameworks (MOFs) and metal-metal oxides [4]–[6]. Some of these adsorbents require a great amount of processing before they can achieve the desired degree of adsorption efficiency. This study chooses to use activated carbon, a carbonaceous material processed to increase the surface area and porosity of the carbons present. AC have been used for a very long time for different purposes, such as the removal of pollutants and dyes from solutions and purification processes . The use of AC over the other adsorbents is more beneficial because it is capable of adsorbing larger molecules such as dibenzothiophene and alkyl dibenzothiophene compounds which are present in large quantities in diesel fuel, and this process occurs without changing the adsorbent chemical characteristics. Furthermore, this type of adsorbent removes sulphur compounds at ambient conditions, resulting in economically friendly attributes. Low energy is consumed during the adsorption desulphurization process by AC, and during the regeneration of the adsorbent (AC). This differs from other processes, whereby these larger molecules of sulphur are difficult to process and result in less removal of total sulphur compounds present in diesel fuel.

The adsorption desulphurization by AC depends on the particle size of the adsorbent, the porosity, and the surface area of the carbon [5]. This is because larger surface area provides a larger area for the reaction to occur, and a wider variety of types of pore such as microporous, mesoporous and macropores. This means that various sizes of sulphur compounds will be trapped inside those pores. ACs are also good for the desulphurization of high sulphur feed even though they attain low levels of total desulphurization at times, and this can become a limitation. The porosity and surface area of AC also depends on the types of raw material used.

1.1.4 Biomass raw materials

Different raw materials have a great impact on the AC produced and also on its adsorption desulphurization. Biomass, a source of greenhouse gas emission for neutral energy, is a biological material obtained from living plant matter that is not used for food or feed [7]. There is a greater preference for biomasses over coal and coke because they are less expensive and are normally obtained from renewable resources. Furthermore, an AC produced from biomass that has fewer inorganic matters, high volatility and relatively high density tend to have a better pore size and surface area. On the other hand, biomass can be used in its natural state as an adsorbent. Several researchers have applied unprocessed biomass as a sorbent mainly for the treatment of water and have reported a very high percentage removal of the pollutants [8]–[10]. However, there are few or no studies on biomass as an unprocessed sorbent for the adsorption of organo-sulphur compounds in diesel fuel. The use of biomass is found to be more advantageous in terms of cost because there is no energy required. It also does not have to undergo process synthesis, which is also time-consuming. Moreover, biomass is available in abundance worldwide. Nevertheless, biomass is seasonal, and this may pose a limitation to large productivity requirements. However, this may be overcome by keeping greater stocks of the biomass and storing it in tanks for further use.

An environmentally friendly and green sustainable biomass waste sourced in Africa was used as an unprocessed sorbent and as a raw material for synthesising low-cost AC adsorbent. The chosen biomass was Amarula waste from the production of Amarula liqueur, a world-wide known spirit [11]. The fruit that is used to produce Amarula liqueur is from the marula tree, which is one of the indigenous trees found mainly in the southern region of Africa such as South Africa, Botswana, and Zimbabwe. The Amarula waste biomass studied in this research, was obtained from the production plant that produces Amarula liqueur, at Limpopo province, in South Africa. The waste was divided into three parts: Amarula fruit waste, Amarula seed wastes and Amarula shell wastes. The best adsorbent, both processed and unprocessed, was determined based on its adsorption desulphurization efficiency, and was further used to determine the adsorption parameters required to design a small-scale adsorption desulphurization plant.

1.2 Problem statement

Distillates of crude oil such as petroleum fuels contain toxic compounds that result in air pollution [1]. These fuels are found to have highly concentrated organo-sulphur compounds such as dibenzothiophene. Therefore, this problem is more observable in industries that produce fuel cells and in transportation fuels [2]. Moreover, sulphur compounds are emitted to the atmosphere and form indirect greenhouse gases such as sulphur trioxide (SO_3), which when reacting with humid air, it forms sulphuric acid. It is this sulphuric acid which causes the acid rain that contaminates the plants and affects the ecology. SO_3 is also indirectly responsible for terrible coldness because it reacts with other gases and forms a layer in the atmosphere that creates excessively low temperatures. Apart from that, in transportation fuels sulphur compounds corrode catalytic converters and have a serious economic impact. In human beings they cause respiratory infection or infertility and with prolonged exposure they may lead to cancer [2]-[6].

Adsorption desulphurization is expected to reduce these toxic organo-sulphur compounds that are very steric and hinder the cleaning process of diesel fuel when other expensive and unstable techniques are used [5]. This will consequently overcome the issues of economic impact, environmental impact and could even lead to saving human lives.

Land pollution and waste management are one of the other major concerns around the world. The production plant that produces Amarula liquor, a worldwide known spirit, discards the Amarula fruits of bad-quality and the Amarula seeds as by-product wastes on the landfill. Biomass wastes can rot and decompose in landfills to produce harmful gasses that contribute to environmental pollution [12]. Hence this study further mitigates the issue of waste management and land pollution by making use of the Amarula wastes biomass in its natural state and, employing it to clean diesel fuel by reducing the organo-sulphur content, and to further process these wastes into AC in order to improve the desulphurization efficiency of diesel fuel.

Biomass has more oxygen functional groups attributed to the hemicelluloses and cellulose components present in abundance [13]. These functional groups are expected to contribute to the mechanism of reducing sulphur content in diesel fuel through interactions of organo-sulphur compound via chemisorption or mass transfer due to Van De Waals forces. On the other hand, AC that has various porosities and a massive surface area is further expected to

improve desulphurization efficiency in transportation fuel by adsorbing the steric sulphur compounds via interface and pore diffusion mechanisms.

The study therefore aimed to utilize the Amarula wastes biomass as a natural sorbent and as a raw material for synthesizing AC adsorbent to reduce the sulphur content in diesel fuel by adsorption desulphurization. Furthermore, it also aims to investigate the desulphurization conditions for designing a small-scale desulphurization plant that is economically friendly and environmentally benign.

1.3 Objectives

The objective of the study was to carry out a green process of deep desulphurization of diesel fuel by adsorption on AC and raw biomass waste using a batch reactor. The objectives were simplified as follows:

1.3.1   To reduce the sulphur content in dibenzothiophene model diesel using Amarula wastes biomass and to characterize it before and after adsorption.

1.3.2   To synthesize AC from the three Amarula wastes biomass raw materials for adsorption desulphurization and the characterization of fresh and used AC.

1.3.3   To compare the performance of Amarula waste AC with ACs from gasification biochar.

1.3.4   To determine the optimal parameters that are economically portable and environmentally friendly for designing a small-scale adsorption desulphurization plant from the best low-cost adsorbent.

1.4 Significance of the study

It is to devise environmentally friendly and sustainable small-scale operations that produce clean diesel fuel with ultra-low sulphur content by an adsorption desulphurization process. This it will do using low-cost adsorbents obtained from the biomass of Africa and in the process, it will contribute towards mitigating the climate change and waste management.

1.5 References

[1]   F. C. Wang, W. K. Robbins, F. P. Di Sanzo, F. C. Mcelroy, "Speciation of sulfur-containing compounds in diesel by comprehensive two-dimensional gas chromatography," *J. Chromatogr. Sci.*, vol. 41, pp. 519–523, 2003.

[2]   C. Song, "An overview of new approaches to deep desulphurization for ultra-clean gasoline, diesel fuel and jet fuel.," *Catal. Today*, vol. 86, pp. 211–263, 2003.

[3]   K. Sertic-Bionda,M. Muzic, "Alternative processes for removing organic sulphur compounds from petroleum fractions," *Chem. Biochem. Eng. Q.*, vol. 27, pp. 101–108, 2013.

[4]   Isam A H, Al Zubaidy, Fatma Bin Tarsh, Noora Naif Darwish, Balsman Sweidan Sana Abdul Majeed, Aysha Al Sharafi, "Adsorption process of sulfur removal from diesel oil using sorbent material," *Clean Energy Technol.*, vol. 1, pp. 66−68, 2013.

[5]   C. Zhang, W. Song, G. Sung, L. Xie, L. Wan, J. Wang, K. Li, "Synthesis, characterization, and evaluation of activated carbon spheres for removal of dibenzothiophene from model diesel fuel," *Ind. Eng. Chem. Res.*, vol. 53, pp. 4271–4276, 2014.

[6]   G. Blanco-Brieva, J. M. Campos-Martin, S. M. Al-Zahrani, and J. L. G. Fierro, "Effectiveness of metal-organic frameworks for removal of refractory organo-sulfur compound present in liquid fuels," *Fuel*, vol. 90, pp. 190−197, 2011.

[7]   P. G. González and Y. B. Pliego-Cuervo, "Physicochemical and microtextural characterization of activated carbons produced from water steam activation of three bamboo species," *J. Anal. Appl. Pyrolysis*, vol. 99, pp. 32–39, 2013.

[8]   Z. Kariuki, J. Kiptoo, and D. Onyancha, "Biosorption studies of lead and copper using rogers mushroom biomass 'Lepiota hystrix'," *South African J. Chem. Eng.*, vol. 23, pp. 62–70, 2017.

[9]   V. Emmanuel, P. Themba, D. Ntuli, and A. Enakpodia, "Biosorption of hexavalent chromium from aqueous solutions by macadamia nutshell powder," *Appl. Water Sci.*, vol. 7, pp. 3015–3030, 2017.

[10]   N. El-naggar, R. A. Hamouda, I. E. Mousa, M. S. Abdel-hamid, and N. H. Rabei, "Biosorption optimization, characterization, immobilization and application of Gelidium amansii biomass for complete Pb^{2+} removal from aqueous solutions," *Sci. Rep.*, vol. 8, pp. 1–19, 2018.

[11]   J. Conway, "Amarula liqueur global market," https://www.statista.com/statistics/308846/aamarula-liqueur-global-sales-volume/, 2019.

[12]   P. Mishra, N. Singh, C. Shrama, A. K. Pathak, "Landfill Emissions and Their Impact on the Environment," Int. J. Eng. Res. Technol., vol. 9, pp. 617-622, 2020.

[13]   P Gonzalez-Garcia, T A Centeno, E Urones-Carrote, D Avila-Brande, L. C. Otero-Dianz "Microstructure and surface properties of lignocellulostic-based activated carbons," *Appl. Surf. Chem.,* vol. 265, pp. 731–737, 2013.

Chapter 2

Literature Review

This chapter reviews the literature on the subject of the sulphur compounds in diesel fuel, the desulphurization techniques, the adsorption desulphurization method, and the adsorbents used in the adsorptive desulphurization of diesel fuel.

2.1 Sulphur compounds and desulphurization processes

2.1.1 Diesel fuel and sulphur compounds

The common type of Diesel fuel is a 60 % distillate of crude oil. It is used for transportation and fuel cells. It contains both direct and indirect sulphur compounds. These toxic compounds when present in high concentrations, they react and produce oxides which corrode catalytic converters [1]-[3]. When emitted to the atmosphere, they result in air pollution and the acid rain they cause has a negative impact on agricultural products. Furthermore, they are known to have long-lasting effects on human life, causing respiratory infections, infertility and even cancer [4],[5].

The toxic sulphur compounds are classified to inorganic compounds such as elemental sulphur (S), hydrogen sulphides (H_2S) and mercaptans, which are easy to remove from diesel fuel. In contrast, the organic sulphur compounds such as thiophenes (TH), benzothiophenes (BT), dibenzothiophenes (DBT) and alkyl dibenzothiophenes (Alkyl DBT), shown in Fig. 2.1, are more toxic and difficult to reduce [1]. Of them all, DBT is the stubborn organo-sulphur molecule to remove, hence it was selected in this study.

Benzothiophene
(BT)

Dibenzothiophene
(DBT)

Alkyl Dibenzothiophene
(4,6 DMDBT)
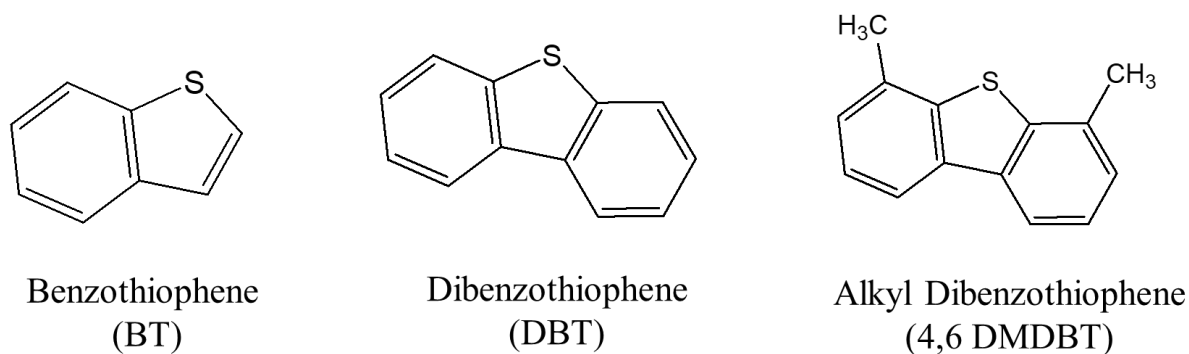
Fig. 2.1. Organo-sulphur compounds in diesel fuel [1]

2.1.2 Desulphurization techniques

Different desulphurization techniques [2]–[4] such as hydrogen desulphurization (HDS), oxidative desulphurization (ODS), bio-desulphurization (BDS) and adsorption desulphurization (ADS), are used to remove these toxic sulphur compounds, but some have limitations over the others. Each of these is described below.

2.1.2.1 Hydrogen desulphurization techniques (HDS)

This is the technique widely used industrially for the removal of sulphur compounds using hydrogen gas, which is an expensive process involving higher temperatures and pressure. Hydrogen (H_2) gas reacts with sulphur that is fused in the sulphur compound via a hydrogenation addition reaction and then later removes sulphur via an elimination reaction to form hydrogen sulphide (H_2S) [3]. This process becomes thermodynamically limited when the sulphur compound is steric, because the sulphur is shielded and this makes its removal difficult under their normal operating conditions [3]–[5]. Therefore, to achieve the removal of a steric hindered sulphur compound (Fig. 2.1), high temperatures and pressure are applied, which becomes a drawback economically. Reaction 2.1 below shows how the HDS reaction occurs. The HDS reaction slows down as the sulphur compound becomes sterically hindered [5].

$$CH_2SH + H_2 \rightarrow C_2H_6 + H_2S \qquad\qquad \textbf{Reaction 2.1}$$

2.1.2.2 Oxidative desulphurization (ODS)

It operates by undergoing a chemical oxidation process for the removal of sulphur to form sulphones, as shown in Reaction 2.2. In this process the fused sulphur in a sulphur compound is bonded to two oxygen atoms [5]–[7]. The second process is by extraction using solvents to separate sulphones to form a sulphur-free compounds [5]–[8], as shown in Fig. 2.2. This extraction process results in product loss, which consequently leads to wasted product. Even though the ODS method is preferred to hydrogen desulphurization (HDS) because of its ambient conditions of operation, it also has its own limitations which emerge from several separations during extraction that requires the use of expensive solvents. Furthermore, the process requires expensive oxidants, such as peroxides to achieve desulphurization efficiency.
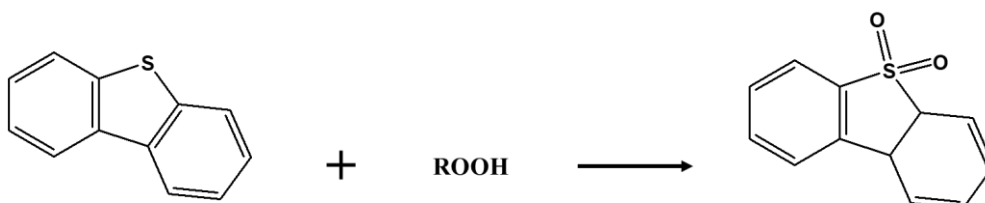
Reaction 2.2 Oxidation of dibenzothiophene in ODS [6]
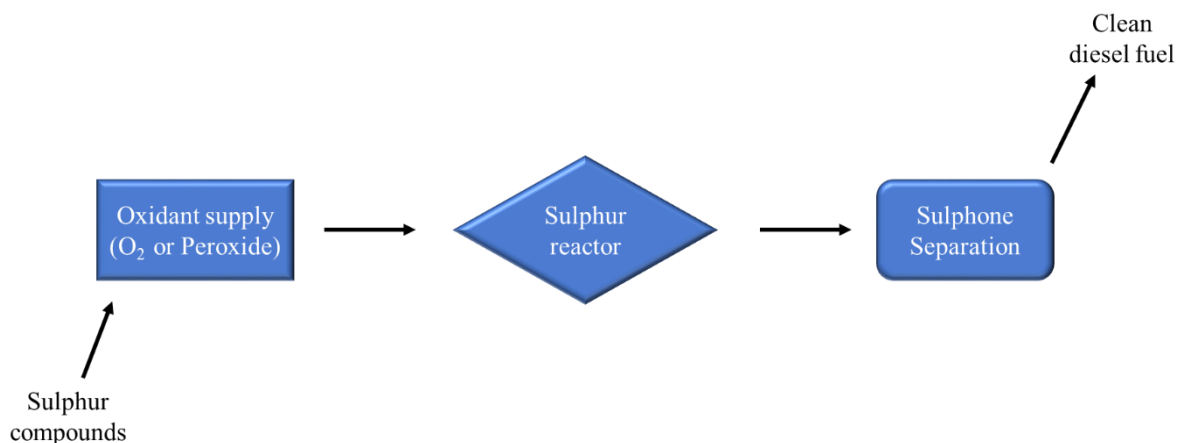
Fig. 2.2. Process flow of oxidative desulphurization [6]

2.1.2.3 Bio-desulphurization technique (BDS)

This is a desulphurization technique that removes sulphur compounds from diesel fuel using a biological catalyst such as enzymes. The BDS process pursues a pathway using a living organism [9], as shown in Reaction 2.3. This technique results in the cleavage of the carbon-

sulphur bond and maintains a calorific value of a sulphur molecule [9]–[11]. It is an acceptable process because of its ambient conditions of operations, but the instability of the enzymes make it difficult for this process to be applied industrially [5].
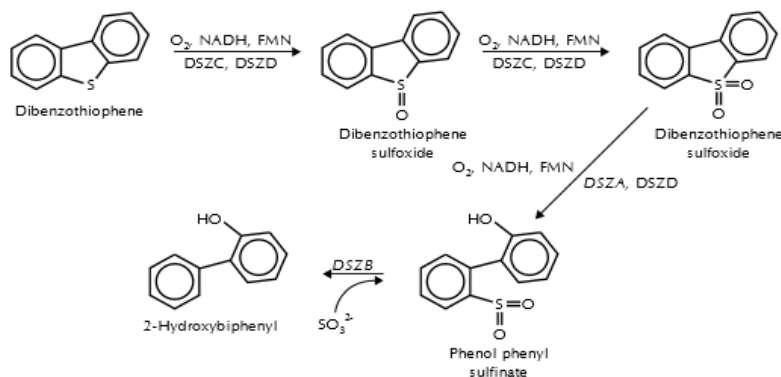
Reaction 2.3 Bio-desulphurization reaction for a pathway of enzyme [5]

2.1.2.4 Adsorption desulphurization technique (ADS)

Adsorption desulphurization (ADS) is one of the techniques of removing sulphur compounds using an adsorption process. It is the process of attaching compounds to another substance by either physisorption or chemisorption. Fig. 2.3 is a schematic diagram of the adsorption process. Physisorption is governed by Van der Wall forces and this type of adsorption is responsible for trapping compounds or substances inside the pores and on the pore surface of the adsorbent. Chemisorption occurs by chemical adsorption which results from the reactive site of an adsorbent that contains various functional groups [12]–[14], possessing an -O group to form sulphur dioxide (SO_2). This SO_2 is further oxidized to form sulphur trioxide (SO_3). The SO_3 then moves to the unreactive site of the adsorbent and becomes adsorbed there. The entire adsorption process occurs at ambient conditions, which is economically favoured and preferred for small-scale operations [5]. The quantity adsorbed is proportional to the surface area of the adsorbent and the pore volume. The longer the adsorption time, the better the removal of sulphur compounds, but this process requires that the adsorbent must be protected from the liquid condensation matters [5],[14],[15], which may mask the adsorption surface and thus reduce the adsorption efficiency of ADS. This problem is overcome by the drying process before use. Furthermore, this technique is thermodynamically limited [12],[15] on the overall rates of conversion, and to overcome this limitation, the reaction temperature is increased

slightly. Its main benefit is that it can also be used for regeneration of the adsorbent at a lower temperature. However, to achieve high adsorptive desulphurization efficiency, an effective adsorbent is required.
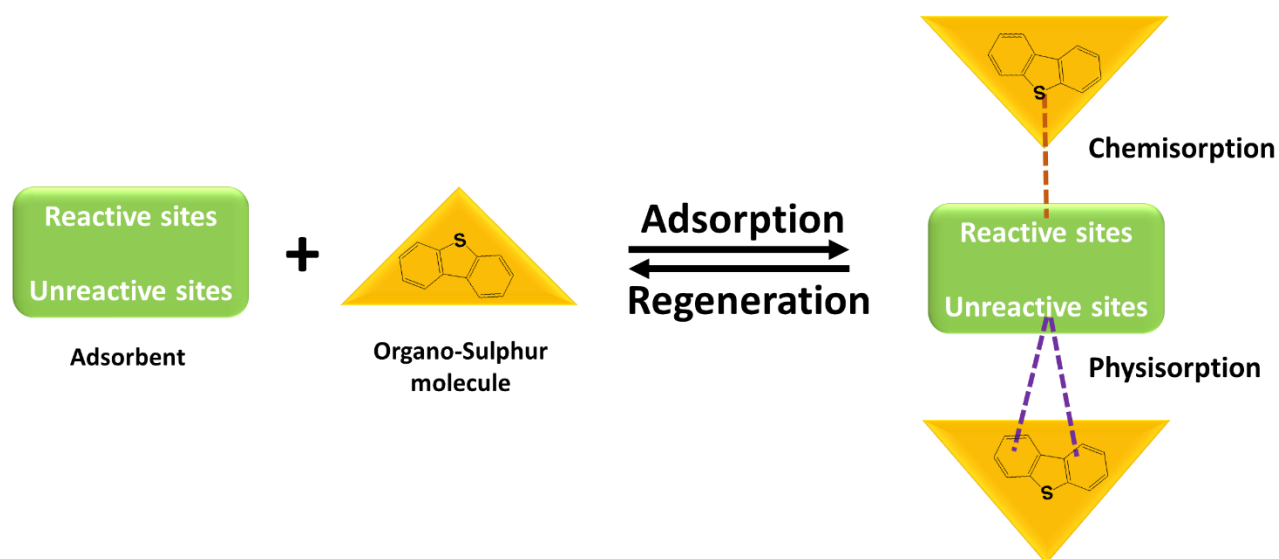
Fig. 2.3. Adsorption desulphurization (ADS) process

2.2 Adsorbents for ADS

Various adsorbents exist; these include zeolites [16],[17],metal–metal oxides [18], MOFs [19],[20] and carbon materials such as AC [21]. They have been used for ADS processes by several researchers. However, the challenge has been that these adsorbents must undergo several expensive synthesis processes before the desired level of efficiency is archived, and this constitutes a limitation. Furthermore, they must use more energy for the regeneration of the adsorbent because they often undergo several chemisorption adsorptions (Fig. 2.3).

2.2.1 Zeolites adsorbents

Zeolites can be produced naturally and are classified as mordenite and clinoptilolite [22]. They can also be synthesized from alkali metals in various ways to produce an inorganic microporous material, as shown in Fig. 2.4. Their main advantage is their high capacity for ion exchange [23]. Their disadvantage is that they can adsorb only micropore-size adsorbate in their pore structure. There are different types of zeolites, such as 5A zeolites, Y-zeolites etc.

Several scientists [24] have produced zeolites from fly ash or waste materials for the treatment of water. Oliveira et al. [25] produced magnetic zeolites for removing metallic contaminants from water and obtained a very high percentage of removal. Song et al. [16] used commercial HY-zeolite to treat jet fuel that had a net sulphur content of 736 ppm in a batch reactor at 80 °C for ≈ 5 hrs and obtained ≈ 30 % sulphur removal. When he further loaded the commercial Y zeolite with transition metals such as Ce and Pd, the percentage of sulphur removal increased to 58 % and 60 % respectively [16].
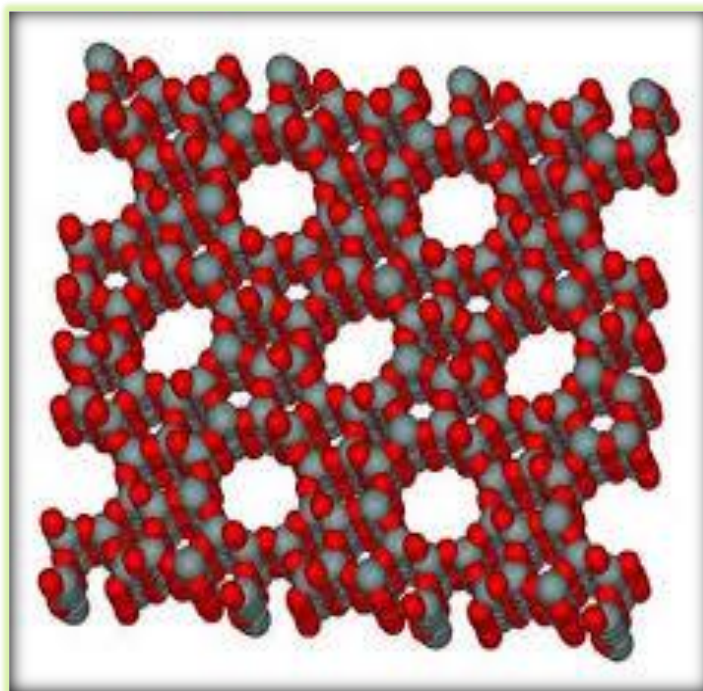
Fig. 2.4. Zeolite structure [23]

2.2.2 MOFs adsorbents

Metal-organic frameworks (MOFs) are a class of highly porous materials with a strikingly high surface area.. These properties occur by varying the type of organic ligands and open metal active sites [26],[27]. Their main disadvantage was that they were found to use expensive organic solvents during their preparation through several stages of synthesis. Recently, they have been incorporated with other materials such as carbon, zeolite or metal-oxides to reduce the use of solvents [27],[28]. Despite that, the synthesis process remains lengthy and costly. MOFs have been used as catalysts [29],[30] or as adsorbents for carbon dioxide and organo-sulphur compounds [31],[32]. MOFs are found to interact with organo-sulphur compounds by π-π interaction [33],[34]. A metal-sulphur coordination bond through unsaturated coordination

sites of selected metal ions has been developed [27]. Shing et al. [19] used MOF-derived porous carbon which underwent several processes before using it to reduce 160 ppm dibenzothiophene in n-hexane model diesel fuel inside a batch reactor, and obtained an adsorption capacity of 26.7 mgS/g. Wang T. used synthesized zinc-copper-based MOFs to reduce dibenzothiophene in model oils using a fixed-bed reactor and obtained $\approx$ 92 % breakthrough capacity and $\approx$ 96 % saturation capacity [20]. The structure of MOF [29] is shown in Fig. 2.5.
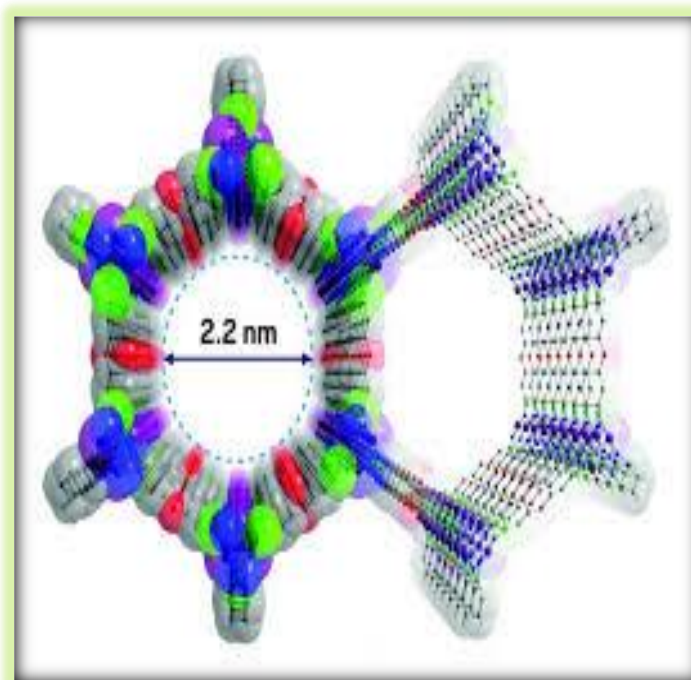
Fig. 2.5. Metal-organic framework (MOF) structure [29]

2.2.3 Metal–metal oxides adsorbents

These adsorbents undergo adsorption by complex formation and chemisorption hence they provide a wide surface area for adsorption [27],[31]. Despite this, the metals are very expensive, and a great amount of energy is required to regenerate the adsorbent. So, poses a limitation to the use of this type of adsorbent.

Kim and his team [35] performed a selectivity study on the adsorption of organo-sulphur compounds and aromatic compounds on $Ni/SiO_2–Al_2O_3$, as shown in Fig. 2.6. They found that sulphur compounds have a higher selectivity on metal–metal oxides compared to aromatic compounds [35].
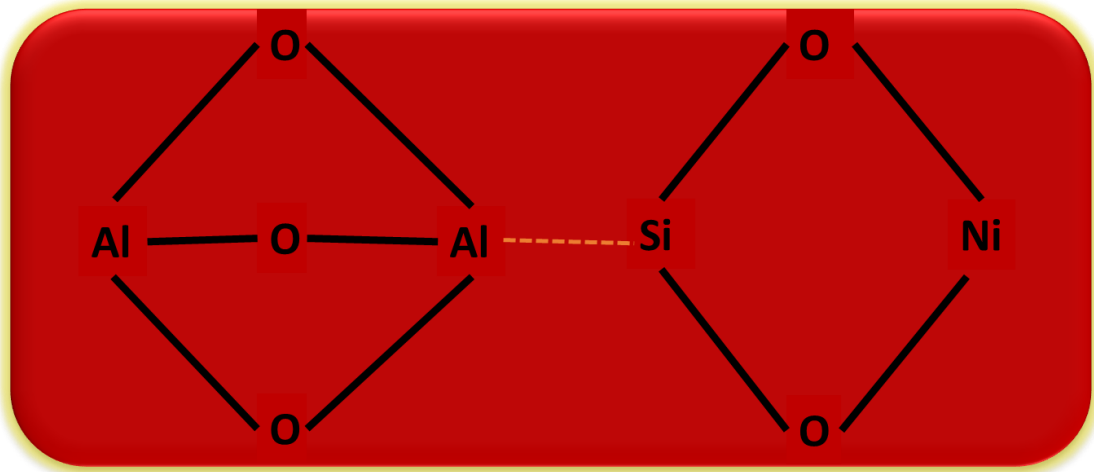
Fig. 2.6. Synthesized metal–metal oxide $Ni/SiO_2–Al_2O_3$ [35]

2.2.4 Activated carbon adsorbent

Studies [5],[12]–[15] have shown that there is a high yield of total sulphur removal from diesel fuel using AC. However, most researchers have used commercial AC in its natural state or modified [12],[21],[36]. Some desulphurization studies show that AC is a better adsorbent compared to others [12],[13],[15]. This is because it can remove those alkyl organo-sulphur compounds which are difficult to remove by other processes, such as HDS.
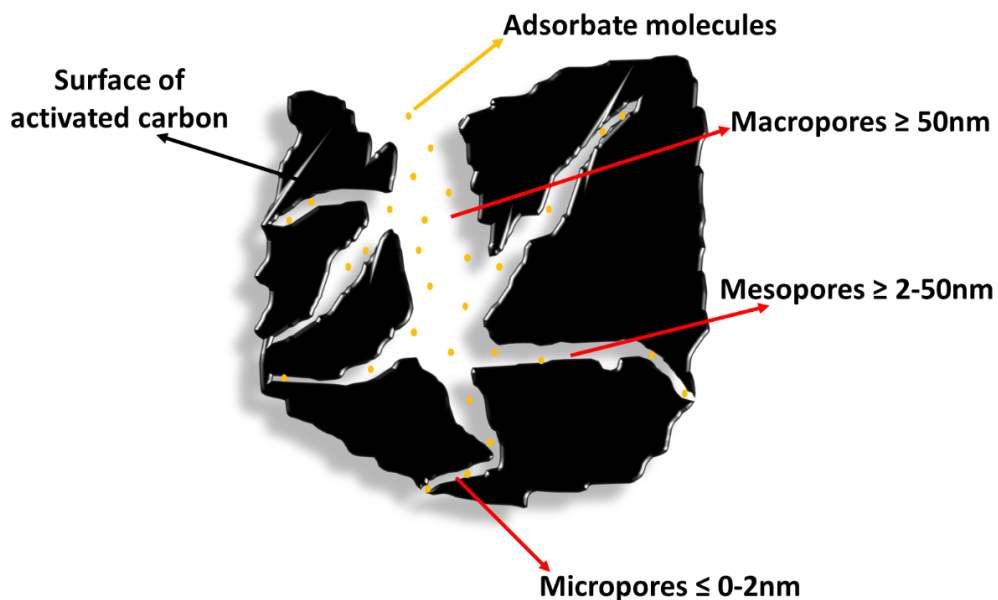
Fig. 2.7. AC with different pore sizes

AC is a carbonaceous material that has been processed to increase pore size and pore shapes together with the surface area, depending on the end-use [14],[15]. Fig. 2.7 shows the pore structure of ACs with different pore sizes. This carbon adsorbent can be synthesized from the raw materials of coke, coal, or biomass [15]. However, its use may be economically viable and environmentally friendly only when the end-product is derived from non-renewable resources such as biomass or waste materials. It has been found that different raw materials have a great impact on the functionality of AC produced, and also on its adsorption desulphurization efficiency. It has also been found that all plant materials have a lignocellulose structure that contributes to their carbon content, and to different carbonyl functional groups found on the surface of the AC [37]. Furthermore, an AC produced from biomass that has less inorganic matter, high volatility and relatively high density tends to have a better pore size and a larger surface area [38]. For this matter, the choice of raw materials depends on the final use of the product.

AC derived from biomass has been found to have greater porosity compared to those obtained from coal and coke [39]. It also has both hydrophobic and hydrophilic properties that render it highly sensitive to moisture. The hydrophilic site (-C–O) is due to the functional groups that have an oxygen atom which is the result of cellulose and hemicellulose fragmentation [12],[40]–[42]. Whereas the hydrophobic site (C–C), known as an unreactive site, is mainly due to the fragmentation of lignin [43], which contributes more to carbon content. These sites or surface areas are favoured for sulphide adsorption, which becomes advantageous for the adsorptive desulphurization process.

$$C–C–C–C–C–C–C–C–C–C–C=O$$
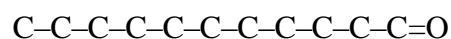
Adsorption on AC occurs by trapping the adsorbate between the pores of the carbon–carbon structure, as shown above. Pores are formed each time a carbon atom is removed between the carbons, making room for absorptivity.

Activating agents such as acids, bases or oxidising gases are utilized to facilitate the activation process. For instance, Po H. used AC prepared by phosphoric acid from date stones to reduce the DBT content in model diesel fuel and obtained an adsorption capacity of ≈ 41 mgS/g [44]. Saleh and Danmaliki [45] prepared ACs from waste tires and then modified it with NaOH and NHO_3 at 90 °C. They then applied these AC adsorbents for the removal of 50 ppm DBT in

16

model fuel and obtained a percentage removal of ≈ 45 %, ≈ 80 % and ≈ 99 % for raw AC, AC-NaOH, and AC-NHO$_3$, respectively [45].

In addition, Muzic et al. [46] performed a study on adsorptive desulphurization using commercial AC and zeolites. They found that the AC had a better adsorption capacity with organo-sulphur compounds in diesel fuel than 13X-type zeolites [46].

2.2.5 Biomass as adsorbent

Despite the mostly favoured adsorbents above, biomass has received little attention when used as an adsorbent, particularly for desulphurization. Biomass is an organic plant material that has a lignocellulose structure which consists of cellulose, hemicelluloses and lignin [37] composites, as shown in Fig. 2.8. Lignin contributes more to the C–C structure during its fragmentation, whereas cellulose and hemicelluloses contribute more to the functional groups such as phenols and carboxylic found on the surface of the carbon material [37],[41]. The different biomass sources shown in Fig. 2.9 produce different quantities of lignocellulose composites, these then result in different adsorption capacities.

Biomass has been used mainly for bio-oil and energy production [47], or as a source of ACs [48]. Therefore, the utilization of biomass as an adsorbent mitigates issues associated with climate change and environmental pollution. Furthermore, biomass is a renewable and sustainable resource that is found in abundance worldwide. Moreover, it can be used either as a fresh or as a waste material. Besides that, no energy is required to produce it, except solar power, which is a natural energy provider. In addition, it is the cheapest low-cost adsorbent that the world needs.
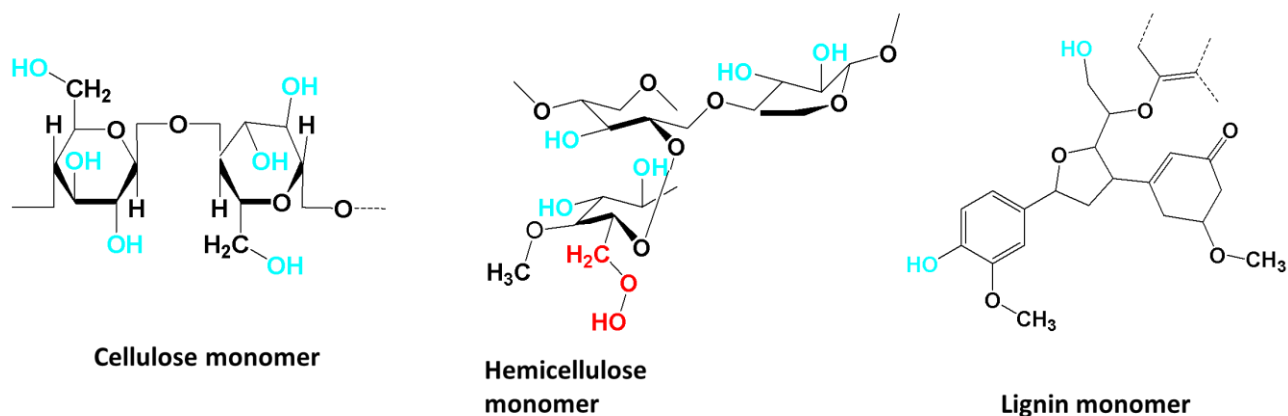
Fig. 2.8. Lignocellulose structure: cellulose, hemicellulose, and lignin [37]
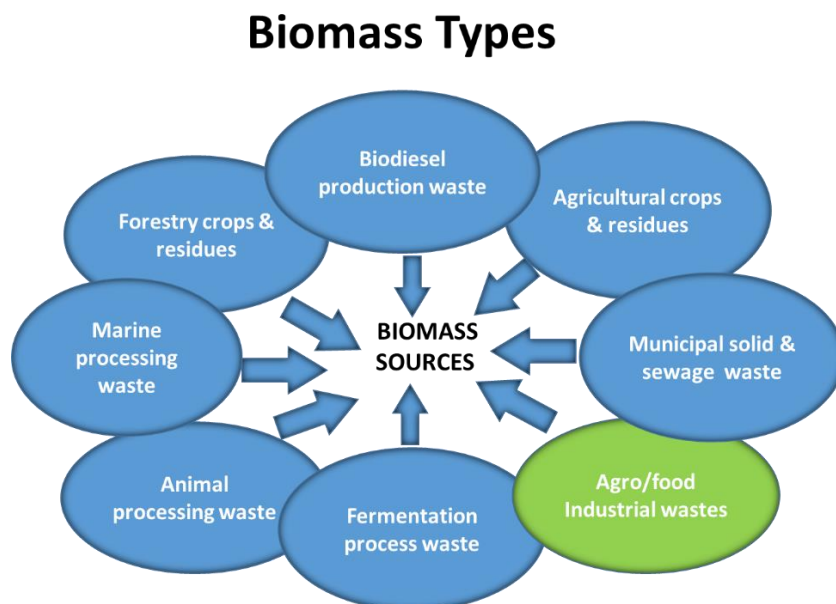
Fig. 2.9. Biomass sources

Recently, some studies have used biomass as a sorbent for the treatment of water. Fadel et al. [49] used the biomass of *Saccharomyces cerevisiae* to remove manganese (Mg^{2+}) from ground water and obtained about 86 % removal. Lokeshwari and Joshi [50] used yeast biomass to remove chromium (VI) in a batch reactor and found that the biomass quantity is a significant factor in effective adsorption. Pakade [51] also used macademia shell powder to remove hexavalent chromium from aqueous solutions. He obtained 91 % uptake of Cr(VI) when using 1.0 g biomass as compared to 32.5 % uptake when using 0.2 g biomass. Huang and Lin [52] used a biomass of dried *Sargassum fusiforme* to adsorb Hg (II) and Cu (II) in an aquatic

solution. Kariuki et al. [53] performed studies on the biosorption of lead and copper in aqueous solutions on roger mushroom biomass, *Lepiota hystrix*. They obtained the maximum adsorption capacity of 3.89 mg/g and 8.50 mg/g respectively in the optimal time of 30 min [53]. Chigondo et al. [54] removed Pb (II) and Cu (II) ions from an aqueous solution by using baobab (*Adononsia digitata*) fruit shells biomass and obtained ≈ 1.2 mg/g for copper at 90 min and ≈ 3.8 mg/g for lead at 120 min. In addition, marula seed husk biomass was used by Moyo M. et al. to remove the Pb (11) and Cu (11) from aqueous solutions [55]. They obtained a maximum percentage removal of 86.7 % at 60 min for Pb (11) and 79.5 % at 180 min for Cu (11) [55]. They concluded that the rate of biosorption decreased after a certain time due to the saturation of the active site and the resulting repulsive forces between the adsorbate and the adsorbent [55]. El-Naggar et al. [56] obtained 45.9 % removal of Pb (11) before Plackette-Burman and 94.3 % removal after Plackette-Burman within 60 min at 50 °C using *Gelidium amansi* biomass under Plackette-Burman at static condition. For water remediation, Muhammad et al. [57] used 0.03 g walnut shell biomass for the removal of 100 mg/g malachite green (a toxic chemical) and obtained an adsorption capacity of 54.5 mg/g in an equilibrium time of 90 min [57]. Guechi et al. [58] also adsorbed malachite green from an aqueous solution by using potato peel biomass at 25 °C, 35 °C and 45 °C and found that the adsorption processes were endothermic because the adsorption capacity increased with an increase in temperature.

Based on the above proven studies, biomass has shown great potential to act as an adsorbent mainly due to the presence of functional groups such as amines, hydroxyl, carbonyls and carboxylic. These functional groups are those that may become active during the adsorptive desulphurization process because they all contain oxygen (-O) group, which is a reactive element due to its high electromagnetic property [41]. The carbon–carbon structure contributed by lignin might be responsible for physical adsorption. However, there is less literature on the adsorption of organo-sulphur compounds in diesel fuel on biomass.

2.2.6 Biochar as adsorbent

Another fast-emerging adsorbent is biochar, which is a carbonaceous material obtained under limited oxidized conditions. This thermal decomposition of organic matter results in the production of biochar, bio-oil, and other gases such as CH_4, CO, H_2 and CO_2. Depending on the objective of the process, the thermal decomposition may favour the formation of slow-yield

char by torrefaction (200–400 °C) and carbonization (400–600 °C), therefore producing a less reactive char. Favouritism of high-yield mobile products by pyrolysis (600–800 °C) and gasification (> 800 °C) results in reactive biochar [43],[59]. Therefore, the heating processes involve heat transfer to the biomass particles by conduction. In addition to that, vapours are formed inside the biomass pores and these are subjected to further cracking, which leads to the formation of gases and thermally stable tars. It is for these reasons that inert gases such as nitrogen are used during this process to prevent an oxidation reaction that may occur due to the presence of water particles. However, the quality of biochar depends on the type of raw materials used, the process conditions and the reactor design.
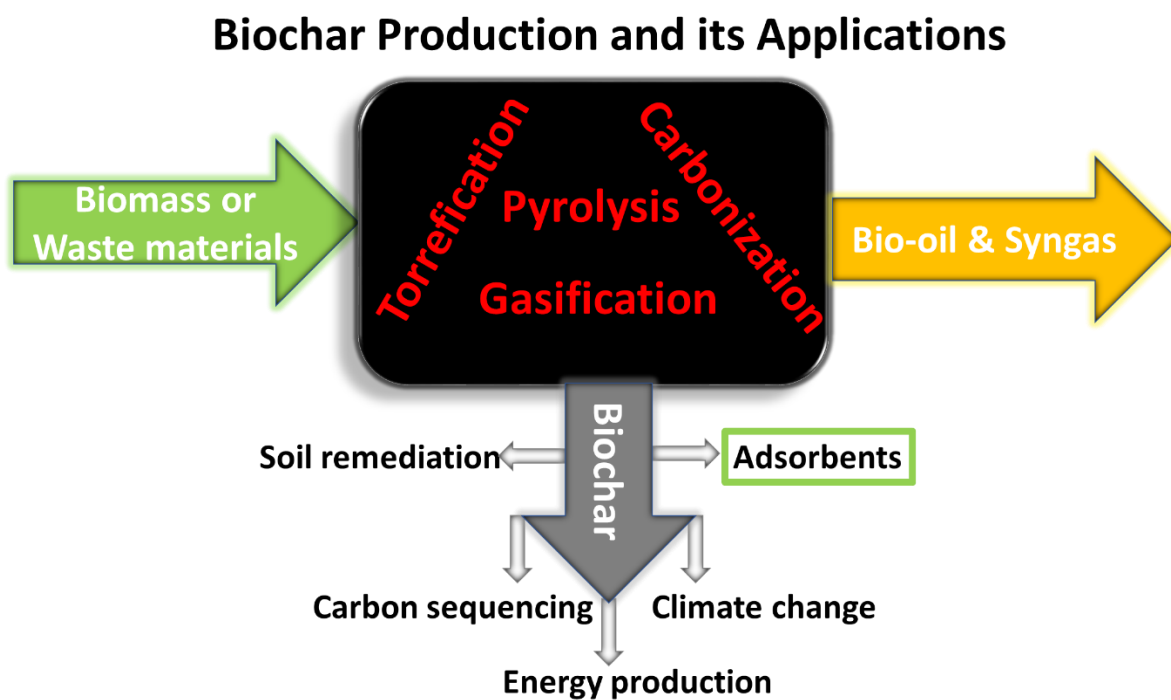
Fig. 2.10. Biochar production and its application

Biochar has been used mainly for soil remediation, carbon sequencing, energy production and environmental management, as shown in Fig. 2.10. Besides these uses, it was mainly used as an intermediate during the production of AC [60],[61]. Recently, it has been used as an adsorbent mainly for water purification or the removal of heavy metals. Its main benefit derives from its ability to resist microbial decay and the high adsorption capacity of ions and molecules [62]. Biochar consists of an ion charge surface, a carbon–carbon structure, C–O, hydrophilic sites, and polar sites, which contribute to the adsorption of various materials [63]. Based on this, Ahmad and his team [63] removed Cu (II), Cd (II) and Pb (II) ions from aqueous solutions

by biochar derived from a potassium-rich biomass of banana and cauliflower. They found that both types of biochar showed similar sorption trends in metal ions in an equilibrium time of 24 hours. However, banana biochar showed faster kinetics compared to cauliflower biochar due to its high electronegativity [63].

Tran et al. [64] used orange peel as a source of biochar to determine the effect of pyrolysis temperature (400–800 °C) on the adsorption of cadmium. They found that the biochar produced at a higher temperature had the highest adsorption capacity of cadmium due to formation of more pores and more carbon structure, which allowed more ions to be adsorbed inside the pores. Ma et al. [65] also determined the carbonization temperature during the production of honeycomb tubular biochar from *fargesia* leaves as an effective adsorbent of pollutants. They reported that the adsorption capacity improved from 52.22 mg/g to 123.59 mg/g, with an increase in the carbonization temperature from 650 to 800°C due to the presence of mesopores. Despite that, he found that further increasing the carbonization temperature from 800 to 900 °C slightly reduced the performance of the biochar because of the damaged structure of the biochar. On the other hand, Sew et al. [66] found that surface area is not the only the controlling factor on adsorption when using biochar produced from Korean cabbage waste [66]. In their study [66], they found that the functional groups and the amount of ash content present in a biochar play an important role in electrostatic and in ion exchange adsorption, respectively.

The gasification of wood from *Eucalyptus grandis* (BC-EG), *Acacia magnium* (BC-AM) and *Gmelina arborea* (BC-GA), which was carried out by Suárez-Hernández et al. [67] at 700 °C using a down-draft gasifier, yielded mesoporous biochar as a by-product with average pore-size range of between 2 nm and 50 nm, with a lower surface area ranging between 4 m^2/g and 50 m^2/g. They were also found to have different morphologies, which were attributed to the different bulk density of the raw biomass, suggesting the importance of the properties of a feed stock [67]. Sun et al. [68] proved that even though the feedstock has a great impact on the properties of biochar, but the temperature used for the production of biochar determines the thermal stability of the biochar and the elemental composition, such as the C, H, N and O content, in the structure of biochar. Chen et al. [69] produced a biochar with high magnetic properties and found that the magnetic biochar had a higher adsorption efficiency on organic pollutants and phosphates than the non-magnetic biochar.

Yanga et al [70] produced biochar from bamboo biomass using $ZnCl_2$ at different temperatures and applied them for the adsorption of dibenzothiophene in model diesel fuel. They found that a bamboo biochar withthe highest micropore ratio had the highest adsorption capacity of DBT as compared to the biochar with the highest surface area, the highest total pore volume and the highest level of acidity [70]. They found out further that when they oxidized bamboo biochar with NHO_3, the percentage removal of DBT improved due to a π–π interaction and an acid–base interaction [70]. However, there are fewer studies on the adsorptive desulphurization of diesel fuel using biochar.

As mentioned above, many options have been investigated for the use of raw biomass and biochar as adsorbents, for water purification. However, there are fewer studies on the adsorptive desulphurization of diesel fuel using biochar or raw biomass. Furthermore, to our best knowledge, there is lack of research projects that have been done on the desulphurization of diesel fuel using biomass from Africa or the materials synthesized by the biomass from Africa.

2.3 References

[1]   F. C. Wang, W. K. Robbins, F. P. Di Sanzo, and F. C. Mcelroy, "Speciation of Sulfur-Containing Compounds in Diesel by Comprehensive Two-Dimensional Gas Chromatography," J. Chromatogr Sci., vol. 41, pp. 519–523, 2003.

[2]   U. Turanga, X. Ma, C. Song, "Desulphurization.," *Encycl. Chem. Process.*, vol. 10, no. 1081/E-ECHP-120007732., 2006.

[3]   K. Sertic-Bionda and M. Muzic, "Alternative Processes for Removing Organic Sulphur Compounds from Petroleum Fractions.," *Chem. Biochem. Eng. Q.*, vol. 27, pp. 101–108, 2013.

[4]   C. Song., "An overview of new approaches to deep desulphurization for ultra-clean gasoline, diesel fuel and jet fuel.," *Catal. Today*, vol. 86, pp. 211–263, 2003.

[5]   J. K. Pratibha R Gawande, "Desulphurization techniques for liquid fuel- a review. Engineering Technology," *Manag. Appl. Sci.*, vol. 2, pp. 2349–4476, 2014.

[6]   J. L. G Fierro, J. M.. Campos-Martin, M.C Capel-Sanchez, and P. Perez-Presas,

"Oxidative Processes of Desulfurization of Liquid Fuels.," *Chem. Technol. Biotechnol.*, vol. 85, pp. 879–890, 2010.

[7]   F. X. Ling, Q. X. Yao, S. J. Wang "Oxidation of dibenzothiophene in an organic biphasic system and its application to oxidative desulphurization of light oil," *Energy fuel*, vol. 15, pp. 1535–1536, 2001.

[8]   D. Antonio Chica, Avelino Corma, Marcelo E, "Catalytic oxidative desulphurization of diesel fuel on continuous fixed bed reactor," *Catalysis*, vol. 242, pp. 299–306, 2006.

[9]   J. A. Claudia Berdugo, and Leonardo Mogollo, "Biodesulphurization process evaluation with a Gordona rubropertinctus STRAIN," *Ciencia Techologia, Y Futoro*, vol. 2, 2003.

[10]   H. Sung-Keun Rhee, Je Hwan Chang, Yong Keun Chang, "Desulphurization of Dibenzothiophene and Diesel oils by newly isolated Gordona Strain, CYKS1.," *Appl. Environ. Microbiol.*, vol 64, pp. 2327–2331, 1998.

[11]   M. A. Douglas Boniek, Debora Figueredo, Antonio Fernando, Batista dos Santos, "Biodesulphurization: a mini review about the immediate search for the future technology.," *Clean Technol. Environ.*, vol. 17, pp. 29–37, 2015.

[12]   A. A. Seyed and H. R. Seyed, "A Review on Diesel Fuel Desulfurization by Adsorption Process.," *Int. Conf. Chem. Agric. Biol. Sci. (ICCABS). Turkey*, 2014.

[13]   I. A. H. Al Zubaidy, F. B. Tarsh, N. N. Darwish, B. S. S. A. Majeed, A. A. Sharafi, L. A. Chacra, "Adsorption Process of Sulfur Removal from Diesel Oil Using Sorbent Materials," *J. clean Energy Technol.*, vol. 1, pp. 66–68, 2013, doi: 10.7763/JOCET.2013.V1.16.

[14]   A S Mestre, J Pire, J. M. F Nogueira, and A. P Carvalh "Activated carbons for adsorption of Ibuprofen.," *Carbons*, vol. 45, pp. 1979–1988, 2007.

[15]   M. P. Xiong L, Chen F, Yan X, "The adsorption of dibenzothiophene using activated carbon loaded with cerium.," *Porous Mater.*, vol. 19, pp. 713–719, 2011.

[16]   C. Song, "Zeolite-based adsorbents for desulfurization of jet fuel by selective adsorption," *Fuel Chem. Div. Prepr.*, vol. 47, pp. 2–4, 2002.

[17]   M. Moradi, R. Karimzadeh, and E. Sadat, "Modified and ion exchanged clinoptilolite

for the adsorptive removal of sulfur compounds in a model fuel : New adsorbents for desulfurization," *Fuel*, vol. 217, pp. 467–477, 2018, doi: 10.1016/j.fuel.2017.12.095.

[18] P. Jeevanandam, K. J. Klabunde, and S. H. Tetzler, "Adsorption of thiophenes out of hydrocarbons using metal impregnated nanocrystalline aluminum oxide," *Microporous Mesoporous Mater.*, vol. 79, pp. 101−110, 2005, doi: 10.1016/j.micromeso.2004.10.029.

[19] Y. Shi, X. Zhang, L. Wang, and G. Liu, "MOF-Derived Porous Carbon for Adsorptive Desulfurization," vol. 60, pp. 2747–2751, 2014, doi: 10.1002/aic.

[20] T. Wang, X. Li, W. Dai, Y. Fang, and H. Huang, "Enhanced adsorption of dibenzothiophene with zinc/copper-based metal–organic frameworks," vol 3, pp. 21044–21050, 2015, doi: 10.1039/c5ta05204a.

[21] Z. Gmzi, M. Muzaic, K. Sertic-Bionda, "Kinetic and Statistical Studies of Adsorptive Desulfurization of Diesel Fuel on Commercial Activated Carbons," *Chem. Eng. Technol.*, vol. 42, pp. 355–364, 2008, doi: 10.1002/ceat.200700341.

[22] B. Shin and N. Kook, "Preparation of zeolitic adsorbents from waste coal fly ash," *Korean. J. Chem. Eng.,* vol. 12, pp. 352–357, 1995.

[23] S. Wang, L. Li, and Z. H. Zhu, "Solid-state conversion of fly ash to effective adsorbents for Cu removal from wastewater," vol. 139, pp. 254–259, 2007, doi: 10.1016/j.jhazmat.2006.06.018.

[24] Y. Wai, K. Ghyselbrecht, R. M. Santos, B. Meesschaert, and J. A. Martens, "Synthesis of zeolitic-type adsorbent material from municipal solid waste incinerator bottom ash and its application in heavy metal adsorption," *Catal. Today*, vol. 190, pp. 23–30, 2012, doi: 10.1016/j.cattod.2011.11.002.

[25] L. C. A. Oliveira, D. I. Petkowicz, A. Smaniotto, and S. B. C. Pergher, "Magnetic zeolites: a new adsorbent for removal of metallic contaminants from water," vol. 38, pp. 3699–3704, 2004, doi: 10.1016/j.watres.2004.06.008.

[26] H. C. Zhou, R. J. Kuppler, D. J. Timmons, Q. R. Fang, J. R. Li, T. A. Makal, M. D. Young, D. Yuan, D. Zhao, W. Zhuang, "Potential applications of metal-organic frame-works, Coord.," *Chem. Rev.*, vol. 253, pp. 3042–3066., 2009.

[27]   Z. Zhao, Z. Zuhra, L. Qin, Y. Zhou, L. Zhang, F. Tang, C. Mu, "Confinement of microporous MOF-74 (Ni) within mesoporous γ-Al2O3 beads for excellent ultra-deep and selective adsorptive desulfurization," *Fuel Process. Technol.*, vol. 176, pp. 276–282, 2018, doi: 10.1016/j.fuproc.2018.03.037.

[28]   M. He, J Yao, Q. Liu, K. Wang, F. Chen, H. Wang "Facile synthesis of zeolitic imidazolate framework-8 from a concentrated aqueous solution," *Microporous Mesoporous Mater*, vol. 184, pp. 55–60., 2014.

[29]   B. N. Bhadra and S. H. Jhung, "Well-dispersed Ni or MnO nanoparticles on mesoporous carbons: preparation via carbonization of bimetallic MOF-74s for highly reactive redox catalysts," *Nanoscale*, vol. 10, pp. 15035−15047, 2018, doi: 10.1039/c8nr04262d.

[30]   B. N. Bhadra, J. Y. Song, N. A. Khan, and S. H. Jhung, "TiO2-Containing Carbon Derived from a Metal-Organic Framework Composite: A Highly Active Catalyst for Oxidative Desulfurization," *ACS Appl. Mater. Interfaces*, vol. 9, pp.31192−31202, 2017, doi: 10.1021/acsami.7b10336.

[31]   G. Blanco-Brieva, J. M. Campos-Martin, S. M. Al-Zahrani, and J. L. G. Fierro, "Effectiveness of metal-organic frameworks for removal of refractory organo-sulfur compound present in liquid fuels," *Fuel*, vol 90, pp 190−197, 2011, doi: 10.1016/j.fuel.2010.08.008.

[32]   B. Arstad, H. Fjellvåg, K. O. Kongshaug, O. Swang, and R. Blom, "Amine functionalised metal organic frameworks (MOFs) as adsorbents for carbon dioxide," *Adsorption*, vol. 14, pp. 755–762, 2008, doi: 10.1007/s10450-008-9137-6.

[33]   N. A. Khan, Z. Hasan, and S. H. Jhung, "Adsorptive removal of hazardous materials using metal-organic frameworks (MOFs): a review," *J. Hazard. Mater.*, pp. 444–456, 2013.

[34]   H. X. Zhang, H. L. Huang, C. X. Li, H. Meng, Y.Z. Lu, C.L. Zhong, D.H. Liu, Q.Y. Yang, "Adsorption behavior of metal–organic frameworks for thiophenic sulfur from diesel oil," *Indonesia*, vol. 51, pp. 12449–12455, 2012.

[35]   J. H. Kim, X. Ma, A. Zhou, and C. Song, "Ultra-deep desulfurization and denitrogenation of diesel fuel by selective adsorption over three different adsorbents : A study on adsorptive selectivity and mechanism," *Catal. Today*, vol. 111, pp. 74–83,

2006, doi: 10.1016/j.cattod.2005.10.017.

[36] A. Saleh, K. O. Sulaiman, S. A. Al-hammadi, H. Dafalla, and I. Danmaliki, "Adsorptive desulfurization of thiophene, benzothiophene and dibenzothiophene over activated carbon manganese oxide nanocomposite: with column system evaluation,"*J. Clean. Prod.,* vol. 154, pp. 401−412, 2017, doi: 10.1016/j.jclepro.2017.03.169.

[37] P Gonzalez-Garcia, T A Centeno, E Urones-Carrote, D Avila-Brande, L. C. Otero-Dianz "Microstructure and surface properties of lignocellulostic-based activated carbons," *Appl. Surf. Chem.*, vol. 265, pp. 731–737, 2013.

[38] P G Gonzalez, Y. B. Pliego-Cuervo, "Physicochemical and microtextural characterization of activated carbons produced from water steam activation of three bamboo species.," *Anal. Appl. pyrolysis*, vol. 99, pp. 32—39, 2013.

[39] S. D. K. Myung Won Seo, Ga Hee Kim, Jae Goo Lee, Ha Myung Jeong, Sanf Mun Jeong, Woon Jae Lee, "Carbonization Characterizatistics of Biomass/Coal Blend for Bio-Coke.," *14th Engineering Conference international ECI Digital Achievers,* 2013.

[40] D. L. Raja, Al-Otaibi, Fusen He, Tian Yu, Mingming Hu, Ahmed Alshammari, Zhanquan Zhang, Linhua song, "Alkali-Impregnated activated carbon: Synthesis and application in Crude Oil Desulfurization.," *Energy Fuels. Am. Chem. Soc.*, vol. 29, pp. 7456–7464, 2015.

[41] H. P. Boehm., "Surface Oxides on carbon and their analysis: a critical assessment.," *Carbon.*, vol. 40, pp. 145–149, 2002.

[42] J.-N. K. Hong-Joo Jeon, Chang Hyun Ko, Sung Hyun Kim, "Removal of Refractory Sulfur Compounds in Diesel Using Activated Carbon with Controlled Porosity.," *Energy Fuel*, vol. 23, pp. 2537–2543, 2009.

[43] R. Zanzi, K. Sjöström, E. Björnbom , "Rapid high-temperature pyrolysis of biomass in a free fall reactor.," *Fuel*, vol. 75, pp. 545–550, 1996.

[44] H. Po, "Adsorption of Dibenzothiophene (DBT) on Activated Carbon from Dates ' Stones Using Phosphoric Acid," *JKAU Eng. Sci.*, vol. 22, pp. 89–105, 2011.

[45] T. A. Saleh and G. I. Danmaliki, "Influence of acidic and basic treatments of activated carbon derived from waste rubber tires on adsorptive desulfurization of thiophenes,"

Taiwan intitut Chem. Eng., vol. 60, pp. 460–468, 2016, doi: 10.1016/j.jtice.2015.11.008.

[46] M. Muzic, K. Sertic-bionda, Z. Gomzi, S. Podolski, and S. Telen, "Chemical Engineering Research and Design Study of diesel fuel desulfurization by adsorption," *Chem. Eng. Res. Des.*, vol. 88, pp. 487–495, 2009, doi: 10.1016/j.cherd.2009.08.016.

[47] A. C. Moitinho, "Production and Characterization of the Bio-Oil Obtained by the Fast Pyrolysis of Spent Coffee Grounds of the Soluble Coffee Industry," vol. 30, pp. 1608–1615, 2019.

[48] D. Bergna, T. Varila, H. Romar, and U. Lassi, "Produced in One-Stage and Two-Stage Processes," *J. Carbon Res.*, vol. 4, pp. 1–10, 2018, doi: 10.3390/c4030041.

[49] M. Fadel, N. M. Hassanein, M. M. Elshafei, A. H. Mostafa, M. A. Ahmed, and H. M. Khater, "Biosorption of manganese from groundwater by biomass of Saccharomyces cerevisiae," *HBRC J.*, vol. 13, pp. 106–113, 2017, doi: 10.1016/j.hbrcj.2014.12.006.

[50] N. Lokeshwari and K. Joshi, "Biosorption of Heavy Metal (Chromium) Using Biomass," vol. 3, pp. 29–35, 2009.

[51] V. Emmanuel, P. Themba, D. Ntuli, and A. Enakpodia, "Biosorption of hexavalent chromium from aqueous solutions by Macadamia nutshell powder," *Appl. Water Sci.*, vol. 7, pp. 3015–3030, 2017, doi: 10.1007/s13201-016-0412-5.

[52] S. Huang and G. Lin, "Biosorption of Hg (II) and Cu (II) by biomass of dried Sargassum fusiforme in aquatic solution," *J. Evironmental Heal. Scie. and Eng.,* vol. 13., pp. 6–13, 2015, doi: 10.1186/s40201-015-0180-4.

[53] Z. Kariuki, J. Kiptoo, and D. Onyancha, "Biosorption studies of lead and copper using rogers mushroom biomass 'Lepiota hystrix,'" *South African J. Chem. Eng.*,vol. 23, pp. 62−70, 2017, doi: 10.1016/j.sajce.2017.02.001.

[54] F. Chigondo, B. C. Nyamunda, S. C. Sithole, and L. Gwatidzo, "Removal of lead (II) and copper (II) ions from aqueous solution by baobab (Adononsia digitata) fruit shells biomass," vol. 5, pp. 43–50, 2013.

[55] M. Moyo, U. Guyo, G. Mawenyiyo, N. P. Zinyama, and B. C. Nyamunda, "Marula seed husk (Sclerocarya birrea) biomass as a low cost biosorbent for removal of Pb (II) and Cu (II) from aqueous solutions," *J. Ind. Eng. Chem.*, vol. 27, pp. 126–132, 2014, doi:

10.1016/j.jiec.2014.12.026.

[56] E. El-naggar, R. A. Hamouda, I. E. Mousa, M. S. Abdel-hamid, and N. H. Rabei, "Biosorption optimization, characterization, immobilization and application of Gelidium amansii biomass for complete Pb 2 + removal from aqueous solutions," *Sci. Rep.*, vol. 18, pp. 1–19, 2018, doi: 10.1038/s41598-018-31660-7.

[57] M. K. Dahri, M. Raziq, R. Kooh, and L. B. L. Lim, "Water remediation using low cost adsorbent walnut shell for removal of malachite green : Equilibrium , kinetics , thermodynamic and regeneration studies," *Biochem. Pharmacol.*, vol. 2, pp. 1434–1444, 2014, doi: 10.1016/j.jece.2014.07.008.

[58] E. Guechi and O. Hamdaoui, "Sorption of malachite green from aqueous solution by potato peel: Kinetics and equilibrium modeling using non-linear analysis method," *Arab. J. Chem.*, vol. 9, pp. S416–S424, 2016, doi: 10.1016/j.arabjc.2011.05.011.

[59] B. E. Zanzi R, Sjostrom K, "Rapid pyrolysis of agricultural residues at high temperatures," *Biomass Bioenergy.*, vol. 23, pp. 357−366, 2002.

[60] X. fei Tan, S. Liu, Y. Liu, Y. Gu, G. Zeng, X. Hu, X. Wang, S. Liu, L. Jiang, "Biochar as potential sustainable precursors for activated carbon production: Multiple applications in environmental protection and energy storage," *Bioresource Technology*, vol. 227, pp. 359–372, 2017, doi: 10.1016/j.biortech.2016.12.083.

[61] A. M. Abioye and F. N. Ani, "The Characteristics of Oil Palm Shell Biochar and Activated Carbon Produced via Microwave Heating," *Appl. Mech. Mater.*, vol. 695, pp. 12–15, 2014, doi: 10.4028/www.scientific.net/AMM.695.12.

[62] J. Lehmann and S. Joseph, *Biochar for Environmental Management*. 2014.

[63] Z. Ahmad,B. Gao, A. Mosa, H. Yu, X. Yin, A. Bashir, H. Ghoveisi, S. Wang, "Removal of Cu (II), Cd (II) and Pb (II) ions from aqueous solutions by biochars derived from potassium-rich biomass," *J. Clean. Prod.*, vol. 180, pp. 437–449, 2018, doi: 10.1016/j.jclepro.2018.01.133.

[64] H. N. Tran, S. You, and H. Chao, "Effect of pyrolysis temperatures and times on the adsorption of cadmium onto orange peel derived biochar," *Waste Manag. Reseach*, vol. 34, no. 2, pp. 129–138, 2016, doi: 10.1177/0734242X15615698.

[65]   C. Ma, H. Huang, X.Gao, T. Wang, Z. Zhu, P. Huo,Y. Liu,Y. Yan, "Honeycomb tubular biochar from fargesia leaves as an effective adsorbent for tetracyclines pollutants," *J. Taiwan Inst. Chem. Eng.*, vol. 91, pp. 299–308, 2018, doi: 10.1016/j.jtice.2018.05.032.

[66]   D. D. Sewu, P. Boakye, and S. H. Woo, "Highly efficient adsorption of cationic dye by biochar produced with Korean cabbage waste," *Bioresour. Technol.*, vol. 224, pp. 206–213, 2017, doi: 10.1016/j.biortech.2016.11.009.

[67]   L. Suárez-Hernández, A. N. Ardila-A, R. Barrera-zapata, "Morphological and physicochemical characterization of biochar produced by gasification of selected forestry species Caracterización morfológica y fisico-química de biocarbones producidos," *Rev. Foculted Lingeneiertia*, vol. 26, pp. 123–130, 2017.

[68]   Y. Sun, B Gau, Y. Yao, J. Fang, M. Zhang, Y. Zhou, H. Chen, L. Yang., "Effects of feedstock type, production method, and pyrolysis temperature on biochar and hydrochar properties," *Chem. Eng. J.*, vol. 240, pp. 574−578, 2014, doi: 10.1016/j.cej.2013.10.081.

[69]   B. Chen, Z. Chen, and S. Lv, "A novel magnetic biochar efficiently sorbs organic pollutants and phosphate," *Bioresour. Technol.*, vol. 102, pp. 716–723, 2011, doi: 10.1016/j.biortech.2010.08.067.

[70]   E. Yang, C. Yao, Y. Liu, C. Zhang, L. Jia, D. Li, Z. Fu, D. Sun, S. R. Kirk, D. Yin., "Bamboo-derived porous biochar for efficient adsorption removal of dibenzothiophene from model fuel," *Fuel*, vol. 211, pp. 121–129, 2018, doi: 10.1016/j.fuel.2017.07.099.

Chapter 3

Materials and Methodology

3.1 Introduction

There may be a degree of repetition of the methodology in this study. This is because the other chapters were written as papers in preparation for publication. Therefore, this chapter summarizes only the experimental method. For safety precautions, the Material Safety Data Sheet (MSDS) was followed where necessary. Moreover, personal protective equipment (PPE) such as googles, lab coats, latex gloves and closed shoes were worn at all times during all the experiments conducted in this study.

Adsorptive desulphurization (ADS) experiments involve mainly an adsorbent (solid material), an adsorbate (a contaminant material in a solution or a solute in a solvent) and a reactor. The adsorption process is usually carried out in a column or a batch adsorption system. However, the latter was used in this study because it does not require a lot of space for laboratory experiments yet it can still achieve all the variables of the adsorption experiments in which we were interested [1]. The ADS efficiency depends on various parameters: adsorbent type, PH of the adsorbent, particle size of the adsorbent, adsorbent quantity, adsorption temperature and concentration of the analyte. However, some of these parameters have been fixed in the literature and in our previous studies (and in Appendix D), for which extensive laboratory experiments were carried out using commercial adsorbent (Com-AC) as our standard reference material (SRM). Therefore, all the desulphurization experiments were eventually conducted at room temperature.

The experimental design also involved the calibration method and the analysis of clean and dirty diesel fuel using chromatographic techniques for both qualitative and quantitative analysis. This is because gas chromatography (GC), when coupled with a pulse flame photometric detector, is sensitive to the analysis of sulphur compounds in petroleum steams up to a level of parts per billion (ppb) [2],[3]. The experimental procedure for either unprocessed Amarula wastes biomass or the synthesis of activated carbons from biomass wastes for the desulphurization of diesel fuel is also discussed. Furthermore, the layout for the use of different

activating agents in the activation of gasification biochar from different reactors is elaborated on for their performance in desulphurizing diesel fuel. The particle size distribution experiment for processed materials is also detailed. The characterization techniques were applied to the qualitative analysis of adsorbents before and after use. Finally, the process for recycling the spent adsorbent and the removed toxic organo-sulphur compound in model diesel fuel is also considered. The hazards associated with this project are also summarized.

3.2 Analysis of Diesel Fuel

3.2.1 Materials

3.2.1.1 Gases

All the gases used were 99.99 % pure hydrogen, oxygen, nitrogen, and helium obtained from Afrox South Africa (SA).

3.2.1.2 Equipment

The equipment used comprised of an Agilent Gas chromatography instrument, IO Analytical PFPD, 1 microlitre syringe, an analytical balance, PPE and MSDS. All the GC consumables were obtained from Agilent.

3.2.1.3 Chemicals and reagents

The reagents were 99.99 % pure dibenzothiophene, hexadecane and toluene purchased from Aldrich Sigma. They were used without any dilution or processing.

3.2.2 Methodology

3.2.2.1 GC analysis

Diesel fuel was analysed for the content of sulphur compounds using the Agilent 7890B GC system. The GC was coupled with OI Analytical 5480 pulse flame photometric detector (PFPD) [2]. Fig. 3.1 is a schematic diagram of the GC-PFPD technique. The fact that diesel fuel also contains competitive hydrocarbons, two DB-1 columns (with specifications in Table 3.1) were therefore used for separating, identifying, and quantifying these compounds to their respective detectors. A flame ionisation detector (FID) inside a GC was used to detect the

hydrocarbons at the temperature of 250 °C, whereas the dibenzothiophene sulphur compounds were detected at 300 °C using a sulphur detector. These set detector temperatures were also suitable in avoiding the tailing of the peaks.
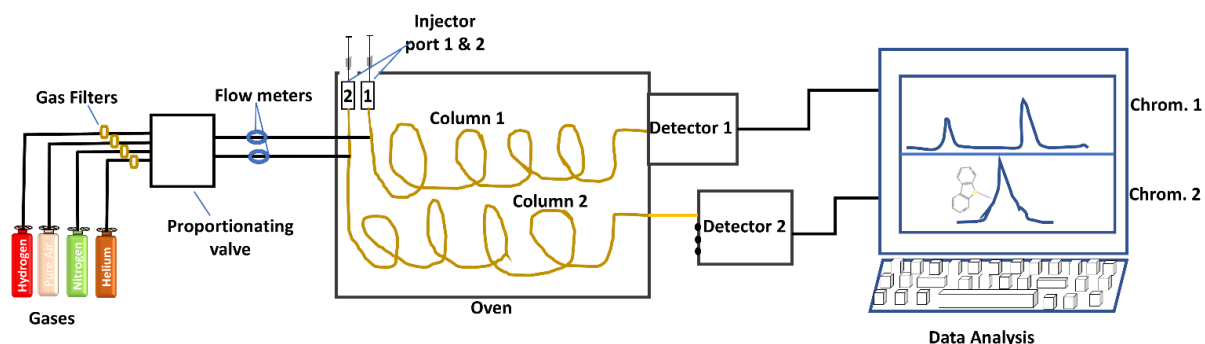
Fig. 3.1. Schematic diagram of GC-PFPD. Chrom. 1 & 2 are chromatographs of hydrocarbons and sulphur compounds, respectively.

Manual injection was used to introduce the sample into the GC using 1 microlitre syringe. The split mode was used for analysis of the analyte. Helium was used as a carrier gas to transport the diesel fuel from the inlet to the column then to the detector at a flow rate of 0.49472 ml/min. A mixture of hydrogen/air gas was used as a fuel for the decomposition of compounds. Nitrogen was used as a make-up gas for high sensitivity in the detectors. The oven temperature was set at 250 °C for a better resolution of the analytes.

The temperature programme (TP) in GC, known as TPGC, is one of the imperative techniques which involves programming the column temperature. Programming the temperature may either be continuous or step by step. The hydrocarbons and organo-sulphur compounds have similar structures; therefore, their separation may be problematic. To overcome this, the gradient temperature programme was used in this study in order to obtain high resolution in a reasonable analysis time. Table 3.2 shows the ramping rates of TPGC for the analysis of diesel fuel.

Table 3.1 Operating conditions for analysis of model diesel fuel using gas chromatography

Parameter	Specifications/Conditions		
GC type	Agilent 7890B GC system		
Sample size	1μl		
Injection	Slit/splitless inlet		
	Split mode		
	Split ratio: 50:1		
	Liner: 4 mm split liner		
Combustion Chamber	3 mm ID		
Column			
DB - 1 Column	Size: 30 m Lenghth, 0.25 mm Diameter, 1.00 μm Film		
	Temperature limit: -60°C - 350°C		
Oven Temperature	250 ^{0}C		
Detectors			
FID	Hydrocarbons attenuation 250 ^{0}C		
PFPD	Model: 5480	Sulphur attenuation 300 ^{0}C	
Detector range	FID: 0.1-10^{4} ppm	PFPD: 10^{7} ppb	
Gases			
		FID	**PFPD**
Carier gas	Helium (He$_2$)	0.49472 ml/min	0.49472 ml/min
Make up gas	Nitrogen (N$_2$)	25.0 ml/min	14.3 ml/min
Fuel gas (H$_2$/Air)	Hydrogen (H$_2$)	30.0 ml/min	11.2 ml/min
	Air	300.0 ml/min	20.0 ml/min

The Win Pulse is PFPD software. It stores all the pulsed flame emission traces for post-run reviewing and reprocessing [4]. It was also used for intergraded gate for each data channel for the high selectivity of sulphur compounds in PFPD [5]. The chromatograms which showed eluted peaks that represented dibenzothiophene and hydrocarbons at a specific retention time and specific area were obtained using Chemetrix Chem-Station software. The area of the dibenzothiophene peak was used to analyse the concentration of sulphur content in diesel fuel.

3.2.2.2 Calibration of the analysis method

Prior to diesel fuel analysis, the calibration of the analysis method was carried out using both internal standard and external standard [2],[3],[6]. However, external standard was found to produce accurate results for the manual injection and so it was used for the entire project.

Standards of dibenzothiophene with different concentrations of 100, 50, 25, 10 and 5 ppmw for sulphur content were accurately prepared in 5 ml volumetric flasks. The 85 % hexadecane and 15 % toluene were used as solvents. The 1 µl of each sulphur standard was injected into the injection port of the GC and analyzed under the conditions in Tables 3.1 and 3.2. The chromatogram was obtained and used to determine the calibration curve using external standard methods.

Table 3.2 Gradient temperature programme in gas chromatography-PFPD

Gradient TPGC				
		Temperature	Rate	Holding time
	Initial temp	50 ^{0}C	0	0.5 min
Column 1	ramp 1	300 ^{0}C	20 ^{0}C/min	7 min
	ramp 2	300 ^{0}C	20 ^{0}C/min	5 min
	post run	50 ^{0}C	-	-
	Initial temp	50 ^{o}C	0	0.5 min
Column 2	ramp 1	300 ^{0}C	20 ^{0}C/min	7 min
	ramp 2	300 ^{o}C	20 ^{0}C/min	5 min
	post run	50 ^{0}C	-	-

3.2.2.3 Adsorptive desulphurization of diesel fuel

The fresh 100 ppmw model diesel fuel of dibenzothiophene was prepared using the similar approach as those of the standards in 3.2.2.2 above. Its actual concentration was analyzed in a GC-PFPD and then used as an adsorbate on Amarula wastes adsorbents. The adsorptive desulphurization experiments were carried out using a batch reactor at room temperature, as shown in the Fig. 3.2 set-up. This experimental design is described in detail in chapters 4–6. The used model diesel fuel was centrifuged and analyzed in a GC-PFPD, as explained in 3.2.2.1 above. This was done to determine how much sulphur content in DBT model diesel was reduced by processed or unprocessed adsorbents.
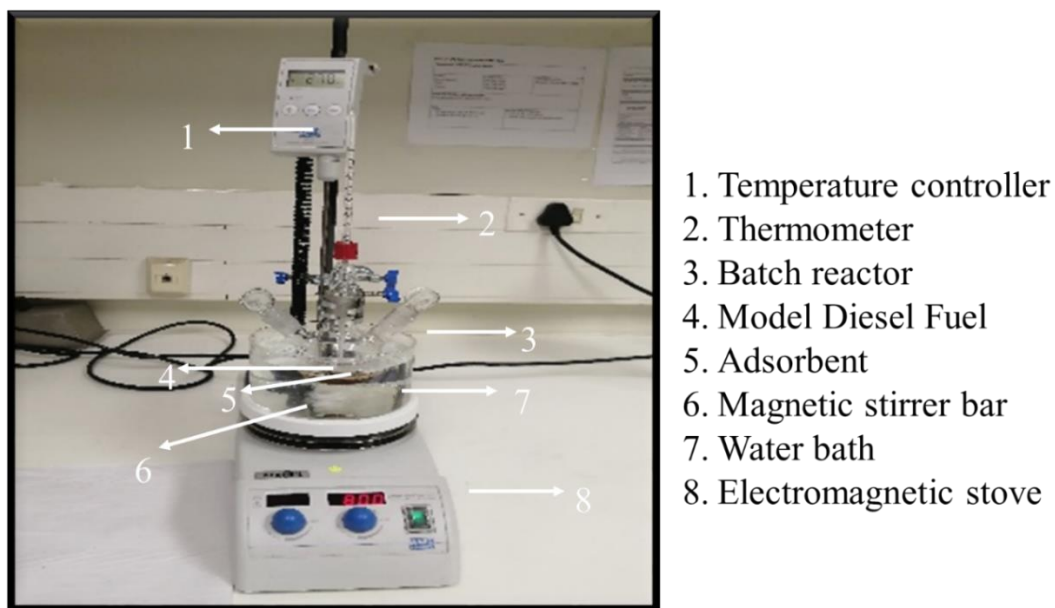
Fig. 3.2. Batch adsorptive desulphurization set-up

3.3 Adsorbent preparation and synthesis

3.3.1 Materials

3.3.1.1 Gases

The 99.99 % nitrogen gas was obtained from Afrox SA and steam from distilled water was used during the thermal processes.

3.3.1.2 Equipment

PPE and MSDS, horizontal tube furnace, quartz tube, quartz boat, analytical balances, sieves, glassware, heat-resistant utensils, tongs, and gloves.

3.3.1.3 Chemical and reagents

The potassium hydroxide (KOH) pellets of 99.99 % purity obtained from Aldrich Sigma were used to prepare a solution of 48 % (m/v) with distilled water.

3.3.2 Methodology

3.3.2.1 Unprocessed Amarula wastes biomass

The Amarula wastes biomass was divided into Amarula fruit wastes, Amarula seeds wastes and Amarula shell wastes. Each Amarula waste was dried first and then used to reduce the sulphur content in dibenzothiophene model diesel fuel, as described in the next chapter at 4.2.4.3. The adsorption process was carried out using the batch reactor shown in Fig. 3.2.
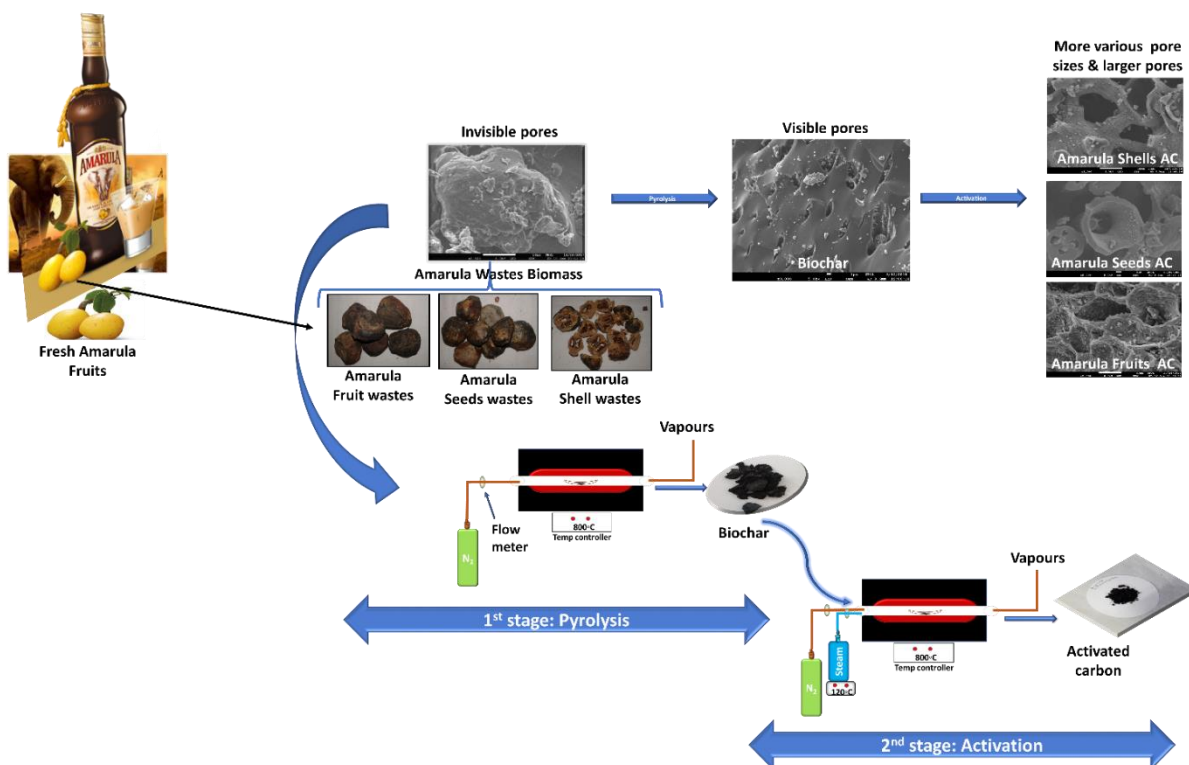
Fig. 3.3. A two-stage experimental design for processing Amarula wastes biomass, and the porous structure of the products

3.3.2.2 Processing of Amarula wastes biomass

The Amarula wastes biomass was thermally processed to activated carbon using steam activation via pyrolysis, as shown in the first and second stages of Fig. 3.3. A horizontal tube furnace that had a maximum specification temperature of 1000 °C was used with a quartz tube as a reactor to obtain both intermediate (biochar) and final (activated carbon) products. This process synthesis was carried out at a higher temperature under nitrogen flow using the conditions described in chapter 5.2.2. The steam residence time was fluctuated for producing the Amarula shells AC while keeping other conditions constant. The processed Amarula wastes

to activated carbons with particle size of about 1–2 mm was then used for desulphurizing diesel fuel using the batch reactor shown in Fig. 3.2 above.

3.3.2.3 Determination of particle size distribution (PSD)

Analyzing particle size is important because it affects the flow characterization and the adsorption kinetics of activate carbon [7]. Therefore, PSD was carried out on processed Amarula wastes biomass. The distribution of the different particle size of activated carbons is necessary in engineering the properties of the adsorbent. For this reason, the powdered and the granular activated carbon were separated, as described in ASTM D 2652 [8].

Fig. 3.4. A picture of the sieve analysis

As a consequence, a manual sieve analysis method was used in this study because it is cheaper, and it requires no energy consumption. In addition, it offers a wide particle size range. The produced Amarula wastes activated carbon was massed on an analytical balance and its mass (m_{AC}) was recorded. Three sets of sieve mashes and a collector pan were used for horizontally sieving, as shown in Fig. 3.4. The clean empty sieve meshes of size 1200 µm, 300 µm, 200 µm and a collecting pan were arranged in ascending order and their masses (m_1) were noted. The massed activated carbon was poured onto the top sieve mesh and manually shaken for 5 min. Each sieve mesh containing activated carbon was then massed (m_2) and recorded after shaking. The retained mass of AC in a sieve mesh was recorded by subtracting m_1 from m_2. The percentage retained passing was calculated using Equations 3.3 and 3.4 (see below). A plot of the semi-logarithm of particle size vs particle finer (quantity passing) was obtained. The particle-size distribution for each of the processed Amarula wastes was determined from the distribution curve.

$$\text{Mass retained } (m_3) = m_1 - m_2 \qquad \qquad \textbf{Eq. 3.1}$$

$$\text{Quantity passing (Q.P)} = \text{total mass} - \text{mass retained} \qquad \textbf{Eq. 3.2}$$

$$\% \text{ mass retained} = m_3/m_{AC} * 100\% \qquad \qquad \textbf{Eq. 3.3}$$

$$\% \text{ passing} = 100 - \text{percentage mass retained} \qquad \qquad \textbf{Eq. 3.4}$$

3.3.2.4 Gasification biochar

Amarula shells biochar (an intermediate product) was selected and compared with gasification biochar (Fig. 3.5) which was obtained as a waste product form syngas production in our research institute (IDEAS). They were applied to the desulphurization of diesel fuel and their performance efficiency was compared. They were then processed to ACs using different activating agents of steam and 48 % m/v KOH. The processed gasification chars were also applied to the reduction of sulphur in DBT model diesel fuel. The experimental methods are detailed in Chapter 6 section 6.2.2.1 for the steam agent and section 6.2.2.2 for the KOH agent.
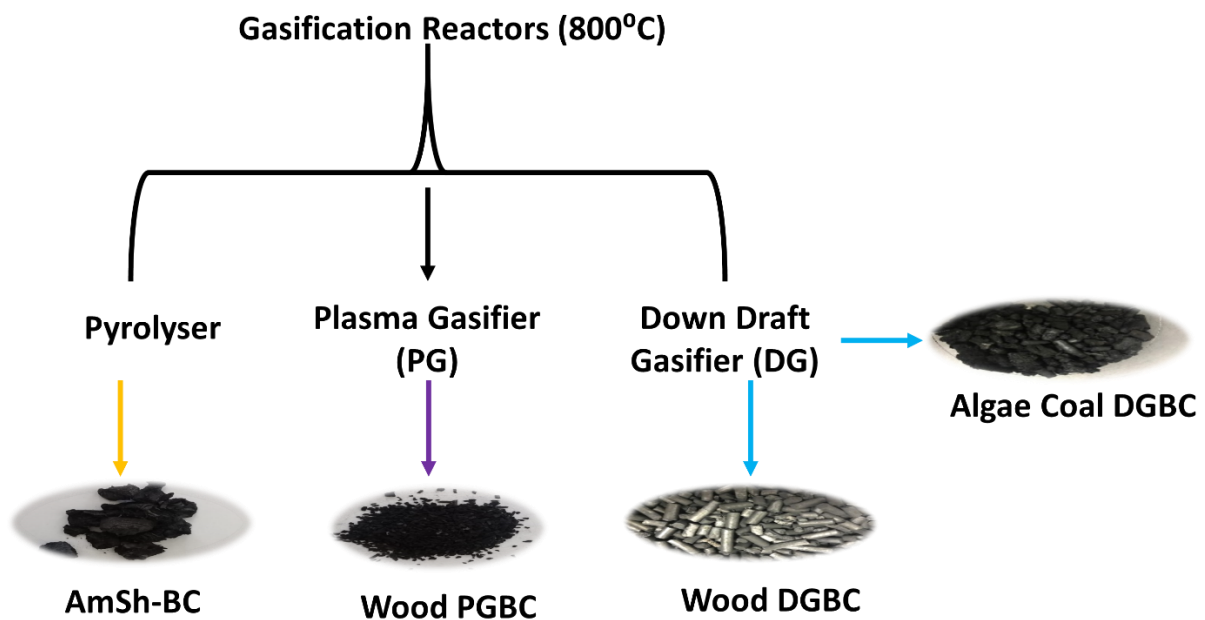
Fig. 3.5. Biochar (BC) from different gasification reactors at 800 °C

3.4 Characterization of adsorbents

The characterization of both processed and unprocessed adsorbents was carried out before and after use in order to determine the thermal, structural, and surface properties of the adsorbents. Techniques such as proximate and thermal analysis, FTIR, XRD, BET, FESEM-EDX and TEM analysis were used in this research. These techniques are elaborated on in depth in chapters 4–6.

3.5 Recycling process

"No waste is waste." With this message in mind, the recycling of spent adsorbents and adsorbate shown in Fig. 3.6 was carried out to further mitigate land pollution. Therefore, the used adsorbents were kept in tightly labelled containers for the regeneration process and for further studies. The diesel fuel waste was stored in tight bottles for the recycling of harmful organo-sulphur compounds to an elemental sulphur substance.

A distillation process will be used to separate sulphur compounds from hydrocarbons in diesel fuel wastes. The obtained residue is the powdered elemental sulphur. After purification, the powdered sulphur will be used as a fertilizer for soil amendment or as an ointment to treat different skin problems such as acne. Another possible use is the manufacture of fire-lighter matches.
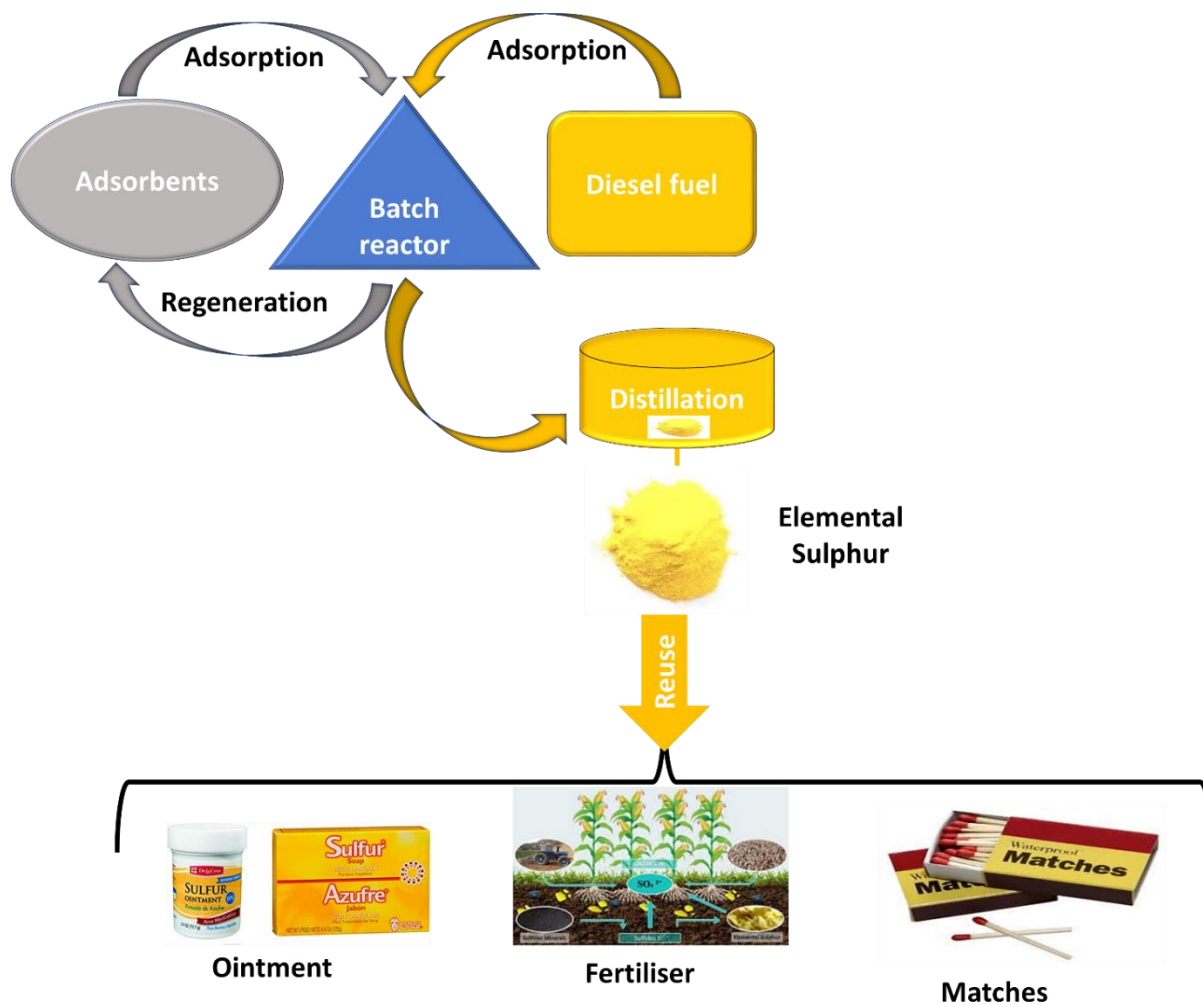
Fig. 3.6. Schematic diagram of the recycling of adsorbents and toxic organ-sulphur compounds

3.6 Hazards and safety precautions

The fumes of the highly concentrated refractory sulphur compounds in diesel fuel may affect respiratory systems. Therefore, to minimize this hazard, an air respiratory mask with an organic chemical filter was used when analyzing the commercial diesel fuel. However, most of the experiments executed in ADS were performed on model diesel fuel, which is less hazardous, with a lower concentration of organo-sulphur compounds. Therefore, the PPE and the MSDS were followed at all times when handling chemicals. Furthermore, KOH is a basic corrosive chemical which has choking fumes and may corrode the skin. Therefore, similar safety precautions including wearing particulate masks, were practised with extra care.

Meanwhile, very high temperatures were experienced during the pyrolysis and activation processes. This presented the likelihood of skin burns and fire hazards. To avoid this, heat-resistant gloves and utensil tongs were used at all times.

Besides that, the thermal processing of biomass is known to produce NOx and COx gases which diffuse into the atmosphere. These gases may cause headaches and affect the lungs when they are inhaled in high concentrations. However, in this study, the raw materials used in each process were ≈ 5 g, which produced low concentrations of gases that enter the atmosphere resulting in minimal hazards. Nevertheless, it is planned to capture these gases and re-use them for syngas production in IDEAS when they are produced in large quantities during scaling up in our next pilot project. This will then minimize the environmental hazards.

3.7 References

[1]   T. Wang, M. Li, and S. Teng, "Bridging the gap between batch and column experiments : A case study of Cs adsorption on granite," *Harzadeous Mater.*, vol. 161, pp. 409–415, 2009, doi: 10.1016/j.jhazmat.2008.03.112.

[2]   D. D. Link, J. P. Baltrus, K. S. Rothenberger, and R. C. Striebich, "Rapid Determination of Total Sulfur in Fuels Using Gas Chromatography with Atomic Emission Detection," *J. Chromatogr.*, vol. 40, pp. 500–504, 2002.

[3]   O. I. Analytical: Application Note. 17630302, "Determination of Total Sulfur Content in Petrochemical Samples Using a Pulsed Flame Photometric Detector (PFPD)," 2002.

[4]   A. G. and G. F. Aviv Amirav, Hongwu Jing, Eitan Atar, Sergey Cheskis, Nitzan Tzanani, "Pulsed Flame Photometric Detector (PFPD) for Gas Chromatography," *https://www.tau.ac.il/chemistry/amirav/pfpd.html*, 2015.

[5]   O. I. Analytical: Application Note 40030214, "Detection of Low-Level Sulfur Compounds in Spearmint Oil Using the Pulsed Flame Photometric Detector (PFPD)," 2014.

[6]   L. Chambers, "ASTM Methods for Sulphur Analysis in Petrochemicals using a Pulsed Flame Photometric Detector (PFPD)," 2009.

[7]   T. Brief, "Particle Size Distribution and its Measurement," *Particle Sciences: Drug Development Services*, vol. 2, 2009.

[8]   "ASTM D2652-05, Standard Terminology Relating to Activated Carbon," *ASTM Int. West Conshohocken, PA,* www.astm.org, 2005.

Chapter 4

Adsorption of Dibenzothiophene in Model Diesel Fuel by Amarula Wastes Biomass as a Low-Cost Adsorbent.

Chapter abstract

Adsorption is an excellent technique used worldwide for purification processes, particularly for the protection of the environment. The effectiveness of the adsorption process is determined by the adsorbent type used, but some adsorbents require lots of processing to achieve the desired quality and this has become a drawback both economically and environmentally. This study focused on mitigating the issue of waste management and land pollution by using the amarula waste biomass, which is a low-cost adsorbent that is obtained from the industrial waste by-product, during the production of Amarula liqueur. The amarula waste biomass was divided into three parts: amarula fruit waste, amarula seed waste, and amarula shell waste. Each waste was used to reduce the sulphur content in dibenzothiophene (DBT) model diesel using a batch reactor for 180 min at 25 °C ±2 °C. The amarula shell waste was found to have a higher adsorption efficiency of 30 ±3 % as compared to the amarula seed waste and the amarula fruit waste, which had an adsorption efficiency of 19 ±5 % and 9,5 ±0.7 %, respectively. The effect of the adsorption temperature was determined at 20 °C–55 °C. It was found that the amarula wastes biomass performed better at lower temperatures. The effect of biomass quantity was performed at room temperature using amarula shell waste biomass. The adsorption capacity was found to decrease with an increase in the quantity of the biomass. Both the kinetic models and the adsorption isotherms were applied to the experimental data. Thermodynamic parameters were also studied to determine the spontaneity of the adsorption process. The characterization of both the fresh and the used amarula waste biomass was analyzed using proximate analysis, FTIR, FESEM-EDS, BET and TGA. It was then concluded that cellulose and hemicellulose structures in amarula waste biomass played a major role in reducing the content of dibenzothiophene in model diesel fuel.

4.1 Introduction

Organo-sulphur compounds such as dibenzothiophene and their alkyl derivatives are present in high concentrations in the distillates of crude oil. These are among the major pollutants of the environment. These toxic refractory compounds have been found to cause indirectly greenhouse gases that affect climate change negatively when such gases are emitted into the atmosphere [1]. Furthermore, they shorten the lifespan of catalytic converters through corrosion and cause health hazards in human beings. One of the simpler techniques to have been used to reduce the concentration of organo-sulphur is an adsorption technique in which the molecules are adhered onto the surface of the other molecule by physisorption or chemisorption. This technique is mostly employed worldwide for separations and purification processes, mainly during the treatment of water or in the petrochemical industries [2]–[11],[12],[13]. Despite that, the effectiveness of the adsorption process depends on the adsorbent type with characteristics such as abrasion, surface morphology, porosity, thermal stability, and adsorption capacity. Hence, industrially, these adsorbents have been classified as polymer-based compounds such as polystyrene sulphonate or poly(allyldimethylammoniumchloride), oxygen-containing compounds such as silica or zeolites, carbonaceous compounds (activated carbon or graphene) and metal-based adsorbents (metal organic framework or metal-metal oxides) which are mainly synthesized for the purposes of catalysis.

Nevertheless, processes such as the adsorptive desulphurization (ADS) of diesel fuel have used these adsorbents on several occasions and obtained high levels of efficiency [2],[6],[8],[9],[14]. However, these adsorbents require major processing before they can achieve the desired degree of adsorption efficiency. Hence, there has been a need to make use of low-cost adsorbent and save non-renewable resources to overcome climate change and thus save planet Earth. Therefore, this study focused on biomass, which is a biological material obtained from living plant matter. It was used as a sorbent because it is an inexpensive renewable resource. The use of biomass over the above adsorbents is more beneficial because less or no energy is required to produce it. Moreover, there is no need for regeneration processes of the adsorbent because it is renewable and found in abundance around the world. It can be used fresh or as waste, which makes it more sustainable and environmentally friendly. The only limitation of biomass

is that it may be seasonal, but this may be overcome by stocking more of it and storing it for further use. Several researchers [4],[5],[10],[12],[13],[15], have used biomass as a sorbent for the treatment of water and obtained high performance, but there is little or no documented research on biomass adsorbent for the treatment of diesel fuel. Biomass is categorized into lignocellulose biomass (wood), plant biomass (grass) and agricultural biomass such as agro-forest waste, which is the interest of this study. The enthusiasm for using waste biomass derives from overcoming the global waste-management problem and land pollution due to a fast-growing population.

Biomass from Africa has received little attention in research hence this study is on an aggro-forest biomass obtained from marula trees which are known scientifically as *Sclerocarya birrea*. The marula tree is a giant tree of about 9–18 m tall [16]. It is found in almost every part of Africa, but mostly in the southern regions such as South Africa, Botswana, and Zimbabwe. The tree is also known as the "elephant tree" because it was found that every time elephants ate marula fruits they would get drunk. When ripe, this fruit is yellow and falls from the tree. It consists of an edible pulp, the seed which contains the edible nut and the shells when the nut is removed. These nuts have been used mostly to produce marula oil, whereas the marula fruit is used to produce a worldwide spirit known as Amarula liqueur. During the production of Amarula liqueur, the large amount of waste is discarded from the plant to the landfill, and therefore cause the waste problem on the land, resulting in environmental pollution. This amarula waste consist of fruits of low quality and seeds from the plant of Amarula liqueur, hence this waste biomass is utilized in this study.

Dibenzothiophene is widely used as a model to represent refractory sulphur compounds. Moreover, compared to its derivatives, it is the most difficult organo-sulphur molecule to be reduced in diesel fuel [17]. Therefore, this study investigated whether this amarula waste biomass could be used to adsorb DBT and thus mitigate the issue of waste management. Furthermore, it aims to determine which part of the amarula waste (fruit, seed, and shell waste) is capable of high adsorption capacity in this organo-sulphur removal in diesel fuel.

Despite the massive characterization of biomass [18]–[20], it was found that there is less investigation of the amarula waste biomass. Researchers [4] used amarula seed husks to remove lead in water, but there was little or no characterization in that research. Therefore, this study further focused in-depth on the characterization of the amarula waste biomass before and after adsorption.

4.2 Materials and methodology

4.2.1 Materials

Amarula waste biomass comprised: amarula fruit (AmWa) waste, amarula seed (AmSe) waste, amarula shell (AmSh) waste. The chemicals (99 % pure reagents from sigma) involved, include: dibenzothiophene (DBT), hexadecane and toluene.

4.2.2 Sampling of biomass

Amarula waste was used as the biomass of Africa and were collected from the landfill of a plant that produced Amarula liqueur at Phalaborwa in Limpopo province. The amarula waste was divided into three parts; each part was used to reduce the sulphur content in model diesel fuel.

4.2.3 Characterization methodology

4.2.3.1 Proximate and thermal analysis

For proximate analysis, the ASTM (the American Society for testing and materials) standards [21] was followed. Thermal Gravimetry Analysis (TGA) and Derivative Thermogravimetry (DTG) were carried out under air and nitrogen atmosphere at a flowrate of 60 ml/min using the TGA5500-0026 model. The process was ramped at the heating rate of 10 ℃/min to 800 ℃. Platinum HT pans were used as sample-holders.

4.2.3.2 FESEM–EDX technique

Microscopic analysis was carried out using Field Emission – Scanning Electron Microscopy (FESEM), JEOL model JSM-7800F. It was coupled with energy-dispersive X-ray spectroscopy (EDS), at which prior analysis the samples were coated with gold using a gold-sputtering device.

4.2.3.3 TEM analysis technique

Prior to analysis, the selected AmSh waste biomass was dispersed in a methanol solution and then sonicated for 15 min. A drop of the suspended aqueous solution of the sample was placed on a copper grid. This was then subjected to transmission electron microscopy (TEM) analysis

using a JEOL 2010F model, equipped with a Schottky field-emission gun operated at keV with an ultra-high-resolution pole piece providing a point resolution of 1,9 Å.

4.2.3.4 Surface chemistry analysis

Fourier transform infrared (FTIR) spectroscopy was carried out to determine the functional groups present in the materials using the Perkier Elmer Frontier model. The surface chemistry analysis was done at a resolution of 8 cm^{-1} and 16 cm^{-1} scans, for which the wavelength was set at 4 000 cm^{-1}–400 cm^{-1}.

4.2.3.5 Powder X-ray diffraction analysis

To determine the crystallinity or amorphous nature of carbons for raw amarula waste, the X-ray patterns were determined by Bruker's D2 Phaser X-ray diffractometer using a Cu-Kα (= 0.15406 Å) radiation source operating under a voltage of 40 kV and a current of 25 mA. The diffraction angle (2θ) was varied from 10º to 90º using a scan rate of 4,2 ºC/min. The lattice size (L) was further determined using Scherrer Equation 4.1:

$$\beta = Ky/LCos\theta \qquad \textbf{Eq. 4.1}$$

where K is constant, ý is the wavelength, β is the full width at half-maximum (FHMW), and θ is the angle of the observed peak [22]. The Crystalline Index CI % was calculated using Equation 4.2, whereby L_{ac} is a lattice size of amorphous carbon and L_{cc} is a lattice size of crystalline carbon [23]:

$$L_{ac}/(L_{ac} + L_{cc})*100 \qquad \textbf{Eq. 4.2}$$

4.2.3.6 Textural properties

Brunauer-Emmett-Teller (BET) surface area and porosity were carried out using Micrometrics TriStar II 3020 under nitrogen adsorption at –196 °C at the range of relative pressure (p/p^o) of 10^{-6}, at which the samples were first degassed for 12 h at 160 °C under inert flow gas. The samples were carried out for BET analysis and a full adsorption isotherm. Micropores and mesopores were determined as a function of pore size using the Barrett-Joyner-Halenda (BJH) method.

4.2.4 Application methodology

4.2.4.1 Preparation of ≈100 ppm model diesel (DBT)

An amount of 1 000 ml of solvent 85 % hexadecane and 15 % toluene was prepared by measuring and weighing 850 ml hexadecane in a 1 L measuring cylinder and 150 ml of toluene. The mixture was then transferred into a tightly closed, labelled bottle. The 250 ml of solvent was measured in another bottle and its mass recorded. The calculated DBT salt was massed into the clean vial and then dissolved in the 250 ml solvent to make model diesel of DBT. The solution mixture was left to dissolve properly overnight. The actual concentration of model diesel (DBT) was calculated and analysed using a gas chromatography (GC) – pulse flame photometric detector (PFPD).

4.2.4.2 Instrument and calibration method

A GC calibrant sample was used to determine the performance of the GC-PFPD instrument. Then method calibration was carried out using both an internal and an external standardization method. Concentrations of 10, 25, 50 and 100 ppmw were prepared from a stock solution of DBT standard using the internal and the external standard methods of calibration. However, the latter was used in this research.
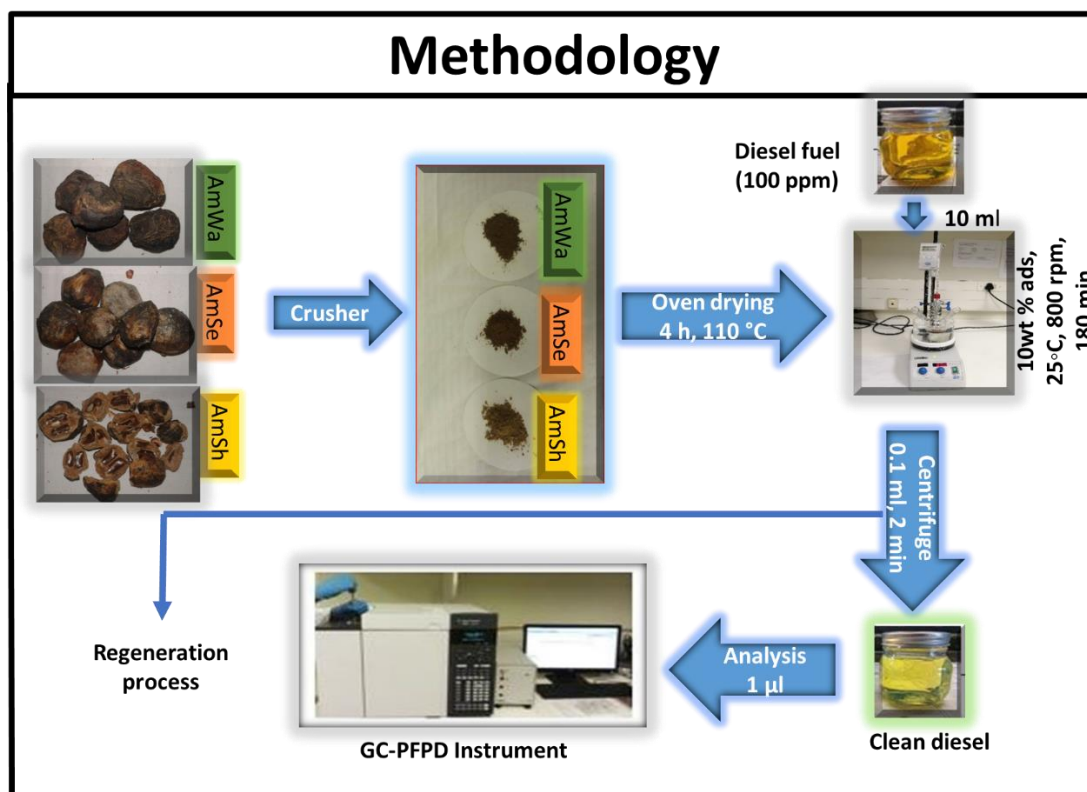
Fig. 4.1. Adsorption desulphurization of DBT model diesel fuel by amarula waste biomass

4.2.4.3 Adsorption of [S] in DBT model diesel fuel

The amarula waste biomass was crushed into powder as shown in Fig. 4.1. The powdered biomass waste was then dried in an oven-dry at 110 ^{0}C for 4 h. The dried biomass adsorbents were then weighed in a 50 ml round-bottomed flask using an analytical balance and its mass recorded. Then 10 ml of model diesel (DBT) was massed into the flask containing the dried biomass. The reactor (flask) was immersed inside a water bath at 25 ^{0}C ± 2 ^{0}C at 800 rpm, on a magnetic stove with a magnet stirrer stirring continuously. This process was immediately started and timed as zero time. The temperature was controlled using a digital thermometer. An amount of 100 µl was pipetted into the 0.5 ml centrifuge tubes at time intervals within 90 min. The equilibrium was reached at 180 min. The pipetted reactor samples were centrifuged using a small centrifuge for 2 min. Then 1 µl of the centrifuged clean model diesel was pipetted and injected into a GC-PFPD for analysis. The content of sulphur in model diesel was determined from the obtained chromatograms. The adsorption efficiency and the adsorption capacity were calculated for the AmWa, AmSe and AmSh amarula waste, using Equations 4.3 and 4.4, respectively:

$$\text{Adsorption Efficiency\%} = ((C_o - C_t)/C_o)* 100 \qquad \textbf{Eq. 4.3}$$

$$q_t = (C_o - C_t)\, W_{soln}/W_{ads} \qquad \textbf{Eq. 4.4}$$

where the C_o and C_t were DBT sulphur content in ppmw at initial and at time t respectively. The q_t was the adsorption capacity (mg/g) at time t. The W_{soln} and W_{ads} were the mass (g) for solution and adsorbent, respectively. The same procedure was followed for the effect of temperature and the effect of adsorption quantity:

4.3 Results and discussion

4.3.1 Characterization results

4.3.1.1 Proximate and thermal analysis

Table 4.1 shows the proximate analysis results obtained through ASTM [21],[24],[25] for the three raw amarula waste biomass samples: AmSh, AmSe and AmWa waste biomass. The moisture content was found to range from 1 % to 4 %. This was attributed to the hydrophilic properties of biomass which attracts water molecules onto its surface. It was further found that raw AmWa waste had a higher ash content of 2,93 %, followed by raw AmSe and AmSh waste, respectively. This was due to the high level of inorganic matter present in the edible pulp of the fruit, which contained lot of minerals in comparison to the AmSe and AmSh waste. Moreover, it was found that the raw amarula fruit waste had a higher fixed carbon content of 35,67 % compared to the AmSe and AmSh waste, which resulted from fibres of the pulp that contributed more to the carbon content. The similar trend of ash and volatile content for the amarula waste was observed further during TGA analysis (Fig. 4.2).

Table 4.1 Proximate analysis of amarula waste biomass by ASTM

Ads type	Proximate analysis			
	Moisture %	Ash %	Volatiles %	Fixed carbon %
Raw AmSh	3,99 ±0,5	0,64 ±0,04	71,2 ±0,4	24,17 ±0,6
Raw AmSe	2,17 ±0,8	0,96 ±0,03	67,2 ±0,9	28,97 ±0,2
Raw AmWa	1,30 ±0,9	2,93 ±0,03	60,1 ±0,8	35,67 ±0,3
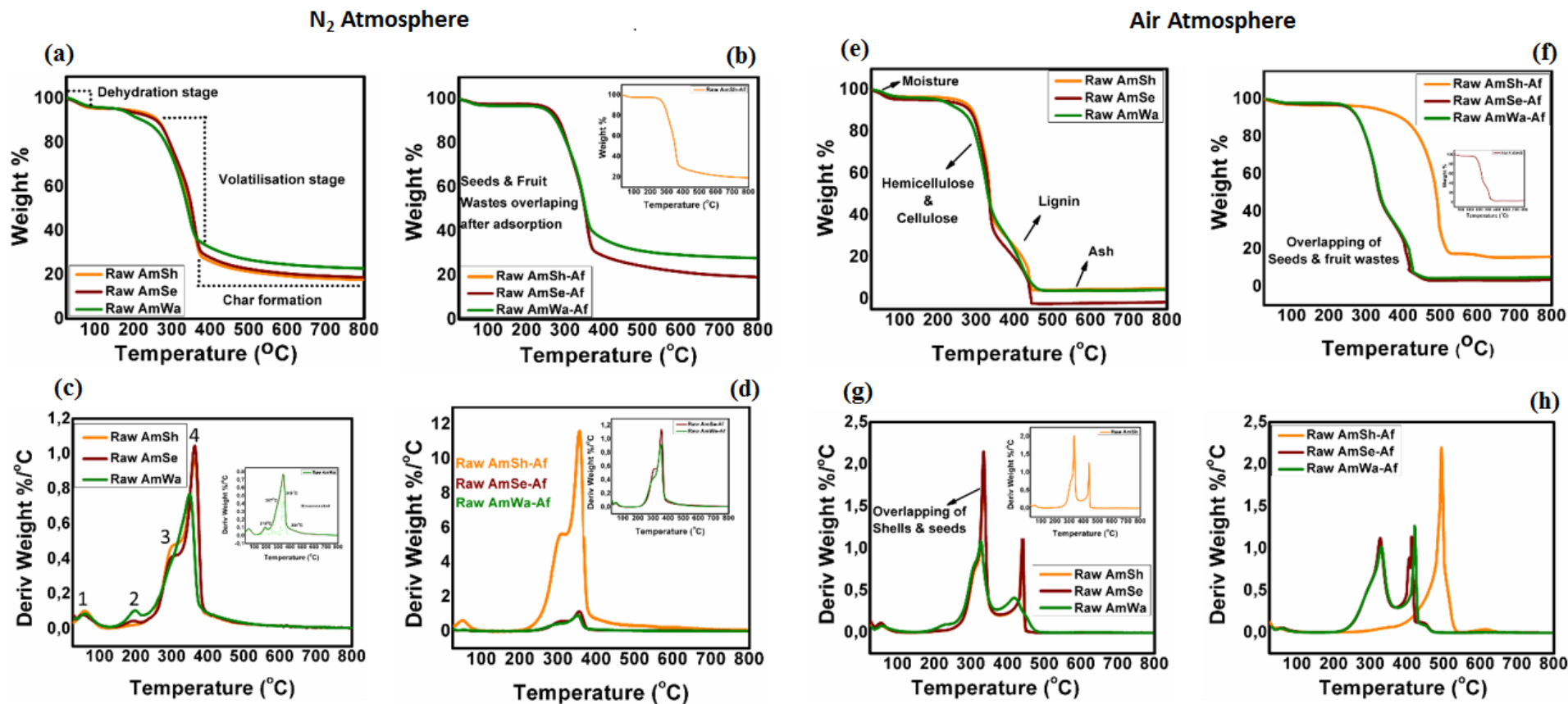
Fig. 4.2. Thermal graphs of raw amarula waste biomass carried out: under N_2 atmosphere TGA (a) before and (b) after adsorption. The (c) and (d) are DTG before and after adsorption. Under air atmosphere TGA (e) before and (f) after adsorption. DTG graphs (g) before and (h) after.

The TGA was used to determine the decomposition of the amarula waste by percentage weight, loss as shown in Fig. 4.2. The thermographs showed three different stages. It was observed that within the first stage of temperatures less than 100 °C there was a weight loss of 1–5 %. This was due to the removal of moisture content on the surface of the amarula waste biomass. Similar observations were found by Salman et al. [26], Rubio et al. [27] and Pathak et al.–[28]. A plateau was further observed at temperatures between 180 °C–240 °C to 400 °C for all the amarula waste at which the AmWa was the first to decompose, with a weight loss range of 63 %, 66 % and 72 % followed by the AmSe and the AmSh, respectively. This plateau was due to the volatilization stage which resulted from the exothermic reactions that occurred as a result of the thermal formation of stronger and stable bonds while replacing the weaker bonds in the biomass structure. It was further attributed as the start of the decomposition of the hemicellulose and cellulose present in amarula waste biomass. This type of decomposition under nitrogen atmosphere was also observed by other researchers [29],[30] who obtained similar results during the thermal analysis of other biomass types under the same conditions. Another mass loss was observed during the last stage between 400 °C and 800 °C. This stage was due to the formation of char resulting from the endothermic reaction, and it was also used to obtain fixed carbons [27],[31] that are thermally stable at higher temperature, as shown in Table 4.2 (a)

Table 4.2 The percentage mass loss at different decomposition stages of TGA: (a) inert and (b) oxidized atmosphere.

(a) Under inert conditions

| Biomass | N₂ Atmosphere | | | | | | | | | |
| | 1st stage | | 2nd stage | | 3rd stage | | Fixed carbon % | | Total mass loss % | |
	Before	After	Before	After	Before	After	Before	After	Before	After
Raw AmSh	3,7	2,5	65,4	65,1	12,9	12,8	18,0	19,6	82,0	80,4
Raw AmSe	3,6	2,5	64,1	64,7	13,6	13,6	18,7	19,2	81,3	80,8
Raw AmWa	3,6	2,4	58,3	55,6	15,6	14,5	22,5	27,5	77,5	72,5

(b) Under oxidized conditions

| Biomass | Air Atmsphere | | | | | | | | | |
| | 1st stage | | 2nd stage | | 3rd stage | | 4th stage | | Total mass loss % | |
	Before	After	Before	After	Before	After	Before	After	Before	After
Raw AmSh	3,7	5,5	58,4	63,9	24,3	12,5	13,6	18,1	86,4	81,9
Raw AmSe	4,4	3,5	61,0	55,5	26,9	19,7	7,7	21,3	92,3	78,7
Raw AmWa	3,7	3,2	55,0	55,8	36,5	22,3	4,8	18,7	95,2	81,3

According to the literature [20],[29]–[32], lignin, another major composite of biomass, starts decomposing at temperatures from 400–800 °C. Therefore, any biomass material that does not decompose after 800 °C is regarded as ash content particularly if it was carried out under airflow atmosphere. For this matter, the TGA was further analysed under air conditions and the results revealed four decomposition stages in Fig. 4.2 (d), with their weight percentage loss listed in Table 4.2 (b). Furthermore, it showed that the amount of inorganic matter that could not decompose any further was 15 %, 14 % and 13 % for AmWa, AmSe and AmSh waste, respectively. The TGA analysis for amarula waste followed a similar trend for ash content as those obtained using proximate analysis by ASTM in Table 4.1. Therefore, TGA has validated that in fact the AmWa waste contained a higher level of inorganic matter than the AmSe and the AmSh waste. It was further concluded that, from the TGA graph, the AmSh waste had higher thermal stability than both the AmSe and the AmWa waste, because its volatile decomposition temperature was higher than that of the AmSe and the AmWa under both N_2 and the air conditions, as shown in Appendix A: Tables A1 and A2.

The derivatives of thermogravimetry analysis were carried out further to determine the actual temperature under inert and oxidising conditions. Each component of biomass that decomposed was listed in Appendix A: Tables A1 and A2. Four peaks were identified from the DTG graphs in Fig. 4.2 (c): the first peak was due to the temperature of moisture removal, the second peak was due to the temperature of light volatiles such as pigments, terpenes and oils present in biomass [32]. The third peak, which appeared as a shouldered peak, upon deconvolution, it was identified as having occurred due to the temperature of the hemicellulose peak, whereas the fourth, longest peak was due to the temperature of a cellulose structure. From there, there was no visible peak, just a tailing until 800 °C. The literature attributed this tailing as being due to the presence of lignin in the biomass [29],[32]. For this reason, upon further deconvolution, a fifth peak was identified as a medium-broad peak that was due to the temperature of lignin decomposition above 400 °C. A similar pattern of derivative temperatures was observed in all three amarula waste types, with AmWa waste showing that there were more light volatiles present in them than in the AmSe and AmSh waste. Besides this, based on peak intensity, the content of the cellulose component in the amarula waste biomass was found to be higher in the AmSh and the AmSe wastes than in the AmWa waste. On the other hand, the DTG graph obtained under air atmosphere in Fig. 4.2 (g) revealed a lignin peak in all biomass types without the deconvolution process. This was due to the combustion of carbon in the lignin component facilitated by oxygen present in the air atmosphere. The peaks for hemicellulose and cellulose

53

became highly intense compared to those in the N_2 atmosphere and remained even more overlapped for both AmSh and AmSe waste, despite exposure to an air atmosphere.

The amarula waste biomass was applied to DBT sulphur molecule in model diesel fuel and then analyzed using TGA and DTG as shown in Fig. 4.2 (b), (d), (f) and (h), under both inert and oxidising atmospheres. The TGA results revealed that there was a slight shift of mass loss in the first stage and the second stages under both graphs (b) and (f); however, the massive difference after adsorption was observed under fixed-carbon content in Table 4.2 (a) at which the fixed-carbon content was higher for raw AmSh waste, followed by AmWa and then AmSe waste. The tables also show that the total mass loss after adsorption was less than that of before adsorption (of di-hexa-cyclic carbon rings fused with a thiophene molecule), signifying an interaction of DBT compound on the amarula waste. Despite that, more elements were also present due to the presence of solvent molecules (hexadecane and toluene) in model diesel fuel, hence more observed fixed-carbon content. Fig. 4.2 (f) under air atmosphere, further revealed that, after adsorption, the AmSh waste became more thermally stable compared to the other waste. This was due to a high interaction of sulphur molecules which formed stronger bonds with the biomass structure.

The Fig. 4.2 (d) is the derivative curve for adsorbents after adsorption under nitrogen atmosphere. It showed no peaks for light volatiles even after deconvolution for all the amarula biomass waste types. However, the peaks of hemicellulose and cellulose shifted slightly to higher temperatures. Meanwhile, the peaks of AmSh waste became very highly intense, confirming a high interaction of sulphur molecule in model diesel to the surface of AmSh waste biomass. Nevertheless, the oxidized atmosphere shown in the DTG curve of Fig. 4.2 (h) after adsorption showed only two peaks, with a massive temperature shift from 334 °C up to 490 °C for a highly intense peak representing cellulose. Another temperature shift of the lignin peak from 425 °C to 716 °C was observed. This confirmed that strong bonds were in fact formed between DBT molecules and AmSh waste biomass, hence the observed high thermal stability.

On the other hand, the light volatiles were still present after adsorption for both the AmSe and the AmWa waste biomass. There were minimum peak shifts for all the components after adsorption, signifying very little interaction of a sulphur molecule with them.

4.3.1.2 FESEM-EDS analysis

The morphology of the three amarula waste samples before and after adsorption is shown in Fig. 4.3. It was observed that the morphology of amarula shells (a) before adsorption revealed a rough surface with some agglomeration due to packed fibres, whereas after adsorption in (b) the morphology changed, at which the fibres dispersed and were mostly rough on the edges. There were some shiny spots on the surface of the fibres, which signified the presence of oily compounds such as DBT. On the other hand, the morphology of AmSe waste in an image (c) showed a very beautiful, smooth surface and some pores, but after the adsorption of DBT molecules in (d) the fingerprint-like morphology was observed on the surface. Moreover, the surface in (d) seemed brighter and shinier, with some more agglomeration, which was attributed to the presence of sulphur compound particles on the surface. Further morphological analysis of AmWa waste in (e) showed the presence of some irregular spheres, but after adsorption the image (f) shows that the spherical morphology disappeared. The surface became distorted and took on the shape of corrugated iron. In addition, the micrograph also showed some roughness, which was due to the organo-sulphur compound on the surface. This agglomeration on the three amarula waste biomasses was attributed to the presence of cellulose and hemicellulose particles held and packed tightly together. A similar morphology for biomass was seen by El-naggar El-nagger et al. [12] and Pathak et al.,[28].

AmSh waste biomass was selected and used for EDS analysis in Fig. 4.3 (g) before and after adsorption. It was found that the raw AmSh waste biomass had a greater content of carbon (C) and oxygen (O) elements and very low content of other elements such as magnesium and silica (not shown in the drawn graph). However, after adsorption, the sulphur (S) element was identified with the content of 0.2wt %. This sulphur element was due to the adsorption of DBT sulphur compounds, signifying that indeed the amarula waste biomass is capable of adhering organo-sulphur compounds. The AmSe and AmWa waste biomass samples were also analysed for EDS but are not reported on here because the content of the sulphur element was too low for instrument detection.
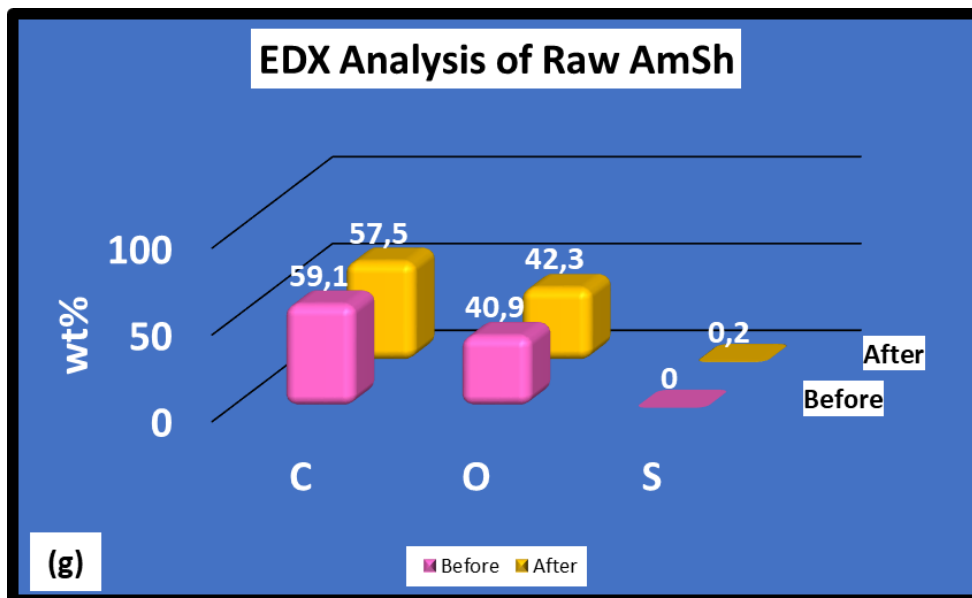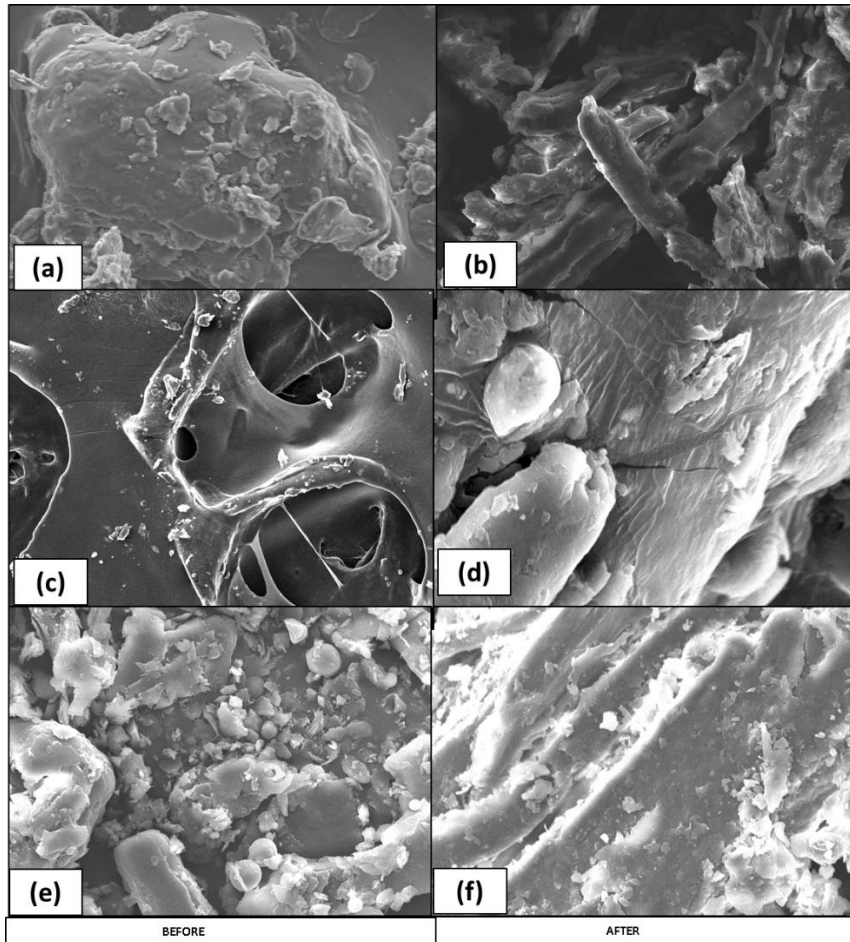
Fig. 4.3. SEM images; for AmSh (a) before (b) after adsorption, for AmSe (c) before and (d) after adsorption, for AmWa (e) before and (f) after adsorption. The (g) graph is an EDS analysis of selected AmSh before, and after adsorption

4.3.1.3 TEM analysis

Further morphological analysis was carried out using the TEM technique shown in Fig. 4.4 for the selected AmSh (a) before and (b) after adsorption of DBT. The results in an image (a) showed an irregular structure with big clusters inside it. This was considered as agglomeration because the material is raw biomass therefore, the fibres and particles are still tightly packed to each other. The image in (b) for after adsorption still showed an irregular shape, but this time with several tiny dark spots on the surface. These spots were attributed to particles of DBT sulphur molecule on the surface of the amarula waste biomass. The TEM results confirmed the EDS results, which showed the presence of a sulphur element after adsorption as seen in Fig. 4.3 (g) above. It can, therefore, be concluded that the amarula waste biomass can adsorb organo-sulphur compounds in diesel fuel, making it a potentially environmentally friendly and sustainable low-cost adsorbent.
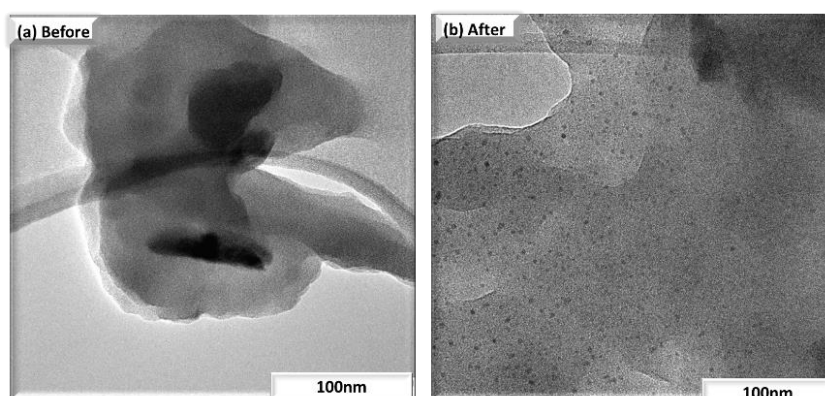
Fig. 4.4. TEM images of amarula shell waste (a) before and (b) after adsorption at 100 nm

4.3.1.4 Surface chemistry analysis

FTIR was used to analyze the functional groups present on the surface of the three amarula waste samples. All the spectrums showed the presence of various functional groups in Fig. 4.5 (a). The broadband at 3 600 cm^{-1}–3 100 cm^{-1} was attributed to an O–H stretching vibration of hydroxyl groups due to the adsorbed moisture which was also visible during TGA analysis at temperatures less than 100 °C. These hydroxyl groups are also assigned to phenols, alcohols and carboxylic groups present in cellulose and hemicellulose. These groups were also reported in various literatures [11]–[13],[28],[33],[34]. There were stretching vibrational bands with medium peaks at 2 925 cm^{-1} and 2 855 cm^{-1} which were attributed to sp^3 C–H asymmetric and symmetric stretch for methane or methylene groups, respectively. The peak at 1 737 cm^{-1} was

assigned to the C=O stretching of the saturated ethers and acetyl groups in the hemicellulose [28],[33],[34]. Peaks at 1 639 cm^{-1} and 1 504 cm^{-1} were attributed to C=C and C–C stretching bends in the aromatic ring, respectively. A weak asymmetric vibrational bend at 1 370 cm^{-1} was due to an N–O functional group present in the biomass. The wave number at 1 236 cm^{-1} showing a weak band represented the C–O aryl functional group in lignin [35]. At 1 168 cm^{-1}, a weak asymmetric bend was observed as being due to acyl and phenyl groups. The strongest bending vibration at 1 031 cm^{-1} was attributed to the C–O functional groups of carbonyl groups present in amarula waste biomass. An out-of-plane bend of sp^2 C–H was observed at 897 cm^{-1}. It can be concluded that although similar functional groups were present in all the spectra of amarula waste biomass, the AmWa waste had highly intense bands, which means that more functional groups were present on its surface because of extra molecules from the edible fruit pulp. It was further observed that for AmSh waste, the intensity of the peak was small compared to the other waste samples, especially for the O–H, C–H and C–O vibrational bands at 3 600 cm^{-1}–3 100 cm^{-1}, 2 925 cm^{-1} and 1 031 cm^{-1}. Generally, it can be concluded that the amarula waste biomass had a higher density of O-functional groups on its surface that resulted from cellulose and hemicellulose. This could mean that the surface of the amarula waste biomass might be acidic and that could contribute to the higher absorptivity of this organo-sulphur compound in model diesel fuel.
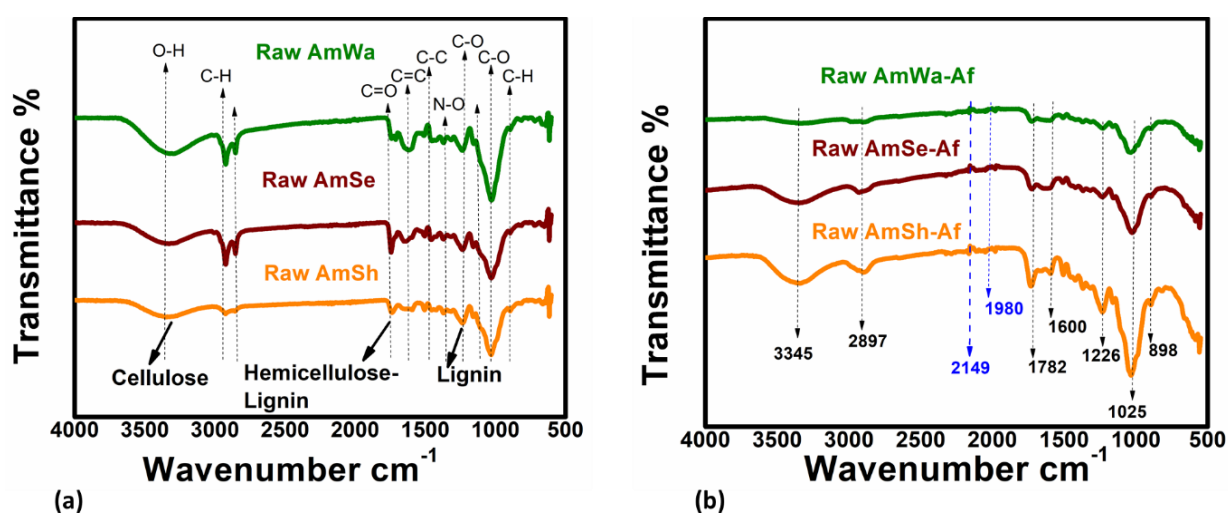
Fig. 4.5. FTIR spectrum of amarula waste biomass (a) before and (b) after adsorption

58

However, the FTIR spectrum of amarula waste after adsorption in Fig. 4.5 (b) - showed more intense peaks compared to the spectrum seen in Fig. 4.5 (a). This was due to the interaction of sulphur compounds (DBT) in model diesel. The peak at 2 925 cm^{-1} disappeared whereas the one at 2 855 cm^{-1} shifted to 2 897 cm^{-1} after adsorption. The FTIR spectra after adsorption also showed a new visible peak at 2 149 cm^{-1} and a weak band at 1 980 cm^{-1}, which was attributed to S–H vibrational stretch and aromatic ring vibrations during the interaction of DBT and amarula waste biomass, respectively. This occurred when weak hydrogen bonds were formed [36]. The peak at 1 737 cm^{-1} shifted to 1 782 cm^{-1} after adsorption due to the formation of conjugated atom rings from model diesel constituents (toluene and hexadecane). The peak at 1 639 cm^{-1} also shifted to 1 600 cm^{-1}. The band at 1 236 cm^{-1} moved to 1 226 cm^{-1} and became more intense, confirming high DBT interaction with it. The peak at 1 031 cm^{-1} also shifted to 1 025 cm^{-1}. Furthermore, the O–H peak of AmWa waste was found to have fewer intensity bends compared to the other AmSe and AmSh waste samples after adsorption. Finally, it can be concluded that even though the SEM morphology of the three amarula waste biomass samples had some similarities (Fig. 4.3) before and after adsorption process, the use of FTIR analysis was able to confirm and show significant differences in their chemical structure in the three types of amarula waste biomass samples before and after adsorption.

4.3.1.5 Powdered X-ray diffraction analysis

Upon exposing the raw amarula waste biomass to X-ray photons, the diffraction spectrum in Fig. 4.6 (a) showed slightly overlapping patterns of broad and sharp intense peaks at 2θ angle values of 16⁰ and 21⁰. These patterns were found to correspond to amorphous carbons, which were due to the presence of lignin composite, and to a crystalline carbon that was due to the presence of cellulose and hemicellulose composites in the structure of amarula waste biomass, respectively. Similar biomass patterns were observed by Rambo et al. [20] and Zhang et al.[23]. The third small pattern that is observable at 2θ angle value of 35⁰ with d spacing of 040 was attributed to the presence of minerals in different phases of calcium in amarula biomass. This was also seen by Rambo et al. [20] for the XRD spectrum of banana fibres. This further confirms a high level of ash content observed during proximate analysis and TG analysis above. Despite the visual similarities of the diffraction patterns on the three types of raw amarula waste biomass, calculations using the Scherrer equation showed that these carbon phases in each type of amarula waste differ in lattice size as shown in Table 4.3 (a). The results revealed that the

lattice size (L) of raw waste biomass followed the trend AmSh < AmSe < AmWa, signifying that amarula shells had a more regular structure compared to the AmSe and AmWa waste biomass.
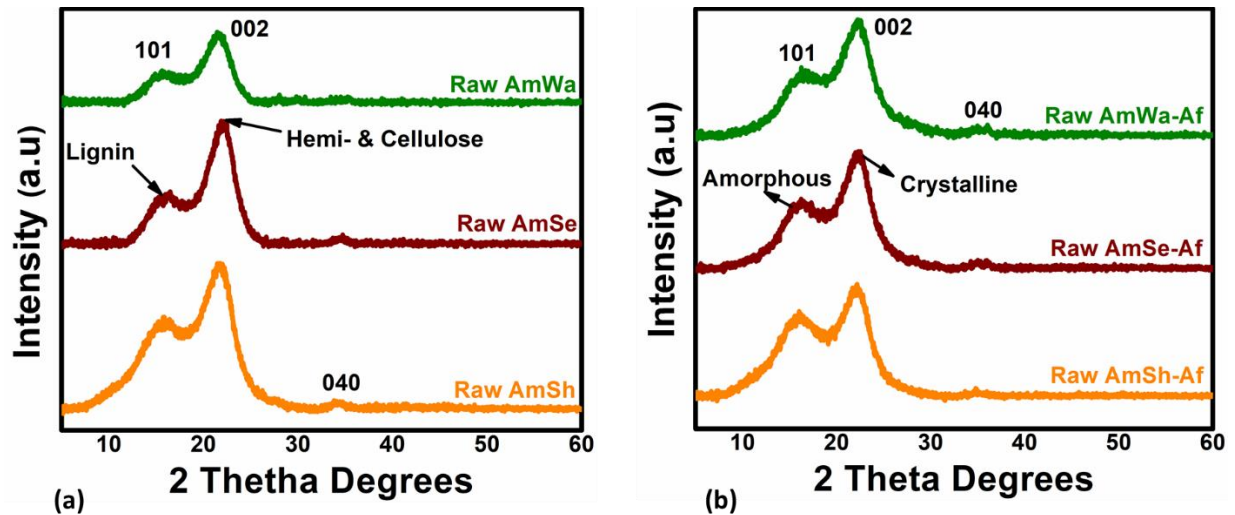
Fig. 4.6. The XRD on the three types of amarula waste biomass (a) before and (b) after adsorption

According to Zhang et al. [23] the crystallinity index (CI %) of the biomass tends to increase when the wax content in biomass is low. This was proven by Rambo et al. [20] who removed the extractives from different lignocellulose biomass types and found that the less the wax content the higher the crystallinity index. Therefore, AmSh waste was found to have a higher crystalline index, followed by AmSe and then AmWa waste as shown in Table 4.3 (a). This was because both the AmSe and the AmWa waste have the nuts inside them and these nuts are waxy, hence they contribute to a higher wax content. This fact was also observed in the FTIR spectrum above, whereby the intensity of the functional groups in the cellulose and hemicellulose region for AmSh waste was very low compared to the intensity of the AmSe and the AmWa waste biomass.

Table 4.3 Crystalline index (CI) % and lattice size of amorphous (L_a) and crystalline (L_c) carbons for the three amarula waste biomass samples (a) before and (b) after adsorption

(a) Before adsorption

Ads type	Lattice size (Å)		Crystalline Index (CI%)
	Amorphours La	Crystalline Lc	
Raw AmSh	10,12	22,11	68,60
Raw AmSe	14,69	24,79	62,79
Raw AmWa	14,98	24,78	62,32

(b) After adsorption

Ads type	Lattice size (Å)		Crystalline Index (CI%)
	Amorphours La	Crystalline Lc	
Raw AmSh-Af	11,10	21,49	65,95
Raw AmSe-Af	12,88	21,07	62,06
Raw AmWa-Af	13,52	19,07	58,51

After applying the three raw amarula waste biomasses, to DBT model diesel fuel, it was found that the crystalline patterns shifted from 2θ value 21° to 2θ value 22°. For the amorphous peak, there was no significant change as shown in Fig. 4.6 (b). It was further observed that the intensity of the peaks for both the amorphous (57°–30°) and the crystalline (18°–13°) patterns decreased to 31°–28° and 22°–11° respectively, after adsorption of the organo-sulphur compound. In addition, the lattice size (L_a and L_c) of amarula waste biomass decreased in the AmSe and AmWa waste samples, but not in the AmSh waste, which showed an increase of L_a from 10,12 Å (before) to 11,10 Å after adsorption as seen in Table 4.3 (b). The crystalline index also decreased after adsorption in a similar trend as before adsorption. This may be due to the hexadecane and toluene solvent in model diesel fuel that facilitates the adsorption of DBT on the amarula waste biomass.

The peak at 040 plane became more observable after adsorption because the amarula waste sorbents had adsorbed the sulphur compound, and that, increased the content of the inorganic matter due to the interaction of DBT sulphur compound on the biomass surface. These sulphur elements were observed on EDX and TEM analysis in Fig. 4.3 and Fig. 4.4 (b) respectively. The low total mass loss percentage observed after adsorption in Table 4.1 (a) and (b) under TG Analysis also confirmed these XRD results.

4.3.1.6 Textural properties of amarula waste

The BET surface area, t-plot external surface area and the BJH surface area are listed in Table 4.4, which summarises the values of the textural properties of amarula waste biomass. The surface area was found to be less than 1 m^2/g for all the types of raw amarula waste, with the AmWa waste being the highest, followed by the AmSh waste, then AmSe waste. A similar trend was also observed for their BJH pore size and pore diameter. This confirms the SEM morphology seen in Fig. 4.3 (a), in which no visible pores were observed except some agglomerations on the surface. The small pore volume found may be due to the blockage caused by the wax arising from the nuts inside the fruit and the AmSe waste biomass. This was also observed in XRD analysis in Table 4.3 (a) under a crystalline index, at which the AmSh waste exhibited high CI %, indicating a lower presence of wax. Pore size is classified according to International Union of Pure and Applied Chemistry (IUPAC) 1985 as macropores (>50 nm), mesopores (2–50 nm) and micropores, which in turn are divided into supermicropores (>1–0.7 nm) and ultra-micropores (<0.7 nm) [37]. From this classification and based on the tabulated results in Table 4.4 (a), it was found that the pore diameter of amarula waste ranged between 10 nm and 15 nm (100 Å–150 Å) and that it fits well as mesopores. This might be advantageous for adsorption of the DBT molecule, which is between 0.65 nm–1 nm in size [38]. Also, the DBT has molecular dimensions of 7.4 Å, 11.6 Å and 3.6 Å, as calculated from the density function theory (DFT) model in the Gaussian 98 software described by Moosavi et al. [39]. The pore distribution of the amarula waste was also analyzed in Fig. 4.6 (a) and all the waste biomass samples revealed the longest peak at the pore width range of 10 Å–20 Å, with the highest increment pore volume being attributed to micropores. The medium peaks observed between 20 Å and 40 Å signified fewer mesopores whereas, from 50 Å upwards, few small peaks were observed, this being ascribed to macropores being in smaller quantities.

Table 4.4 Textural properties values of raw amarula waste biomass using BET

Ads type	Surface Analysis				
	BET-S-area (m^2/g)	t-plot Ext S-ar (m^2/g)	BJH-S-area (m^2/g)	BJH Pore Vol (cm^3/g)	BJH Pore diameter (Å)
Raw AmSh	0,54 ±0,6	0,65	0,559	0,0018	131,3
Raw AmSe	0,18 ±0,7	0,25	0,198	0,0007	141,5
Raw AmWa	0,67 ±0,1	0,93	0,748	0,002	107,8

The adsorption–desorption isotherm was further determined to understand which adsorption isotherm the amarula waste biomass will follow. According to Fig. 4.7 (b), the amarula waste biomass exhibited similar adsorption–desorption isotherms with a tiny hysteresis loop. It was observed from the graph that at a low relative pressure of between 0.0 p/p° and 0.2 p/p° the pores were quickly filled only up to 0.15 cm^3/g, showing a less distinctive gradual curve, with the AmSe waste being the lowest filled followed by AmSh and then AmWa waste. This indicated that there was an overlap of monolayer coverage and an onset of multilayer adsorption [40]. At high relative pressures $\approx$ 0.8–1.0 p/p° the volume adsorbed increased without limit to $\approx$ 0.4 cm^3/g, 1.1 cm^3/g and 1.2 cm^3/g for AmSe, AmSh and AmWa waste respectively. This observed shape was regarded as a Type II isotherm, which also normally occurs in non-porous or macro-porous material [37],[40]. This is indeed true, because the amarula waste biomass was found to have a non-porous morphology under microscopic analysis in Fig. 4.3. Furthermore, a sharp step-down branch for the desorption process created a slim loop in all the amarula waste, and it closed at a relative pressure of $\approx$ 0.5 p/p°. This type of loop signified the Type H3 hysteresis loop that is identified in the origin of the IUPAC classification [37].
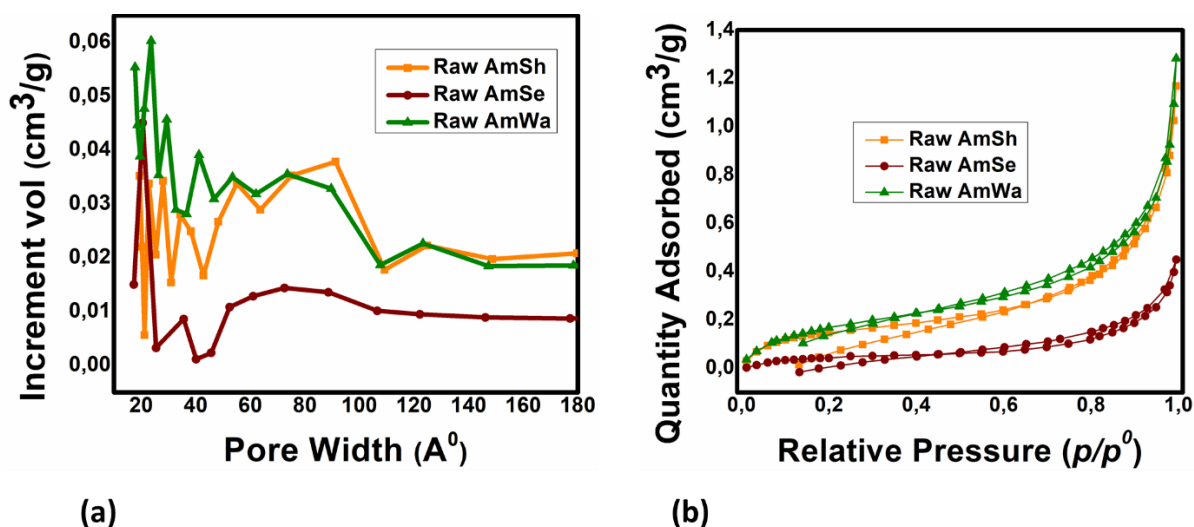
Fig. 4.7. (a) Pore distribution and (b) N_2 adsorption-desorption isotherm of amarula waste biomass

4.3.2 Adsorption of dibenzothiophene

4.3.2.1 Analysis of model diesel fuel before and after processing

Analysis of DBT model diesel fuel was carried out using the GC-PFPD technique coupled with a flame ionisation detector (FID). The quality of the instrumental operation and the method of analysis were validated by performing a calibration method. The calibration curve results are shown in Appendix A: Fig. A1.

4.3.2.2 Effect of adsorption time on adsorption of DBT

The three types of amarula waste biomass were applied to a batch adsorption process at time intervals within 180 min for the 93 ppmw DBT model diesel fuel at room temperature (25 °C) and, their performances were determined. It was found that the concentration of DBT sulphur content decreased as adsorption time increased as seen in Fig. 4.8 (a). This implied that the amarula waste can in fact reduce the sulphur content in model diesel by 30 %, 19 % and 9,5 % within 3 h for raw AmSh, AmSe and AmWa waste respectively as shown in Fig. 4.8 (b). Table 4.5 shows further that the extent of the adsorption (q_e) followed the similar trend of three amarula waste biomasses, suggesting that the AmSh waste had a higher adsorption capacity of 0.278 mg/g than the other two waste biomasses. It was observed that the AmWa waste biomass quickly became saturated within 30 min whereas the AmSe and AmSh wastes became saturated at around 60 min only.

(a)   (b)
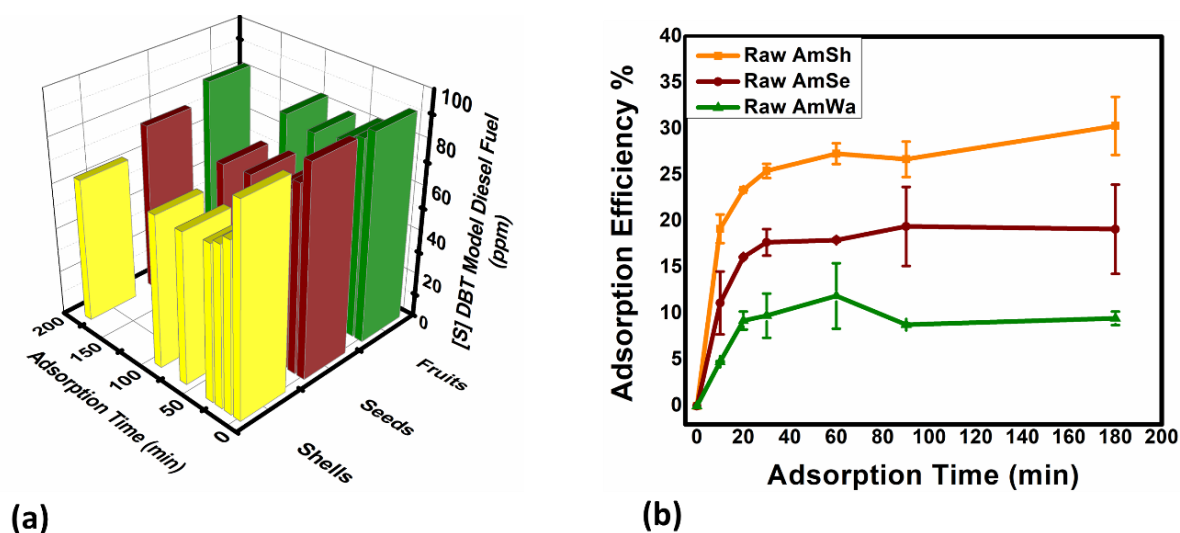
Fig. 4.8. The graphs of (a) sulphur content in DBT model diesel and (b) adsorption efficiency at 800 rpm within 180 min using a 10wt % adsorbent of amarula waste biomass

This means that the adsorption of DBT in model diesel fuel on AmWa waste was controlled by fast kinetics and it could undergo monolayer adsorption. On the other hand, the AmSe and the AmSh waste underwent slower kinetics and could undergo multilayer adsorption. A similar scenario with biomass was observed in [11]. This is because, as time passes, more adsorption occurred until a certain plateau was reached. It was found that the adsorption of AmSe and AmSh waste occurred in two stages. The first stage was due to physical adsorption that occurred on the surface of the biomass and was faster, occurring within 30 min. Then the second stage, known as the active stage, became slower as it reached equilibrium at around 60–90 min. It was also observed that the adsorption capacity increases with adsorption time too. It was concluded that the effect of time showed less or no significant change in adsorption efficiency from 90 min to 180 min for all three amarula waste biomasses. Therefore, 90 min was regarded as the equilibrium time for the adsorption of DBT in model diesel fuel on amarula waste biomass.

Table 4.5 Values of adsorption capacity and adsorption efficiency of the three amarula waste biomasses

Ads type	Ads capacity qe (mg/g)	Ads eff % @ 25 ℃	
		90 min	180 min
Raw AmSh	0,278 ±0,16	26,7 ±2	30,3 ±3
Raw AmSe	0,175 ±0,24	19,4 ±4	19,1 ±5
Raw AmWa	0,087 ±0,07	8,8 ±0,1	9,5 ±0,7

The faster kinetics on AmWa waste may also be attributed to the larger pore size of 141Å observed during textural analysis in Table 4.4. It is said that a material that has a mixture of micropores and mesopores tends to facilitate the faster movement of adsorbate to the micropores [41]. Researchers in articles [4],[11],[42],[43] obtained similar trends for the effect of time when they were using biomass as a sorbent for different applications. It can be concluded that among the three amarula sorbents, AmSh performed better for the adsorption of DBT in model diesel fuel, with AmWa waste being the lowest performer despite having a higher surface area than the other waste samples. This may also be attributed to the fact that AmWa waste had a higher ash content of about 2,9 % as shown in Table 4.1 of proximate analysis compared to AmSe and AmSh waste, respectively. It is reported that adsorbents with high levels of inorganic matter tend to be less favoured for high adsorption efficiency [44].

4.3.2.3 Effect of Adsorption temperature

The temperature has a great impact on adsorption processes depending on whether the process is endothermic or exothermic. The effect of the adsorption temperature of DBT in model diesel fuel was tested on AmWa, AmSe and AmSh waste within 180 min at a stirring rate of 800 rpm using a 10wt % biomass sorbent. From the graph of Fig. 4.9, it was observed that the adsorption efficiency increased from 20 °C to 25 °C by ≈ 10 % for AmSh and AmSe waste. It then decreased substantially to 35 °C, where it became stable until it reached 45 °C. It further decreased again as the temperature increased to 55 °C. The adsorption efficiency values are shown in Appendix A: Table A3.

This decline in adsorption efficiency with the increase in adsorption temperature might have been due to the rate of desorption that occurred on the surface of the amarula waste biomass. Similar results for the effect of adsorption temperature were experienced by other researchers [45]. Researchers in [9]–[12] used biomass as a sorbent to reduce the content of heavy metals in water and found out that the optimal temperature was 35 °C. On the other hand, Ahmad et al. [46] used modified sorbent loaded with metals to reduce the sulphur content of DBT in model diesel and found a higher desulphurization efficiency of about 63 % at room temperature of 25 °C after six hours, whereas Ahmadi et al. [47] reported that adsorption desulphurization in other studies reached equilibrium in just 60 min. For AmWa waste, the adsorption efficiency was found to increase linearly from 20 °C to 25 °C and to 35 °C by 5 % and then it dropped as the temperature increased to 45 °C and 55 °C. Despite this temperature effect, the AmWa waste still had lower adsorption efficiencies as compared to AmSe and AmSh waste and this might still be due to a high level of inorganic matter present in the sorbent.

Moreover, based on the result, it was further found that the adsorption of DBT in model diesel fuel on all raw amarula waste biomass favours a lower temperature. Consequently, 25 °C was the optimal temperature for AmSh and AmSe waste, with 30 % and 22 % adsorption efficiency, whereas for AmWa waste the optimal adsorption temperature was 35 °C, with the highest adsorption efficiency of 9,5 %. It can further be concluded that the rise in temperature decreased the adsorption efficiency of AmWa waste due to the exothermic nature of the adsorption process.
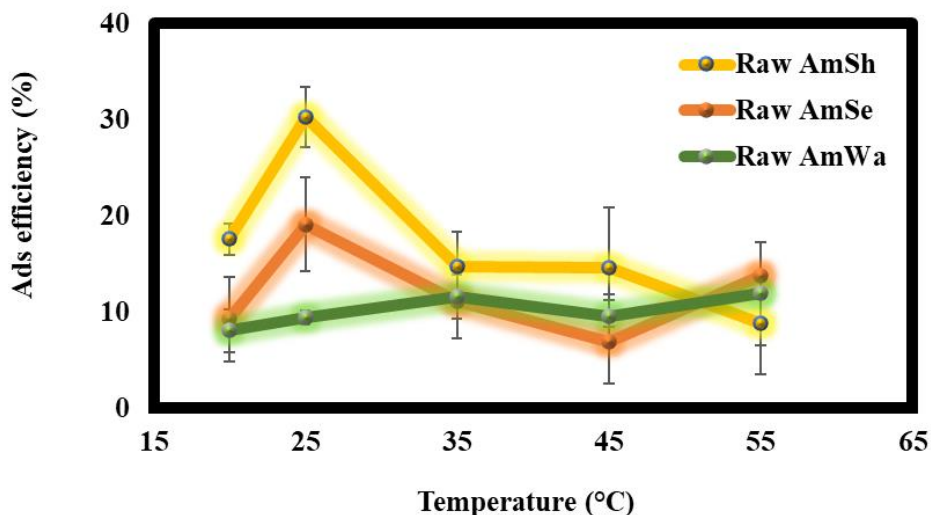
Fig. 4.9. The effect of adsorption temperature on amarula waste samples: conditions: 10wt % ads quantity 800 rpm, 180 min

4.3.2.4 Effect of adsorbent quantity

Minimised cost is found to attract inventions, and it allows competition among other production industries, hence adsorbent quantity was found to be a crucial parameter in the adsorption process for scaling-up purposes because of its economic impact. Therefore, AmSh waste was selected to determine the effect of biomass quantity on DBT adsorption based on the above results, because of its better performance out of the three amarula waste samples. The results . for both the adsorption efficiency and the adsorption capacity are shown in Fig. 4.10. Various biomass concentrations, ranging from 2wt % to 20wt % were used while keeping the other parameters constant. The results revealed that as the concentration of AmSh waste biomass increased from 2wt % to 10wt %, the adsorption efficiency also increased to 30 %. This was because the biomass was more concentrated and that offered more surface area for adsorption, hence more adsorption sites available for DBT adsorption [48].

It was also observed that as the biomass quantity was further increased from 10wt % to 20wt %, the adsorption efficiency decreased from 30 % to 15 %. This was attributed to the fact that some active sites of adsorbent remained unoccupied or exposed to the adsorption of the DBT molecule, and this resulted in the aggregation of adsorbent particles on the surface. This type of trend was reported on by Kosa et al. [48]. Further analysis of the extent of adsorption results also revealed that the adsorption capacity decreased as the quantity of biomass increased. In addition, the mathematical expression in Equation 4.2 which shows that the ratio of adsorbate solution to mass adsorbent increases if the mass of adsorbent increases. This trend of adsorption capacity was also attributed to the unsaturated active sites for adsorption reaction and the agglomeration of biomass particles due to the higher content of biomass, which led to the decrease in surface area and the increase in the diffusion path length. A similar observation was obtained by Prajapati et al. [49]
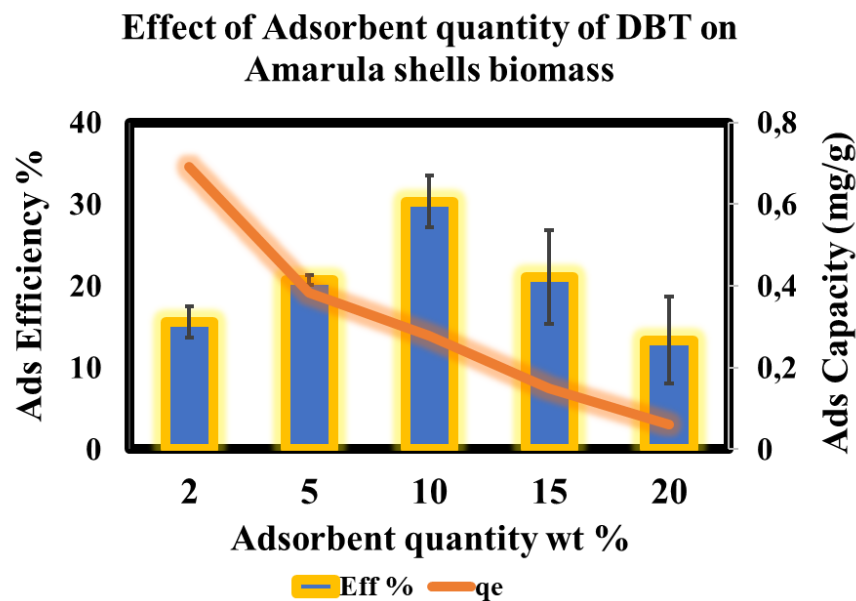
Fig. 4.10. Adsorption capacity and adsorption efficiency for the effect of adsorbent quantity on selected raw AmSh at 25 °C, 800 rpm and 180 min

4.3.2.5 Adsorption kinetics

Adsorptive kinetics, particularly in a batch system, are found to be very imperative for designing adsorption column and for industrial applications. For this matter, the kinetic models of pseudo-1st-order, pseudo-2nd-order and intraparticle diffusion models were applied to experimental data to understand the sorption mechanism. These models have been applied by

several researchers previously during adsorptive desulphurization of diesel fuel on synthesized adsorbents [3],[6],[8],[9],[50],[51]. Pseudo 1st order, which was first discovered by Lagergren [52] is expressed in Equation 4.5 as:

$$rq_t = K_1(q_e-q_t) = dq/dt \qquad \textbf{Eq. 4.5}$$

Table 4.6 Constants and correlation values of the kinetic models of DBT on amarula waste biomass at room temperature

Constants and Correlation values of kinetic models for Amarula wastes biomass								
Adsorbent type	Pseudo 1st order		Pseudo 2nd order				Intraparticle diffusion		
	K_1	R^2	K_2	R^2	$q_{e\ calc}$	$q_{e\ exp}$	K_i	C	R^2
Raw AmSh	-0,0093	0,2051	256,92	0,9956	0,280	0,278	0,002	0,1472	0,399
Raw AmSe	-0,0184	0,3693	5,57	0,9983	0,179	0,175	0,001	0,089	0,3596
Raw AmWa	-0,0128	0,3856	1798,69	0,9876	0,088	0,087	6E-04	0,055	0,233

The r is the reaction rate, the q_t (mg/g) and q_e (mg/g) are the adsorption capacity of sulphur at time t (min) and equilibrium, respectively, K_1 (min^{-1}) is the rate constant of pseudo 1st-order sorption. The integrated Equation 4.5 gives Equation 4.6:

$$\ln(q_e - q_t) = K_1t + \ln q_e \qquad \textbf{Eq. 4.6}$$

where the plot of $\ln(q_e-q_t)$ vs t from the linear Equation 4.6 was used to determine the q_e and the K_1 shown in Fig. 4.11 (a).

The type 1 linear pseudo 2nd-order model, which was first proposed by Blanchard et al. [53] and then applied by Ho et al. [54], is written in Equation 4.7 as:

$$rq_t = K_2(q_e - q)^2 = dq/dt \qquad \textbf{Eq. 4.7}$$

at which K_2 (g mg^{-1}min^{-1}) is the rate constant of pseudo 2nd-order sorption [53],[54]. When Equation 4.7 was integrated, it gave Equation 4.8 as:

$$t/q_t = (1/q_e)t + 1/K_2q_e^2 \qquad \textbf{Eq. 4.8}$$

where the values of q_e and K_2 were obtained from a linear plot of $1/q_t$ vs t as shown in Fig. 4.11 (b). In this application, q_e was not estimated from experimental data. The same approach was followed when applying the intraparticle diffusion model that was first established by Weber and Morris [55], which is expressed in Equation 4.9.

$$q_t = K_i t^{1/2} + C \qquad \qquad \textbf{Eq. 4.9}$$

in which K_i (mgg^{-1}min^{-1}) is the intraparticle diffusion constant and C (mgg^{-1}) is the constant related to the energy of sorption or thickness of the boundary layer. These intraparticle diffusion constants K_i and C were determined in Fig. 4.11 (c) from the linear plot of q_t vs $t^{1/2}$ as slope and intercept, respectively. This model assumes rate-limiting step only if the plot is linear and passes through the origin.
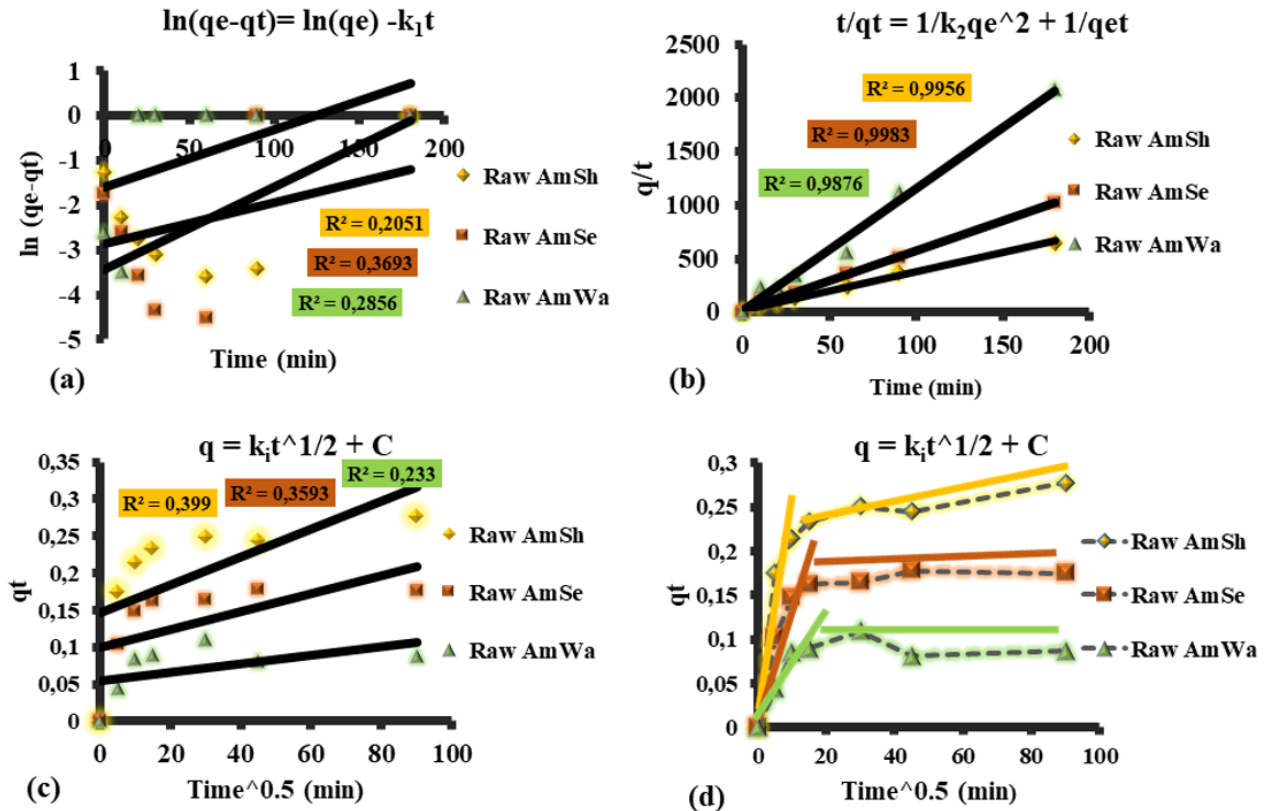
Fig. 4.11. Graphs of (a) pseudo 1st order, (b) pseudo 2nd order, (c) intraparticle diffusion and (d) two linear regions in the intraparticle diffusion graph on the three types of amarula waste biomass at 25 °C

Table 4.6 shows the correlation and constant values obtained from kinetic models at time t for the amarula waste at room temperature. According to Bucchianico [56], the coefficient of determination r^2 in the range of [0,9, 1] means a good fit between the data and the values predicted by a model. The correlation values of pseudo 1st order were found to be less than 0,5; therefore, they did not fit best with the model which requires the r^2 values to be close to 1. Moreover, the experimental data ($q_{e\ exp}$) were very different from the calculated data ($q_{e\ calc}$), which further confirmed the deviation from the model. This discrepancy in the 1st-order kinetic

model was attributed to the presence of a boundary layer or an external resistance controlling the beginning of the sorption process [57].

The pseudo 2nd-order model was found to be a better fit for all the amarula waste biomass samples, with high correlation values of 0,9956, 0,9983 and 0,9876 for raw AmSh, AmSe and AmWa waste biomass samples, respectively. This was because the values were close to unity, as discussed by Nazal et al. [58]. The 2nd-order kinetic model assumes that chemical adsorption could be a rate-limiting step [50],[58],[59]. In that case, it was therefore concluded that the sorption mechanism may have occurred via hydrogen bonding between hydroxyl and carbonyl functional groups in amarula waste biomass and thiols in DBT model diesel fuel as shown in Fig. 4.12. These findings were found to be in line with the FTIR spectra before and after adsorption in Fig. 4.5 (a) and (b).

On the other hand, the plot of the graph in Fig. 4.11 (c) did not pass through the origin. This was because the rate of mass transfer was different from the initial and the final stages of adsorption [60]. Nevertheless, Fig. 4.11 (d), which is an extended intraparticle diffusion graph of Fig. 4.11 (c), showed two diffusion stages predicted by the diffusion model for DBT and are attributed to two linear parts.
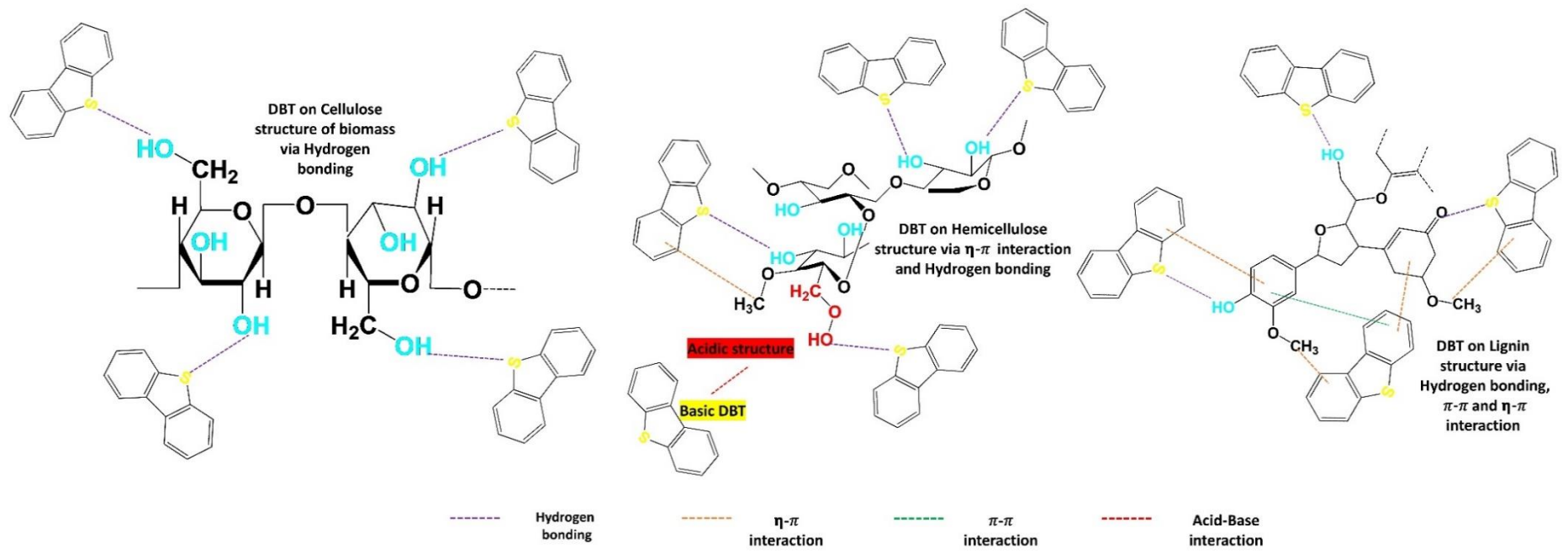
Fig. 4.12. Adsorption mechanism of DBT on amarula waste biomass

The 1st linear part is attributed to film diffusion which transported the DBT molecule from the bulk of model diesel solution to the external surface of the amarula waste. The 2nd linear region was regarded as the intraparticle diffusion of DBT molecule from the exterior of the amarula waste biomass into its small pores or along pore wall surfaces which were then followed by the establishment of equilibrium. Similar findings on biomass as a sorbent in aqueous solutions were observed by researchers in [60],[61]. Whereas other similar findings were seen on desulphurization of model fuels on mesoporous materials [47]. It was for these reasons that this stage was found to be in line with the results of the textural properties seen in Fig. 4.7 and Table 4.4, which show the presence of micropores in amarula waste biomass. It can be concluded that the adsorption process was controlled by multiple mechanisms because the intraparticle diffusion gave out multiple linear regions in Fig. 4.11 (c). This was also confirmed by adsorption–desorption isotherms in Fig. 4.7 (b) which showed an overlap of monolayer and multilayer adsorption of reversible Type 11 isotherm.

Table 4.7 Impact of ads temperature on second-order kinetic parameters on amarula waste biomass

Adsorption Temp. (°C)	Pseudo 2nd order											
	Raw AmSh				Raw AmSe				Raw AmWa			
	$q_{e\,exp}$	$q_{e\,calc}$	K_2	R^2	$q_{e\,exp}$	$q_{e\,calc}$	K_2	R^2	$q_{e\,exp}$	$q_{e\,calc}$	K_2	R^2
20	0,16	0,16	1,09E+03	0,9963	0,09	0,08	3,58E+03	0,9922	0,07	0,07	1,63E+04	0,9736
25	0,28	0,28	2,57E+02	0,9956	0,18	0,18	6,30E+02	0,9983	0,09	0,09	1,80E+03	0,9876
35	0,14	0,14	1,21E+03	0,9968	0,10	0,10	5,69E+03	0,9879	0,11	0,11	3,61E+03	0,997
45	0,13	0,14	3,43E+03	0,9869	0,10	0,10	5,69E+03	0,9971	0,09	0,09	7,54E+03	0,9937
55	0,08	0,09	1,32E+04	0,976	0,13	0,13	5,99E+03	0,9846	0,11	0,12	6,31E+03	0,8727
Chi square x^2	0,00039				0,00027				0,00066			

The kinetic models were further applied to experimental results for the effect of adsorption temperature, and pseudo 2nd order was still found to be the best fit. For this reason, the pseudo kinetic constants and correlation values were the only ones reported on in Table 4.7, whereas the other models are in the Appendix A: Tables A4, A5, and A6. The results further revealed that the values of $q_{e\,exp}$ and $q_{e\,calc}$ were very close to each other on this type of model for all the amarula waste types, as shown in Table 4.7. This confirms that indeed pseudo 2nd order was the best fit model as compared to first order and intraparticle diffusion models in the Appendix A: Tables A4 and A5. It was finally observed that the k_2 values increased as the temperature increased up to a point when the temperature no longer had a positive impact on adsorption process, further confirming that adsorption of DBT on amarula waste was favoured at lower temperatures. However, the coefficient of determination alone is not enough to provide the

criterion of the best fit of the model [56],[59],[62]. Therefore, these kinetic models were further validated by applying the Chi-square (χ^2) statistic model.

The Chi-square test model is described as the sum of the squares of differences between experimental data ($q_{e\ exp}$) and calculated or predicated data ($q_{e\ calc}$) from the model [11],[63],[64]. Chi-square test is given by Equation 4.10 where it states that if the values from the model is similar to the experimental data, then x^2 value would be a small value and vice versa.

$$\chi^2 = \Sigma(q_{e\ exp} - q_{e\ calc})^2/\Sigma q_{e\ calc} \qquad \textbf{Eq. 4.10}$$

The results revealed that pseudo second-order kinetic model had smallest values of x^2 for all the amarula waste types, as shown in Table 4.8, when compared to values obtained in pseudo 1st order kinetics and intraparticle diffusion kinetic models. Therefore, it was concluded that chemisorption was the rate-controlling step for the overall adsorption mechanism in adsorption of DBT in model diesel fuel on amarula waste biomass.

Table 4.8 Chi-square values of amarula waste biomass from the kinetic models

Calculated Chi squre (x^2) values			
	1st order	**2nd order**	**Intra**
Raw AmSh	0,513	0,00039	0,021
Raw AmSe	0,971	0,00027	0,010
Raw AmWa	0,065	0,00066	0,019

4.3.2.6 Adsorption isotherms

Adsorption isotherms were used to describe the distribution of the DBT molecule in model diesel fuel on the three types of amarula waste biomass. The interest arose from the fact that these isotherms' assumptions are based (i) on the surface homogeneity or heterogeneity of the adsorbent, (ii) the type of adsorbent coverage during the adsorption process, (iii) and the interactions between the adsorbent and the adsorbate. Moreover, they interpret the efficiency of the adsorbent that will adsorb in an undertaken system. For this matter, different adsorption isotherms have been applied for different adsorption processes by different scientists and researchers [3],[11],[51],[64],[65]. Therefore, in this study, Langmuir isotherms and

Freundlich isotherms were used to determine the equilibrium characteristics during sorption of the DBT sulphur molecule in model diesel fuel.

Table 4.9 Parameters of separation factor

Separation factor (S_f)	Parameters
$0 < s_f < 1$	Favoured
$s_f > 1$	Unfavoured
$s_f = 1$	Linear
$s_f = 0$	Reversible

Table 4.10 Adsorption isotherm of raw amarula shell biomass waste

Adsorption Isotherm on Raw AmSh							
Temperature	Langmuir				Freundlich		
(K)	q_m	K_L	S_f	r^2	K_F	n	r^2
293,15	0,00350	-0,013	1,32	0,9969	6,98E-08	8,28	0,5488
298,15	0,00860	-0,015	1,79	0,9907	5,02E-04	3,80	0,6371
308,15	0,00060	-0,013	1,06	0,9992	1,66E-12	13,80	0,9216
318,15	0,00004	-77,519	1,00	0,9969	6,94E-10	10,56	0,4311
328,15	0,00002	-82,645	1,00	0,9986	4,59E-17	18,92	0,3982

The Langmuir isotherm is expressed in Equation 4.11 [66]:

$$q_e = q_m K_L C_e / 1 + K_L C_e \qquad \text{Eq. 4.11}$$

where q_e(mg/g) and C_e (ppmw) are the amount of organo-sulphur adsorbed on the amarula waste samples and the content of the DBT in model diesel at equilibrium, respectively. The theoretical capacity monolayer is denoted by constant q_m(mgg^{-1}), whereas the affinity of binding energy is given by Langmuir constant K_L(gmg^{-1}). Equation 4.11 was linearized to obtain the Eadiee-Hoffsiee linearized Langmuir Type 3 expressed in Equation 4.12 by Tran et al. [67].

$$q_e = q_m - (1/K_L)(q_e/C_e) \qquad \text{Eq. 4.12}$$

Here the plot of q_e vs q_e/C_e was obtained for the three amarula waste as shown in Fig. 4.13(a). The constants q_m and K_L were determined from the intercept and the slope, respectively. The adsorption isotherm parameters for the effect of adsorption temperature on amarula waste samples are shown in Tables 4.10, 4.11 and 4.12. The results showed that, as the adsorption temperature increased from 20 °C to 25 °C, the q_{max} on the raw AmSh, AmSe and AmWa waste increased to 0.0086 mg/g, 0.0035 mg/g and 0.0015 mg/g respectively. As the temperature increased further, the q_{max} then decreased. This implies that the adsorption monolayer was highly favoured at 25 °C because that is where the maximum adsorption capacity was higher. Furthermore, the adequacy of the sorption process was evaluated by the separation factor (s_f), which was proposed by Hall in 1966 and is expressed in Equation 4.13 [68]:

Table 4.11 Adsorption isotherms of amarula seed biomass

Adsorption Isotherm on Raw AmSe							
Temperature	Langmuir				Freundlich		
(K)	q_m	K_L	S_f	r^2	K_F	n	r^2
293,15	0,0008	-0,0121	-0,11	0,999	1,76E-20	23,11	0,811
298,15	0,0035	-0,0134	-0,24	0,997	4,53E-07	7,33	0,5866
308,15	0,0011	-0,0122	-0,12	0,999	3,49E-17	19,18	0,6427
318,15	0,0005	-0,0118	-0,08	0,9996	4,21E-26	29,69	0,7381
328,15	0,0025	-0,0126	-0,16	0,9981	5,73E-01	-377,27	0,2323

$$s_f = 1/1 + K_L C_o \qquad \textbf{Eq. 4.13}$$

The C_o is the initial concentration of sulphur in DBT model diesel. It is reported by researchers in [51],[64],[65],[68] that when the sorption is favoured, then the separation factor will follow the trend in Table 4.9, which shows the relationship of isotherm parameters and isotherm shape. For this reason, the values of s_f for AmSe and AmWa waste were found to be higher than 1, signifying unfavorability of adsorption, whereas for the AmSh waste the values were less than 0, showing the irreversibility of the adsorption.
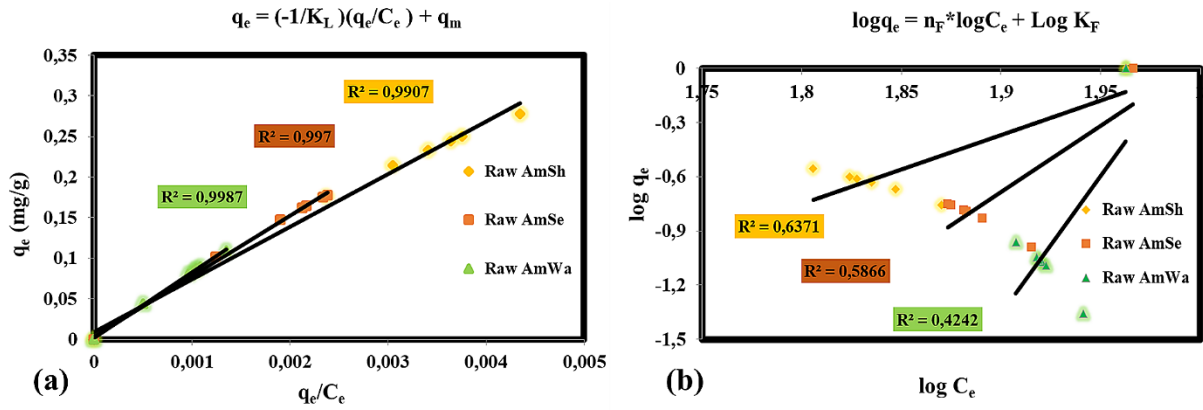
Fig. 4.13. The graphs of (a) Type 3 Langmuir isotherm and (b) Freundlich isotherm for DBT on amarula waste biomass

Freundlich isotherms is a model that assumes the heterogeneous sorption due to various sorption sites and it is denoted by a non-linear Equation 4.14 as in [69]:

$$q_e = K_F(C_e)^n \qquad\qquad \textbf{Eq. 4.14}$$

where K_F (mg/g) and n are the constants related to sorption capacity and sorption intensity. The linearized form of Equation 4.14 is shown in Equation 4.15 as:

$$\log q_e = n\log C_e + \log K_F \qquad\qquad \textbf{Eq. 4.15}$$

Table 4.12 Adsorption isotherm of raw amarula fruit waste biomass

Adsorption Isotherm on Raw AmWa							
Temperature	Langmuir				Freundlich		
(K)	q_m	K_L	S_f	r^2	K_F	n	r^2
293,15	0,000300	0,0118	2,08	0,9996	6,01E-31	35,40	0,8581
298,15	0,001500	0,0123	2,13	0,9987	6,65E-14	15,25	0,4242
308,15	1,30E-03	0,0124	2,13	0,9988	5,11E-15	16,64	0,6334
318,15	6,00E-04	0,0120	2,10	0,993	1,34E-22	25,59	0,79
328,15	1,90E-03	0,0129	2,18	0,9987	2,79E-02	1,40	0,6066

at which a plot of log q_e vs log C_e (shown in Fig. 4.13 (b)) was used to calculate the constant n and K_F. This isotherm states that if n constant is greater than 1, then the adsorption was physical.

In conclusion, the maximum monolayer adsorption of DBT in model diesel fuel on AmSh, AmSe and AmWa waste biomass was favoured at 25 °C and below. This was shown in Tables 4.10, 4.11 and 4.12 at which the q_{max} was the highest. Above 25 °C the q_{max} decreased and fluctuated. In addition, these isotherm findings were found to be consistent with the discussions in section 2.2 above, at which the highest percentage adsorption efficiency of DBT on raw AmWa was observed at 20 °C, whereas for raw AmSh and raw AmSe the highest percentage removal of DBT was observed at 25 °C.

4.3.2.7 Sorption thermodynamic study

4.3.2.7.1 Activation energy

The activation energy (E_a) is the minimum kinetic energy required to carry out a reaction. In sorption processes, it measures the energetic barrier that the adsorbate molecule must ride on to the sorption sites. To determine the activation energy of the sorption process of organo-sulphur by raw amarula waste biomass, the pseudo 2nd-order rate constants, K_2, were used in Arrhenius Equation 4.16, which is expressed as [51].

$$lnK_2 = lnA - (E_a/R)1/T \qquad \textbf{Eq. 4.16}$$

This equation was used to evaluate the relationship between rate constant and sorption temperature at which E_a (KJ/mol) is the activation energy, A is the Arrhenius constant, K_2 is a pseudo-2nd order kinetics constant, R is the gas constant (KJ/mol) and T is the absolute temperature in kelvin (K). Table 4.13 shows the activation energy of the sorption process which was then obtained from a plot of lnK_2 vs 1/T for raw AmSh, AmSe and AmWa wastes. It is reported that if the activation energy of an adsorption process is less than 21 KJ/mol, then the sorption process is controlled by mass transfer [51]. For this reason, it can be concluded that the sorption process of the organo-sulphur molecule on raw AmSe and AmWa waste biomasses mainly occurred via mass transfer. This therefore confirms the kinetics observed in Fig. 4.11 (d) for multiple steps during intraparticle diffusion model: that the adsorption of the organo-sulphur molecule was controlled not only by chemisorption, but also by other adsorption mechanisms. Raw AmWa waste biomass was further found to have a negative activation energy, implying the presence of multiple steps during the diffusion process. This was also stated by Samaniego et al. [51].

4.3.2.7.2 Thermodynamic parameters

Table 4.13 further shows the values of the thermodynamic parameters; Gibbs free energy change ($\Delta G°$), enthalpy change ($\Delta H°$) and entropy change ($\Delta S°$). They were used to evaluate the spontaneity and the heat change of the sorption process by applying the following equations from [51],[70],[47],[71]:

$$K_d = q_e/C_e \qquad \textbf{Eq. 4.17}$$

The dimensionless constant K_d was obtained from a ratio of the amount adsorbed at equilibrium to the concentration of the adsorbed solution at equilibrium as shown in Equation 4.17. It was then used in the Van Hoff plot in Equation 4.18. This was done to determine the enthalpy change and the entropy change from the graph of $\ln K_d$ vs $1/T$ shown in Appendix A: Fig. A2:

$$\ln K_d = -\Delta H°/RT + \Delta S°/R \qquad \textbf{Eq. 4.18}$$

$$\Delta G° = -RT\ln K_d \qquad \textbf{Eq. 4.19}$$

$$\Delta G° = \Delta H° - T\,\Delta S° \qquad \textbf{Eq. 4.20}$$

Equation 4.19 was therefore used to determine the Gibbs free energy whereas Equation 4.20 simply showed that Gibbs free energy is a function of enthalpy and a change in entropy.

Table 4.13 Values of activation energy and thermodynamic parameters of DBT adsorption on amarula waste biomass samples

Ads type	Ea (kJ/mol)	$\Delta H°$ (kJ/mol)	$\Delta S°$ (kJ/mol)	$\Delta G°$ (kJ/mol)				
				293,15K	298,15 K	308,15 K	318,15 K	328,15 K
Raw AmSh	0,071	-23,68	-0,13	14,99	13,48	16,28	16,86	18,92
Raw AmSe	0,030	0,84	-0,05	16,78	15,02	17,13	17,81	17,58
Raw AmWa	6,1E-05	4,99E-06	-7,48E-06	17,15	17,01	16,99	18,12	18,02

Therefore, the results in Table 4.13 showed the positive values for Gibbs free energy ($\Delta G°$) of the DBT sulphur molecule for the amarula waste biomass, revealing non-spontaneous adsorption process. However, as the absolute temperature increased from 293,15 K to 298,15 K, the positive values in Gibbs free energy change decreased, but as the temperature further increased from 298.15 K to 328.15K, the Gibbs free energy change increased indicating that the optimal temperature for adsorption of DBT on this waste biomass was 298.15K, where the

lowest value of ΔG° was observed. Despite this, other researchers used natural biomass as a sorbent for the removal of a steric molecule (Congo red) or metals and found negative ΔG° [70],[71]. These negative values of ΔG° were also found during adsorptive desulphurisation of model fuels on novel mesoporous materials [47]. Nevertheless, some researchers obtained similar positive values for ΔG° as in this study during the adsorption of sulphur compounds on synthesised adsorbents such as activated carbons [51],[72].

Calculations of enthalpy change (ΔH°) for AmSh waste showed negative values, revealing the exothermic process due to the interaction of the DBT molecule and the AmSh surface [70],[71]. This may also be due to the higher intraparticle diffusion, which was also observed in section 4.3.2.5 above for the kinetic model. On the contrary, the AmSe and AmWa waste had positive values of enthalpy change, indicating endothermic adsorption [47]. The negative values of the entropy change (ΔS°) proved that there was the decrease randomness and the decrease in the degrees of freedom at the interface between the amarula waste biomass and the DBT model diesel fuel.

4.4 Economic feasibility and environmental impact

Cost is as important as the quality of the adsorption process, but it is found to be difficult to have fixed values because the cost may differ from sales to sales representative even if the adsorbent is derived from the same materials. The cost of the adsorption process depends also on the adsorbent type used to reduce the sulphur content in diesel fuel. The abundant amarula waste was found on a landfill; therefore, there is no cost associated with it, except the cost of transportation. Instead, the use of the waste serves as a waste management and a land pollution solution, which makes it a green adsorbent that is more environmentally friendly. On the other hand, the cost of activated carbon production accounts for the energy used during production, handling, transportation chemicals, and the materials used.

4.5 Conclusion

The AmSh, AmSe and AmWa waste biomasses were found to be capable of reducing organo-sulphur content in Dibenzothiophene model diesel fuel by 30 %, 19 % and 9,5 %, respectively.

The high adsorptivity of DBT on AmSh waste biomass was based on its structural properties which confirmed its high crystallinity compared to the AmSe and AmWa waste biomasses. The three amarula waste samples were found to have an agglomerated morphology, but surface analysis confirmed the high density of O-functional groups, which also contributed in the adsorption of the sulphur molecule. The XRD analysis confirmed that all three biomass types exhibited a crystalline structure due to the high presence of cellulose. The thermal analysis confirmed that the AmSh waste is more thermally stable before and after adsorption. The surface textural analysis confirmed that the adsorption depends not only on the surface area, but also on the type of pores present in the amarula waste biomass. Moreover, crystallinity was also found to play an important role in the adsorption of the DBT molecule. The kinetic models confirmed that the adsorption mechanism involved multi-steps, with chemisorption being the overall rate-controlling step and diffusion being the rate-limiting step. In addition, the adsorption isotherms revealed Langmuir as the favoured isotherm in this study. It was also concluded that based on the result of adsorption thermodynamic studies, the adsorption of DBT on AmSh waste biomass was exothermic whereas for AmSe and AmWa waste biomasses the adsorption was endothermic. Overall, amarula waste biomass was found to be an environmentally friendly and sustainable green adsorbent that can mitigate the issue of waste management and therefore overcome problems of climate change at a lower cost.

4.6 Acknowledgements

4.7 References

[1]   C. Song, "An overview of new approaches to deep desulfurization for ultra-clean gasoline, diesel fuel and jet fuel," *Catal. Today*, vol. 86, pp. 211–263, 2003, doi: 10.1016/S0920-5861(03)00412-7.

[2]   R. Zhao, Z. Jin, J. Wang, G. Zhang, D. Zhang and Y. Sun, "Adsorptive desulfurization of model fuel by S, N-codoped porous carbons based on polybenzoxazine," *Fuel*, vol. 218, pp. 258–265, 2018, doi: 10.1016/j.fuel.2018.01.043.

[3]   T. A. Saleh and G. I. Danmaliki, "Adsorptive desulfurization of dibenzothiophene from fuels by rubber tyres-derived carbons: Kinetics and isotherms evaluation," *Process Saf. Environ. Prot.*, vol. 102, pp. 9−19, 2016, doi: 10.1016/j.psep.2016.02.005.

[4]   M. Moyo, U. Guyo, G. Mawenyiyo, N. P. Zinyama, and B. C. Nyamunda, "Marula seed husk (*Sclerocarya birrea*) biomass as a low cost biosorbent for removal of Pb (II) and Cu (II) from aqueous solutions," *J. Ind. Eng. Chem.*, vol. 27, pp. 126–132, 2014, doi: 10.1016/j.jiec.2014.12.026.

[5]   M. Abdelkreem, "Adsorption of phenol from industrial wastewater using olive mill waste," *APCBEE Procedia*, vol. 5, pp. 349–357, 2013, doi: 10.1016/j.apcbee.2013.05.060.

[6]   A. B. F. Câmara, R. V Sales, L. C. Bertolino, R. P. P. Furlanetto and E. Rodríguez, "Novel application for palygorskite clay mineral: A kinetic and thermodynamic assessment of diesel fuel desulfurization," *Adsorption*, vol. 26, pp. 267−282, 2020.

[7]   M. Ishaq, S. Sultan, I. Ahmad, H. Ullah, M. Yaseen and A. Amir, "Adsorptive desulfurization of model oil using untreated, acid activated and magnetite nanoparticle loaded bentonite as adsorbent," *J. Saudi Chem. Soc.*, vol. 21, pp. 143−151, 2017, doi: 10.1016/j.jscs.2015.02.003.

[8]   C. Song, "Zeolite-based adsorbents for desulfurization of jet fuel by selective adsorption," *Fuel Chem. Div. Prepr.*, vol. 47, pp. 2–4, 2002.

[9]   T. Wang, X. Li, W. Dai, Y. Fang and H. Huang, "Enhanced adsorption of dibenzothiophene with zinc/copper-based metal–organic frameworks," *J. Mater. Chem. A*, vol. 3, pp. 21044–21050, 2015, doi: 10.1039/C5TA05204A.

[10] M. Fadel, N. M. Hassanein, M. M. Elshafei, A. H. Mostafa, M. A. Ahmed, and H. M. Khater, "Biosorption of manganese from groundwater by biomass of Saccharomyces cerevisiae," *HBRC J.*, vol. 13, pp. 106–113, 2017, doi: 10.1016/j.hbrcj.2014.12.006.

[11] V. Emmanuel, P. Themba, D. Ntuli, and A. Enakpodia, "Biosorption of hexavalent chromium from aqueous solutions by macadamia nutshell powder," *Appl. Water Sci.*, vol. 7, pp. 3015–3030, 2017, doi: 10.1007/s13201-016-0412-5.

[12] N. E. El-Naggar, R. A. Hamouda, I. E. Mousa, M. S. Abdel-hamid, and N. H. Rabei, "Biosorption optimization, characterization, immobilization and application of Gelidium amansii biomass for complete Pb^{2+} removal from aqueous solutions," *Sci. Rep.*, vol. 8, pp. 1–19, 2018, doi: 10.1038/s41598-018-31660-7.

[13] Z. Kariuki, J. Kiptoo, and D. Onyancha, "Biosorption studies of lead and copper using rogers mushroom biomass 'Lepiota hystrix,'" *South African J. Chem. Eng.*, vol. 23, pp. 62−70, 2017, doi: 10.1016/j.sajce.2017.02.001.

[14] P. Baltzopoulou, K. X. Kallis, G. Karagiannakis, and A. G. Konstandopoulos, "Diesel fuel desulfurization via adsorption with the aid of activated carbon: Laboratory- and pilot-scale studies," *Energy & Fuels*, vol. 29, pp. 5640–5648, 2015, doi: 10.1021/acs.energyfuels.5b01133.

[15] R. Zhang, J. Zhang, X. Zhang, C. Dou, and R. Han, "Adsorption of Congo red from aqueous solutions using cationic surfactant modified wheat straw in batch mode: Kinetic and equilibrium study," *J. Taiwan Inst. Chem. Eng.*, vol. 45, pp. 2578–2583, 2014, doi: 10.1016/j.jtice.2014.06.009.

[16] A. A. Mariod and S. I. Abdelwahab, "*Sclerocarya birrea* (marula), an African tree of nutritional and medicinal uses: A review *Sclerocarya birrea* (marula)," *Food Reviews international*, vol. 28, pp. 375 −388, 2017, doi: 10.1080/87559129.2012.660716.

[17] T. A. Saleh, "Simultaneous adsorptive desulfurization of diesel fuel over bimetallic nanoparticles loaded on activated carbon," *J. Clean. Prod.*, vol. 173, pp. 2123–2132, 2018, doi: 10.1016/j.jclepro.2017.11.208.

[18] M. Thyrel, "Spectroscopic Characterization of Lignocellulosic Biomass" *Thesis - Sweden Univ of agric Scie*, 2014.

[19] P. Bajpai, "Structure of lignocellulosic biomass, In: Pretreatment of lignocelosic biomass for biofuel production," *Green Chem. for Sustainability,* vol, 34, pp. 7−12, 2016, doi: 10.1007/978-981-10-0687-6.

[20] M. K. D. Rambo, F. L. Schmidt and M. M. C. Ferreira, "Analysis of the lignocellulosic components of biomass residues for biorefinery opportunities," *Talanta*, vol. 144, pp. 696–703, 2015, doi: 10.1016/j.talanta.2015.06.045.

[21] "ASTM, standard method for determination of moisture content in biomass, Society of Testing Materials International (2003), West Conshohocken, USA," *Soc. Test. Mater. Int.*, 2003.

[22] A. Monshi, M. R. Foroughi and M. R. Monshi, "Modified Scherrer equation to estimate more accurately nano-crystallite size using XRD," *World J. Nano Sci. Eng.*, vol. 2, pp. 154–160, 2012.

[23] C. X. D. Zhang L.H., Dong L., Wang L.J., Wang T. P. Zhang L., "Effect of steam-explosion on biodegradation of lignin in wheat straw," *Bioresour. Technol.*, vol. 99, pp. 8512–8515, 2008.

[24] "ASTM D 3174-04, standard method for ash in the analysis sample of coal and coke," *West Conshohocken, USA*, 2004.

[25] "ASTM D 3175-07, Standard method for volatile matter in the analysis sample of coal and coke," *West Conshohocken, USA*.

[26] B. Salman, M. Y. Ong, S. Nomanbhay, A. A. Salema, R. Sankaran and P. L. Show, "Thermal analysis of Nigerian oil palm biomass with Sachet-Water plastic wastes for sustainable production of biofuel.", *Processes,* vol. 7, 2019.

[27] B. Rubio, M. C. Mayoral, M. T. Izquierdo and J. M. Andre, "Different approaches to proximate analysis by thermogravimetry analysis," vol. 370, pp. 91–97, 2001.

[28] P. D. Pathak, S. A. Mandavgane and B. D. Kulkarni, "Fruit peel waste: characterization and its potential uses," *Curr. Sci.*, vol. 113, pp. 444−454, 2017.

[29] H. Yang, "Characteristics of hemicellulose, cellulose and lignin pyrolysis," *Fuel*, vol. 86, pp. 1781−1788, 2007, doi: 10.1016/j.fuel.2006.12.013.

[30] L. C. Terron and M. Zamorano, "Thermal events during the combustion of agricultural and forestry lopping residues," *Material and Processes for Energy; Com. Curr. Resea. Techno. Dev.,* pp. 407–413, 2013.

[31] R. Muktham, A. S. Ball, S. K. Bhargava, and S. Bankupalli, "Study of thermal behavior of deoiled karanja seed cake biomass: Thermogravimetric analysis and pyrolysis kinetics," *Energ. Scie. Snd Eng.*, vol. 4, pp. 86−95, 2016, doi: 10.1002/ese3.109.

[32] L. Burhenne, J. Messmer, T. Aicher and M. P. Laborie, "The effect of the biomass components lignin, cellulose and hemicellulose on TGA and fixed bed pyrolysis," *J. Anal. Appl. Pyrolysis*, vol. 101, pp. 177–184, 2013, doi: 10.1016/j.jaap.2013.01.012.

[33] H. Yang, "Characteristics of hemicellulose, cellulose and lignin pyrolysis," *Fuel*, vol. 86, pp. 1781–1788, 2007, doi: 10.1016/j.fuel.2006.12.013.

[34] H. Say, "High surface area mesoporous activated carbon from tomato processing solid waste by zinc chloride activation: Process optimization, characterization and dyes adsorption," *J. Clean Prod.,* vol. 113, pp. 995−1004, 2016, doi: 10.1016/j.jclepro.2015.12.055.

[35] F. Dowell and D. Wang, "Qualitative and quantitative analysis of lignocellulosic biomass using infrared techniques: A," *Appl. Energy*, vol. 104, pp. 801–809, 2013.

[36] M. Seredych and T. J. Bandosz, "Applied catalysis B: Environmental removal of dibenzothiophenes from model diesel fuel on sulfur rich activated carbons," *Applied Catal. B, Environ.*, vol. 106, pp. 133–141, 2011, doi: 10.1016/j.apcatb.2011.05.016.

[37] S. T. Sing, S. W. Kenneth, E. H. . Everett, R. A. Haul and J. Rougerol, "Reporting physisorption data for gas/solid systems with special reference to the determination of surface area and porosity," *Pure Appl. Chem.*, vol. 54, pp. 603, 1985.

[38] L. Deng B. Lu, T. Li, G. Lv, S. Du, J. Shi, Y. Yang., "Effect of pore structure and oxygen-containing groups on adsorption of dibenzothiophene over activated carbon," *Fuel*, vol. 200, pp. 54–61, 2017, doi: 10.1016/j.fuel.2017.03.018.

[39] E. S. Moosavi, S. A. Dastgheib and R. Karimzadeh, "Adsorption of thiophenic compounds from model diesel fuel," *Energies,* vol 10, pp. 4233–4250, 2012, doi: 10.3390/en5104233.

[40] M. Thommes, K. Kaneko, A Neimark, J. P. Olivier, F. Rodriguez-Reinoso, J. Rouquerol, K. S.W. Sing., "Physisorption of gases, with special reference to the evaluation of surface area and pore size distribution (IUPAC Technical Report)," *Pure & Appled Chem.,* vol. 87, pp. 1051–1069, 2015, doi: 10.1515/pac-2014-1117.

[41] A. U. Rajapaksha, M. Vithanage and S. S. Lee, "Steam activation of biochars facilitates kinetics and pH-resilience of sulfamethazine sorption," *J. Soils Sediments*, vol. 16, pp. 889−895, 2015, doi: 10.1007/s11368-015-1325-x.

[42] S. Huang and G. Lin, "Biosorption of Hg (II) and Cu (II) by biomass of dried Sargassum fusiforme in aquatic solution," *J. Evironmental Heal Scie and Eng.*, vol. 13, pp. 6–13, 2015, doi: 10.1186/s40201-015-0180-4.

[43] B. Nagy, C. Mânzatu, A. Măicăneanu, C. Indolean, L. Barbu-Tudoran and C. Majdik, "Linear and nonlinear regression analysis for heavy metals removal using Agaricus bisporus macrofungus," *Arab. J. Chem.*, vol. 10, pp. S3569−S3579, 2017, doi: 10.1016/j.arabjc.2014.03.004.

[44] P. G. González and Y. B. Pliego-cuervo, "Physicochemical and microtextural characterization of activated carbons produced from water steam activation of three bamboo species," *J. Anal. Appl. Pyrolysis*, vol. 99, pp. 32–39, 2013, doi: 10.1016/j.jaap.2012.11.004.

[45] A. Saleh, K. O. Sulaiman, S. A. Al-hammadi, H. Dafalla and I. Danmaliki, "Adsorptive desulfurization of thiophene, benzothiophene and dibenzothiophene over activated carbon manganese oxide nanocomposite: With column system evaluation," *J. Clean. Prod.,* vol. 154, pp. 401−412, 2017, doi: 10.1016/j.jclepro.2017.03.169.

[46] W. Ahmad, I. Ahmad, M. Ishaq and K. Ihsan, "Adsorptive desulfurization of kerosene and diesel oil by Zn impregnated montmorollonite clay," *Arab. J. Chem.*, vol. 10, pp. S3263–S3269, 2017, doi: 10.1016/j.arabjc.2013.12.025.

[47] M. Ahmadi, M. Mohammadian and M. R. Khosravi-nikou, "Experimental, kinetic, and thermodynamic studies of adsorptive desulfurization and denitrogenation of model fuels using novel mesoporous materials," *J. Hazard. Mater.*, vol. 374, pp. 129–139, 2019, doi: 10.1016/j.jhazmat.2019.04.029.

[48] A. Kosa, A., Al-Zhrani, G., Salam, "Removal of heavy metal from aqueous solution by

multi-walled carbon nanotubes modified with 8-hydroxyquinoline," *Chem. Eng.*, vol. 181, pp. 159–168, 2012.

[49]   Y. N. Prajapati, B. Bhaduri, H. C. Joshi, A. Srivastava and N. Verma, "Chemosphere Aqueous phase adsorption of different sized molecules on activated carbon fibres: Effect of textural properties," *Chemo*, vol. 155, pp. 62–69, 2016, doi: 10.1016/j.chemosphere.2016.04.040.

[50]   M. Muzic, K. Sertic-bionda, Z. Gomzi, S. Podolski and S. Telen, "Chemical engineering research and design study of diesel fuel desulfurization by adsorption," *Chem. Eng. Res. Des.*, vol. 88, pp. 487–495, 2009, doi: 10.1016/j.cherd.2009.08.016.

[51]   M. L. Samaniego, M. D. G. de Luna, D. C. Ong, M. Wan and M. Lu, "Isotherm and thermodynamic studies on the removal of sulfur from diesel fuel by mixing-assisted oxidative − adsorptive desulfurization technology," *Energy & Fuels*, vol. 33, pp. 1098–1105, 2019, doi: 10.1021/acs.energyfuels.8b04242.

[52]   Lagergren. S Zur, "Theorie der Sogenannten Adsorption Gelöster Stoffe, Kungliga Svenska Vetenskapsakademiens," *Handlingar*, vol. 24, pp. 1–39, 1898.

[53]   M. Blanchard G, Maunaye.M, "Removal of heavy-metals from waters by means of natural zeolites," *Water Resour.*, vol. 8, pp. 1501–1507, 1984.

[54]   Y. Ho, "Adsorption of heavy metals from waste streams by peat," PhD. thesis,. *The University of Birmingham*, 1995.

[55]   W. J. Weber Jr, J. C. Morris, "Kinetics of adsorption on carbon from solution," *J. Sanit. Eng. Div.*, vol. 89, pp. 31–60, 1963.

[56]   A. D. Bucchianico, "Coefficient of determination (R^2)," *Encycl. Stat. Qual. Reliab. Wiley Online Libr.*, 2008.

[57]   H. Nguyen, S. You, and A. Hosseini-bandegharaei, "Mistakes and inconsistencies regarding adsorption of contaminants from aqueous solutions: A critical review," *Water Res.*, vol. 120, pp. 88–116, 2017, doi: 10.1016/j.watres.2017.04.014.

[58]   M. K. Nazal, M. Khaled, M. A. Atieh, I. H. Aljundi, G. A. Oweimreen and A. M. Abulkibash, "The nature and kinetics of the adsorption of dibenzothiophene in model diesel fuel on carbonaceous materials loaded with aluminum oxide particles," *Arab. J.*

Chem., vol 12, pp. 3678−3691, 2019, doi: 10.1016/j.arabjc.2015.12.003.

[59]   J. Simonin, "On the comparison of pseudo-first order and pseudo-second order rate laws in the modeling of adsorption kinetics," *Chem. Eng. J.*, vol. 300, pp. 254–263, 2016, doi: 10.1016/j.cej.2016.04.079.

[60]   M. A. Abuh, G. K. Akpomie, N. K. Nwagbara, N. A. Bassey, and D. I. Ape, "Kinetic rate equations application on the removal of copper (II) and Zinc (II) by unmodified lignocellulosic fibrous layer of palm tree trunk – single component system studies," *Int. J. Rece. Appl. Scie.,* vol 1, pp. 800–809, 2010.

[61]   T. S. Pant and K. K. & Sing, "Equilibrium, kinetics and thermodynamics study for adsorption of As(II) ions on activated alumina," *Sep. Purifications Technol.*, vol. 3, pp. 139–147, 2004.

[62]   W. Guthrie, "Engineering statistics handbook, section 4.4: Model validation," <http://www.itl.nist.gov/div898/handbook/index.htm>, NIST/SEMATECH, 2013.

[63]   A. Kaushal, "Critical analysis of adsorption data statistically," *Appl. Water Sci.*, vol. 7, no. 6, pp. 3191–3196, 2017, doi: 10.1007/s13201-016-0466-4.

[64]   A. A. Inyinbor, F. A. Adekola, and G. A. Olatunji, "Kinetics, isotherms and thermodynamic modeling of liquid phase adsorption of rhodamine B dye onto raphia hookerie fruit epicarp," *Water Resour. Ind.*, vol. 15, pp. 14−27, 2016, doi: 10.1016/j.wri.2016.06.001.

[65]   A. O. Dada, A. P. Olalekan, O. Dada, "Langmuir, Freundlich, Temkin and Dubinin – Radushkevich isotherms studies of equilibrium sorption of Zn 2 + unto phosphoric acid modified rice husk," *IOSR. J. App. Chem.,* vol. 3, pp. 38–45, 2012.

[66]   I. Langmuir,. The adsorption of gases on plane surfaces of glass, mica and platinum. " *Am. Chem. Soc.*, vol. 40, pp. 1361–1403, 1918.

[67]   H. N. Tran, S. J. You, A. Hosseini-Bandegharaei and H. P. Chao, "Mistakes and inconsistencies regarding adsorption of contaminants from aqueous solutions: A critical review," *Water Research.*, vol 120, pp 88−116, 2017, doi: 10.1016/j.watres.2017.04.014.

[68]   T. Hall, K. R. Eagleton, L.C. Acrivos and A. Vermeulen, "Pore and solid-diffusion

kinetics in fixed-bed adsorption under constant-pattern conditions," *Indutrial Eng. Chem Fundam.*, vol. 5, pp. 212–223, 1966.

[69] H. Freundlich, "Über die Adsorption in L€osungen.," *Phys. Chem.*, vol. 57, pp. 385–471, 1906.

[70] A. A. Inyinbor, F. A. Adekola and G. A. Olatunji, "Kinetics, isotherms and thermodynamic modeling of liquid phase adsorption of rhodamine B dye onto raphia hookerie fruit epicarp," *Water Resour. Ind.*, vol. 15, pp. 14–27, 2016, doi: 10.1016/j.wri.2016.06.001.

[71] S. Mustapha, M. M. Ndamitso, U. M. Mohammed, N. O. Adeosun and M. Idris, "Study on activated from melon (*Citrullus lanatus*) husk as natural adsorbent for removal of hardness in water," vol. 6, pp. 1–9, 2016, doi: 10.5923/j.aac.20160601.01.

[72] D. Stan, A. Mohammed, A. Usman and M. M. Oloruntoba, "Adsorptive desulfurization of diesel using activated sewage sludge: Kinetics, equilibrium and thermodynamics studies," *Appl. Petrochemical Res.*, vol. 10, pp. 1−12, 2019, doi: 10.1007/s13203-019-00239-2.

Chapter 5

Deep Desulphurization of Diesel Fuel by Processed Amarula Waste to Activated Carbon a Low-Cost Adsorbent

Chapter abstract

This study focused on environmental pollution by mitigating the issue of waste management and climate change. Therefore, amarula waste biomass from the production of Amarula liqueur, was processed thermally by conventional heating methods. The porous activated carbons from amarula waste were produced via steam activation within 45 min. The activated carbons of amarula fruit, seed and shell waste were found to be microporous and mesoporous, with a surface area of 740 m^2/g, 437 m^2/g and 245 m^2/g respectively, and a total pore volume of 0.37, 0.21 and 0.17 cm^3/g respectively. Amarula shell waste was selected and exposed to steam for 90 min longer. The surface area was found to increase to 1 194 cm^2/g, with a total pore volume of 0.98 cm^3/g. The processed amarula waste was used for removing the toxic DBT molecule in diesel fuel using a batch reactor. These DBT molecules and their alkyl derivatives contribute to air pollution when emitted into the atmosphere. The results showed a high desulphurization efficiency of 65 ±4 %, 54 ±3 % and 31 ±6 %, respectively, at equilibrium. The activated carbon (AC) of the amarula shells was produced with a longer steam residence time and displayed an adsorption efficiency of more than 50 % within 30 min and 73 ±3 % at equilibrium. Thermal, spectroscopic, and microscopic analysis was carried out on amarula-activated carbons before and after the desulphurization of model diesel fuel.

5.1 Introduction

The marula (*Sclerocarya birrea*) fruit is an indigenous product of Africa. The marula trees are now cultivated for industrial purposes to produce large quantities of a spirit known worldwide as "Amarula" liquor, with approximately 1.2 million 9 L cases sold per year [1]. Large amount of waste is produced during the production of Amarula liqueur. These amarula wastes constist of fruits of low quality, and seeds wastes, after the pulp has been squashed during production. These wastes are discarded and dumped to the landfill, which rot and decompose to produce harmful gasses that contribute to environmental pollution [2] . It is for these reasons that this study chose to convert biomass of amarula waste (fruits, seeds, shells) to valuable products such as activated carbon, in order to develop a process to help mitigate the issue of waste management.

Activated carbons (AC) are carbonaceous materials that have been processed to create materials with various pore sizes and a high surface area. They consist mainly of cyclic carbons bonded to each other by sp^2 and sp^3 hybridization, with heteroatoms on the surface as seen in Fig. 5.1. Depending on the type of processing, the AC produced may be either graphitic or non-graphitic [3]–[4]. The global market size for AC was estimated at USD 4,72 billion in 2018, and this number is expected to increase by 17,5 % at a compound annual growth rate (CAGR) during the forecast period [5]. ACs are used as adsorbents and catalysts, and for catalytic support in various industries, such as the medicinal field, the food industry, and the nuclear, automobile, chemical, vacuum, and petrochemical industries [6].
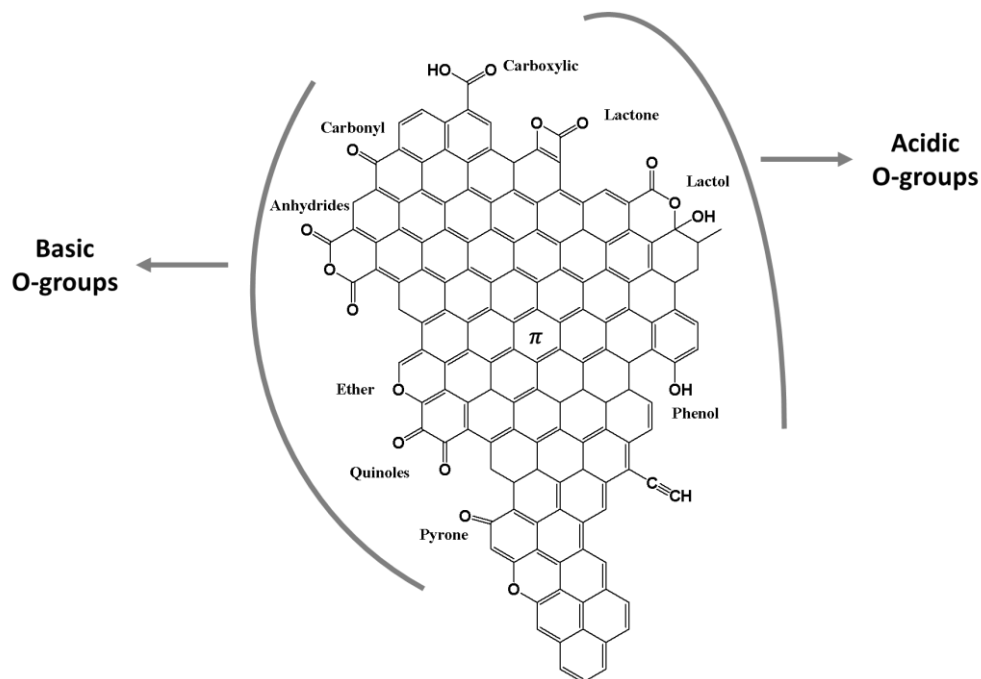
Fig. 5.1. Molecular structure of AC with basic and acidic groups

ACs are also used to remove inorganic and organic impurities during purification, separation, or water treatment. In addition, they are used for energy and gas storage, the filtration of mobile substances and the production of high-purity substances [7]. ACs are derived mostly from renewable resources such as coal which is a fossil fuel; but the use of this resource is environmentally unfriendly, and the cost of production is very high. As a result of the effects of climate change, it is advisable to resort to renewable resources such as biomass, particularly biomass waste, in order to produce ACs. In recent years, several researchers have resorted to using agricultural waste as the source of ACs to reduce costs [8]–[22].

Different carbonaceous materials produce AC with different characteristics. Marsh and Rodrigue [3] and Savova et al [23] used olive stones, cherry stones, apricot stones, and almond shells to produce AC under the same conditions and found that a precursor plays an important role in textural properties. Lo et al. [24] used Ma bamboo and Moso bamboo as precursors for ACs and found that the ACs of these bamboos had different characteristics, despite their habitats being the same.

However, the production of ACs involves microwave and conventional heating treatment. In this study, the latter treatment has been used because it is suitable for scaling-up purposes. Researchers, such as Crombi [25], Huang et al. [26], Figueiredo et al [27] and Lin et al. [28],

compared the production of ACs in their studies using both microwave and conventional heating methods and found that although the conventional heating method is time-consuming and wastes energy; but for large-scale production it is widely preferred.

It was also found that the properties of the AC depend on the activation methods used for processing. Therefore, the production of AC involves either single-step or two-step synthesis process, which is about carbonization or pyrolysis under inert conditions, followed by an activation process at an elevated temperature. The activation process can occur by chemical activation [8],[18],[27],[29]–[35],[36]–[41], such as KOH, K_2CO_3, HNO_3, H_2SO_4, PO_4H_2 or $ZnCl_2$; or by physical activation [3],[8],[15],[42]–[45],[46] such as steam, CO_2 or O_2; or by combining both chemical and physical activation [14],[11] in one process. Some researchers compared the properties of AC produced from steam and AC produced from CO_2 [3],[47]–[51]. They found that the activated carbons from steam had wider micropores and mesopores were present whereas the AC from CO_2 had narrower micropores. Some researchers determined the effect of steam residence time and found that the longer the steam stays in the system, the more the micropores are widened, the more mesopores are formed and the more the surface area increases [52].

Other researchers found that as the steam increases, the micropores widen, but the volume of the mesopores decreases and the surface area decreases [8],[20],[53]. Some researchers determined the effect of the activation temperature and found that as the temperature increases, the surface area increases along with the pore volume [53],[54]. Some researchers found that the more the temperature is increased, the more the surface area is ruptured and destroyed, which creates more macropores, but fewer micropores. Moreover, the material becomes more graphitic [9],[15],[55],[56].

For these reasons, this study used physical activation for the production of AC using steam, because it is environmentally friendly and sustainable. The mechanism of steam activation has been studied by several researchers [3],[46],[57]. It involves steam from water (H_2O) molecules; the steam oxidizes carbon (C) from a carbonaceous solid to form a water–gas product which consists of carbon monoxide (CO) and hydrogen (H_2) gas as shown in Reactions 5.1 and 5.2 below. Hydrogen gas then burns to form a water (H_2O) molecule, which further oxidizes CO to CO_2. The CO_2 continues to extract carbon from its structure and oxidizes it to CO, which goes away as a gas (Reaction 5.3), forming more mesopores and macropores.

$$C + H_2O \rightleftharpoons CO + H_2 \qquad\qquad \Delta H = 117 \text{ KJ/mol} \qquad\qquad \textbf{Reaction 5.1}$$

$$CO + H_2O \rightleftharpoons CO_2 + H_2 \qquad \Delta H = -41 \text{ KJ/mol} \qquad \textbf{Reaction 5.2}$$

$$C + H_2O \rightleftharpoons CO \qquad\qquad\qquad \textbf{Reaction 5.3}$$

In addition, steam reduces the interference of heteroatoms in the carbon structure; the water vapour produces activated carbon, which has a lower specific surface area compared to that produced from CO_2 gas. Moreover, the reaction of steam is endothermic and easy to control. For these reasons, AC that has microporosity, mesoporosity and macroporosity may be beneficial for the adsorption of larger molecules. Therefore, this study applied the processed amarula waste to AC to remove the DBT molecules in diesel fuel.

The study also looked at a possible way to mitigate the issue of climate change. Recently, the world has faced floods, tornados and excessive heat or coldness, due to global warming. This is caused by direct and indirect greenhouse gases (COx, SOx, NOx) that are emitted into the atmosphere. One of the main causes is air pollution that results from fuel-hungry industries, mainly from transportation. Transportation creates 29 % of air pollution worldwide [58], which poses a major concern; therefore, this study focused on purifying diesel fuel.

Diesel fuel is a distillate of crude oil. It contains toxic compounds such as the organo-sulphur compounds; dibenzothiophene and its alkyl derivatives. When present in high concentrations, these sulphur compounds have a negative impact on the environmental (agriculture and global warming), on the economy (corrosion), and on health (respiratory infections in human beings) []. Moreover, they are difficult to remove using available technologies, such as hydrodesulphurization (HDS) under ambient conditions [59]. In order for them to be removed, an expensive hydrogen gas must be used, and the operation must occur at a higher temperature and pressure, which is a limitation to this technique. Oxidative desulphurization (ODS) has also been employed to reduce the sulphur content in diesel fuel, using extractive solvents [60],[61]. However, these solvents are very expensive, and several processes involved are time-consuming, and present other drawbacks. The other technique that has been used is bio-desulphurization (BOD), which uses enzymes to create several pathways for the removal of organo-sulphur compounds [62]–[65], but there is a limitation in terms of instability with the process, which means it is difficult for it to be applied industrially, because the enzymes degrade at some point. The more interesting desulphurization technique is adsorptive desulphurization (ADS). It has been used by other researchers and was found to be effective [12],[61],[66]–[84]. This technique has been found to be preferable to others because it involves both reactive and unreactive adsorption. It is operated under ambient conditions. For

these reasons, there is less energy consumption, which makes it easier to regenerate the adsorbent, that may also require less energy. Moreover, ADS has been found to be capable of desulphurising the steric-alkyl organo-sulphur compounds that are difficult to reduce using other techniques, such as HDS. It has been found to be cost-effective compared to both ODS and HDS. It also provides stable processes unlike BOD, because it can be carried out using either batch or fixed-bed reactors.

The major benefit of ADS is that it is mostly suitable for small-scale operations. Despite its advantages, ADS has certain limitations: it has been found that it is mostly selective to organo-sulphur compounds and to low high-sulphur feed. Some studies have overcome this problem by connecting ADS in parallel with ODS to obtain high efficiency, particularly if needed for large-scale applications [69],[85].

ADS uses different adsorbents to obtain better efficiency for desulphurization. Several adsorbents such as metal–metal oxides [86], zeolites [87],[88], MOFs [83],[89], and other forms of carbon [73],[75],[76],[80],[90]–[92], such as ACs are mainly used in the ADS. In this study, AC was preferred because it is cheaper to produce than other adsorbents, which require several synthesis processes, in order for them to achieve high adsorption efficiency. Moreover, ACs can reduce the larger molecules of organo-sulphur compounds in diesel fuel, because of their high porosity and large surface area, which can be tuned as needed. Furthermore, it is easier to regenerate the adsorbent because the process is mainly via unreactive adsorption, which usually occurs through the Van Der Waal force's reaction. Despite its benefit in desulphurization, it has been found that AC is mainly hydrophilic and therefore can adsorb moisture that may mask the reactive surface and thus reduce its adsorption capacity. This drawback may be overcome by drying the AC before use.

The novelty of this study lies in utilizing the amarula waste biomass to ACs and using it to reduce toxic organo-sulphur content in diesel fuel, in order to mitigate environmental pollution using sustainable processes.

5.2 Materials and methodology

AC was prepared using a two-step synthesis process that involved pyrolysis and steam activation. The desulphurization process was carried out using a batch reactor.

5.2.1 Materials

The biomass used was amarula waste biomass (waste fruit, waste seeds, waste shells). The following was also used:

- horizontal electric tube furnace
- quartz tubes and quartz crucible boats
- Afrox nitrogen gas (99% purity)
- Chemicals: (99% pure reagents from sigma), dibenzothiophene (DBT), hexadecane and toluene.

5.2.2 Sampling and processing of amarula waste biomass

Amarula waste was used as the biomass. It was collected in Phalaborwa, Limpopo province. The amarula waste samples collected were divided into three categories: the amarula fruit (AmWa), the amarula seeds (AmSe) and the amarula shells (AmSh). Each part was used to produce AC under the same conditions using the heating method, a two-step synthesis.

AmSh waste biomass was used to determine the effects of applying pyrolysis temperature (600 °C, 700 °C and 800 °C) on biochar in our previous work (not reported). A temperature of 800 °C was selected as the best pyrolysis temperature for steam-activated carbon. The pyrolysis of amarula waste biomass was carried out by weighing ≈3g of dried AmSh waste in a quartz boat crucible three times, to obtain the three samples. The sample was placed inside a quartz tube and then subjected to a horizontal furnace with set parameters: temp 800 °C; ramp 10 °C/min; residence time 2 h (Fig. 5.2.). The pyrolysis process was carried out under the nitrogen gas at the flow rate of 60 ml/min, which was allowed to flow for 10min before energy was applied to the process. At the end of the process, the system was cooled to room temperature and the percentage yield of biochar was obtained. The pyrolyzed biochar was then stored for later use in a tightly sealed container after being labelled AmSh-B-800,"B" denotes biochar and "800" denotes the pyrolysis temperature. The AmSe and the AmWa waste samples were pyrolyzed as above and named AmSe-B-800 and AmWa-B-800, respectively. Fig. 5.2 is a photograph of the steam-activation process.
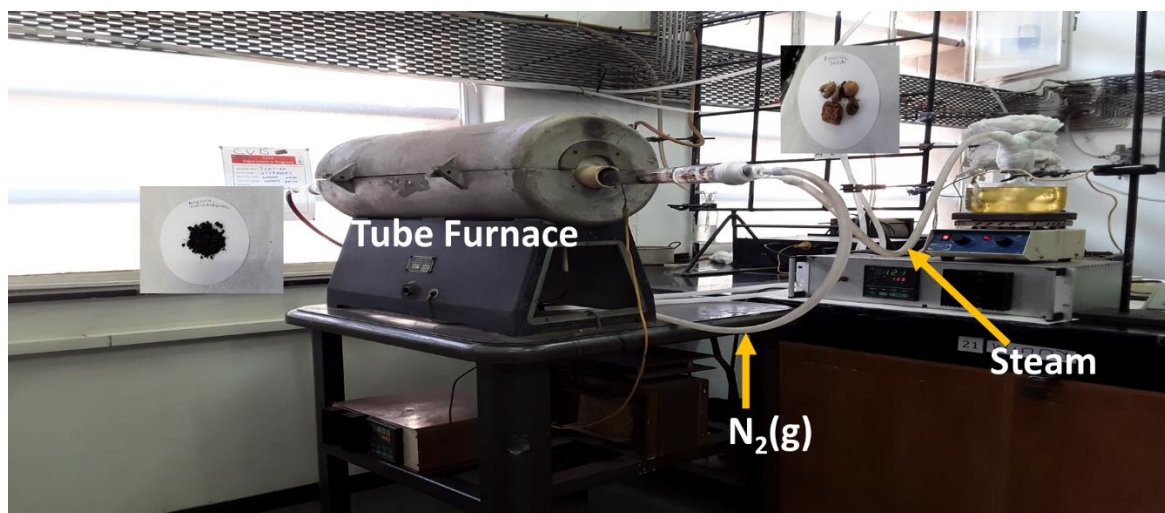
1. Pyrolysis temp = 800 °C, Pyrolysis residence time = 120 min; 2. Activation temp = 800 °C, Heating rate =10 ml/min, Inert gas = N_2 (60 ml/min), Steam residence time = 45 min (5 ml/min)

Fig. 5.2. Synthesis of ACs from amarula waste biomass

The effect of steam residence time was recorded at 30, 45, 60, 75 and 90 min intervals, when using the AmSh biochar. A steam residence time of 45 min was selected and used for the other amarula waste samples. The steam activation was carried out by crushing biochar AmSh-B-800 (>3mm) and massing it first into a crucible and then placing it in a horizontal tube furnace. Thermal energy was applied at a rate of 10 ml/min to 800 °C under the nitrogen flow rate of 60 ml/min. The supply of inert gas (N_2) was stopped when the set temperature was reached. The temperature of the activating gas (steam) was kept constant at 120 °C, using a temperature controller connected to a magnetic-stirring heating mantle. The steam was fed into a horizontal reactor at a rate of 5 ml/min for 45 min. The supply of steam was stopped, and the N_2 flow was then resumed until the reaction cooled down to room temperature. The steam-AC produced was massed to determine the percentage yield and the percentage burn-off, before being stored in a tightly sealed container and labelled: AmShAC-800ST-45min for the AmSh waste; AmSeAC-800ST-45min for the AmSe waste; and AmWaAC-800ST-45min for the AmWa waste.

5.2.3 Characterization of processed amarula waste biomass

5.2.3.1 Thermal analysis of processed amarula waste biomass

An AC with a higher percentage burn-off tends to have higher activity than one with a lower percentage burn-off. For this reason, ACs were characterized by calculating the percentage yield, as shown in Equation 5.1, in order to obtain the percentage burn-off by difference.

$$\% \text{ Yield} = (m_i - m_f/m_i)*100 \qquad \textbf{Eq. 5.1}$$

Where: m_i is the initial mass before thermal treatment; m_f is the final mass after steam activation.

The percentage burn-off characterizes the mass loss of carbon during the pyrolysis or activation process. Proximate analysis was obtained from the Thermal Gravimetry Analysis (TGA) technique under air atmosphere at a flowrate of 60 ml/min, using the TGA5500-0026 model. The process was ramped up using a heating rate of 10 °C/min to a maximum of 800 °C. Platinum HT pans were used as sample holders. Derivative Thermogravimetry (DTG) analysis was also performed under the same conditions.

5.2.3.2 Microscopic analysis

Micrograms of processed amarula waste were obtained using Field Emission – Scanning Electron Microscopy (FESEM) – JEOL JSM-7800F, coupled with energy dispersive x-ray spectroscopy (EDS). Before analysis, the samples were coated with gold, using a gold-sputtering device. Transmission electron microscopy (TEM) analysis was done on selected AmSh waste ACs; the selected AC was dispersed in the methanol solution and then sonicated for 15 min. A drop of the suspended aqueous solution of the sample was then placed onto a copper grid. This was subjected to the TEM technique using a JEOL 2010F equipped with a Schottky field-emission gun that was operated at keV, and with an ultra-high-resolution pole piece providing a point resolution of 1,9 Å.

5.2.3.3 Spectroscopic analysis

A previously-dried potassium bromide (KBr) was mixed with each thermally-processed amarula waste biomass sample to make pellets in a ratio of 1:100. Pelleted AC samples were subjected to the Fourier transform infrared (FTIR) spectroscopic technique using the Perkier Elmer Frontier model. The analysis of the functional groups present was carried out at a resolution of 8 cm^{-1} and 16 cm^{-1} scans, at which the wavelength was set at 4 000 cm^{-1}–400 cm^{-1}.

The X-ray diffraction patterns, were determined using Bruker's D2 Phaser X-ray diffractometer, and using Cu-Kα (= 0.15406 Å). The radiation source was operated under a voltage of 40 kV, with a current of 25 mA. The diffraction angle (2θ) was varied from 10º to 90º, using a scan rate of 4,2 °C/min. Peak analysis was carried out using Origin Pro 8.5 software and the deconvolution of peaks was done by peak fitting using Gaussian type. The lattice (L) size for crystalline (Lc) and amorphous (La) was further determined using Scherrer Equation 5.2:

$$\beta = K\lambda/Lcos\theta \qquad\qquad \textbf{Eq. 5.2}$$

Where: K is the constant -at which 0,9 was for Lc, and 1,84 was for La; $\acute{y}$ is the wavelength; β is the full width at half maximum (FHMW); θ is the angle of the observed peak. The interlayer spacing d$_{002}$ was carried out using Equation 5.3:

$$d_{002} = \lambda/2sin\theta \qquad\qquad \textbf{Eq. 5.3}$$

5.2.3.4 Textural properties

Branauer - Emmett - Teller (BET) surface area and porosity analyses were carried out using Micrometrics TriStar II3020 under N$_2$ adsorption at $-196°C$ at a range of relative pressure (p/p°) of 10^{-6}, at which the samples were first degassed for 12 h at 160 °C under inert gas flow. Micropores and mesopores were determined as a function of pore size using Barrett-Joyner-Halenda (BJH).

5.2.4 Application to desulphurization of model diesel DBT

5.2.4.1 Preparation of ≈ 100 ppm DBT model diesel

100 ppm dibenzothiophene (DBT) model diesel fuel was prepared by dissolving it in a solvent mixture of 85 % hexadecane and 15 % toluene, as discussed previously (see Chapter 4). All the analyses of clean and dirty diesel were carried out using the gas chromatography-pulse flame photometric detector (GC-PFPD) technique.
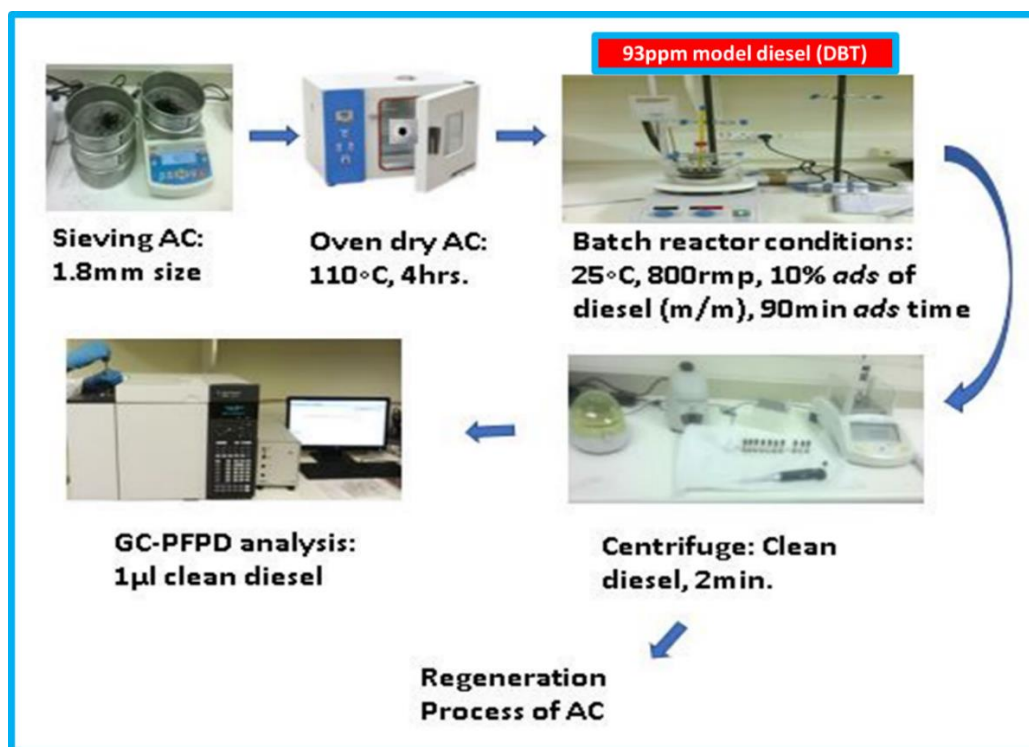
Fig. 5.3. Desulphurization process of DBT model diesel fuel, using processed amarula waste

5.2.4.2 Desulphurization of model diesel (DBT)

The synthesized AC of AmSh waste was sieved to obtain a 1–2 mm particle size (Fig. 5.3.). The sieved AmShAC-800ST was then dried in an oven-dry at 110 °C for 4 h. The dried AC was then weighed into a 50 ml round-bottomed flask using an analytical balance, and its mass was recorded. Then 10 ml of model diesel (DBT) was massed and poured into the flask containing the massed AC. The reactor (flask) was immersed in a water bath at 27 °C ±2 °C at 800 rpm with a continuous stirring of a magnetic stirrer, which was immediately started and timed as zero time. The temperature was controlled using a digital thermometer. 100 µl was pipetted into the 0,5 ml centrifuge tubes at 10 min intervals within 180 min. The pipetted reactor

samples were centrifuged using a small centrifuge for 5 min. Then 1 µl of the centrifuged clean model diesel was pipetted and injected into a GC-PFPD for analysis. The content of organo-sulphur in model diesel was determined from the chromatograms obtained. The adsorption efficiency percentage and the adsorption capacity were calculated according to Equations 5.4 and 5.5 for all synthesized ACs labelled as AmWaAC-800ST, AmSeAC-800ST and AmShAC-800ST. The C_o and C_t are the concentrations of DBT in the model diesel at the initial time and at time t in ppm, respectively. The q_t was the adsorption capacity at time t in mg/g; W_{soln} and W_{ads} are the mass of the DBT model diesel solution and the mass of processed amarula waste, respectively.

$$\text{Desulphurization efficiency \%} = ((C_o - C_t)/C_o) * 100 \qquad \textbf{Eq. 5.4}$$

$$q_t = (C_o - C_t)\, W_{soln}/W_{ads} \qquad \textbf{Eq. 5.5}$$

The AmSh ACs that were produced at different steam residence times were also subjected to desulphurization, as per Fig. 5.3.

5.3 Results and discussion

5.3.1 Characterization

5.3.1.1 The percentage burn-off for processed amarula waste

Fig. 5.4 (a) shows the effect of steam residence time on the percentage burn-off for AmShAC. The results show that as the steam residence time increases, the percentage burn-off also increases. This was because the longer the carbons are exposed to water molecules, the more the active carbon layers are extracted from the solid carbon, and the more the pores are widened. However, the indirect proportionality of percentage yield on residence time was attributable to carbons being burnt or oxidized, because they stay longer and are exposed to water vapour at high temperatures, thus eventually forming more ash. Trends such as those seen in Table 5.1 have been observed by other researchers [20],[93],[94]. Bergna et al. [46] also found similar results when they produced AC using steam at 800 °C witha holding time of 60 min. A yield of 34,3 % is achieved. But when using 240 min as the holding time, they obtained a lower percentage yield [46]. In 2018, the research team of Bergna et al. [52] used wood chips to produce ACs with a steam residence time of 120 min and 240 min, respectively, and found similar trends in percentage yield. On the other hand, Asensio et al. [95] found that in order to obtain 50 % burn-off at 800 °C at a flow rate of 1,5 µmf, a residence time of 5 h was needed but when using 850 °C under the same conditions, 50 % burn-off was obtained at 2 h (120 min) residence time.
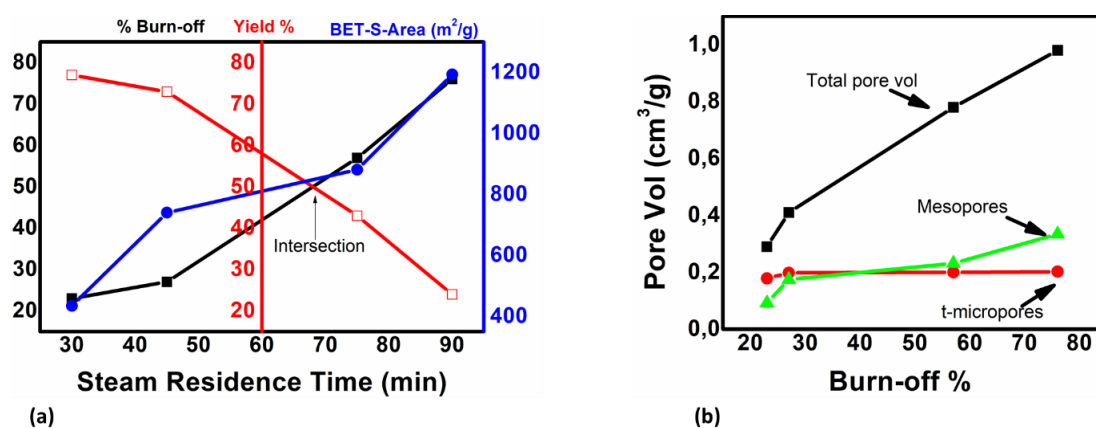
Fig. 5.4. Effect of steam residence time on (a) percentage burn-off and (b) porosity

In this study, using AmSh waste as a precursor showed that a 50 % burn-off could be obtained at 80 min residence time, with a temperature of 800 °C as shown at the intersection point (Fig

5.4 (a)). This would be ideal for industrial purposes or for scaling up to balance both the yield and the percentage burn-off, without compromising the quality of the product.

Fig. 5.4 (b) also shows that, when the percentage burn-off increased as steam residence time increased, the porosity of the AmSh ACs also increased. The graph also shows, that more mesopores were developed at above 50 % burn-off. This is contrary to the findings obtained by Rodríguez-Reinoso et al. [49]: at a higher percentage burn-off, the volume of the mesopores and the macropores decreased.

Table 5.1 Percentage burn-off of AmShAC-ST at different steam residence times

Effect of steam residence time using Amarula shells waste activated carbon		
Time (min)	% Burn-off	% Yield
30	23 ±2	77 ± 2
45	27 ±4	73 ±4
75	57 ±5	43 ±5
90	76 ±2	24 ±2

Upon comparing the percentage burn-off for different amarula waste ACs (Table 5.2), it was found that the AmWa waste had a higher percentage burn-off, followed by the AmSh waste and then the AmSe waste ACs. This is attributed to the different materials producing different percentages of burn-off, due to the different constituents in the precursor. The AmWa waste ACs precursor had the edible pulp and a nut inside the shells. The precursor of the amarula seed waste AC had only the nuts inside the shell, whereas the precursor of the shell waste AC had the pulp, but the nuts were removed. Savova et al. [23] found a different percentage burn-off when they produced ACs from almond shells, nut shells, apricot stones, cherry stones and grape seeds.

Table 5.2 Percentage burn-off for three types of amarula waste ACs

Percentage burn-off for Amarula wastes activated carbons		
AC type	% Burn-off	% Yield
AmShAC-ST	27 ±4	73 ±2
AmSeAC-ST	25 ±3	75 ±3
AmWaAC-ST	30 ±5	69 ±4

5.3.1.2 Thermal analysis of processed amarula waste

Thermal analysis has been applied by several researchers to determine the decomposition stages of the material [9],[42],[45]. In this study, TGA was performed on the processed amarula waste (AmSeAC-ST, AmSeAC-ST, and AmWaAC-ST), which showed three decomposition stages in each graph (Fig. 5.5.). The first stage (< 100 °C) was due to dehydration. It showed a tiny curve, signifying less moisture content on the surface of processed amarula wastes compared to the unprocessed amarula waste (Chapter 4). This was because the processed amarula waste was then less hydrophobic, due to a loss of polarity during processing. The second stage between 400 °C and 600 °C was due to devolatilization. It was caused by thermal decomposition of oxygen groups on the surface of ACs and during the cracking and deformation of C=C and C–H in the aromatic ring of AC [96]. The third stage - between 600 C and 800 C was due to retained residue product that consists of inorganic matter and fixed carbon.
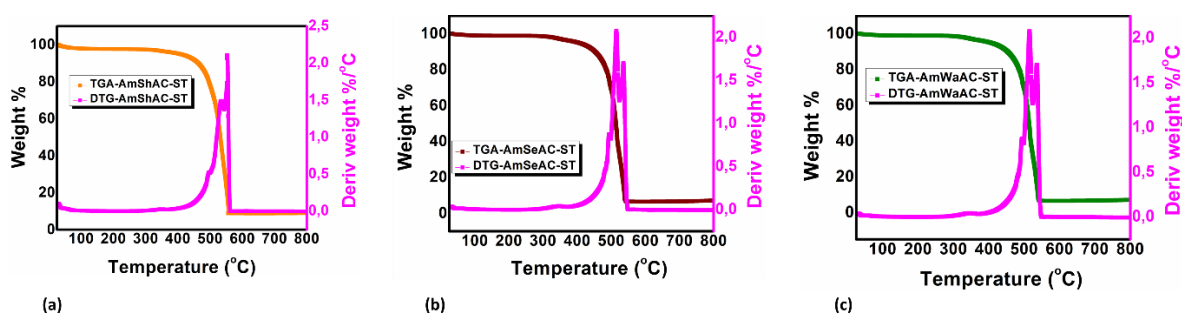
Fig. 5.5. TGA/DTG graph under air atmosphere for amarula waste ACs (a) AmWaAC-ST, (b) AmSeAC-ST and (c) AmWaAC-ST

The total mass loss during thermal analysis was found to be 91,7 %, 93,6 % and 98,8 % for AmShAC-ST, AmSeAC-ST, and AmWaAC-ST, respectively. Despite the same habitant of the precursor, the differences in mass loss confirm that the precursor of AC does play an important role in the thermal characters of the final product, as stated by other researchers [93],[20],[94]. It was further found that the processed amarula waste was more thermally stable than the unprocessed amarula waste from our previous work (Chapter 4). This was due to the strong bonds formed between carbon–carbon atoms during thermal processing. This formation of strong bonds occurred because of the breakdown of the volatiles that were present, leaving only a carbon structure, which is single-bonded to one another by sigma bonds. Other researchers obtained a similar TGA curve when analysing ACs derived from biomass [9].

Table 5.3 TGA/DTG's peak temperatures for amarula waste ACs

| AC type | TGA/DTG | | | |
| | Peaks Temperature °C | | | Total mass loss % |
	1st peak	2nd peak	3rd peak	
AmShAC-ST	504	536	556	91,7
AmSeAC-ST	492	515	537	93,6
AmWaAC-ST	495	518	537	98,8

The peak temperatures for each of the amarula waste ACs from DTG curve are shown in Table 5.3. The three identified peaks, in each graph show the amount of evolved volatiles, such as CO_2, CO and CH_4, during thermal decomposition of volatiles on ACs [96]. It was further observed that peak identification of amarula shell ACs occurred at a much higher temperature compared to that of the AmSe and the AmWa waste ACs. This confirms the ability of the AmShAC-ST to be more resistant to thermal treatment than the other two sample. Even though the amarula waste ACs can be used as an adsorbent at room temperature, the TGA/DTG results show that there is great potential in this type of waste for use as a catalyst or catalytic support for processes that occur at temperatures ≈ 500 °C.

5.3.1.3 SEM-EDX analysis

The morphology of the amarula waste ACs is shown in Fig. 5.6. It reveals the presence of cavities and large pores on the surface – unlike in the unprocessed amarula waste biomass discussed previously in Chapter 4, which showed only a smooth surface with no observable pores. These types of morphologies were also observed on ACs by other researchers [97],[98]. The formation of the observed pores is said to be due to the elimination of volatiles from the biomass during the first stage of thermal processing, which is called pyrolysis. This process leaves only a carbon material called biochar. The application of steam to the biochar tends to widen the pores, depending on the source type. This process occurs because every time a layer of carbon is removed, a hole or pore is formed. The removed carbon dissipates into the environment as carbon monoxide (CO)/carbon dioxide (CO_2) formed from the oxygen in the water molecule, as shown in chemical Reactions 5.1, 5.2 and 5.3.
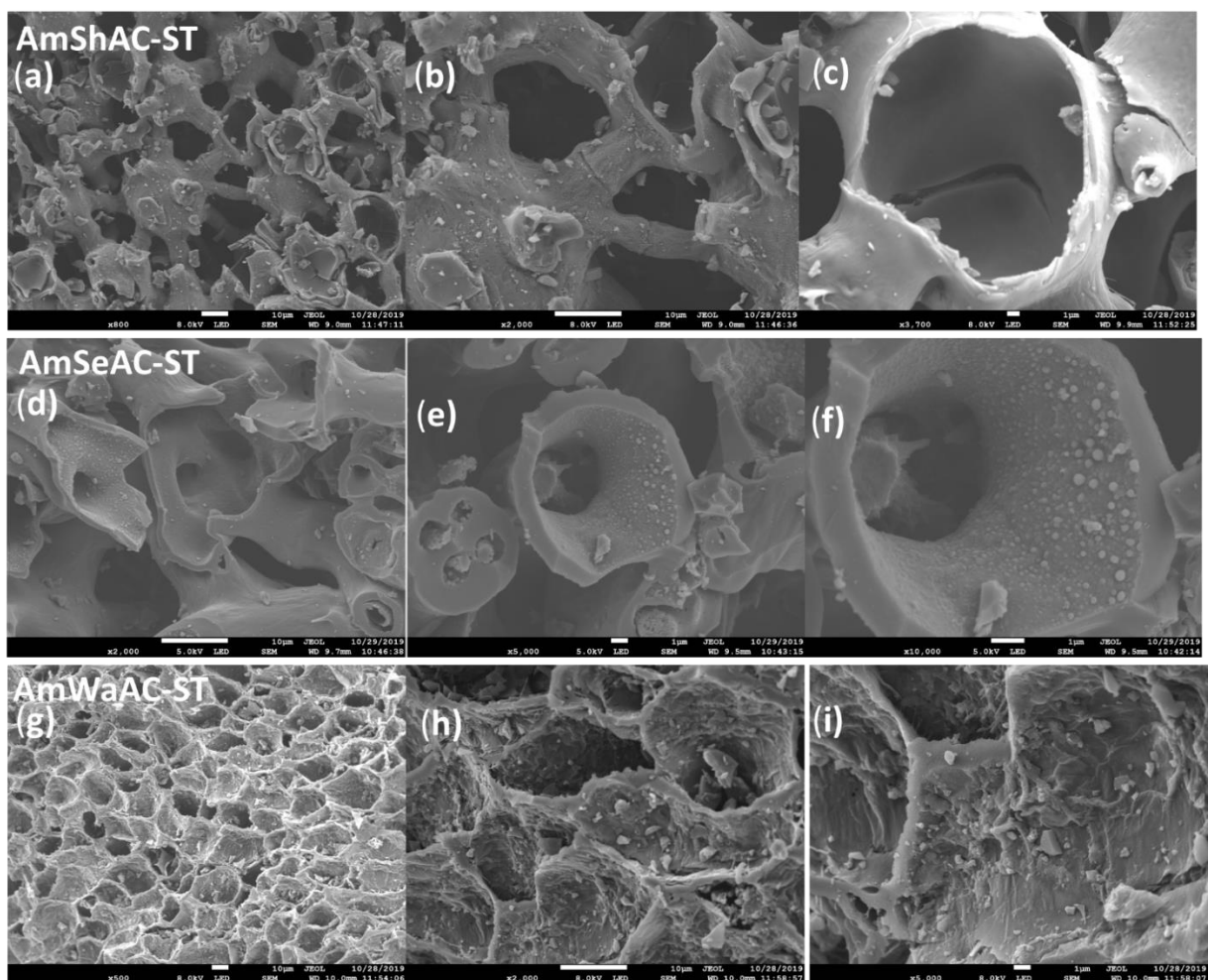
Fig. 5.6. SEM images for amarula waste ACs at different magnifications: Images (a), (b), (c) are for AmShAC-ST; (d), (e), (f) are for AmSeAC-ST; and (g), (h), (i), are for AmWaAC-ST

The amarula shells waste processed to AC, showed a network of holes and tiny particles on a surface, and large, deep open pores in a network format (Fig. 5.6 (a). Further magnification (Fig. 5.6 (b) and (c)) revealed large, irregular semi-open pores with smooth walls, and observable cracks inside the pores. This microgram resembles that of a glassy carbon image which was computer visualized by O'Molley [99]. According to the model, the AC structure is a tangle of threads of carbon atoms arranged in different ring structures. The spaces in between the threads result to various pore sizes, which makes it easy for molecules of different sizes to be adsorbed [100]. On the other hand, the morphology of amarula seed ACs (Fig. 5.6 (d)) have a smoother surface compared to that of the amarula shell AC, except that the pores have a cone-like shape with smooth edges. Further magnification (Fig. 5.6 (e) and (f)),of the SEM image revealed tiny spheres inside the walls of the pores. The spheres inside the pores possessed a similar structure to the carbon aerogels structure modelled by Gavalda et al and Zhang et al. [101],[102]. The spheres in AmSe AC appeared naturally, unlike in carbon aerogel, as they are synthesized by polycondensation. According to Gavalda et al, the structure of the spheres depicts the graphitic microcrystalline with some layers, which contribute further to the heterogeneous adsorption process [101]. The spherical morphology was also seen on other synthesized carbon materials by Nath et al. [80], Li et al. [90], and Zhang et al. [103].

The AmWa waste AC (Fig. 5.6 (g)) showed a cage-like morphology with a rough surface and roughness on the walls of the pores. The pores appeared to be wider, but these pores did not extend deep to the end (Fig. 5.6 (h) and (i)), unlike the AmSe and the AmSh waste ACs. This type of morphology exhibited a similar model of carbon as that first proposed by Gibson et al (1946) and Riley (1947), and as discussed in by Byrne and Marsh [100], and Ruthven et al. [104], which describe a low-density carbon. This morphology also looks like the model of potato chips and wedges, as described in Chapter 9 of the book, *Origins of Carbon* [104]. This type of structure reveals slit-like pores, which result in non-homogeneity for adsorption sites.

Table 5.4 Elements identified by EDX for processed amarula waste

| Elements | EDX analysis of processed Amarula wastes | | | | | |
| | AmShAC-ST | | AmSeAC-ST | | AmWaAC-ST | |
	Element wt %	Atom %	Element wt %	Atom %	Element wt %	Atom %
C	78,4	97,0	68,0	86,2	59,9	84,2
O	0,8	0,7	3,5	3,3	8,1	8,6
N	-	-	7,7	8,4	-	-
K	0,9	0,4	1,7	0,7	9,5	4,1
Mg	0,3	0,2	-	-	0,6	0,4
Ca	1,0	0,4	-	-	-	-
Si	-	-	-	-	1,5	0,9

The SEM images also revealed some particles on the surface of the amarula waste ACs. These particles were identified during EDX analysis. They were found to be due to the inorganic elements of potassium, magnesium, calcium, and silica as shown in Table 5.4. They confirmed the presence of ash content found during TGA analysis.

5.3.1.4 TEM analysis

TEM analysis was carried out on the selected AmSh ACs, as shown in Fig. 5.7. The observed dark parts in image (a) in Fig. 5.7 signify agglomeration on the surface which might have resulted in a higher surface area of AmShAC-ST, whereas the bright parts were considered to be pores, confirming the SEM analysis above. The holes observed in the magnified images (b) and (c) in Fig. 5.7 were caused by the tangling of fibres, as observed in SEM micrographs. Therefore, these images confirm that a porous AC was indeed synthesized from AmSh waste biomass. Similar images were observed by other researchers [105]–[107].
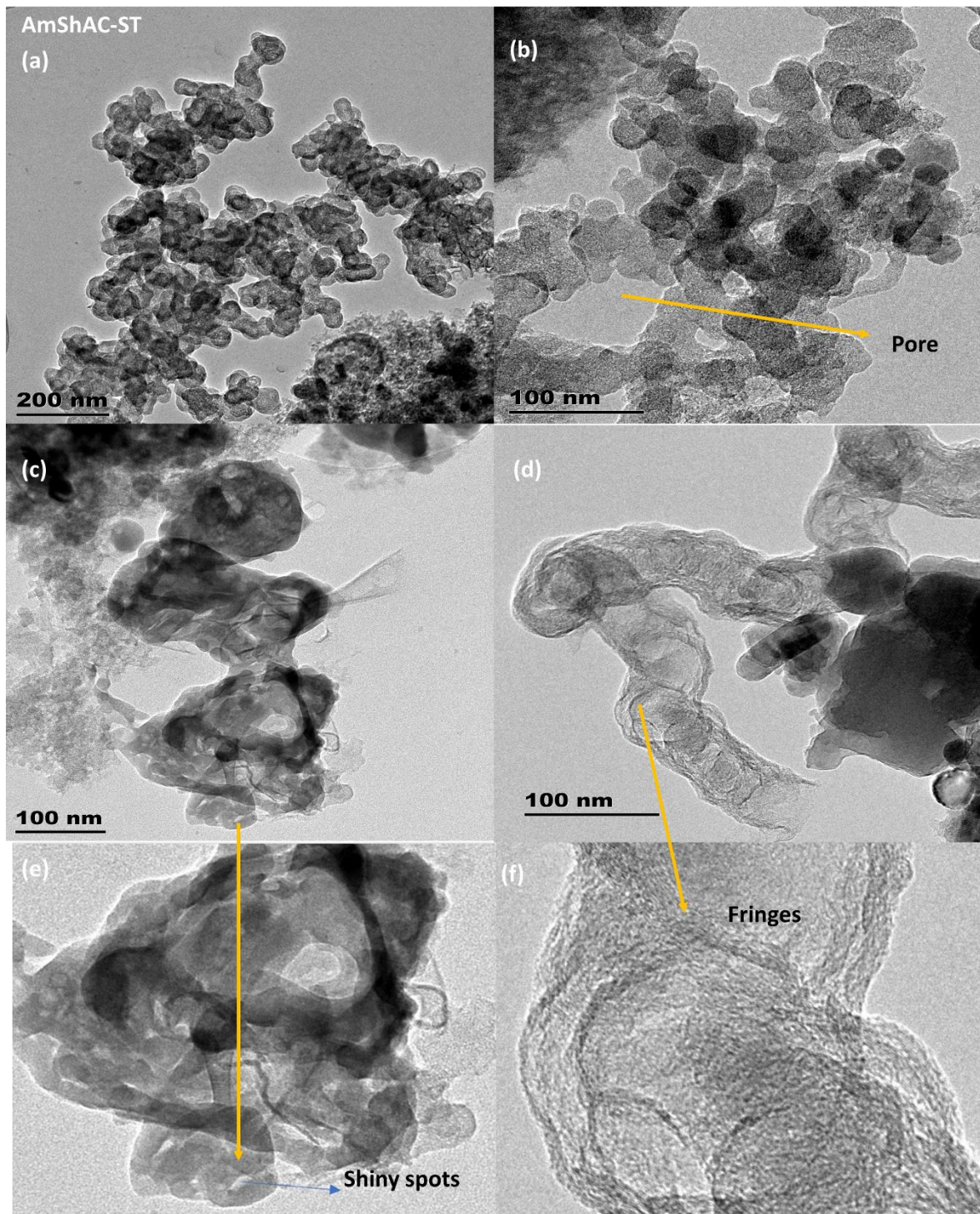
Fig. 5.7. TEM images of amarula shell ACs at different magnification showing different structures

The structure in Fig. 5.7 (d) looked like a hollow-ring fibre which represents an amorphous carbon observed in 2θ value 23°. The morphology in Fig. 5.7 (e) further showed some white dots that are more like shiny particles in the structure of AC, as in the TEM image in Saleh [74]. This may be attributed to the geometry of a diamond structure. This shiny structure may be attributed to another carbon type that is crystalline in AC, as confirmed by the XRD at 2θ

value 44°. The fringes observed in (f) confirm the stickering of carbon layers for 5-, 6- or 7-membered rings in the structure of AmSh waste AC [97],[108]–[111].

5.3.1.5 XRD analysis of amarula waste ACs

The XRD analysis of unprocessed amarula waste biomass in our previous work had shown a highly intense peak at the 002 plane, which was due to crystalline cellulose and hemicellulose (Chapter 4). The thermal processing of these amarula waste samples broke down the cellulose and hemicellulose, therefore reducing the intensity of the (002) reflection peak and then broadening it. This was due to the decrease in the order of crystallinity as a result of heat treatment. This consequently shifted the asymmetric bands of 002 to 2θ angles valued at 22.9°, 23.2° and 24.7° for AmSh, AmSe and AmWa waste ACs respectively, as shown in Fig. 5.8 (a). The second weak broad peak was observed at approximately 2θ value at 44° with a basal reflection plane of (10). This peak was formed in response to a high degree of randomness in the processed amarula wastes. It denotes the presence of amorphous carbon [71],[109],[112]–[114]. It was for these reasons that the Scherrer expression in Equation 5.1 above was used to calculate the lattice size L_c and L_a using 0,9 and, 1,84 as K constants, respectively. It was found that AmSh waste AC had a higher crystalline size (L_c), followed by AmWa waste and then AmSe waste ACs, as shown in Table 5.5.
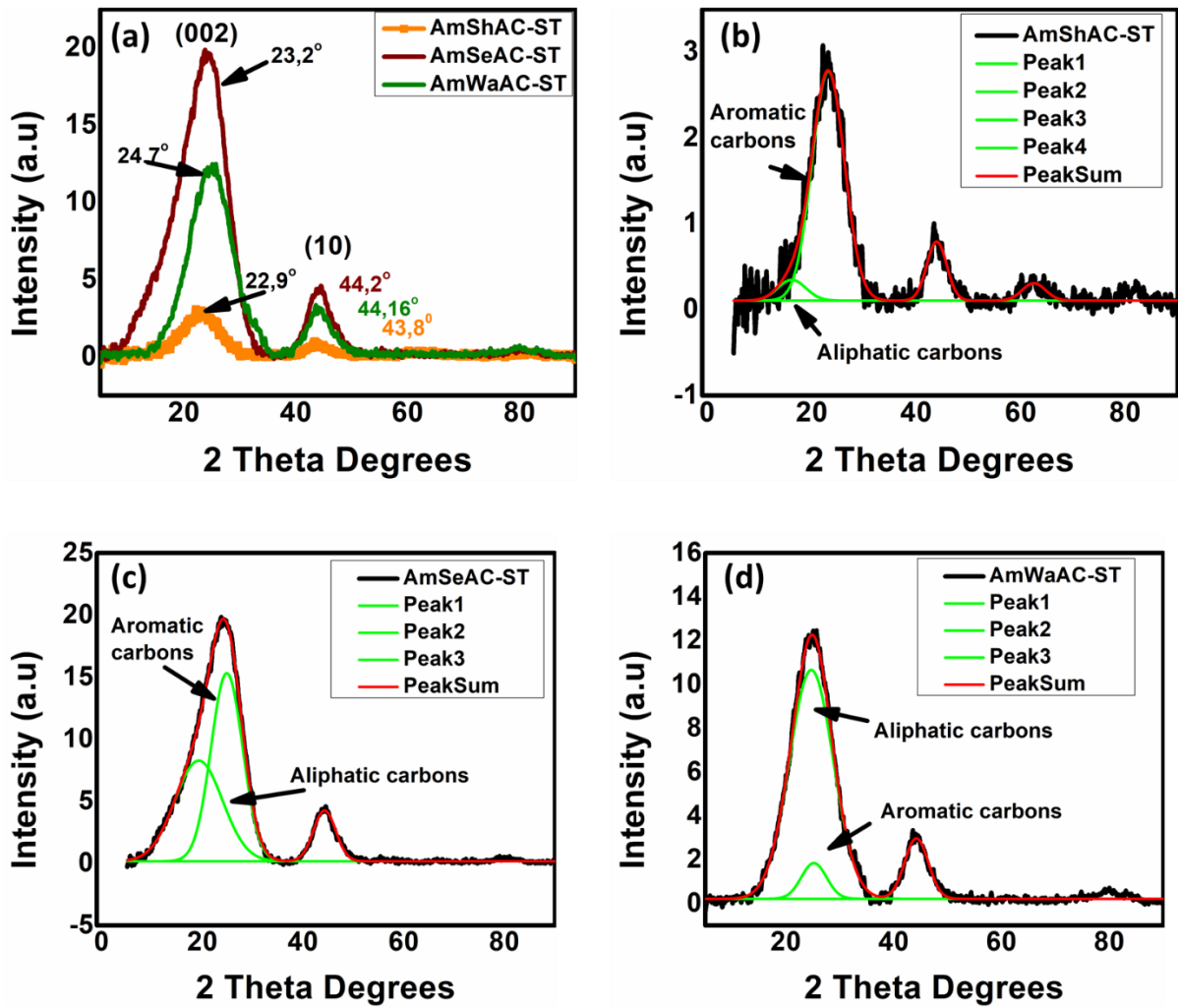
Fig. 5.8. XRD patterns of amarula waste ACs

It was further found that the AmShAC is more graphitic because the interlayer d-spacing was found to be higher in Table 5.5 and followed the trend AmShAC-ST > AmSeAC-ST > AmWaAC-ST.

Table 5.5 Crystallinity parameters of amarula waste ACs

AC type	Lattice size Å		d_{002} (Å)	I∏/Iγ	$\square_a$
	L_c	L_a			
AmShAC-ST	10,66	41,68	3,88	8,63	0,93
AmSeAC-ST	7,81	34,30	3,83	1,87	0,55
AmWaAC-ST	9,04	34,04	3,60	0,16	0,24

Upon deconvolution in Figs. 5.8 (b), (c), and (d), it was found that the 002 reflection basal planes possessed two bands (λ band & Π band). The first band (λ) on the left side at 2θ valued $16.1°$, $19.2°$ and $24.7°$, were attributed to the aliphatic carbon chains for AmSh, AmSe and AmWa waste ACs, respectively. The second peak was due to the Π band emerging from carbons in the aromatic rings [113] at 2θ angle valued at $23.1°$, $24.8°$ and $25.1°$ respectively. The ratio of the carbon atoms in the aliphatic to that of the aromatic rings was determined using the integrated area under each fitted curve using Equation 5.6 [113]:

$$F_a = A_\Pi/A_\Pi + A_\lambda \qquad\qquad \textbf{Eq. 5.6}$$

where f_a is the aromaticity of AC, A_Π was the area of carbons in the aromatic rings and A_λ is the area of the aliphatic carbon chains in ACs. From the results in Table 5.3, it was observed that the aromaticity (f_a) followed the trend AmShAC-ST > AmSeAC-ST > AmWaAC-ST.

Mannoj (2012) ranked coal production using the intensity ratio of the deconvoluted peaks. A similar approach was followed in this study. The ACs were ranked by determining the ratio of intensities (I) of the deconvoluted peaks, as shown in Table 5.5. AmSh ACs were found to have a higher rank value, which makes it more feasible for industrial application. Furthermore, a similar trend was observed for all three amarula waste ACs as that of f_a, d_{002} and L_a.

5.3.1.6 FTIR analysis

The FTIR spectra of the processed amarula waste in Fig. 5.9 showed fewer vibrational bands compared to the unprocessed amarula waste discussed previously (Chapter 4). The O–H stretching band, which was very broad at $3\ 600\ cm^{-1}$–$3\ 100\ cm^{-1}$, has now become very strong, highly intense, and less broad in the current study (comparison is shown in the Appendix B: Fig. B5). This is because processed amarula waste has lost its hydrophilicity, meaning less moisture absorbed by the material. This confirms the TGA analysis in Fig. 5.5, where the first stage of decomposition which was attributed to moisture loss has decreased due to a lack of moisture on the surface, resulting from the degraded hemicellulose and cellulose. Therefore, the present O–H functional groups at $3\ 442\ cm^{-1}$ in the amarula waste ACs spectra, are due mainly to the phenols, lactones, and carboxylic groups.
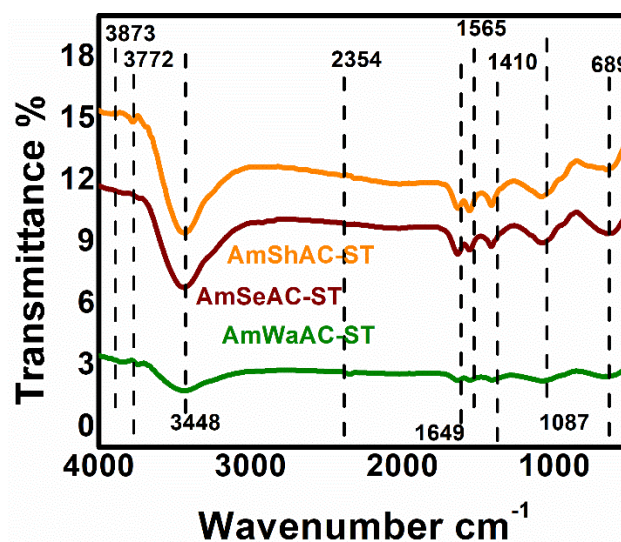
Fig. 5.9. FTIR spectra of processed amarula wastes

More of these acidic groups were mainly formed because of the steam that was passed through during thermal processing, as shown in the chemical Reactions 5.1, 5.2, and 5.3. It was also observed that the two vibrational bands that were due to C–H symmetric and asymmetric bands of methyl and ethyl at the range 2 850 cm^{-1}–2 950 cm^{-1} in the unprocessed amarula waste biomass (Chapter 4), have either now disappeared or are too tiny to identify in the processed amarula waste. This was attributed to the oxidation of the aliphatic carbon chains during steam activation and the cause of more stable C=C and C≡C functional groups being established on the surface. Moreover, other new, weak vibrational bands were observed at the range of 3 700 cm^{-1}–3 900 cm^{-1} which were attributed to the sp C–H of alkynes [32]. These bands were confirmed by the presence of a C≡C functional group, which appeared as a weak band between 2 300 cm^{-1}–2 400cm^{-1}. This C≡C triple bond functional group was also observed by Ali and Idris [105], Saka [115], and Tran et al. [116]. The peak which was due to a C=O vibrational band at 1 737 cm^{-1}in the unprocessed amarula waste (Chapter 4) has now disappeared in the processed amarula waste, because of the thermal breakdown of the hemicellulose and has formed more of the carboxylic groups. The C=O stretch at 1 649cm^{-1} is attributed to the carbon–oxygen conjugated with carbon basal planes of carbonyl, quinols, lactose, and carboxylic groups in ACs [32]. The respective C=C and C–C stretching bends at 1 565 cm^{-1} and 1 410 cm^{-1} are the confirmation of vibrating bands in the condensed skeleton of aromatic rings in the amarula waste ACs. It was further observed that the peak which was very strong and highly intense at 1 031 cm^{-1} in the unprocessed amarula waste (Fig. 4.5) has shifted to 1 087 cm^{-1} and has become very weak and less intense in these processed amarula waste. This is because of

thermal processing which broke down the C=O bonds of the carbonyl functional groups that were present and formed more of the C–O bonds for carboxylic, lactone and phenolic groups, therefore reducing the vibrational bend of the C–O bands. The sp^2 C–H out-of-plane bend shifted from 897 cm^{-1} to 659 cm^{-1} in the processed amarula waste, confirming the formation of more aromatic rings. Other researchers [32],[37] also found similar FTIR bends of ACs as in this study. It can therefore be concluded that, of the three amarula waste ACs in the current study, the AmWaAC-ST had the strongest bends of alkynes. This was due to the high content of volatiles and aliphatic carbon, as confirmed in Fig. 5.5 (c) of the TGA analysis and in Fig. 5.8 (d) of the deconvoluted peaks of XRD analysis, respectively. Despite that, it was found that the AmSh ACs had more of the hydroxyl groups and the carboxylic groups present because it had the strongest peaks at 3 443 cm^{-1} and at 1 087 cm^{-1} followed by the AmSe waste and then the AmWa waste ACs.

5.3.1.7 Textural properties

Upon analysis of amarula waste ACs produced at 45 min steam residence time, it was found that the AmSh AC had the highest BET surface area of 740 m^2/g and the highest total pore volume of 0,37 cm^3/g, followed by the AmWa waste then the AmSe waste AC, as shown in Table 5.6 (green, brown, and yellow colour). These results confirm the SEM analysis in Fig. 5.6, where the three amarula waste ACs had a morphology showing very large pores of different shapes in each AC type.

Table 5.6 Comparison of textural surface analysis of amarula waste ACs with ACs from literature.

| AC Precursor | Conditions | | | Surface area | | | | Pore Volume | | | Pore Size | | Ref |
	Activation method	Temperature (°C)	Steam Residence time (min)	BET S-Area m²/g	t-micropore S-Area m²/g	External S-Area m²/g	BJH S-Area m²/g	BJH Pore vol cm²/g	t-micropore Vol cm³/g	Total Pore vol (cm³/g)	Total Pore Size (nm)	BJH pore Size (nm)	
Outs hulls	steam	800	120	625	-	-	-	-	-	-	-	-	[93]
Corn stove	steam	800	120	311	-	-	-	-	-	-	-	-	[93]
Corn corb	steam	850	60	607	-	-	-	-	-	-	-	-	[13]
Bamboo wastes	steam	850	60	870	-	-	-	-	-	-	-	-	[119]
Guayule Bugasse	steam	800	45	716	-	-	-	-	-	-	-	-	[115]
Apricot stones	steam	700	120	820	-	-	-	-	0,46	0,5	-	-	[53]
Almond shells	steam	-	-	484	-	-	-	-	-	-	-	-	[118]
Rubber seeds shells	steam	-	-	948	-	-	-	-	-	-	-	-	[117]
Moso Bamboo	steam	800	60	486,8	385,51	-	-	-	-	0,2354	1,9231	-	[24]
Ma Bamboo	steam	800	60	464,7	391,95	-	-	-	-	0,2329	2,0049	-	[24]
Wood chips Birch	steam	800	240	617	318,00	300	-	-	0,136	0,509	-	-	[122]
Wood chips Spruce	steam	800	240	679	317,00	369	-	-	0,136	0,555	-	-	[122]
Peat	steam	800	240	543	-	-	-	-	-	0,18	-	-	[46]
Commercial AC	unknown	-	-	541	-	-	-	-	-	0,42	0,33	-	Sigma Aldridge-SA
Amarula fruit wastes	steam	800	45	425,98	357,35	68,63	38,86	0,0351	0,0187	0,23	2,20	3,60	This study
Amarula seeds wastes	steam	800	45	279,36	238,36	41,00	19,1	0,01695	0,0170	0,15	2,16	3,55	This Study
Amarula shell wastes	steam	800	30	434,47	345,67	88,80	182	0,0923	0,1783	0,29	2,66	3,15	This Study
			45	740,36	498,54	241,76	201	0,1749	0,1983	0,37	2,75	3,47	
			75	881,08	557,08	324,00	312	0,2314	0,1998	0,78	2,89	3,85	
			90	1193,25	404,00	789,00	905	0,3345	0,2023	0,98	3,27	4,40	

The observed high surface area and the increased porosity in the thermally processed amarula waste is attributed to the removal of volatiles from the amarula waste biomass precursors during the pyrolysis stage. This first stage formed mainly micropores and more carbon atoms, which contributed to the greater surface area and porosity of an intermediate product (biochar) as shown in the Appendix B: Table B2. The second stage, which involved the application of steam to the biochar, created more pores, widened them, and further deepened them, depending on the structure of the precursor or the biochar. Similar results were also found by other researchers such as Sheng-Fong, Lima and Rajapaksha, who also produced ACs from various precursors using a steam-activation process [24],[117],[118]. The textural properties of amarula waste ACs in this study are listed in Table 5.6, where they were compared with other ACs produced in other literatures [13],[24],[46],[52],[53],[94],[117],[119]–[121]. Amarula waste ACs were found to be compatible with the other ACs in the literature. The surface area of AmSh waste ACs was also compared with the commercial AC which was purchased from sigma Aldrich in South Africa. It was found that the AmSh AC produced at 45min had a higher BET surface area of 740 m^2/g compared to commercial AC that had a BET surface area of 541 m^2/g with a total pore volume of 0,42 cm^3/g. This confirms that the AmSh ACs can be commercialized and be competent in the AC industry. Besides that, the SEM morphology did confirm that amarula shells AC had a glassy-like structure of carbon which is suitable for industrial purposes.
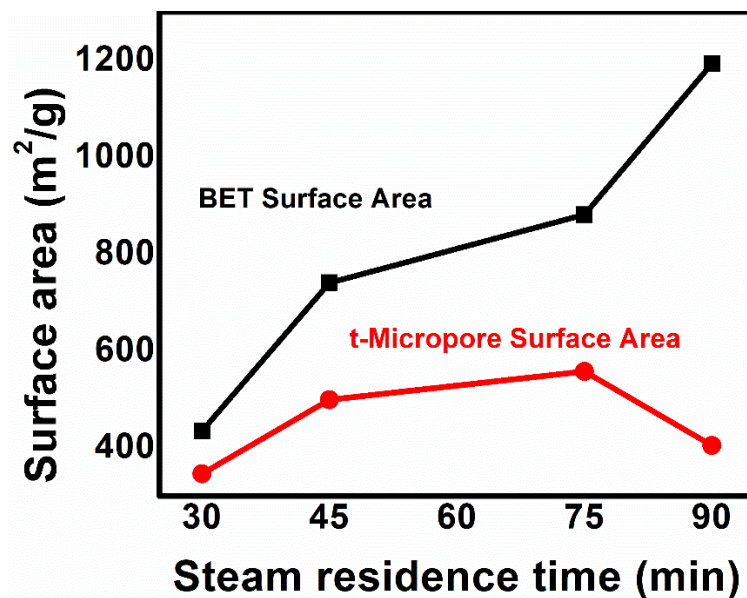
Fig. 5.10. BET and micropore surface area with steam residence time of AmShAC-ST

Textural properties were further carried out on the selected AmShAC for the effect of steam residence time. It was found that as the steam residence time increased from 30 min to 90 min, the BET surface area increased from 434 m^2/g to 1 193 m^2/g. It was also found that even the porosity increased with an increase in steam residence time, as shown in Table 5.6 (yellow colours). This is attributed to the fact that steam activation removes the sp^3 bulk carbon; therefore, the longer the steam is exposed to the char, the more carbons are removed, and the more pores are formed, resulting in a higher surface area. Besides that, there is enough diffusion of water vapour throughout the porous network of the char. The formation of more mesopores is due to the H_2O molecule that has easy access to the already available micropores on the solid. In addition, as the H_2O molecule removes the carbon atoms, it occupies the space that was occupied by the carbon and therefore creates more mesopores. Again, it is because the longer the material is exposed to steam, the more the entire surface of the material gets enough exposure for reactivity, consequently increasing the BET surface area. As a consequence, more pores are widened and deepened, which leads to more mesopores and macropores being observed at 90 min residence time. Similar trends of results as in this study were obtained by other researchers who determined the effect of steam residence time on ACs [46]. However, some researchers, such as Zhang and his team [121], found the opposite of this. They prepared AC via pyrolysis and then used the steam-activation time effect as in this study and found that as they increased the steam residence time, the BET surface area and the pore volume decreased [121]. Fu et al. [122] also found similar results. For this reason, further textural analysis was done to determine the t-micropores surface area of amarula waste ACs. It was found that the t-micropore surface area increased with steam residence time up to a certain plateau, at 75 min residence time as shown in Fig. 5.10. The micropore surface area then decreased as the steam residence time increased further to 90 min. This was attributed to the fact that the already present micropore surface area became raptured as the available micro-pores were widened and deepened by more steam. The effect of this was a reduced surface area of the micropores. Therefore, in this study, it was found that it is the micropore surface area that "decreased" at a certain point in time when the steam residence time was increased, whereas the BET surface area increased with an increase in the steam residence time.

5.3.2 Desulphurization of ≈ 100 ppm model diesel fuel

5.3.2.1 Effect of adsorption time on processed amarula waste

Fig. 5.11 shows the results for the effect of adsorption time of DBT in model diesel on processed amarula waste. It was found that all the amarula waste ACs improved the adsorption of the DBT molecule in model diesel fuel compared to the unprocessed amarula waste discussed previously. This could have been due to the presence of micropores and mesopores that were introduced by thermal processing with steam together with the O-functional groups on the surface. More of the DBT was reduced within 60 min due to the available active sites on the surface of ACs. The adsorption process slowed down to 90 min and there was almost no change until 180 min because the surface was now being covered by the DBT molecules and the pores were now filled, consequently reducing the activity. It was found that the removal of the DBT molecule increased massively to almost 60 % within 90 min adsorption time for the AmSh ACs. From there the curve flattened, showing only a small significant change in adsorption efficiency up to 180 min. A similar trend was observed in all the amarula waste ACs.
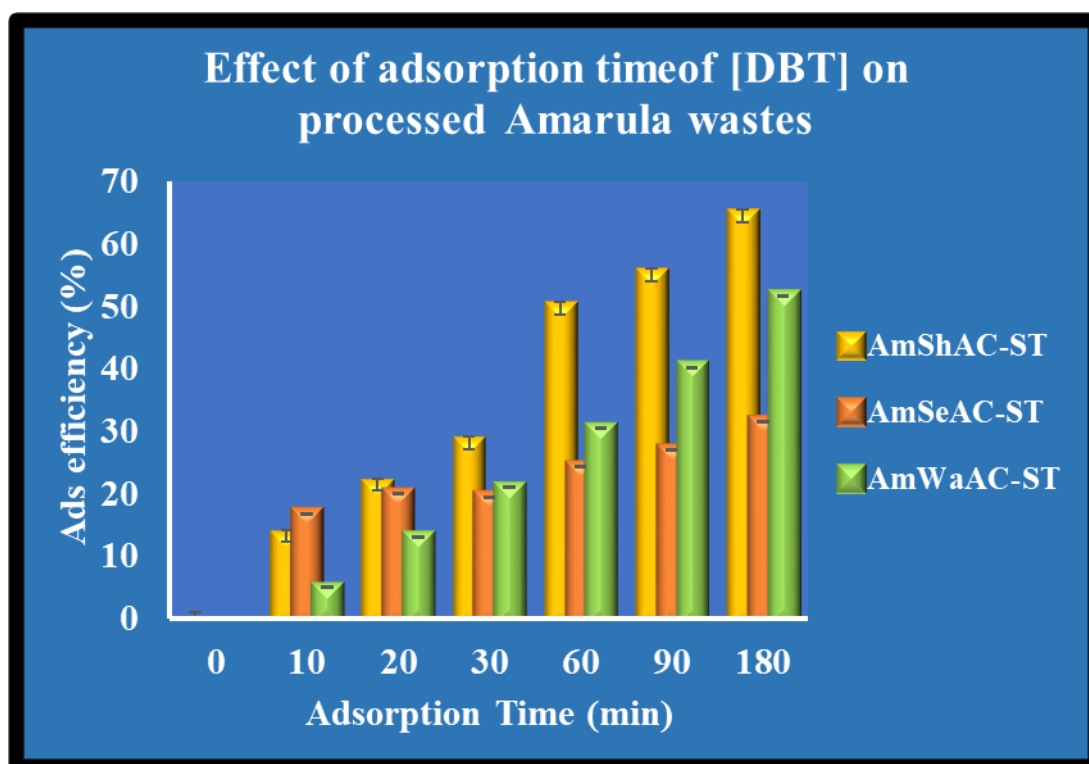
Fig. 5.11. Effect of adsorption time of DBT on amarula waste ACs

However, for AmSe waste AC, the removal of the DBT molecule within the first 10 min was higher than that of the AmSh and the AmWa waste ACs. After 30 min and up to 180 min, the AmSe reduced less of the DBT molecule. The fast activity of AmSe AC within 30 min might be due to pi–pi bonding, that resulted from the aromatic rings of ACs (Fig. 5.1) and the aromatic rings of the DBT molecule (Fig. 5.15) mentioned later. In addition, Fig. 5.3 (b) for a deconvoluted peak of 002 showed that the AmSe waste ACs had more of the aromatic carbons than the other two amarula waste ACs. This could have been attributed to the AmSeAC having higher activity within the first 10 min. The lack of higher activity on the AmSeAC-ST as time progresses may be due to having the smallest t-micropore volume of 0,017 cm^3/g which, was observed during textural analysis in Table 5.6 above. This volume is too small to accommodate a molecule of $\approx$ 1 nm size. This then proves that not only the pi–pi bonding contributed to adsorption of DBT molecule, but the porosity of the AC plays an important role. This was proved by other researchers such as Deng et al. [123] and Jha et al.[124].

The AmSh waste AC were found to have higher activity from 30 min to 180 min. This could have been due to more mesopores present, which then quickly facilitated the movement of the DBT molecule to the micropores until they were filled. Rajapaksha et al. [118] found that steamed biochar facilitated the adsorption of sulfamethazine because of the presence of mesopores. Despite that, owing to the presence of more mesopores, more DBT molecules were adsorbed until all the pores were filled. This porosity was also confirmed by the textural analysis in Table 5.6. The active site of the AC, which comprises the O-functional groups, may also have contributed to more adsorption capacity in the AmSh ACs because the FTIR showed a highly intense peak of O–H and C–O which belonged mainly to carboxylic acids. This type of bonding may have occurred by electrophilic addition because oxygen is an electron-withdrawing element that can form O–S bonds. Therefore, the trend of adsorption capacity for amarula waste AC was AmShAC-ST >AmWaAC-ST > AmSeAC-ST within 30–180 min. It can then be concluded that the amarula seed waste ACs showed higher initial adsorption rate of DBT in model diesel within 10 min, followed by the amarula shells then the fruit waste ACs.
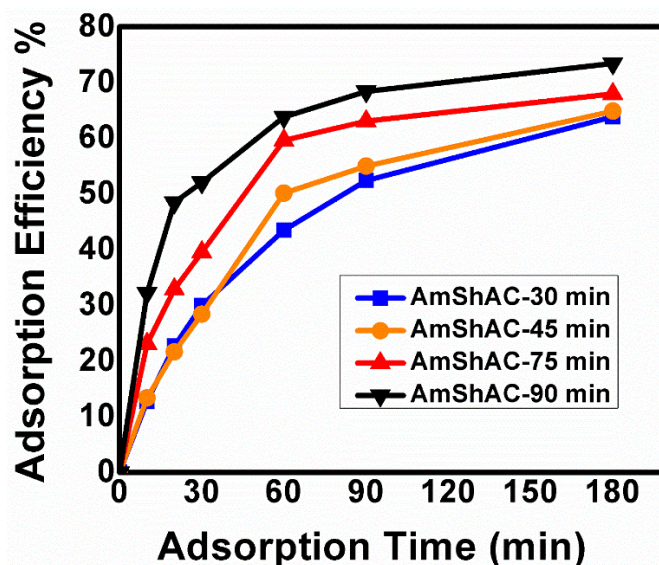
Fig. 5.12. Adsorption efficiency of amarula shell ACs produced at different steam residence time

AmSh waste ACs, which were selected and used to determine the effect of steam residence time, were then applied to reducing the DBT molecule in diesel fuel, as shown in Fig. 5.12. It was found that the adsorption capacity increased with the ACs produced at a longer time. In addition, it was observed that the AmShAC-ST-45min adsorbed 50 % of DBT within 60 min, whereas AmShAC-ST-90min adsorbed more than 50 % of DBT molecules in model diesel within just 30 min, as shown in Fig. 5.12; despite that, the adsorption quickly slowed down towards equilibrium. This is because the ACs produced at the longer time had more of the micro-pores and more of the mesopores and macropores, as confirmed in Table 5.6. Furthermore, the FTIR spectra in Appendix B: Fig. B6 confirmed the intense broader peak of C–O of the carboxylic groups at 1 087 cm^{-1}. These improved textural, and surface characters, allowed more of the DBT molecules to be adsorbed, which then reduced the concentration of the organo-sulphur compound massively. Zhang et al. [121], in their study of bamboo waste, also showed that the ACs produced by steam activation increased the oxygen density on the surface, which further increased the activity of the adsorbent.

5.3.2.2 Kinetic models

Kinetic models were applied to the experimental data for the processed amarula waste ACs, as shown in Fig. 5.13. Equations 5.7, 5.8 and 5.9 were used to determine the best fit of the model

$$\ln(q_e - q_t) = \ln(q_e) - k_1 t \qquad \qquad \textbf{Eq. 5.7}$$

$$t/q_t = 1/k_2 q_e{}^{\wedge 2} + (1/q_e)\, t \qquad \qquad \textbf{Eq. 5.8}$$

$$q_e = k_i{}^{\wedge 1/2} + C \qquad \qquad \textbf{Eq. 5.9}$$

at which q_t and q_e (in mg/g) were the adsorption capacity at time (t) and at equilibrium (e). The C represents the intercept which describes the thickness of the boundary layer on the surface of the adsorbent, whereas k_1, k_2, and k_i are kinetic constants in 1/mg, mg/g.min, and mg/g.mg$^{1/2}$ for pseudo 1st order, pseudo 2nd order and intraparticle diffusion models respectively [116],[125]–[127]. According to some of the literature, when a correlation value (r^2) is close to unity (1), then the fitted results follow that model [69],[74],[76],[78],[91].

The results in this study showed that AmShAC-ST and AmSeAC-ST followed both the pseudo 1st-order and the pseudo 2nd-order kinetics models because their highest r^2 values were close to unity with values above 0,9 as shown in Table 5.7. This implies that both the chemisorption and the physisorption might have been involved mainly in the adsorption process of DBT. On the other side, the AmWaAC-ST had the highest r^2 value for intraparticle diffusion (of 0,8847) followed by pseudo 2nd-order kinetics (with 0,7334). This indicates that the adsorption on the AmWa waste might have occurred mainly via both particle diffusion and chemisorption.

Some scientists and researchers also applied kinetics on the experimental results for adsorption of DBT and found that they followed pseudo 2nd order kinetic therefore the adsorption was through chemisorption [67],[68],[78],[79],[115],[128]. On the contrary, Samaniego found that their results followed pseudo 1st order kinetics and therefore the adsorption was via physical adsorption [69]. Based on the structure of amarula ACs, adsorption occurred via physisorption when the organo-sulphur molecules were adsorbed inside the pores of ACs, and when the aromatic rings were breaking to form pi–pi complex interaction with the aromatic rings of the DBT molecule. A chemisorption adsorption may have also occurred because of the presence of the C–O and O–H groups. The O–H functional groups formed an electrophilic addition reaction between S–O via hydrogen bonding.

It is stated that when the calculated adsorption capacity ($q_{e\,calc}$) values are close to experimental adsorption capacity ($q_{e\,exp}$) values under that particular kinetic model, then that model is considered as the best fit [91],[115],[128]. For this reason, the $q_{e\,exp}$ data was compared with the $q_{e\,calc}$ data under each kinetic model. According to the results in Table 5.7, the $q_{e\,calc}$ values were consistent with the $q_{e\,exp}$ values for AmShAC-ST under pseudo 2nd-order kinetics, for

AmSeAC-ST under the intraparticle diffusion model, and for AmWaAC-ST under the pseudo 1st-order kinetic model.
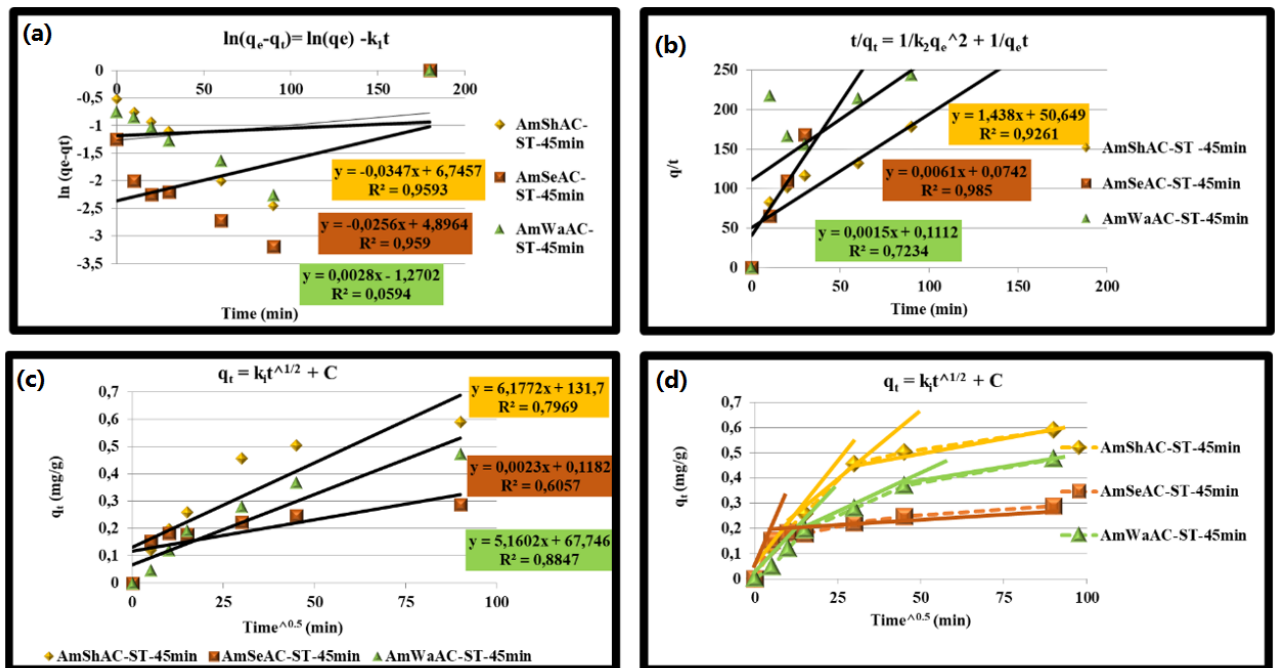
Fig. 5.13. Kinetic models of (a) pseudo 1st order, (b) pseudo 2nd order, (c) intraparticle diffusion and (d) intraparticle diffusion, showing multi-linear steps of adsorption

Table 5.7 Kinetic parameters of amarula waste ACs

| Ads Type | Pseudo 1st order | | | Pseudo 2nd order | | | Intraparticle diffusion | | | | q_e exp |
	$q_{e\ calc}$ (mg/g)	K_1 (1/mg)	r^2	$q_{e\ calc}$ (mg/g)	K_2 (mg/g.min)	r^2	$q_{e\ calc}$ (mg/g)	K_i (mg/g.mg ^{0,5})	C	r^2	
AmShAC-ST-45min	850,394	-3,47E-02	0,9593	0,69541	1,05E+02	0,9261	687,65	6,1772	131,7	0,7969	0,5905
AmSeAC-ST-45min	133,807	-2,56E-02	0,9590	163,9344	2,76E-06	0,9850	0,33	0,0023	0,1182	0,6054	0,2884
AmWaAC-ST-45min	0,28078	2,80E-03	0,0594	666,6667	2,50E-07	0,7234	532,16	5,1602	67,746	0,8847	0,4733

Furthermore, this study used chi-square (x^2) to validate the best-fit kinetic models obtained for the results. Chi-squared (x^2) test is normally analysed under the same abscissa and ordinate to determine the best-fit model, which makes it more advantageous. It states that if the calculated Chi-squared value (x^2) is smaller under that model, then the results followed that model [129]. The x^2 results for the adsorption of DBT in model diesel on processed amarula waste samples seen in Table 5.8 were obtained using Equation 5.10, where $q_{e\ exp}$ and $q_{e\ calc}$ are the equilibrium adsorption capacity for experimental and calculated data, respectively. Therefore, the smallest x^2 values were found to be 0,019 for AmShAC-ST under the pseudo 2nd-order model, 0,0047 for AmSeAC-ST under the intraparticle diffusion model and 0,078 for AmWaAC-ST under the pseudo 1st-order kinetic model. These x^2 results are consistent with the results in Table 5.7 in terms of comparison of $q_{e\ calc}$ and $q_{e\ exp}$:

$$X^2 = \sum (q_{e\ exp} - q_{e\ calc})^2 / q_{e\ calc} \qquad \textbf{Eq. 5.10}$$

For this reason, it can be concluded that the adsorption mechanism of AmSh waste AC occurred mainly via chemisorption, at which there was involvement of valence forces through the exchange or sharing of electrons between the outer surface of AmShAC and the DBT molecules in model diesel fuel. The AmSeAC, however, followed intraparticle diffusion, implying that further adsorption of molecules from the outer surface to the pores of the adsorbent occurred. On the other hand, the AmWaAC followed mainly the pseudo 1st-order according to x^2 values, but there might also be intraparticle diffusion that occurred because of its r^2 values, which were highest.

Table 5.8 Chi-squared values for amarula waste ACs

AC type	Pseudo 1st order	Pseudo 2nd order	Itraparticle diffusion
Chi square (x^2) values in the processed Amarula wastes			
AmShAC-ST-45min	1,22E+06	1,86E-02	7,99E+05
AmSeAC-ST-45min	6,18E+04	9,29E+04	0,0047
AmWaAC-ST-45min	7,83E-02	9,38E+05	5,97E+05

Although the x^2 values of the amarula waste ACs showed consistency of q_e values for calculated and experimental data, the graph in Fig. 5.13 (c) showed that the plots did not pass through the origin. Therefore, the intraparticle diffusion model is not the sole rate-limiting step for adsorption mechanism; other adsorption mechanisms are involved on the surface [78]. The intercept C, which is referred to as a boundary layer effect, showed a high value of 132 for AmShAC than that for AmWaAC, confirming that there was a greater contribution of surface adsorption in the rate-limiting step. This may be valid for AmShAC which had an r^2 value of 0,9261 under pseudo 2nd-order model, a value that is not that far from unity. On the other side, the same graph extended in Fig. 5.13 (d) also showed multi-linear plots for amarula waste ACs, which further confirms different adsorption mechanisms. This was attributed to the rate of mass transfer, which is different at the initial and the final adsorption stages. In the initial stage, which was fast, the adsorption occurred via film diffusion while, in the second stage, it was through pore diffusion and intraparticle transportation. Pant and Sing [130] had a similar finding in his study.

It can be concluded that, the adsorption of DBT in model diesel on AmSh and AmWa waste ACs, was controlled by pore diffusion and intraparticle diffusion whereas for the AmSe waste ACs, the adsorption process was controlled by film diffusion. This then validated those observed O-functional groups on the outer surface of AC in Fig. 5.9 and those various pore sizes analysed in Table 5.6.and in Fig. 5.6. These properties are the main contributors to the multiple adsorption mechanism of DBT molecules in diesel fuel on amarula waste ACs. It can further be concluded that the rate-limiting step was film diffusion for AmShAC and AmWaAC, whereas for AmSeAC it was pore diffusion.

5.3.2.3 Adsorption isotherms

Adsorption isotherms are models that represent the amount of solute adsorbed by adsorbent during the adsorption process. Hence, they are imperative for designing adsorption systems for determining the correlation of experimental data. Several researchers have applied adsorption isotherms to various applications [76],[79],[131],[132]. In this study, linear Langmuir and Freundlich isotherms were applied to experimental data to determine the best fit of adsorption isotherms using Equations 5.11 and 5.12 respectively [133].

$$q_e = q_m - (1/K_L)(q_e/C_e) \qquad\qquad \textbf{Eq. 5.11}$$

$$\log q_e = n\log C_e + \log K_F \qquad\qquad \textbf{Eq. 5.12}$$

The q_e and q_m is the adsorption capacity of amarula waste ACs at equilibrium and the latter at maximum for monolayer coverage in mg/g. The C_e is the equilibrium concentration of DBT on the processed amarula ACs in mg/g. The K_L and K_F are isotherm constants for Langmuir and Freundlich, respectively. The latter indicates the adsorption capacity and the strength of the adsorption bond, whereas the n constant is the heterogeneity factor that describes the bond distribution [133]. The constants were determined from the linear plot of q_e vs q_e/C_e and from log q_e vs log C_e respectively (Fig. 5.14.). The separation factor s_f was calculated by Ahmadi et al. [78]. The isotherm parameters for amarula waste AC are listed in Table 5.9.
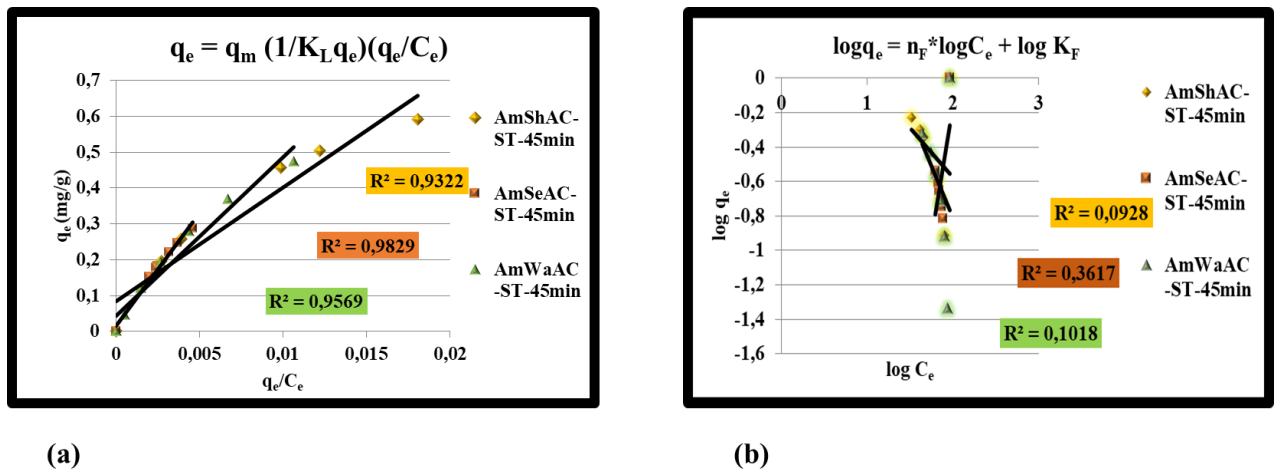
Fig. 5.14. (a) Langmuir and (b) Freundlich adsorption isotherms for amarula waste ACs

The correlation values r^2 were found to be close to unity for Langmuir isotherms in all the amarula waste ACs confirming the literature that says when experimental data is fitted to the

adsorption isotherm model, then the correlation value should be close to unity for the model to be considered the best fit [69]. The value of q_m for AmShAC-ST was 0,85 mg/g, which was higher, followed by AmWaAC-ST with 0,044 mg/g. These indicate that the adsorption of the DBT molecule on them followed more monolayer coverage compared to AmSeAC-ST, which had a lower q_{max} of 0,016 mg/g.

Table 5.9 Parameters of adsorption isotherms for amarula waste ACs

Ads type	Langmuir				Freundluich			
	r^2	q_m (mg/g)	K_L (g/mg)	sf	r^2	K_F (g/mg)	C	n
AmShAC-ST	0,9322	0,085	-0,032	-1,89	0,0928	1,78	0,58	-0,58
AmSeAC-ST	0,9829	0,016	-0,016	-0,47	0,3613	0,61	-0,49	3,17
AmWaAC-ST	0,9569	0,045	-0,023	-1,08	0,1018	5,05	1,62	-1,22

In the Freundlich isotherm, the correlation (r^2) values for amarula waste ACs were less than 0,5 and they were smaller than those in the Langmuir isotherms. This confirmed that the Freundlich isotherm was not the best fit. AmWaAC-ST had a higher K_F value of 5,05, indicating that it had a higher interaction of DBT on its surface. This was attributed to more aliphatic carbons, which were observed in the deconvoluted XRD analysis above.

The n values for amarula waste ACs were higher compared to the s_f values of the Langmuir isotherms. This indicates that there could also be some heterogeneous sites that may have occurred but in less quantity. On the other hand, AmSeAC-ST had the highest n value of 3,17 compared to the other ACs, indicating that its heterogeneity had the strongest bond distribution compared to those of other amarula waste ACs. These confirmed the kinetics discussed above.
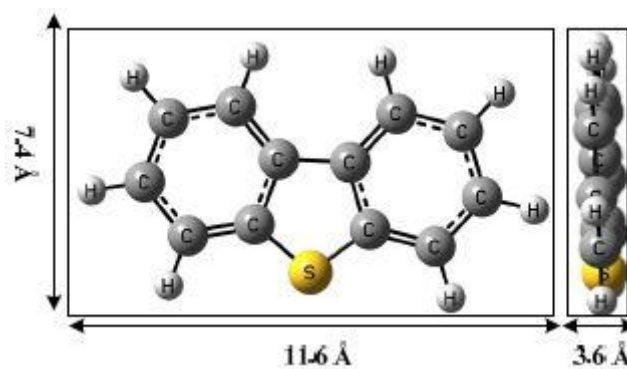
Fig. 5.15. Molecule and dimensions of DBT [134]

5.4 Conclusion

The amarula waste biomass from the production of Amarula liqueur, was successfully processed thermally by steam to ACs. The content of the DBT in model diesel fuel was successfully reduced further to 64 %, 54 % and 31 % by low-cost AmSh, AmWa and AmSe waste ACs, respectively. Thermal analysis (TGA/DTG) showed that the AmSh waste ACs were more thermally stable than the AmSe and AmWa waste ACs. It was concluded that despite the habitant of the amarula waste precursors, the microscopic analysis of the three amarula waste ACs had a morphology of sponge-like pores with a different pore shape which possessed slit-like shape porosity, concave, and tangled-like porosity that made it easier for more DBT molecules to diffuse through the pores via Van De Waal forces. The spectroscopic analysis of FTIR confirmed that the presence of dense O-functional groups on the acidic surface of ACs played an important role by increasing the desulphurization efficiency of the DBT molecule in model diesel fuel. Here, AmShAC performed better than the other amarula waste ACs. This surface adsorption occurred via chemisorption and Lewis acid–base interaction, whereas the XRD spectroscopy showed diffractograms that revealed the presence of hexagonal and cubic structure in all the amarula waste ACs. This further confirmed that the produced amarula waste ACs are amorphous. The deconvoluted XRD patterns showed that there were more aromatic carbons in AmSh ACs than in AmWa and AmSe ACs, making it more crystalline than the others. This contributes further to the much higher absorptivity of DBT. Textural properties further confirmed a massive improvement of (740 m^2/g, 430 m^2/g and 240 m^2/g) on the surface area for AmShAC-ST, AmWaAC-ST, and AmSeAC-ST respectively. In addition, pore sizes and pore volumes increased in the ACs when compared to the unprocessed amarula waste biomass in our previous work (Chapter 4) The AmShAC which were synthesized for a much longer steam residence time of 90 min revealed an improved surface area of approximately 1 200 m^2/g and a total pore volume of 0,4 cm^3/g. Therefore, this textural improvement resulted to a much higher adsorption efficiency of 73 %, which was close to the 72% of commercial AC that had a surface area of 540 m^2/g and total pore volume of 0,42 cm^3/g.

It was generally found that the adsorption of organo-sulphur compounds in diesel fuel depends on different adsorption mechanisms, which involves both the reactive and the unreactive active sites of AC. This was confirmed by one of the kinetic models and the adsorption isotherms applied to our experimental results. Despite that, it can finally be concluded that this study

successfully mitigated the waste-management issues by using amarula waste on the landfill to produce valuable products using environmentally friendly and sustainable operations. Some studies [46] have proved that the quantity of initial mass during the steam activation process does not have any impact on the product properties because the carbon–steam reaction is a gas–surface reaction not a gas–mass interaction. For these reasons, we can proudly conclude further that the production of amarula waste ACs by steam can be scaled up for commercial purposes at a particular rate, depending on the quality of production and the end-use, without compromising the quality of the product. This study further proved that the valuable product AC from the amarula waste successfully reduced the content of toxic substances such as DBT in diesel fuel that contribute negatively to climate change when emitted into the atmosphere.

5.5 Acknowledgements

5.6 References

[1]   J. Conway, "Amarula liqueur global market," https://www.statista.com/statistics/308846/aamarula-liqueur-global-sales-volume/, 2019.

[2]   P. Mishra, N. Singh, C. Shrama, A. K. Pathak, "Landfill Emissions and Their Impact on the Environment," *Int. J. Eng. Res. Technol.*, vol. 9, pp. 617-622, 2020.

[3]   H. Marsh and F. Rodríguez-Reinoso, "Activation processes (thermal or physical)," *Act. Carbon*, vol. 2, pp. 243–321, 2006, doi: http://dx.doi.org/10.1016/B978-008044463-5/50019-4.

[4]   K. S. Yang, Y. J. Yoon, M. S. Lee, W. J. Lee, and J. H. Kim, "Further carbonization of anisotropic and isotropic pitch-based carbons by microwave irradiation," *Carbon*, vol. 40, pp. 897–903, 2002.

[5]   Https://www.grandviewresearch.com/industry-analysis/activated-carbon-market, "Activated carbon market size, share/global industry report 2019–2025," *Global Industry Report 2019-2025*, 2019.

[6]   V. K. Gupta and Suhas, "Application of low-cost adsorbents for dye removal – A review," *J. of Environmental Management*, vol. 90, pp. 2313–2342, 2009, doi: 10.1016/j.jenvman.2008.11.017.

[7]   J. Guo and A. C. Lua, "Preparation of activated carbons from oil-palm-stone chars by microwave-induced carbon dioxide activation," *Carbon*, vol. 38, pp. 1985–1993, 2000, doi: 10.1016/S0008-6223(00)00046-4.

[8]   G. Selvaraju and N. K. A. Bakar, "Production of a new industrially viable green-activated carbon from Artocarpus integer fruit processing waste and evaluation of its chemical, morphological and adsorption properties," *J. Clean. Prod.*, vol. 141, pp. 989−999, 2017, doi: 10.1016/j.jclepro.2016.09.056.

[9]   C. I. Contescu, S. P. Adhikari, N. C. Gallego, and N. D. Evans, "Activated carbons derived from high-temperature pyrolysis of lignocellulosic biomass," *J. Carbon Res.*, vol. 4, pp. 9–13, 2018, doi: 10.3390/c4030051.

[10]   W. Mohd, A. Wan, W. Shabuddin, and W. Ali, "Comparison of pore development of activated carbon produced from palm shell and coconut shell," *Bioresource Technology*, vol. 93, pp. 63–69, 2004, doi: 10.1016/j.biortech.2003.09.015.

[11]   A. S. Mestre, J. Pires, J. M. F. Nogueira, and A. P. Carvalho, "Activated carbons for the adsorption of ibuprofen," *Carbon*, vol. 45, pp. 1979–1988, 2007, doi: 10.1016/j.carbon.2007.06.005.

[12]   H. Po, "Adsorption of dibenzothiophene (DBT) on activated carbon from date stones using phosphoric acid," *JKAU Eng. Sci.*, vol. 22, pp. 89–105, 2011.

[13]   A. N. A. El-Hendawy, S. E. Samra, and B. S. Girgis, "Adsorption characteristics of activated carbons obtained from corncobs," *Colloids Surfaces A Physicochem. Eng. Asp.*, vol. 180, pp. 209–221, 2001, doi: 10.1016/S0927-7757(00)00682-8.

[14]   A. Garba, H. Basri, N. S. Nasri, and R. Isma, "Synthesis and characterisation of porous carbon from biomass using KOH and K_2CO_3 chemical activation," *ARPN J. Eng. Appl.*

Sci., vol. 11, pp. 1613–1617, 2016.

[15]   J. Zhou, A. Luo, and Y. Zhao, "Preparation and characterisation of activated carbon from waste tea by physical activation using steam," *J. Air Waste Manage. Assoc.*, vol. 68, pp. 1269–1277, 2018, doi: 10.1080/10962247.2018.1460282.

[16]   B. Xiaofeng, Z. Xiaoqin, L. Zifu, N. Jiewen and B. Xue, "Properties and applications of biochars derived from different biomass feedstock sources," *Int. J. Agric. Biol Eng.*, vol. 10, pp. 242–250, 2017, doi: 10.3965/j.ijabe.20171002.2878.

[17]   P. D. Pathak, S. A. Mandavgane, and B. D. Kulkarni, "Fruit peel waste: Characterization and its potential uses," *Curr. Sci.*, vol. 113, pp. 444−454, 2017.

[18]   A. A. Arie and A. Putranto, "Activated carbons from KOH-activation of salacca peels as low cost potential adsorbents for dye removal," *Adv. Mater. Lett.*, vol. 7, pp. 226–229, 2016, doi: 10.5185/amlett.2016.6194.

[19]   H. Say, "High surface area mesoporous activated carbon from tomato processing solid waste by zinc chloride activation: Process optimization, characterization and dyes adsorption," *J. Clean. Prod.*, vol. 113, pp. 995–1004, 2016, doi: 10.1016/j.jclepro.2015.12.055.

[20]   W. A. Hall, D. E. Bellamy, and S. S. Walse, "Activated carbons from end-products of tree nut and tree fruit production as sorbents for removing methyl bromide in ventilation effluent following postharvest chamber fumigation," *J. Agric. Food Chem.*, vol. 63, pp. 3094–3103, 2015, doi: 10.1021/jf505193e.

[21]   T. M. Alslaibi , I. Abustan, M. A. Ahmad, A. A. Foul, "A review: Production of activated carbon from agricultural byproducts via conventional and microwave heating. *J. Chem. Technol. Biotechnol.,* vol. 88, pp. 1183−1190, 2015, doi: 10.1002/jctb.4028.

[22]   R. H. Gumus and I. Okpeku, "Production of activated carbon and characterization from snail shell waste (Helix pomatia)," *Adv. Chem. Eng. Sci.*, vol. 5, pp. 51–61, 2015, doi: 10.4236/aces.2015.51006.

[23]   D. Savova, E. Apak, E. Ekinci, F. Yardim, N. Petrov, T. Budinova, M. Razvigorova, V. Minkova, "Biomass conversion to carbon adsorbents and gas," *Biomass and Bioenergy*, vol. 21, pp. 133–142, 2001, doi: 10.1016/S0961-9534(01)00027-7.

[24] S. Lo, S. Wang, M. Tsai, and L. Lin, "Adsorption capacity and removal efficiency of heavy metal ions by Moso and Ma bamboo activated carbons," *Chem. Eng. Res. Des.*, vol. 90, pp. 1397–1406, 2011, doi: 10.1016/j.cherd.2011.11.020.

[25] K. N. Crombie, "Torrefaction/biochar production by microwave and conventional slow pyrolysis – comparison of energy properties," vol. 2, pp. 144–152, 2013, doi: 10.1111/gcbb.12021.

[26] L. Huang, Y. Sun, W. Wang, Q. Yue, and T. Yang, "Comparative study on characterization of activated carbons prepared by microwave and conventional heating methods and application in removal of oxytetracycline (OTC)," *Chem. Eng. J.*, vol. 171, pp. 1446–1453, 2011, doi: 10.1016/j.cej.2011.05.041.

[27] J. L. Figueiredo, M. M. A Freika, M. F. R. Perei, J.J.M. Orfao, "Modification of surface chemistry of activated carbon," *Carbon*, vol. 37, pp. 1379–1389, 1999.

[28] B-J. Lin and W-H. Chen, "Sugarcane bagasse pyrolysis in a carbon dioxide atmosphere with conventional and microwave-assisted heating," *Front. Energy Res.*, vol. 3, pp. 1–9, 2015, doi: 10.3389/fenrg.2015.00004.

[29] E. Villota, H. Lei, M. Qian, Z. Yang, S. M. A. Villota, Y. Zhang and G Yadavalli,, "Optimizing microwave-assisted pyrolysis of phosphoric acid-activated biomass: Impact of concentration on heating rate and carbonization time," *ACS Sustain. Chem. Eng.*, vol. 6, pp. 1319−1326, 2018, doi: 10.1021/acssuschemeng.7b03669.

[30] H. N. Tran, S. J. You, and H. P. Chao, "Fast and efficient adsorption of methylene green 5 on activated carbon prepared from new chemical activation method," *J. Environ. Manage.*, vol. 188, pp. 322−336, 2017, doi: 10.1016/j.jenvman.2016.12.003.

[31] H. Sayğili and F. Güzel, "High surface area mesoporous activated carbon from tomato processing solid waste by zinc chloride activation: Process optimization, characterization and dyes adsorption," *J. Clean. Prod.*, vol. 113, pp. 995−1004, 2016, doi: 10.1016/j.jclepro.2015.12.055.

[32] H. N. Tran, H. Chao, and S. You, "Activated carbons from golden shower upon different chemical activation methods: Synthesis and characterizations," *Adsorpt. Sci. Tchnology*, vol. 36, pp. 95–113, 2018, doi: 10.1177/0263617416684837.

[33] N. Dejang, O. Somprasit, and S. Chindaruksa, "A preparation of activated carbon from macadamia shell by microwave irradiation activation," *Energy Procedia*, vol. 79, pp. 727−732, 2015, doi: 10.1016/j.egypro.2015.11.556.

[34] Y. Liu, Z. Huo, Z. Song, C. Zhang, D. Ren, H. Zhong, and F. Jin, "Preparing a magnetic activated carbon with expired beverage as carbon source and KOH as activator," *J. Taiwan Inst. Chem. Eng.*, vol. 96, pp. 575−587, 2019, doi: 10.1016/j.jtice.2018.11.017.

[35] M. A. A. Elsayed and O. A. A. Zalat, "Factor affecting microwave assisted preparation of activated carbon from local raw materials," *Int. Lett. Chem. Phys. Astron.*, vol. 47, pp. 15–23, 2015, doi: 10.18052/www.scipress.com/ILCPA.47.15.

[36] S. Yang, H. Hu, and G. Chen, "Preparation of carbon adsorbents with high surface area and a model for calculating surface area," vol. 40, pp. 277–284, 2002.

[37] M. Zbair, K. Ainassaari, A. Drif, and S. Ojala, "Toward new benchmark adsorbents: Preparation and characterization of activated carbon from argan nut shell for bisphenol A removal," *Env. Scie. & Pollution Research.,* vol. 25, pp. 1869–1882, 2018.

[38] H. M. Al-swaidan and A. Ahmad, "Synthesis and characterization of activated carbon from Saudi Arabian date tree fronds wastes," vol. 20, pp. 25–31, 2011.

[39] D. P. Vargas-delgadillo, L. Giraldo and J. C. Moreno-piraján, "Preparation and characterization of activated carbon monoliths with potential application as phenol adsorbents," vol. 7, pp. 531–539, 2010.

[40] B. Tsyntsarski, S. Marinov, T. Budinova, M. F. Yardim, and N. Petrov, "Synthesis and characterization of activated carbon from natural asphaltites," *Fuel Process. Technol.*, vol. 116, pp. 346–349, 2013, doi: 10.1016/j.fuproc.2013.07.020.

[41] P. Thue, M. Abdebayo, E. Lima, J. M. Sieliechi, F. M. Machadod, G.L.Dotto, J. C.P.Vaghetti and S. L.P. Dias, "Preparation, characterization and application of microwave-assisted activated carbons from wood chips for removal of phenol from aqueous solution," *J. Mol. Liq.*, vol. 223, pp. 1067−1080, 2016, doi: 10.1016/j.molliq.2016.09.032.

[42] R. Pietrzak, A. Bazan, P. Nowicki, and P. Po, "Thermal analysis of activated carbon obtained from residue after supercritical extraction of hops," *J. Therm. Anal. Calorim.*,

vol. 125, pp. 1199–1204, 2016, doi: 10.1007/s10973-016-5419-5.

[43] J. Kazmierczak-Razna, P. Nowicki, and R. Pietrzak, "The use of microwave radiation for obtaining activated carbons enriched in nitrogen," *Powder Technol.*, vol. 273, pp. 71–75, 2015, doi: 10.1016/j.powtec.2014.12.037.

[44] Z. Qiang Zheng, H. Ying Xia, C. Srinivasakannan, J. Hui Peng, and L. Bo Zhang, "Utilization of crofton weed for preparation of activated carbon by microwave induced CO_2 activation," *Chem. Eng. Process. Process Intensif.*, vol. 82, pp. 1–8, 2014, doi: 10.1016/j.cep.2014.05.001.

[45] M. D. F. Salgado, A. M. Abioye, and M. Mat, "Preparation of activated carbon from babassu endocarpunder microwave radiation by physical activation," in *2nd International Renewable Energy Conference*, pp. 1–13, 2018.

[46] D. Bergna, T. Hu. H. Prokkola, H. Romar, and U. Lassi, "Effect of some process parameters on the main properties of activated carbon produced from peat in a lab-scale process," *Waste and Biomass Valorization*, vol. 11, pp. 2837−2848, 2020, doi: 10.1007/s12649-019-00584-2.

[47] J. Pallarés, A. González-Cencerrado, and I. Arauzo, "Production and characterization of activated carbon from barley straw by physical activation with carbon dioxide and steam," *Biomass and Bioenergy*, vol. 115, pp. 64−73, 2018, doi: 10.1016/j.biombioe.2018.04.015.

[48] Z. Zhang, W. Qu, J. Peng, L. Zhang, X. Ma, Z. Zhang and W. Li, "Comparison between microwave and conventional thermal reactivations of spent activated carbon generated from vinyl acetate synthesis," *Desalination*, vol. 249, pp. 247–252, 2009, doi: 10.1016/j.desal.2009.03.008.

[49] F. Rodríguez-Reinoso, M. Molina-Sabio, and M. T. González, "The use of steam and CO2 as activating agents in the preparation of activated carbons," *Carbon.*, vol. 33, pp. 15−23, 1995, doi: 10.1016/0008-6223(94)00100-E.

[50] M. T. Gonzalez, "The use of steam and CO_2 as activating agents in the preparation of activated carbons," *Carbon,* vol. 33, pp. 15–23, 1995.

[51] Y. Fernández, A. Arenillas, J. M. Bermúdez, and J. A. Menéndez, "Comparative study

of conventional and microwave-assisted pyrolysis, steam and dry reforming of glycerol for syngas production, using a carbonaceous catalyst," *J. Anal. Appl. Pyrolysis*, vol. 88, pp. 155–159, 2010, doi: 10.1016/j.jaap.2010.03.009.

[52]   D. Bergna, T. Varila, H. Romar, and U. Lassi, "Produced in one-stage and two-stage processes," *J. Carbon Res.*, vol. 4, pp. 1–10, 2018, doi: 10.3390/c4030041.

[53]   V. Minkova, M. Razvigorova, E. Bjornbom, R. Zanzi, T. Budinova, and N. Petrov, "Effect of water vapour and biomass nature on the yield and quality of the pyrolysis products from biomass," *Fuel Process. Technol.*, 2001, doi: 10.1016/S0378-3820(00)00153-3.

[54]   N. Mohamad Nor, L. C. Lau, K. T. Lee, and A. R. Mohamed, "Synthesis of activated carbon from lignocellulosic biomass and its applications in air pollution control – a review," *J. Environ. Chem. Eng.*, vol. 1, pp. 658–666, 2013, doi: 10.1016/j.jece.2013.09.017.

[55]   M. M. Yashim, N. Razali, N. Saadon, and N. A. Rahman, "Effect of activation temperature on properties of activated carbon prepared from oil palm kernel shell (Opks)," *ARPN J. Eng. Appl. Sci.*, vol. 11, pp. 6389–6392, 2016, [Online]. Available: http://www.arpnjournals.org/jeas/research_papers/rp_2016/jeas_0516_4285.pdf.

[56]   S. Lee and S. Park, "Effect of temperature on activated carbon nanotubes for hydrogen storage behaviors," *J. Hydrog. Energy*, vol. 35, pp. 6757–6762, 2010, doi: 10.1016/j.ijhydene.2010.03.114.

[57]   A. U. Rajapaksha, M. Vithage, M. Ahmad, D. C. Seo, J. S. Cho, S. E. Lee, S. S. Lee, Y. S. Ok, "Enhanced sulfamethazine removal by steam-activated invasive plant-derived biochar," *J. Hazard. Mater.*, vol. 290, pp. 43–50, 2015, doi: 10.1016/j.jhazmat.2015.02.046.

[58]   Https://www.epa.gov/greenvehicles/fast-facts-transportation-greenhouse-gas-emissions:, "Transportation Greenhouse Gas Emission," 2019.

[59]   V. Chandra Srivastava, "An evaluation of desulfurization technologies for sulfur removal from liquid fuels," *RSC Advances*. 2012, doi: 10.1039/c1ra00309g.

[60]   J. T. Sampanthar, H. Xiao, J. Dou, and T. Y. Nah, "A novel oxidative desulfurization

process to remove refractory sulfur compounds from diesel fuel," vol. 63, pp. 85–93, 2006, doi: 10.1016/j.apcatb.2005.09.007.

[61] Y. Yang, G. Lv, L. Deng, B. Lu, J. Li, J. Zhang, J. Shi, S. Du, "Ultra-deep desulfurization of diesel fuel via selective adsorption over modified activated carbon assisted by pre-oxidation," *J. Clean. Prod.*, vol. 161, pp. 422–430, 2017, doi: 10.1016/j.jclepro.2017.05.112.

[62] M. M. Oloruntoba, D. S. Aribike, and S. C. U. Nwachukwu, "A review on bio- and adsorptive desulfurization of diesel fuel," *J. Sci. Res. Reports*, vol. 11, pp. 1–6, 2016, doi: 10.9734/JSRR/2016/26909.

[63] P. R. Gawande, "Desulphurization techniques for liquid fuel: A review," *Int. J. Eng. Technol. Manag. Appl. Sci.*, vol. 2, pp. 121–127, 2014

[64] S. Chen and C. Zhao, "Biodesulfurization of diesel oil in oil – water two phase reaction system by Gordonia sp. SC-10," *Biotechnol. Lett.*, vol. 41, pp. 547–554, 2019, doi: 10.1007/s10529-019-02663-9.

[65] O. O. Sadare, F. Obazu, and M. O. Daramola, "Biodesulfurization of petroleum distillates – current status, opportunities and future challenges," *Environment MPI*, 2017, doi: 10.3390/environments4040085.

[66] M. Moradi, R. Karimzadeh, and E. Sadat, "Modified and ion exchanged clinoptilolite for the adsorptive removal of sulfur compounds in a model fuel: New adsorbents for desulfurization," *Fuel*, vol. 217, pp. 467–477, 2018, doi: 10.1016/j.fuel.2017.12.095.

[67] X. Li, H. Zhu, C. Liu, P. Yuan, Z. Lin, J. Yang, Y. Yue, Z. Bai, T. Wang, X. Bao, "Synthesis, modification, and application of hollow mesoporous carbon submicrospheres for adsorptive desulfurization," *Ind. & Eng. Chem. Res.,* vol. 54, pp. 15020−15030, 2018, doi: 10.1021/acs.iecr.8b02780.

[68] W. Ahmad, I. Ahmad, M. Ishaq and K. Ihsan, "Adsorptive desulfurization of kerosene and diesel oil by Zn impregnated montmorollonite clay," *Arab. J. Chem.*, vol. 10, pp. S3263–S3269, 2017, doi: 10.1016/j.arabjc.2013.12.025.

[69] M. L. Samaniego, M. D. G. De Luna, D. C. Ong, M. Wan and M. Lu, "Isotherm and thermodynamic studies on the removal of sulfur from diesel fuel by mixing-assisted

oxidative − adsorptive desulfurization technology," *Energy & Fuels*, vol. 33, pp. 1098–1105, 2019, doi: 10.1021/acs.energyfuels.8b04242.

[70] G. I. Danmaliki, T. A. Saleh, and A. A. Shamsuddeen, "Response surface methodology optimization of adsorptive desulfurization on nickel/activated carbon," *Chem. Eng. J.*, vol. 313, pp. 993–1003, 2017, doi: 10.1016/j.cej.2016.10.141.

[71] T. A. Saleh and G. I. Danmaliki, "Influence of acidic and basic treatments of activated carbon derived from waste rubber tires on adsorptive desulfurization of thiophenes," *Taiwan Institute Chem. Eng.*, vol. 60, pp. 460–468, 2016, doi: 10.1016/j.jtice.2015.11.008.

[72] G. I. Danmaliki and T. A. Saleh, "Effects of bimetallic Ce/ Fe nanoparticles on the desulfurization of thiophenes using activated carbon," *Chem. Eng. J.*, vol. 307, pp. 914–927, 2017, doi: 10.1016/j.cej.2016.08.143.

[73] P. Baltzopoulou, K. X. Kallis, G. Karagiannakis, and A. G. Konstandopoulos, "Diesel fuel desulfurization via adsorption with the aid of activated carbon: Laboratory- and pilot-scale studies," *Energy & Fuels*, vol. 29, pp. 5640–5648, 2015, doi: 10.1021/acs.energyfuels.5b01133.

[74] T. A. Saleh, "Simultaneous adsorptive desulfurization of diesel fuel over bimetallic nanoparticles loaded on activated carbon," *J. Clean. Prod.*, vol. 173, pp. 2123–2132, 2018, doi: 10.1016/j.jclepro.2017.11.208.

[75] E. Yang C. Yao, Y. Liu, C. Zhang, L. Jia, D. Li, Z. Fu, D. Sun, S. R. Kirk, D. Yin , "Bamboo-derived porous biochar for efficient adsorption removal of dibenzothiophene from model fuel," *Fuel*, vol. 211, pp. 121–129, 2018, doi: 10.1016/j.fuel.2017.07.099.

[76] D. Stan, A. Mohammed, A. Usman, and M. M. Oloruntoba, "Adsorptive desulfurization of diesel using activated sewage sludge: Kinetics, equilibrium and thermodynamics studies," *Appl. Petrochemical Res.*, vol. 10, pp. 1−12, 2019, doi: 10.1007/s13203-019-00239-2.

[77] A. R. Lopes, A. Scheer, G. Silva, C. I. Yamamoto, "Palladium loaded on activated carbon for sulphur compounds adsorption in commercial diesel," *XXI Congreso Brasileiro de Engenharia Quimica conference,* 2016, and Machado 2013.

[78] M. Ahmadi, M. Mohammadian, and M. R. Khosravi-nikou, "Experimental, kinetic, and thermodynamic studies of adsorptive desulfurization and denitrogenation of model fuels using novel mesoporous materials," *J. Hazard. Mater.*, vol. 374, pp. 129–139, 2019, doi: 10.1016/j.jhazmat.2019.04.029.

[79] A. Saleh, K. O. Sulaiman, S. A. Al-hammadi, H. Dafalla, and I. Danmaliki, "Adsorptive desulfurization of thiophene, benzothiophene and dibenzothiophene over activated carbon manganese oxide nanocomposite: With column system evaluation," *Clean. Prod.*, vol. 154, pp. 401–412, 2017, doi: 10.1016/j.jclepro.2017.03.169.

[80] Y. Nath and N. Verma, "Adsorptive desulfurization of diesel oil using nickel nanoparticle-doped activated carbon beads with/without carbon nanofibers: Effects of adsorbate size and adsorbent texture," *Fuel*, vol. 189, pp. 186–194, 2017, doi: 10.1016/j.fuel.2016.10.044.

[81] R. Zhao, Z. Jin, J. Wang, G. Zhang, D. Zhang, and Y. Sun, "Adsorptive desulfurization of model fuel by S, N-codoped porous carbons based on polybenzoxazine," *Fuel*, vol. 218, pp. 258–265, 2018, doi: 10.1016/j.fuel.2018.01.043.

[82] S. Velu, X. Ma, and C. Song, "Zeolite-based adsorbents for desulfurization of jet fuel by selective adsorption," *ACS Div. Fuel Chem. Prepr.*, vol. 47, pp. 447–448, 2002.

[83] Y. Shi, X. Zhang, L. Wang, and G. Liu, "MOF-derived porous carbon for adsorptive desulfurization," vol. 60, pp. 2747–2751, 2014, doi: 10.1002/aic.

[84] J. A. Arcibar-orozco, J. R. Rangel-mendez, and T. J. Bandosz, "Desulfurization of model diesel fuel on activated carbon modified with iron oxyhydroxide nanoparticles: Effect of tert-butylbenzene and naphthalene concentrations," *Energy & Fuels*, vol 27, pp. 5380−5387, 2013, doi: 10.1021/ef400999g.

[85] X. Ma, A. Zhou, and C. Song, "A novel method for oxidative desulfurization of liquid hydrocarbon fuels based on catalytic oxidation using molecular oxygen coupled with selective adsorption," *Catal. Today*, vol. 123, pp. 276–284, 2007, doi: 10.1016/j.cattod.2007.02.036.

[86] M. K. Nazal, M. Khaled, M. A. Atieh, I. H. Aljundi, G. A. Oweimreen, and A. M. Abulkibash, "The nature and kinetics of the adsorption of dibenzothiophene in model diesel fuel on carbonaceous materials loaded with aluminum oxide particles," *Arab. J.*

Chem., vol. 12, pp. 3678−3691, 2015, doi: 10.1016/j.arabjc.2015.12.003.

[87] T. T. Ng Flora, A. Rahman, T. Ohasi, and M. Jiang, "A study of the adsorption of thiophenic sulfur compounds using flow calorimetry," *Appl. Catal. B Environ.*, vol. 56, pp. 127−136, 2005, doi: 10.1016/j.apcatb.2004.07.018.

[88] M. A. Abdulwahhab, "Naphtha desulfurization by prepare Cu-Ni-zeolite adsorbent," *Iragi J. Chem. Pet. Eng.*, vol. 15, pp. 9–14, 2014.

[89] Z. Zhao, Z. Zuhra, L. Qin, Y. Zhou, L. Zhang, F. Tang, C. Mu., "Confinement of microporous MOF-74 (Ni) within mesoporous γ-Al$_2$O$_3$ beads for excellent ultra-deep and selective adsorptive desulfurization," *Fuel Process. Technol.*, vol. 176, pp. 276–282, 2018, doi: 10.1016/j.fuproc.2018.03.037.

[90] Q. Li, Z. Li, L. Lin, X.Y. Wang, Y. Wang, C. Zhang and H. Wang, "Facile synthesis of activated carbon/carbon nanotubes compound for supercapacitor application," *Chem. Eng. J.*, vol. 156, pp. 500–504, 2010, doi: 10.1016/j.cej.2009.10.025.

[91] Z. G. Marko Muzaic, Katica Sertic-Bionda, "Kinetic and statistical studies of Adsorptive desulfurization of diesel fuel on commercial activated carbons," *Chem. Eng. Technol.*, vol. 154, pp. 355–364, 2008, doi: 10.1002/ceat.200700341.

[92] I. Danmaliki and A. Saleh, "Influence of conversion parameters of waste tires to activated carbon on adsorption of dibenzothiophene from model fuels," *J. Cleaner Prod.* vol. 117, pp. 50–55, 2016, doi: 10.1016/j.jclepro.2016.01.026.

[93] W. Mohd, A. Wan, W. Shabuddin and W. Ali, "Comparison of pore development of activated carbon produced from palm shell and coconut shell," *Boresource Technol.*, vol. 93, pp. 63–69, 2004, doi: 10.1016/j.biortech.2003.09.015.

[94] M. Fan, "Steam activation of chars produced from oat hulls and corn stover," *Bioresource Technol.*, vol. 93, pp. 103–107, 2004, doi: 10.1016/j.biortech.2003.08.016.

[95] M. Asensio, R. Font, and A. Marcilla, "Steam activated carbons from bituminous coal in a continous multibed fluidized bed pilot plant," *Carbon*, vol. 34, pp. 1515–1520, 1996.

[96] G. De Oliveira, R. De Andrade, M. Trindade, H. M. C. Andrade, C. T. de Carvalho, "Thermogravimetric and spectroscopic study (TG–DTA/FT–IR) of activated carbon

from the renewable biomass source babassu," *Quim. Nova*, vol. 40, pp. 284–292, 2017.

[97]   H. Marsh and F. Rodríguez-Reinoso, "SEM and TEM images of structures in activated carbons," *Activated Carbon*, pp. 366–382, 2006.

[98]   O. Onay, "Influence of pyrolysis temperature and heating rate on the production of bio-oil and char from safflower seed by pyrolysis, using a well-swept fixed-bed reactor," *Fuel Process. Technol.*, vol. 88, pp. 523–531, 2007, doi: 10.1016/j.fuproc.2007.01.001.

[99]   I. Snook and D. Mcculloch, "Reverse Monte Carlo analysis of the structure of glassy carbon using electron-microscopy data," vol. 57, pp. 148–157, 2006.

[100] J. Byrne and H. Marsh, "Porosity in carbons," *Origins of Carbons*, pp. 2–12, 1995.

[101] S. Gavalda, K. Kaneko, K. T. Thomson, and K. E. Gubbins, "Molecular modeling of carbon aerogels," *Colloids & Suraces A: Physicochem. & Eng. Asp.* vol. 187, pp. 531−538, 2001, doi: 10.1016/S0927-7757(01)00641-0.

[102] S. Gavalda, K. E. Gubbins, Y. Hanzawa, K. Kaneko, and K. T. Thomson, "Nitrogen adsorption in carbon aerogels: A molecular," *Langmuir*, vol. 18, pp. 2141–2151, 2002.

[103] C. Zhang, W. Song, G. Sun, L. Xie, L. Wan, J. Wang and K. Li, "Synthesis, characterization, and evaluation of activated carbon spheres for removal of dibenzothiophene from model diesel fuel," *Ind. Eng. Chem. Res.*, vol. 53, pp. 4271–4276, 2014.

[104] I. Ruthven, A. Processes, A. Society, and T. Materials, "Porosity in carbons: Modeling," in *Origins of Carbons*, pp. 87–142, 1995.

[105] A. Ali and R. Idris, "Utilization of low-cost activated carbon from rapid synthesis of microwave pyrolysis for WC nanoparticles preparation," *Adv. Mater. Lett.*, vol. 8, pp. 70–76, 2017, doi: 10.5185/amlett.2017.6964.

[106] T. Miyazaki, T. Oshida, T. nakutsuka, M. Okanmoto and M. Endo., "Analysis of pore structure of activated carbon by using image processing of Tem images," *Mol. Cryst. Liq. Cryst.*, vol. 388, pp. 499–504, 2010, doi: 10.1080/10587250215278.

[107] M. R. Endo, T. Furuta, F. Minoura, and C. Kim, "Visualized observation of pores in activated carbon fibres by HRTEM and combined image processor," *Supermolecular

Sci., vol. 5, pp. 261–266, 1998.

[108] M. S. N. Yoshizawa, Y. Yamada, "TEM lattice images and their evaluation by image analysis for activated carbons with disordered microtexture," *J. Mater. Sci.*, vol. 3, pp. 199–206, 1998.

[109] N. Yoshizawa, K. Maruyama, and Y. Yamada, "XRD evaluation of CO_2 activation process of coal- and coconut shell-based carbons," *Fuel*, vol. 79, pp. 1461–1466, 2000.

[110] N. M. Oberlin, "Graphitizability of carbonaceous materials as studied by TEM and X-ray diffraction," *J. Microsc.*, vol. 132, pp. 353–363, 1983.

[111] A. Ali and R. Idris, "Utilization of low-cost activated carbon from rapid synthesis of microwave pyrolysis for WC nanoparticles preparation," *Adv. Mater. Lett.*, vol. 8, pp. 70–76, 2017, doi: 10.5185/amlett.2017.6964.

[112] A. Dandekar, R.T.K,. Barker and M.A. Vinnice "Characterization of activated carbon, graphitized carbon fibres and synthetic," *Carbon,* vol. 36, pp. 1821–1831, 1998.

[113] B. Manoj and A. G. Kunjomana, "Study of stacking structure of amorphous carbon by X-ray diffraction technique," *Int. J. Electrochem. Scie.,* vol. 7, pp. 3127–3134, 2012.

[114] M. S. Shamsuddin, N. R. N. Yusoff, and M. A. Sulaiman, "Synthesis and characterization of activated carbon produced from kenaf core fiber using H3PO4 activation," *Procedia Chem.*, vol. 19, pp. 558–565, 2016, doi: 10.1016/j.proche.2016.03.053.

[115] C. Saka, "BET, TG – DTG, FT-IR, SEM, iodine number analysis and preparation of activated carbon from acorn shell by chemical activation with ZnCl 2," *J. Anal. Appl. Pyrolysis*, vol. 95, pp. 21–24, 2012, doi: 10.1016/j.jaap.2011.12.020.

[116] H. N. Tran, S. J. You, A. Hosseini-Bandegharaei, and H. P. Chao, "Mistakes and inconsistencies regarding adsorption of contaminants from aqueous solutions: A critical review," *Water Research*. vol. 120, pp. 88−116, 2017, doi: 10.1016/j.watres.2017.04.014.

[117] I. M. Lima, A. Boateng, and K. T. Klasson, "Physicochemical and adsorptive properties of fast-pyrolysis bio-chars and their steam activated counterparts†," *J. chem Technol Biotechnol.*, vol. 85, pp. 1515–1521, 2010, doi: 10.1002/jctb.2461.

[118] A. U. Rajapaksha, M. Vithanage, and S. S. Lee, "Steam activation of biochars facilitates kinetics and pH-resilience of sulfamethazine sorption," *J. Soils Sediments*, vol. 16, pp. 889−895, 2015, doi: 10.1007/s11368-015-1325-x.

[119] K. Sun and Jiang. J. C. Jiang "Preparation and characterization of activated carbon from rubber-seed shell by physical activation with steam," *Biomass Bioenerg*, vol. 34, pp. 539–544, 2010.

[120] C. A Toles, L. H Wartelle and McAloon A, "Acid activated carbons from almond shells: Physical, chemical and adsorptive properties and estimated cost of production," *Bioresour. Technol.*, vol. 71, pp. 87-92., 2000.

[121] Y. Zhang, Z. Xing, Z. Duan, M. Li, and Y. Wang, "Effects of steam activation on the pore structure and surface chemistry of activated carbon derived from bamboo waste," *Appl. Surf. Sci.*, vol. 315, pp. 279–286, 2014, doi: 10.1016/j.apsusc.2014.07.126.

[122] L. J. Fu, K. F. Yue, Q.Y. Gao, B.Y. Sun, Y.Y. Zhu, "Preparation, characterization and application of lignin-based activated carbon from black liquor lignin by steam activation.," *Chem. Eng. J.*, vol. 228, pp. 1074–1082., 2013.

[123] L. Deng, B. Lu, J.Li, G. Lv, S. Du, J. Shi, Y. Yang, "Effect of pore structure and oxygen-containing groups on adsorption of dibenzothiophene over activated carbon," *Fuel*, vol. 200, pp. 54−61, 2017, doi: 10.1016/j.fuel.2017.03.018.

[124] D. Jha, M. Haider, R. Kumar, N. Byamba-Ochir, W. Shim, B. M. Sivagnanam and H. Moon, "Enhanced adsorptive desulfurization using Mongolian anthracite-based activated carbon," *ACS Omega*, vol. 4, pp. 20844−20853, 2019, doi: 10.1021/acsomega.9b03432.

[125] S. Zur Lagergren., "Theorie der Sogenannten Adsorption Gelöster Stoffe, Kungliga Svenska Vetenskapsakademiens," *Handlingar*, vol. 24, pp. 1–39, 1898.

[126] M. Blanchard, G. Maunaye, "Removal of heavy-metals from waters by means of natural zeolites," *Water Resour.*, vol. 8, pp. 1501–1507, 1984.

[127] W. J. Weber, "Kinetics of adsorption on carbon from solution.," *J. Sanit. Eng. Div.*, vol. 89, pp. 31–60, 1963.

[128] M. Muzic, K. Sertic-bionda, Z. Gomzi, S. Podolski, and S. Telen, "Chemical

engineering research and design study of diesel fuel desulfurization by adsorption," *Chem. Eng. Res. Des.*, vol. 88, pp. 487–495, 2009, doi: 10.1016/j.cherd.2009.08.016.

[129] M. Hadi, G. Mckay, and A. Maleki, "Prediction of optimum adsorption isotherm: Comparison of chi-square and Log-likelihood statistics,"*Desalination and Water Treatment,* vol 49, pp 81−94, 2012, doi: 10.1080/19443994.2012.708202.

[130] K. K. Pant, and T.S. Sing, "Equilibrium, kinetics and thermodynamics study for adsorption of As(II) ions on activated alumina," *Sep. Purifications Technol.*, vol. 3, pp. 139–147, 2004.

[131] A. B. F. Câmara, R. V Sales, L. C. Bertolino, R. P. P. Furlanetto and E. Rodríguez, "Novel application for palygorskite clay mineral: A kinetic and thermodynamic assessment of diesel fuel desulfurization," *Adsorption*, vol. 26, pp.267−282, 2019.

[132] B. Saha, A. Singh and S. Sengupta, "Advances compounds present in fuel†," *RSC Adv.*, vol. 6, pp. 76434–76447, 2016, doi: 10.1039/C6RA16367J.

[133] I. Langmuir, "The adsorption of gases on plane surfaces of glass, mica and platinum," vol. 345, pp. 1361−1403, 1918, doi: 10.1021/ja02242a004.

[134] E. S. Moosavi, S. A. Dastgheib and R. Karimzadeh, "Adsorption of thiophenic compounds from model diesel fuel," *Energies,* vol. 10, pp. 4233–4250, 2012, doi: 10.3390/en5104233.

Chapter 6

Gasification Biochar as a Potential Adsorbent in Adsorptive Desulphurization of Diesel Fuel

Chapter abstract

With the aim of seeking highly efficient and low-cost adsorbents, for small scale adsorptive desulfurization (ADS) of diesel fuel, gasification chars which are solid carbon-based materials with highly porous structure were used as adsorption agents for ADS of diesel fuel. Four chars were used as adsorbents for the ADS of model diesel fuels in a stirred basket reactor: Char-1 from the gasification of coal fines mixed with an algae binder; Char-2 from the gasification of wood pellets; Char-3 from plasma gasification of wood pellets; Char-4 from amarula shell waste. The clean and dirty diesel samples were analyzed using the GC-PFPD technique. The performance of this biochar was compared with a commercial activated carbon (COMAC). The gasification chars were further activated using two different activation agents (KOH and steam) and used in the ADS process. The laboratory results show that the gasification char had to be modified before use, to improve the ADS efficiency of diesel fuels. Although the gasification chars showed a lower sulphur-removing capacity than the one with commercial activated carbon, due to processing conditions, there are potential opportunities for using gasification char for desulphurization. The fresh and used adsorbents were characterized using TGA, BET, XRD, SEM-EDX and FTIR. The research outcome of this study could provide information needed for the design of a small-scale ADS of diesel fuel.

6.1 Introduction

Dibenzothiophene (DBT) is a toxic organo-sulphur molecule that is mainly found in distillates of crude oil, such as diesel fuel [1]. When the sulphur compounds (DBT and their alkyl derivatives) are present in high concentrations, it has a negative impact on the environment, as the compounds are emitted into the atmosphere and indirectly cause green-house gases that contaminate the atmosphere and result in global warming [2]. Furthermore, they corrode catalytic converters and eventually strain the economy. In addition, with long-term exposure, they cause health problems such as carcinogen and infertility in human beings. Furthermore, transportation fuel also contributes to the air pollution, hence its toxic constituents are a major concern [3]–[5].

Different desulphurization techniques have been developed, such as hydrodesulphurization (HDS), oxidative desulphurization (ODS), bio-desulphurization (BOD) and adsorption desulphurization (ADS) [1]–[5]. The latter was selected for this study, due to its low energy consumption during adsorption and regeneration of the adsorbents. The challenge with ADS has been that some adsorbents - such as metal-metal oxides, zeolites, and MOFs - are not economical for use in production, because they have to undergo various expensive processes before reaching the desired efficiency. Therefore, alternative cheaper adsorbents are preferred, such as activated carbon [6]–[14]. However, the use of activated carbon has an economic drawback when it is produced from non-renewable resources such as coal; but, when it is produced from biomass or waste carbon materials, it becomes a cheaper and more sustainable product. Likewise, biochar is an emerging sustainable adsorbent that has been found to be cost-effective when sourced from biomass or biomass waste as in articles [15],[16],[17]–[24] [25],[26]. Biochar is produced by means of carbonization, pyrolysis, or gasification processes. During syngas production, biochar is produced as a waste product. Therefore, the use of biochar from gasification reactors becomes a sustainable way of utilizing waste biochar as a green adsorbent.

Biochar is a microporous carbonaceous material that is produced under an inert or limited oxygen atmosphere condition. Fig. 6.1 shows the molecular structure of biochar. Joseph and Shackley defined biochar as: "The porous carbonaceous solid produced by the thermochemical conversion of organic materials in an oxygen depleted atmosphere that has physicochemical properties suitable for safe and long-term storage of carbon in the environment" [27],[28]. The International Biochar Initiative (IBI 2012) defined biochar as a solid material that is obtained

by thermochemical conversion of biomass in an oxygen-limited environment [29]. Biochar is considered different from charcoal, in that charcoal is a source of charred organic matter for producing fuel and energy, whereas biochar can be applied for carbon sequestration and environmental management [30],[31]. The quality of the biochar also depends on production conditions, such as feedstock type [19],[32],[33], temperature [22],[34], heating rate [35],[36], atmospheric conditions [22],[24],[32],[37], and the type of reactor. However, fewer studies have been done on the properties of biochar when using different gasification reactors, hence a core focus of this study was to determine the impact of a gasification reactor on biochar properties.
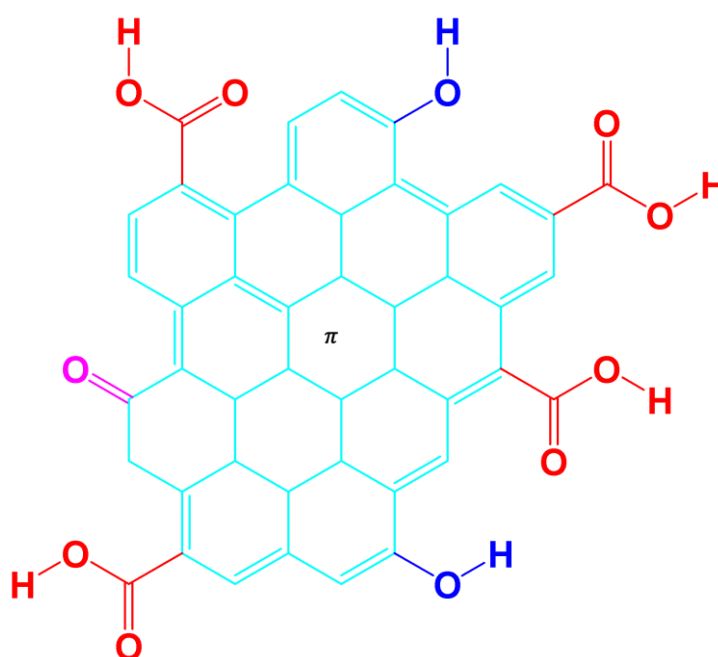
Fig. 6.1. Molecular structure of biochar

Biochar has been in existence since the 18th century when it was used to improve soil quality. In the 19th century, it became more popular and was found to mitigate climate change, environmental management and energy production issues [30]. Other scientists have made use of biochar in the treatment of water [31],[34],[38]. It was also concluded that it is advantageous to the environment due to its resistance to microbial decay and because it has a high adsorption capacity for ions and molecules. Therefore, in recent years, some researchers have used biochar as an adsorbent for removing organic and inorganic contaminants, such as heavy metals or for gas and energy storage [22],[25],[26],[38]–[42]. However, there is fewer literature on removing

organo-pollutants in diesel fuel when using biochar as an adsorbent. Therefore, this study used a biochar waste material during syngas production from different gasification reactors, in order to reduce the sulphur content in DBT model diesel fuel.

This biochar was then activated by means of KOH and a steam activating agent, to enhance the adsorption properties of the DBT molecule. The approach of using chemical and physical activation with biochar was reported by several researchers [18],[37],[43]–[52]. It is stated that the use of KOH as an activating agent is a tool for creating micropores in the material [47],[48],[53],[54]. However, Arie [55] obtained mesoporous activated carbons in his study when using a KOH activating agent with biochar. This could have been due to a different feed stock or activating conditions used by individual researchers in their studies. When steam is used as an activating agent, it enhances the surface functional groups and the porosity of the material. Rajapaksha et al. [37] activated biochar with steam, and found that the BET surface area and total pore volume of biochar increased from 421.31 m^2/g to 576.09 m^2/g, and from 0.0219 cm^3/g to 0.1091 cm^3/g, respectively.

6.2 Methodology

The biochar from gasification reaction was applied as they are, and later processed by chemical (KOH) activating agent and by physical (steam) activating agent. The application was done through adsorptive desulphurization, using a stirred batch reactor.

6.2.1 Materials

The materials used were as follows: amarula shell waste biochar (AmSh-BC); wood biochar (Wood-DGBC); algae-coal biochar (ALGC-DGBC); wood biochar (Wood-PGBC); a horizontal electric tube furnace; quartz tubes and quartz crucible boats; Afrox nitrogen gas (99 % purity); chemicals (99 % pure reagents from sigma): KOH pellets, dibenzothiophene (DBT), hexadecane and toluene.

6.2.2 Sampling and activating of gasification char

AmSh-BC was sampled after the pyrolysis of amarula shell waste, as described in Chapter 5. Wood-DGBC and Wood-PGBC were sampled from biochar waste after gasification of wood from a down draft gasifier (DG) and a plasma gasifier (PG) respectively. ALGC-DGBC was a biochar waste obtained using the down draft gasifier (DG) and pellets made of algae and coal fines. All the biochar was sieved to obtained ≈ 1-2 mm particle size and applied for the adsorption of DBT in model diesel, as described in Chapters 4 and 5.

6.2.2.1 Steam activation

The biochar was then processed by steam activation according to the procedure described in Chapter 5. The samples were labelled AmSh-BC-ST, Wood DGBC-ST, Wood-PGBC-ST, and ALGC-DGBC-ST, and then used for desulphurization of model diesel fuel.
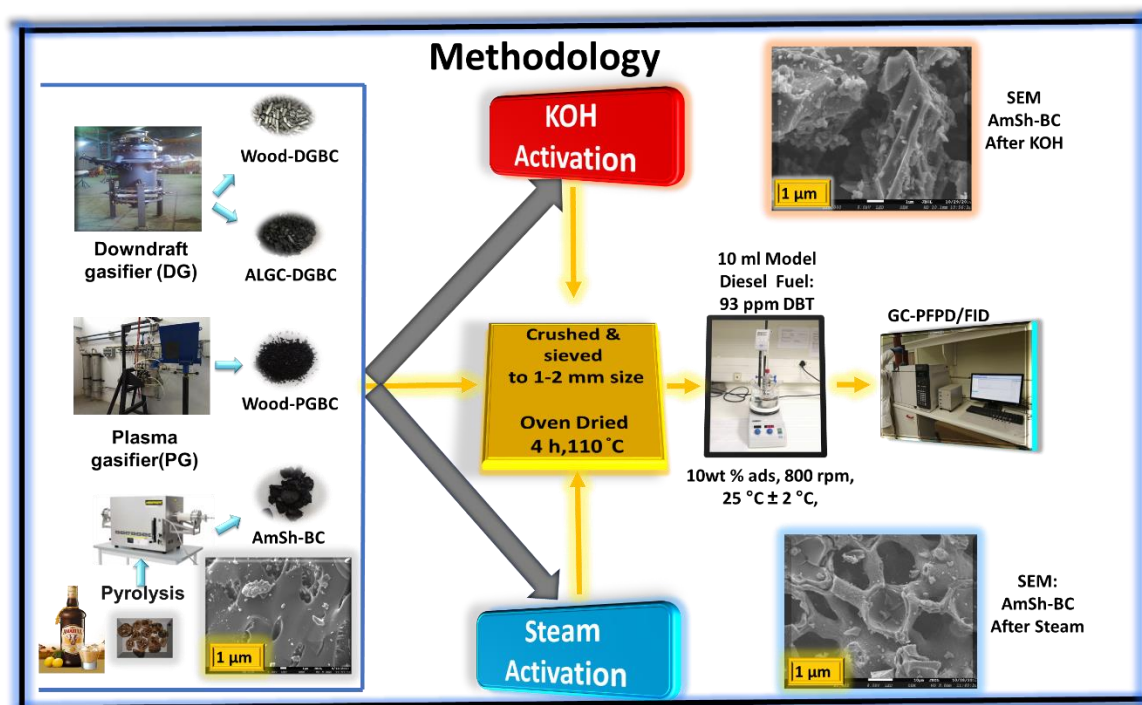
Fig. 6.2. Schematic for activating gasification chars

6.2.2.2 Potassium hydroxide (KOH) activation

The 48 % (w/v) KOH solution was used as a different activating agent to process the biochar. Each massed biochar sample was impregnated with a KOH solution with a ratio of 1:3 (C:KOH). The mixture was stirred continuously at room temperature for 1 h in an open system. The slurry was filtered and dried at 110 °C in an oven over-night. The dried impregnated biochar was subjected to a horizontal furnace using a quartz tube as a reactor. The 800 °C of conventional heat was applied to the system at 10 °C/min together with a nitrogen flow of 60 ml/min. The temperature was held for 2 h, before allowing the system to cool to room temperature. The biochar was washed with hot and cold distilled water until neutral PH was obtained. The samples were oven dried, labelled as AmSh-BC-KOH, Wood DGBC-KOH, Wood-PGBC-KOH, and ALGC-DGBC-KOH, and then subjected to adsorption of DBT in model diesel (Fig. 6.1).

Both processed and unprocessed biochar were characterized using FTIR, BET and SEM-EDX techniques for surface analysis, textural properties, and for microscopic analysis respectively, as per our previous work (chapter 4 and 6).

6.3 Results and discussion

6.3.1 Performance of biochar in terms of desulphurization of diesel fuel

The biochar was found to reduce DBT in model diesel fuel, as shown by the adsorption mechanism in Fig. 6.3. However, it had to be activated by KOH and steam activating agents, after which the desulphurization efficiency increased three times.
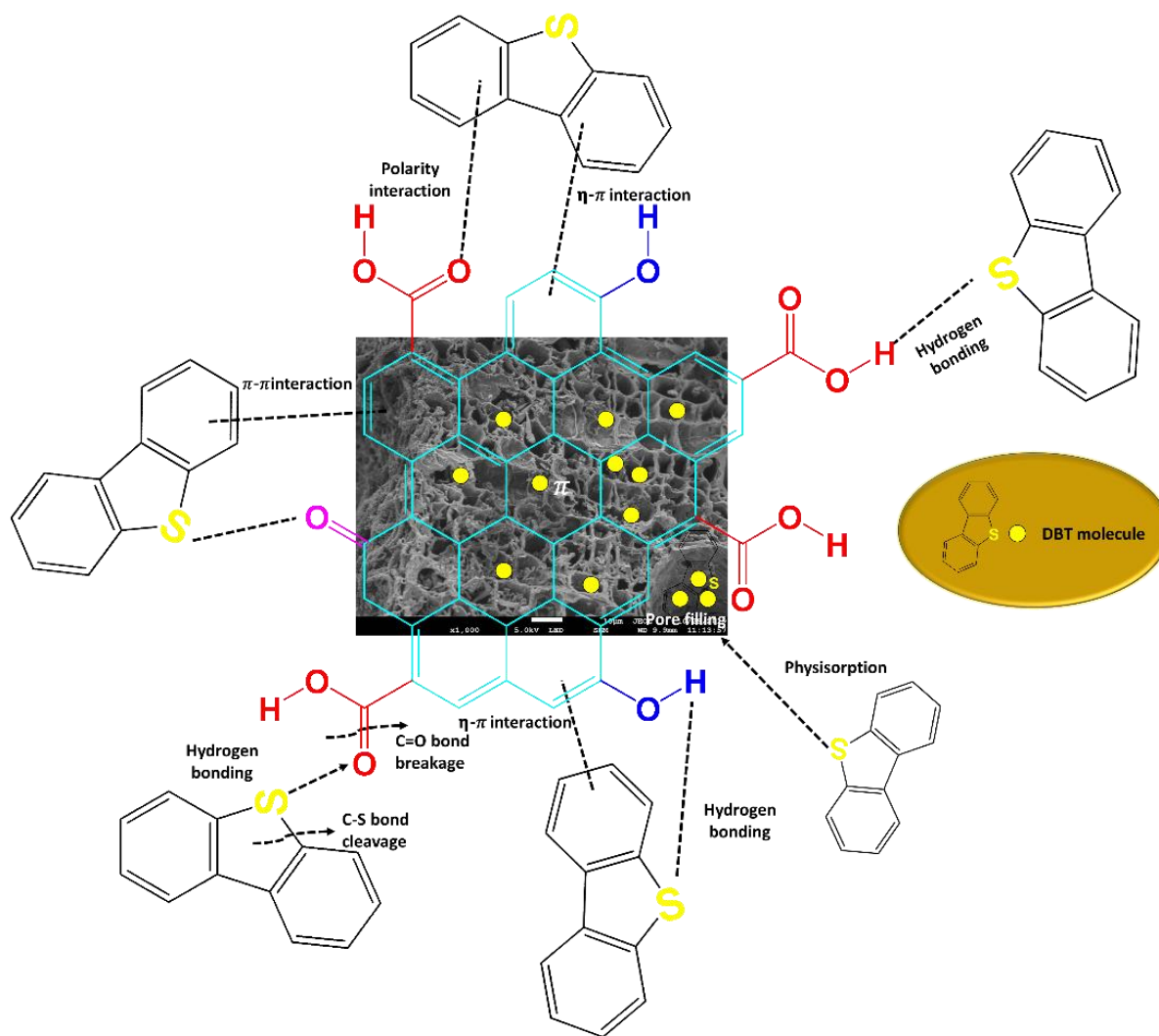
Fig. 6.3. Adsorption mechanism of DBT molecule on biochar

6.3.1.1 Performance of biochar before activation

Fig. 6.4 (a) shows the adsorption of DBT in model diesel fuel by biochar from different sources and when using different gasification reactors, before processing. The biochar was able to reduce the organo-sulphur molecule; however, the percentage removal was found to be very low when compared to COMAC, which was used as the reference standard. This could have been due to the very small BET surface area and total pore volume, as observed in Table 6.1 of the textural analysis. The smaller surface area provided less area for electrostatic adsorption of DBT on the biochar. The diffusion of DBT molecules that occurred via physical attraction was limited to the tiny pores of biochar, because the molecule was too large to penetrate through the pores. Despite this, it was found that the unprocessed biochar could have adsorbed

some DBT molecules via heteroatoms of oxygen on the surface of biochar, as shown in Fig. 6.3. The FTIR spectra in Fig. 6.5 (a) confirmed the presence of O-H, C=O, and C-O functional groups on the biochar at 3 441 cm^{-1}, 1 662 cm^{-1} and 1 064 cm^{-1} respectively. The O-functional groups observed were attributed to phenols, lactose, carboxylic, carbonyls and quinols on the surface of the biochar. These functional groups could have interacted with the fused sulphur atom in a DBT molecule via hydrogen bonding to create exothermic adsorption. Other researchers [44],[56],[57] also found that the O-functional groups enhanced the adsorption of organo-pollutants. In addition, both the biochar and the DBT molecule possessed the benzene ring structure. Therefore, the C=C functional group observed at 1 541 cm^{-1} provided validation for the vibrational bend of the aromatic ring skeletons found in the biochar. It was this type of functional group that further contributed to the formation of a π-π complex between the biochar and the DBT molecule. The BET analysis for each individual biochar was found to be similar to that obtained by other researchers [19],[17],[32] who used different precursors for biochar production. The gasification reactor may have also contributed to this adsorption difference, at which the wood biochar from the down-draft gasifier (DG) had higher textural properties than the one from the plasma gasifier (PG). This could be attributed to the high energy ions from the plasma, which destroyed the surface of the material. So, it was found that the performance of gasification biochar on DBT adsorption, was in the order of AmSh-BC > ALGC-DGBC > Wood-DBGC > Wood-PGBC.
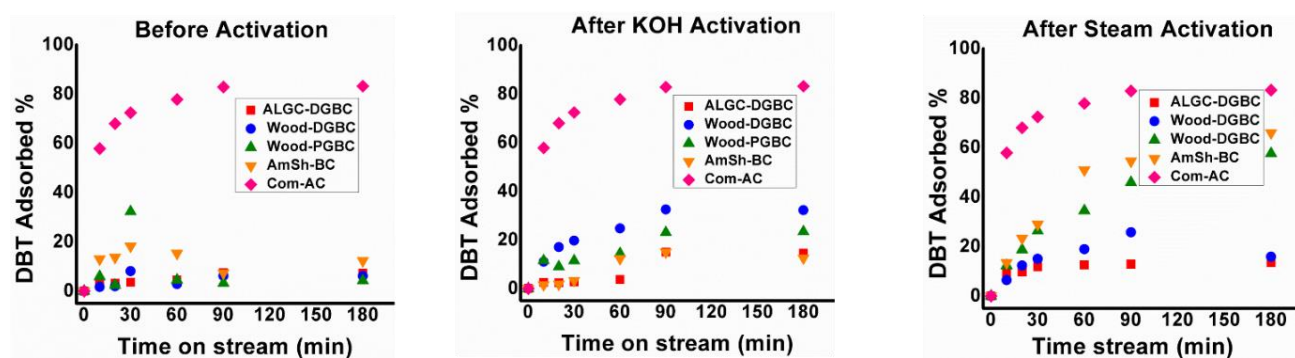
Fig. 6.4. Desulphurization efficiency of biochar (a) before KOH, (b) after KOH and (c) after steam activation (Temp. 25 ℃, ads 10wt % (m/v), stirring 800 rpm)

6.3.1.2 Biochar after KOH processing

The biochar processed by KOH showed an increase in surface area, despite it being impregnated for just 1 h of continuous stirring at room temperature, compared to the unprocessed biochar. The activation of carbon with KOH is described by Reactions 6.1 - 6.8 [45],[47],[53],[55],[58]–[61]

$C + 4KOH \rightleftarrows K_2CO_3 + K_2O + 2H_2$…...…………………………………………**Reaction 6.1**

$K_2CO_3 + C \rightleftarrows 2K + 2CO$…..…………………………………………**Reaction 6.2**

$K_2O + C \rightleftarrows C\text{-}O\text{-}K + K$ ……………………………………………**Reaction 6.3**

$C\text{-}O\text{-}K + H_2O \rightleftarrows C\text{-}O\text{-}H + KOH$ …….……………………………………**Reaction 6.4**
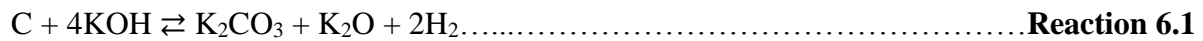
The K_2CO_3 that was formed in Reaction 6.1 was reduced by C to form K, CO, CO_2 and H_2. This resulted in the formation of more pores. The boiling point of potassium is 780 °C [47], however, the activation temperature used in this study was 800 °C. This resulted in Reactions 6.5 & 6.6, and the K_2O produced in Reaction 6.1 was further reduced by the hydrogen and carbon present in the system, to form potassium (K) metals. It was these K metals that further created more voids in the existing pores of biochar, and thus increased the porosity and the surface area of the gasification chars (Table 6.1 of the textural analysis).

$K_2O + H_2 \rightleftarrows 2K + H_2O$……………………………………………………..**Reaction 6.5**

$K_2O + C \rightleftarrows 2K + CO$…………………………………………………….**Reaction 6.6**

In this study, the textural properties of KOH/BC were compared with the KOH/BC in literature [39],[45],[55]. These differences could have been due to the impregnation time and impregnation temperature applied. Luo J. soaked biochar with 1 L of 2M KOH for 4 h at 25 °C, and found a BET surface area of 128.42 m^2/g from 75.30 m^2/g [39]. Garba A. produced AC by impregnating biochar with KOH at 70 °C and obtained a surface area of 305.1 m^2/g from [45]. Arie et al. [55] . impregnated salacca peel biochar with 10 % KOH (1:2) for 20 h and recorded a surface area of 813 m^2/g. In this study, the impregnation was done for just 1 h at room temperature, so as to save energy, and to see how active the biochar would be if it was slightly exposed to KOH.

Table 6.1 Textural analysis of biochar before KOH, after KOH and after steam activation

Adsorbent Type	Before Activation				After KOH activation				After Steam Activation			
	Surface Area (m^2/g)	Pore Size (nm)	Pore Vol (cm^3/g)	Adsorption Efficiency % @ 180min	Surface Area (m^2/g)	Pore Size (nm)	Pore Vol (cm^3/g)	Adsorption Efficiency % @ 180min	Surface Area (m^2/g)	Pore Size (nm)	Pore Vol (cm^3/g)	Adsorption Efficiency % @ 180min
ALGC-DGBC	18,83	6,68	0,03	7±4	30,26	6,45	0,05	15 ±5	111,26	2,74	0,08	13 ±7
Wood-DGBC	60,83	4,47	0,07	6 ±5	217,99	2,63	0,14	32 ±3	153,91	2,95	0,11	27,34
Wood-PGBC	45,86	4,7	0,05	4 ±7	241,16	2,6	0,16	23 ±4	249,36	2,61	0,16	58 ±4
AmSh-BC	19,69	4,33	0,02	12 ±3	199,84	2,15	0,11	15 ±6	740,7	2,7	0,37	66 ±2
Com-AC	540,73	3,39	0,42	82 ±4	540,73	3,39	0,42	82 ±4	540,73	3,39	0,42	82 ±4

The outcomes detailed in this section, may suggest that when the gasifier char was totally immersed in a highly-concentrated KOH, it was assumed that the film of KOH covered the external surface and the entire internal surface of the char for a complete reaction [53]. However, the process may not have been completed. In this work, the activation process was carried out under inert conditions; therefore, it may have been difficult for the surface pyrolysis to occur on the surface of the char. This could have then resulted in the surface structure of the carbon being partially activated.

Fig. 6.4 (b) shows the improved adsorption efficiency of DBT in model diesel on biochar processed by KOH. These results are similar to the results of the study done by Saleh T.A.: he treated biochar with basic and acidic chemicals and found that the basic chemicals had a lower adsorption efficiency of DBT at optimal conditions than the acid-treated biochar [14]. As explained above, the O-functional groups also contributed to the adsorption of DBT in model diesel. Therefore, the FTIR spectra of KOH/BC showed similar functional groups as the raw biochar, except that the vibrational bends of OH, C=O, C-O and C=C shifted to a higher value wavenumber, as shown in Fig. 6.5 (b). This was because the KOH adds more of the O-functional groups to the carbon. The activation process detailed above, also showed that the K_2CO_3 is one of the by-products seen during activation, which adds more C-O groups to the char. Hence the spectra showed more intense peaks and more shifting of the peaks. In addition, the KOH/BC spectra showed two strong bands between 3 700 cm^{-1} – 3 900 cm^{-1}. This was attributed to the sp C-H band from the C-C triple bond of the alkynes and was confirmed by the vibrational bands at 2 376 cm^{-1} for C≡C function group on the surface [45],[62],[63].

To further understand the impact of KOH on the surface of biochar and its desulphurization, a protocol known as Boehm titration was proposed by Oickle et al. [64] and applied by other researchers [14],[19],[62]. This approach will be used in our next research study. This is to quantitatively determine the acidic groups (carboxylic, lactones, phenols and quinones) and the

basic groups (ethers, pyrone, and carbonyl). This technique will be incorporated into the TPD analysis.

So, under KOH activation, the ADS efficiency was found to be in the order of Wood-DGBC-KOH > Wood- PGBC-KOH > AmShBC-KOH > ALGC-DGBC-KOH.

6.3.1.3 Biochar after steam processing

The biochar was found to have more increased surface area after steam processing compared to KOH/BC and unprocessed char (except Wood- DGBC). This improvement was attributed to steam creating more micropores and widening the micropores already present to create mesopores. This phenomenon occurred because the steam removed trapped products from incomplete combustion during thermal treatment [37]. This then increased the surface area of the steamed biochar. Similar results were obtained by other researchers [42],[49],[50],[65],[66]. There was also increased desulphurization efficiency of DBT in model diesel on the steamed biochar, as shown in Fig. 6.4 (c) above. Furthermore, the presence of mesopores speeds up the movement of the DBT molecules to the micropores - hence more DBT was removed. Some researchers found similar results; that the presence of micropores and mesopores improved the adsorption of organo-sulphur compounds in diesel fuel [9],[13],[67]–[70]. Our previous work (chapter 4 and 5) confirmed that it is not only the porosity that contributes to the adsorption of organo-sulphur pollutants, but that even the heteroatoms, such as oxygen on the surface plays an important role. Therefore, analysis of the functional groups of steamed biochar was carried out, as shown in Fig. 6.5 (c) spectrum below. The FTIR spectra confirmed the presence of O-H, C=O, C-O and C=C functional groups, which were highly intense and had shifted to 3 459 cm^{-1}, 1 624 cm^{-1}, 1 054 cm^{-1} and 1 541 cm^{-1} respectively, due to steam activation on biochar. The spectra also showed that there were no visible bands after 3 700 cm^{-1}, compared to the BC and KOH/BC, except in ALGC-DGBC, which had a very weak peak at 2 330 cm^{-1}.

However, the steam could have contributed more to the acidic functional groups forming, which then made the steam-biochar more acidic, and further contributed to acid-base interaction with the DBT molecule, which is basic in nature. Shafeeyan et al. [71] showed the structure of activated carbon with basic and acidic functional groups. Some researchers [9],[11],[13] also stated that the organo-sulphur molecules are bound to favour the adsorption

on an acidic adsorbent, because of their basic nature . Therefore, the KOH activation could have increased the basic functional groups on biochar, and thus limiting acid-base interaction with the DBT molecules; hence KOH/BC had a lower desulphurization efficiency than steam/BC.

Yang E. obtained 80 % and 62 % adsorption efficiency in 50 ppm DBT model diesel using modified bamboo biochar that was oxidized and un-oxidized [16]. This percentage removal was found to be higher than in this study (64 %). The major differences in desulphurization efficiency were attributed to the textural and structural properties of the adsorbent. In Yang's study [13], $ZnCl_2$ was used to process bamboo biochar at 500 °C; later the $ZnCl_2$/Bamboo BC was modified with HNO_3 at 700 °C before applying it for desulphurization. In our study, a one-step process was used that required less energy, less chemicals (KOH) and a shorter production time, which means a more sustainable process when steam is utilized.

Upon comparing, the individual performance of gasification char after steam activation, it was found that their desulphurization efficiency was in the order of AmSh-BC-ST > Wood-PGBC-ST > Wood-DGBC-ST > ALGC-DGBC-ST. This might have been attributed to the higher pore volume of AmSh-BC-ST as seen in Table 6.1 above.
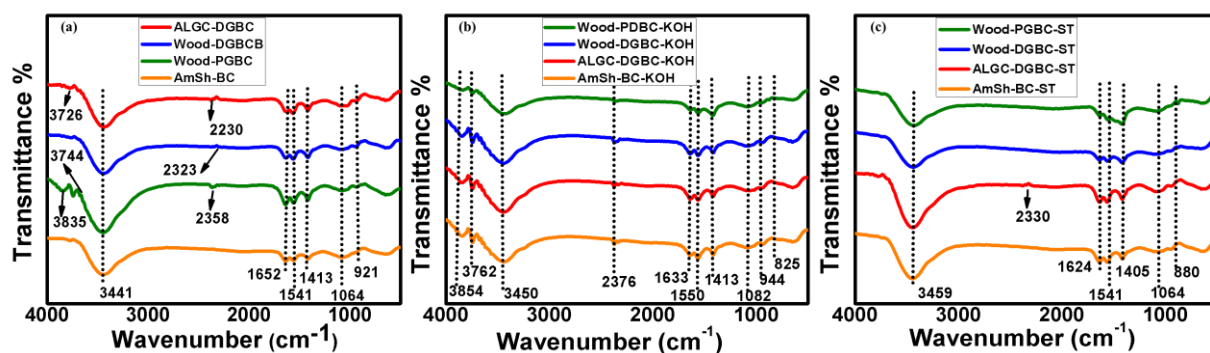

Fig. 6.5. FTIR spectra of biochar (a) before (b) after KOH, and (c) after steam activation

6.3.2 Microscopic analysis of gasification char

The morphology of biochar before activation, after KOH activation, and after steam activation is shown in Fig. 6.6. All the biochar before processing biochar showed the presence of tiny

pores on the surface. These existing pores could have been due to gasification of the carbonaceous precursor, which removed the volatiles and thus left the carbon structure with micropores. Micropores are classified as ultra-micropores (≤ 0.7 nm) and super-micropores (0.7-2.0 nm). The KOH processed biochar is shown in Fig. 6.6 (e), (f), (g) and (h). It showed that some surfaces had cavities, whereas other surfaces did not have cavities. This could have been due to partial activation of biochar by KOH, which only occurred within 1 hr of impregnation time. This then confirms the results above; that even though there was improved surface area and porosity of KOH/BC compared to raw biochar (Table 6.1), when compared to some studies, the surface area was smaller. The steamed biochar showed a morphology with more pores of different sizes: micropores (≤ 2 nm), mesopores (2-50 nm) and macropores (>50 nm). There were also some particles on the surface on both the processed and unprocessed biochar. These particles were identified as potassium (K), sodium (Na), magnesium (Mg) and calcium (Ca) during the EDS analysis shown in Appendix C: Tables C1, C2, and C3. However, EDX is not a suitable technique for determining the actual amount of the elements identified. Therefore, the observed carbon (C) and oxygen (O) elements will be quantitatively analyzed using the CHNSO analyzer in the next part of the research.

6.3.2.1 Morphology of biochar before activation

When analyzing different biochar samples before activation, it was found that the amarula shell waste biochar (Fig. 6.6 (a) (i)) showed well-defined micropores with an oval pore shape on the surface (Fig. 6.6 (a) (iii)). Image (a)(IV) further showed that there was some roughness inside some of the pores. This could have limited the smooth diffusion of the DBT molecule inside the AmSh-BC, confirming the low adsorption efficiency seen in Fig. 6.4 (a).

Fig. 6.6 (b) shows the morphology of wood biochar (wood-DGBC) from a down-draft gasifier. The micrograms shown in Fig. 6.6 (b) (i) and (ii) show the upper view with more micropores close to each other, and a cross-sectional area that had more particles on the surface, respectively. This explains why the Wood-DGBC had a higher BET surface area than the AmSh-BC in Table 6.1. Upon magnification, the micrograms in Fig. 6.6 (b) (iii) & (iv) showed irregular pores, with some clustering inside the pores and some of the clusters consisting of branch-like trees. The clusters inside the pores could also have inhibited complete diffusion of the DBT, even though this biochar had larger pore sizes, compared to AmSh-BC. The larger

pore size is indicated in Table 6.1; however, the adsorption efficiency of DBT was lower than that of AmSh-BC.

After analyzing the wood biochar (Wood-PGBC) from the plasma gasifier (Fig. 6.6 (c)), it was found that the microgram showed various morphology, as shown in Fig. 6.6 (c) (i). The magnification of the first point in Fig.6.6 (c) (ii) showed the presence of irregular pores filled with lots of clusters that nearly filled the pores. This morphology is like that of wood biochar from the down-draft gasifier, except that it had less clustering inside the pores. The magnification of the second point of analysis in 6.6 (c) (iii) showed the presence of round pores on the biochar, with no clustering and a smooth surface. This morphology 6.6 (c) (iii) was found to be similar to the one obtained by Bardestani R. for steamed activated biochar using a mixture of spruce and pine wood [18]. Further magnification of the inside of the pores (image 6.6 (c) (iv) revealed that the clusters exhibited more tiny pores, while the clusters in wood-DGBC did not have any tiny pores. This difference in wood biochar morphology is attributed to the design of the gasification reactor and different pore sizes in this biochar may be due to super-micropores and ultra-micropores.

These differences in the biochar structure were also attributed to the precursor that was used to produce the biochar. Some researchers also found different morphological properties in biochar products when using different precursors [17],[32],[72]. Wood DGBC and ALGC-DGBC were obtained from the downs-draft gasifier, but had different morphology traits, due to the feed-stocks inlet. Similarly, Barrera-Zapata's team [17] also used different wood types during gasification at 700 °C and found different pore morphology types. Furthermore, the design of a reactor for gasification also plays an important role in the properties of the product. This was confirmed when using wood biochar that showed different morphology traits when using a down-draft gasifier and a plasma gasifier. There is less literature that provides a comparison of biochar obtained from different gasification reactors.

Why did the AmSh-BC have a higher desulphurization efficiency than the other biochar samples studied, yet it had lower textural properties? It may be that more adsorption of DBT was controlled by chemisorption because of the high number of dense O-functional groups on the surface. This was confirmed using an FTIR spectrum of AmSh-BC, which was quite different to the other gasification chars. On the other hand, it could have been that the other gasification biochar was more basic. Sun et al. [32] produced biochar from different feedstock samples and found that they have different PH values, which was more basic. Therefore,

AmSh-BC could have been slightly acidic, which then resulted in more DBT being removed due to acid-base interaction.

6.3.2.2 Morphology of biochar after KOH activation

The AmSh-KOH micrograms are shown in Fig. 6.6 (e). The image shows parallel pores that are semi-closed. These pores are not distributed on the entire surface. Therefore, this morphology confirms that there was partial activation of amarula shell waste biochar, due to minimum exposure of the KOH particles, as described above. No tiny pores were observed, despite the increased magnification. Based on this morphology, it can be concluded that the KOH agent created mesopores from the existing micropores that were observed in unprocessed AmSh-BC. The surface of AmSh-BC-KOH had more particles on the surface compared to raw biochar. This was attributed to the increased content of potassium elements (K) from the KOH agent, as confirmed by EDS analysis (Appendix C: Table C2).

The Wood-DGBC-KOH microscopic analysis showed two different morphologies: (i) and (ii) in Fig. 6.6 (f). Image 6.6 (i) shows lots of particles on the surface, despite 5 times magnification in (iii), which signifies that some surfaces were difficult to activate under the given conditions. The other microgram (6.6 (ii)) showed lots of semi-closed pore that were parallel to each other and close to each other. The pores exhibited some tiny pores inside the bigger pores. This morphology shows that the Wood-DGBC-KOH had both mesopores and micropores. The micrograms also showed more particles on the surface compared to the unprocessed wood biochar from the down-draft gasifier. These particles were also identified as Mg and K elements in higher quantity by means of the EDS shown in the Appendix C: Tables C2 and C3, respectively.

6.3.2.3 Morphology of biochar after steam activation

Fig. 6.6 (i), (j), (k) and (l) shows the morphology of biochar after steam activation for AmSh-BC, Wood-DGBC, Wood-PGBC and ALGC-DGBC, respectively. The overview in the microgram of AmSh-BC-ST shows lots of deep wide large pores at just x300 magnification. Upon further magnification - x5 000 and x10 000, it was found that there were also tiny pores of different sizes covering the entire surface. This confirmed that AmSh-BC-ST contained

various size micropores, mesopores and macropores, and that these mesopores and macropores helped to speed up the movement of DBT, resulting in high desulphurization efficiency, as confirmed above. Th(is again validates the higher surface area and the pore volume of 0.39 cm^3/g observed in textural properties of AmSh-BC-ST (Table 6.1).
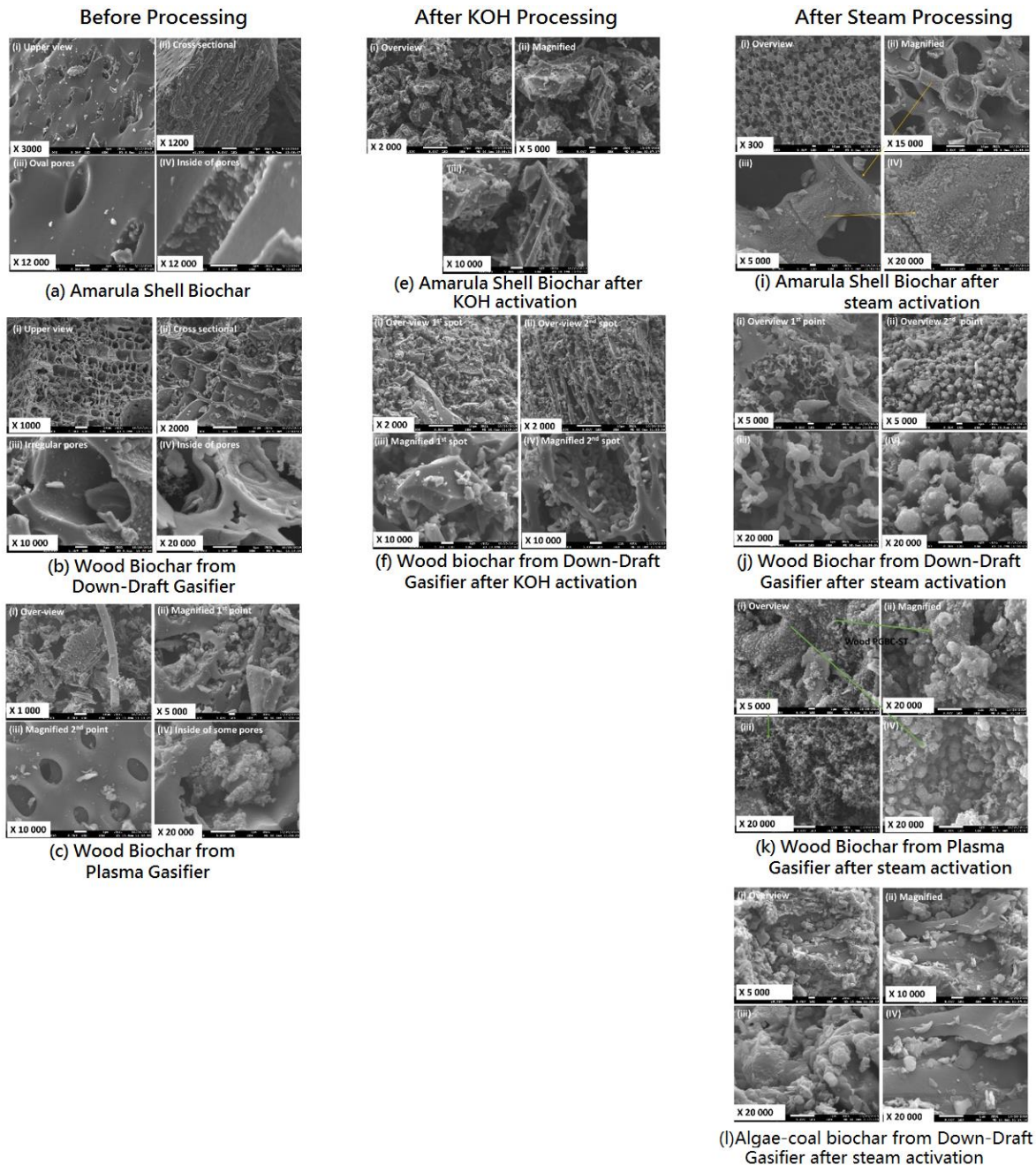

Fig. 6.6. Micrograms showing the morphology of biochar: before - (a), (b), (c) (d); after KOH - (e), (f), (g), (h); and after steam - (i), (j), (k), (l) activation at different magnifications

The Wood-DGBC-ST showed an overview image that had two different morphology types. The microgram in Fig. 6.6 (j) (i) showed the presence of irregular pores with some ring- worm like fibres inside the large pores at x5 000 magnification. Upon further magnification (x20 000), it was found that these rings had a smooth surface with no extra pores, but with goose-bumps. This morphology resembles that of activated meso-carbon microbeads on carbon nanotubes (AMCMB/CNT), and that of activated carbon beads loaded with carbon nanofibers and nickel (Ni/CNF/ACB) obtained in articles [58] and [70]. The other microgram shown in (j) (ii) showed an overview morphology of lots of sphere-like-balls at x5 000 magnification. Upon further magnification to x20 000, it was found that some of these balls possessed some cracks and micropores on the surface. This morphology was similar to that found in [58],[67],[70],[73].

Wood-PGBC-ST is shown in microgram Fig. 6 (k) (i). It has lots of spherical balls and branch-like trees at x5 000 magnification. This microgram was further analyzed for three different sport at x20 000 magnification. It was found that the micrograms in (k) (ii) and (iv) had tiny pores of different sizes on the surface of the spherical balls. The microgram in (k) (iii) also showed tiny pores on the branch-like trees. These pores covered the entire surface and could have been due to the ultra-micropores (≤ 0.7 nm) and super-micropores (0.7-2.0 nm) in the steamed biochar from the plasma gasifier. The bead-like or aerosol morphology in this steamed biochar was also seen in [58],[67],[70],[73]. This morphology explains why this wood biochar had a higher desulphurization efficiency of DBT in model diesel fuel than the one from the down-draft gasifier. It also confirms that for DBT adsorption, there were more super-micropores in the material, which contributed more to the desulphurization efficiency of organo-sulphur compounds. Other researchers [67],[70] also proved a similar scenario; that the micropores allow more of the DBT adsorption.

The overview of the ALGC-DGBC-ST microgram seen in Fig. 6.6 (l) (i) shows a flake-like morphology, and a smooth surface on a scapula-like morphology at x5 000 magnification. The scapula was further magnified to x10 000 and then to x20 000 in image (ii) and (iv) respectively. There were no observable pores. Upon magnification to x20 000 of another point in microgram (iii), it was found that there were some large pores and a few lines on the surface of some flakes. These lines signified that there is the potential for pore formation if the steam reside for a longer period of time. This confirms why the desulphurization efficiency of DBT in model diesel from this gasifier biochar was the lowest. The difficulty in activating algae-coal biochar under the same conditions as with the other samples was that its precursor was

made up of algae biomass combined with coal fines. Some coal materials might be destructive, making it difficult to activate under mild conditions [74]–[76].

6.4 Conclusions

It was concluded that the use of biochar waste obtained during syngas production has the potential for use as an adsorbent for adsorptive desulphurization of diesel fuel. In addition, it was found that biochar obtained when using different gasification reactors possessed different morphology and structural properties, which confirmed that the type of gasifier reactor design has a major impact on the biochar type. Moreover, the properties of biochar were also found to be influenced by the type of feedstock. These properties had a major influence on their capabilities for desulphurization of DBT in model diesel fuel. Nevertheless, this gasifier biochar had to be processed in order to enhance porosity and O-functional groups for higher adsorption efficiency.

It was concluded that: (1) for steam activation the AmSh-BC performed better than the wood-PGBC, Wood-DGBC and ALGC-DGBC in terms of desulphurization of DBT in model diesel fuel, irrespective of any processing approach; (2) for KOH activation, the Wood-DGBC had better desulphurization capacity than the other three BCs. It was further concluded that the use of steam activation with biochar improved the desulphurization efficiency significantly compared to KOH activation of Wood-PGBC and AmSh-BC. This was because these two steamed/BCs had better textural and structural surface properties than the KOH biochar. This was revealed by BET and FTIR analysis, respectively.

It was also concluded that the KOH/BC showed improved activity on DBT in model diesel fuel, even though the preparation of the adsorbent involved exposure of biochar with a chemical for just 1 h. Therefore, longer impregnation time and a higher temperature during adsorbent preparation may be required for improved performance of KOH/BC on DBT adsorption. Microscopic analysis (SEM) confirmed the presence of various micropores on biochar, except in algae-coal biochar. The micrograms further showed improved porosity after using KOH and steam as activating agents on gasifier biochar. However, it was found that wood biochar had more than one morphology compared to ALGC-DGBC and AmSh-BC. This confirmed that some feedstock can possess more than one morphology under the same processing conditions.

Finally, it was concluded that the amarula shell waste biochar performed better than the wood-PGBC, Wood-DGBC and ALGC-DGBC in terms of desulphurization of DBT in model diesel

fuel, irrespective of any processing approach. It was generally found that KOH produced processed biochar that is more microporous, whereas steam produced micro porosity, mesopores and macropores in the processed biochar. Despite this, the outcomes of the research provided valuable information for designing a small-scale plant for adsorptive desulphurization of diesel fuel.

6.5 Acknowledgements

6.6 References

[1]   C. Song, "An overview of new approaches to deep desulfurization for ultra-clean gasoline, diesel fuel and jet fuel.," *Catal. Today*, vol. 86, pp. 211–263, 2003, doi: 10.1016/S0920-5861(03)00412-7.

[2]   J. H. Kim, X. Ma, A. Zhou, and C. Song, "Ultra-deep desulfurization and denitrogenation of diesel fuel by selective adsorption over three different adsorbents : A study on adsorptive selectivity and mechanism," *Catal. Today*, vol. 111, pp. 74–83, 2006, doi: 10.1016/j.cattod.2005.10.017.

[3]   J. Zongxuan, L. Ü. Hongying, Z. Yongna, and L. I. Can, "Oxidative Desulfurization of Fuel Oils," *Chinese J. Catal.*, vol. 32, pp. 707–715, 2011, doi: 10.1016/S1872-2067(10)60246-X.

[4]   A. Chica, A. Corma, and M. E. Dómine, "Catalytic oxidative desulfurization (ODS) of diesel fuel on a continuous fixed-bed reactor," *J. Catal.*, vol. 242, pp. 299–308, 2006, doi: 10.1016/j.jcat.2006.06.013.

[5]   M. M. Oloruntoba, D. S. Aribike, and S. C. U. Nwachukwu, "A Review on Bio- And Adsorptive Desulfurization of Diesel Fuel," *J. Sci. Res. Reports*, vol. 11, pp. 1–6, 2016, doi: 10.9734/JSRR/2016/26909.

[6]   P. Baltzopoulou, K. X. Kallis, G. Karagiannakis, and A. G. Konstandopoulos, "Diesel

Fuel Desulfurization via Adsorption with the Aid of Activated Carbon : Laboratory- and Pilot-Scale Studies," *Energy & Fuels*, vol. 29, pp. 5640–5648, 2015, doi: 10.1021/acs.energyfuels.5b01133.

[7]   I. Danmaliki and A. Saleh, "Influence of conversion parameters of waste tires to activated carbon on adsorption of dibenzothiophene from model fuels," J. *Cleaner. Prod.*, vol. 117, pp. 50–55, 2016, doi: 10.1016/j.jclepro.2016.01.026.

[8]   G. I. Danmaliki and T. A. Saleh, "Effects of bimetallic Ce/Fe nanoparticles on the desulfurization of thiophenes using activated carbon," *Chem. Eng. J.*, vol. 307, pp. 914–927, 2017, doi: 10.1016/j.cej.2016.08.143.

[9]   L. Deng, B. Lu, T. Li, G. Lv, S. Du, J. Shi, Y. Yang, "Effect of pore structure and oxygen-containing groups on adsorption of dibenzothiophene over activated carbon," *Fuel*, vol. 200, pp. 54–61, 2017, doi: 10.1016/j.fuel.2017.03.018.

[10]   J. Bu, G. Loh, C. G. Gwie, S. Dewiyanti, M. Tasrif, and A. Borgna, "Desulfurization of diesel fuels by selective adsorption on activated carbons : Competitive adsorption of polycyclic aromatic sulfur heterocycles and polycyclic aromatic hydrocarbons," *Chem. Eng. J.*, vol. 166, pp. 207–217, 2011, doi: 10.1016/j.cej.2010.10.063.

[11]   S. A. Ganiyu, O. Ajumobi, S. A. Lateef, K. O. Sulaiman, I. A.Bakare, M. Qamaruddin, K. Alhooshani., "Boron-doped activated carbon as efficient and selective adsorbent for ultra-deep desulfurization of 4 , 6-dimethyldibenzothiophene," *Chem. Eng. J.*, vol. 321, pp. 651–661, 2017, doi: 10.1016/j.cej.2017.03.132.

[12]   A. Saleh, K. O. Sulaiman, S. A. Al-hammadi, H. Dafalla, and I. Danmaliki, "Adsorptive desulfurization of thiophene , benzothiophene and dibenzothiophene over activated carbon manganese oxide nanocomposite : with column system evaluation," *Clean. Prod.*, vol. 154, pp. 401–412, 2017, doi: 10.1016/j.jclepro.2017.03.169.

[13]   Y. Yang, G. Lv, L. Deng, B. Lu, J. Li, J. Zhang, J. Shi, S. Du, "Ultra-deep desulfurization of diesel fuel via selective adsorption over modi fi ed activated carbon assisted by pre-oxidation," *J. Clean. Prod.*, vol. 161, pp. 422–430, 2017, doi: 10.1016/j.jclepro.2017.05.112.

[14]   T. A. Saleh and G. I. Danmaliki, "Influence of acidic and basic treatments of activated carbon derived from waste rubber tires on adsorptive desulfurization of thiophenes,"

Taiwan Inst. Chem. Eng., vol. 60, pp. 460–468, 2016, doi: 10.1016/j.jtice.2015.11.008.

[15] M. Danish and T. Ahmad, "A review on utilization of wood biomass as a sustainable precursor for activated carbon production and application," *Renewable and Sustainable Energy Reviews*, vol. 87. 2018, doi: 10.1016/j.rser.2018.02.003.

[16] E. Yang, C. Yao, Y. Liu, C. Zhang, L. Jia, D. Li, Z. Fu, D. Sun, S. R. Kirk, D. Yin, "Bamboo-derived porous biochar for e ffi cient adsorption removal of dibenzothiophene from model fuel," *Fuel*, vol. 211, pp. 121–129, 2018, doi: 10.1016/j.fuel.2017.07.099.

[17] L. Suárez-Hernández, A. N. Ardila-A, R. Barrera-zapata, , "Morphological and physicochemical characterization of biochar produced by gasification of selected forestry species Caracterización morfológica y fisico-química de biocarbones producidos," *Rev. Foculted Lingeneiertia*, vol. 26, pp. 123–130, 2017.

[18] R. Bardestani and S. Kaliaguine, "Steam activation and mild air oxidation of vacuum pyrolysis biochar," *Biomass and Bioenergy*, vol. 108, pp. 101−112, 2018, doi: 10.1016/j.biombioe.2017.10.011.

[19] W. Suliman, J. B. Harsh, N. I. Abu-lail, A. Fortuna, I. Dallmeyer, and M. Garcia-perez, "Biomass and Bioenergy Influence of feedstock source and pyrolysis temperature on biochar bulk and surface properties," *Biomass and Bioenergy*, vol. 84, pp. 37–48, 2016, doi: 10.1016/j.biombioe.2015.11.010.

[20] Y. Huang, M. Anderson, D.Mcilveen-Wright, G. A. Lyons, W. C. McRoberts, Y. Wang, T. Roskilly, N. Hewitt, "Biochar and renewable energy generation from poultry litter waste : A technical and economic analysis based on computational simulations," *Appl. Energy*, vol. 160, pp. 656–663, 2015, doi: 10.1016/j.apenergy.2015.01.029.

[21] S. Lin, L. Hsu, C. Chou, J. Jhang, and P. Wu, "Carbonization process of Moso bamboo (Phyllostachys pubescens) charcoal and its governing thermodynamics," *J. Anal. Appl. Pyrolysis*, vol. 107, pp. 9–16, 2014, doi: 10.1016/j.jaap.2014.01.001.

[22] Y. Chen, Y. Lin, S. Ho, Y. Zhou, and N. Ren, "Highly e fficient adsorption of dyes by biochar derived from pigments-extracted macroalgae pyrolyzed at different temperature," *Bioresour. Technol.*, vol. 259, pp. 104–110, 2018, doi: 10.1016/j.biortech.2018.02.094.

[23] D. D. Sewu, P. Boakye, and S. H. Woo, "Highly efficient adsorption of cationic dye by

biochar produced with Korean cabbage waste," *Bioresour. Technol.*, vol. 224, pp. 206–213, 2017, doi: 10.1016/j.biortech.2016.11.009.

[24]   H. N. Tran, S. You, and H. Chao, "Effect of pyrolysis temperatures and times on the adsorption of cadmium onto orange peel derived biochar," *Waste Manag. Reseach*, vol. 34, pp. 129–138, 2016, doi: 10.1177/0734242X15615698.

[25]   Z. Ahmad, B. Gau, A. Mosa, H. Yu, X. Yin, A. Bashir, H. Ghoveisi, S. Wang, "Removal of Cu (II), Cd (II) and Pb (II) ions from aqueous solutions by biochars derived from potassium-rich biomass," *J. Clean. Prod.*, vol. 180, pp. 437–449, 2018, doi: 10.1016/j.jclepro.2018.01.133.

[26]   B. Chen, Z. Chen, and S. Lv, "A novel magnetic biochar efficiently sorbs organic pollutants and phosphate," *Bioresour. Technol.*, vol. 102, pp. 716–723, 2011, doi: 10.1016/j.biortech.2010.08.067.

[27]   J. Lehmann and S. Joseph, "Biochar for Environmental Management: Science and Technology," *First Edition,* pp. 1–399, 2009.

[28]   S. Shackley, S. Carter, T. Knowles, E. Middelink, S. Haefele, and S. Haszeldine, "Sustainable gasification – biochar systems? A case-study of rice-husk gasification in Cambodia , Part II : Field trial results , carbon abatement , economic assessment and conclusions," *Energy Policy*, vol. 41, pp. 618–623, 2012, doi: 10.1016/j.enpol.2011.11.023.

[29]   "IBI Biochar Standards and Testing Guidelines Completed and Approved: New IBI Organization Member: Biochar Greenhouse Gas Protocol Development," *Internationa Biochar Inititiative*, 2012. https://www.biochar-international.org/wp-content/uploads/2018/04/IBI_Newsletter_May_2012.pdf

[30]   J. Lehmann and S. Joseph, "Biochar for Environmental Management: An Introduction", *Second Edition,* 2015.

[31]   M. Ahmad, A. U. Rajapaksha, F. E. Lim, M. Zhang, N. Bolan, D. Mohan, M. Vithanage, S. S. Lee, Y. S. Ok, "Biochar as a sorbent for contaminant management in soil and water: A review," *Chemosphere*, vol. 99, pp. 19–33, 2014, doi: 10.1016/j.chemosphere.2013.10.071.

[32] Y. Sun, B. Gao, Y. Yao, J. Fang, M Zhang, Y. Zhou, H. Chen, and L. Yang, "Effects of feedstock type, production method, and pyrolysis temperature on biochar and hydrochar properties," *Chem. Eng. J.*, vol. 240, pp. 574-578, 2014, doi: 10.1016/j.cej.2013.10.081.

[33] B. Xiaofeng, Z. Xiaoqin, L. Zifu, N. Jiewen, and B. Xue, "Properties and applications of biochars derived from different biomass feedstock sources," *Int. J. Agric. Biol Eng.*, vol. 10, pp. 242–250, 2017, doi: 10.3965/j.ijabe.20171002.2878.

[34] M. Ahmad, S. Soo, X. Dou, D. Mohan, J. K. Sung, J. E. Yang, Y. S. Ok, "Effects of pyrolysis temperature on soybean stover- and peanut shell-derived biochar properties and TCE adsorption in water," *Bioresour. Technol.*, vol. 118, pp. 536–544, 2012, doi: 10.1016/j.biortech.2012.05.042.

[35] D. Chen, J. Zhou, and Q. Zhang, "Effects of heating rate on slow pyrolysis behavior, kinetic parameters and products properties of moso bamboo," *Bioresour. Technol.*, vol. 169, pp. 313–319, 2014, doi: 10.1016/j.biortech.2014.07.009.

[36] H. Haykiri-Acma, S. Yaman, and S. Kucukbayrak, "Effect of heating rate on the pyrolysis yields of rapeseed," *Renew. Energy*, vol. 31, pp. 803–810, 2006, doi: 10.1016/j.renene.2005.03.013.

[37] A. Upamali Rajapaksha, M. Vithanage, M. Zhang, and M. Ahmad, "Pyrolysis condition affected sulfamethazine sorption by tea waste biochars," *Bioresour. Technol.*, vol. 166, pp. 303–308, 2014, doi: 10.1016/j.biortech.2014.05.029.

[38] M. Zhang, B. Gao, S. Varnoosfaderani, A. Hebard, Y. Yao, and M. Inyang, "Preparation and characterization of a novel magnetic biochar for arsenic removal," *Bioresour. Technol.*, vol. 130, pp. 457–462, 2013, doi: 10.1016/j.biortech.2012.11.132.

[39] J. Luo, X. Li, C. Ge, K. Müller, H. Yu, P. Huang, J. Li, D. C. W.Tsang, N. S. Bolan, J. Rinklebe, H. Wang, "Sorption of norfloxacin , sulfamerazine and oxytetracycline by KOH-modified biochar under single and ternary systems," *Bioresour. Technol.*, vol. 263, pp. 385–392, 2018, doi: 10.1016/j.biortech.2018.05.022.

[40] X. Tan, Y. Liu, G. Zeng, X. Wang, X. Hu, and Y. Gu, "Chemosphere Application of biochar for the removal of pollutants from aqueous solutions," *Chemosphere*, vol. 125, pp. 70–85, 2015, doi: 10.1016/j.chemosphere.2014.12.058.

[41]   D. H. K. Reddy and S. Lee, "Physicochemical and Engineering Aspects Magnetic biochar composite: Facile synthesis, characterization, and application for heavy metal removal," *Colloids Surfaces A Physicochem. Eng. Asp.*, vol. 454, pp. 96–103, 2014, doi: 10.1016/j.colsurfa.2014.03.105.

[42]   X. fei Tan, S. Liu, Y. Liu, Y. Gu, G. Zeng, X. Hu, X. Wang, S. Liu, L. Jiang, "Biochar as potential sustainable precursors for activated carbon production: Multiple applications in environmental protection and energy storage," *Bioresource Technology*. vol. 227, pp. 359−372, 2017, doi: 10.1016/j.biortech.2016.12.083.

[43]   Y. Moxin, N. Zhang, L. Fan, C. Zhang, X. He, and M. Zheng, "Removal of organic sulfur compounds from diesel by adsorption on carbon materials," *Revis. Chem. Eng.*, vol. 31, pp. 27–43, 2015, doi: 10.1515/revce-2014-0017.

[44]   H. N. Tran, S. J. You, and H. P. Chao, "Fast and efficient adsorption of methylene green 5 on activated carbon prepared from new chemical activation method," *J. Environ. Manage.*, vol. 188, pp. 322−336, 2017, doi: 10.1016/j.jenvman.2016.12.003.

[45]   A. Garba, H. Basri, N. S. Nasri, and R. Isma, "Synthesis and characterisation of porous carbon from biomass using KOH and K_2CO_3 chemical activation," *ARPN J. Eng. Appl. Sci.*, vol. 11, pp. 1613–1617, 2016.

[46]   R. Tseng and S. Tseng, "Pore structure and adsorption performance of the KOH-activated carbons prepared from corncob," *J. Colloid Interface Sci.*, vol. 287, pp. 428–437, 2005, doi: 10.1016/j.jcis.2005.02.033.

[47]   R. Tseng, S. Tseng, and F. Wu, "Effects of micropore development on the physicochemical properties of KOH-activated carbons," *Chinese Inst. Chinese Institude Chem. Eng.*, vol. 39, pp. 37–47, 2008, doi: 10.1016/j.jcice.2007.11.005.

[48]   Y. Zheng, Q. Li, C. Yuan, Q. Tao, and Y. Zhao, "In fluence of temperature on adsorption selectivity: Coal-based activated carbon for CH4 enrichment from coal mine methane," *Powder Technol.*, vol. 347, pp. 42–49, 2019, doi: 10.1016/j.powtec.2019.02.042.

[49]   A. U. Rajapaksha, M. Vithanoge, M. Ahmad, D. C. Seo, J. S. Cho, S. E. Lee, S. S. Lee, Y. S. Ok, "Enhanced sulfamethazine removal by steam-activated invasive plant-derived biochar," *J. Hazard. Mater.*, vol. 290, pp. 43–50, 2015, doi: 10.1016/j.jhazmat.2015.02.046.

[50] I. M. Lima, A. Boateng, and K. T. Klasson, "Physicochemical and adsorptive properties of fast-pyrolysis bio-chars and their steam activated counterparts," *J. chem Technol Biotechnol.*, vol. 85, pp. 1515–1521, 2010, doi: 10.1002/jctb.2461.

[51] M. Fan, "Steam activation of chars produced from oat hulls and corn stover," *Bioresour. Technol.*, vol. 93, pp. 103–107, 2004, doi: 10.1016/j.biortech.2003.08.016.

[52] P. G. González and Y. B. Pliego-cuervo, "Physicochemical and microtextural characterization of activated carbons produced from water steam activation of three bamboo species," *J. Anal. Appl. Pyrolysis*, vol. 99, pp. 32–39, 2013, doi: 10.1016/j.jaap.2012.11.004.

[53] S. Mopoung, P. Moonsri, W. Palas, and S. Khumpai, "Characterization and Properties of Activated Carbon Prepared from Tamarind Seeds by KOH Activation for Fe (III) Adsorption from Aqueous Solution," *Sci. World J.*, vol. 2015, pp. 1–9, 2015.

[54] G. Gatti, M. Errahali, L. Tei, M. Cossi, and L. Marchese, "On the Gas Storage Properties of 3D Porous Carbons Derived from Hyper-Crosslinked Polymers," *J. Polym.*, vol. 302, pp. 1–18, 2019, doi: 10.3390/polym11040588.

[55] A. A. Arie, Vincent and A. Putranto, "Activated carbons from KOH-activation of salacca peels as low cost potential adsorbents for dye removal," *Adv. Mater. Lett.*, vol. 7, pp. 226–229, 2016, doi: 10.5185/amlett.2016.6194.

[56] J. L. Rivera, P. Navarro-santos, R. Guerra-gonzalez, and E. Lima, "Interaction of Refractory Dibenzothiophenes and Polymerizable Structures," *Int. J. Polym. Sci.*, vol. 2014, pp. 1–12, 2014.

[57] H. N. Tran, S. You, and H. Chao, "Insight into adsorption mechanism of cationic dye onto agricultural residues-derived hydrochars: Negligible role of π-π interaction," *Korean J. Chem. Eng.*, vol. 34, pp. 1708–1720, 2017, doi: 10.1007/s11814-017-0056-7.

[58] Q. Li, Z. Li, L. Lin, X.Y. Wang, Y. Wang, C. Zhang, H. Wang, "Facile synthesis of activated carbon / carbon nanotubes compound for supercapacitor application," *Chem. Eng. J.*, vol. 156, pp. 500–504, 2010, doi: 10.1016/j.cej.2009.10.025.

[59] A. Ali and R. Idris, "Utilization of low-cost activated carbon from rapid synthesis of microwave pyrolysis for WC nanoparticles preparation," *Adv. Mater. Lett.*, vol. 8, pp.

70–76, 2017, doi: 10.5185/amlett.2017.6964.

[60] K. Y. Foo and B. H. Hameed, "Microwave-assisted preparation of oil palm fiber activated carbon for methylene blue adsorption," *Chem. Eng. J.*, vol. 166, pp. 792–795, 2011, doi: 10.1016/j.cej.2010.11.019.

[61] D. W. McKee, "Mechanisms of the alkali metal catalysed gasif ication of carbon," *Fuel*, vol. 62, pp. 170–175, 1983.

[62] H. N. Tran, H. Chao, and S. You, "Activated carbons from golden shower upon different chemical activation methods : Synthesis and characterizations," *Adsorpt. Sci. Tchnology*, vol. 36, pp. 95–113, 2018, doi: 10.1177/0263617416684837.

[63] A. Dandekar, R. T. K. Baker, M.A. Vannice, "Characterization of Activated carbon, Graphitized carbon fibres and synthetic diamond powder using TPD and DRIFTS," *Carbon*, vol. 36, pp. 1821–1831, 1998.

[64] A. M. Oickle, S. L. Goertzen, K. R. Hopper, Y. O. Abdalla, and H. A. Andreas, "Standardization of the Boehm titration: Part II . Method of agitation, effect of filtering and dilute titrant," *Carbon*, vol. 48, pp. 3313–3322, 2010, doi: 10.1016/j.carbon.2010.05.004.

[65] A. U. Rajapaksha, M. Vithanage, and S. S. Lee, "Steam activation of biochars facilitates kinetics and pH-resilience of sulfamethazine sorption," *J. Soils Sediments*, vol. 16, pp. 889−895, 2015, doi: 10.1007/s11368-015-1325-x.

[66] A U. Rajapaksha, S. S. Chen, D. C. W. Tsang*,* M. Zhang, M. Vithanage, S. Mandal, B. Gao, N. S. Bolan, Y. S. Ok , "Engineered/designer biochar for contaminant removal/immobilization from soil and water: Potential and implication of biochar modi fi cation," *Chemosphere*, vol. 148, pp. 276–291, 2016, doi: 10.1016/j.chemosphere.2016.01.043.

[67] C. Zhang, W. Song, G. Sun, L. Xie, L. Wan, J. Wang, K. Li, "Synthesis , Characterization , and Evaluation of Activated Carbon Spheres for Removal of Dibenzothiophene from Model Diesel Fuel," *Ind. Eng. Chem. Res.*, vol. 53, pp. 4271−4276, 2014.

[68] C. O. Ania and T. J. Bandosz, "Importance of Structural and Chemical Heterogeneity of

Activated Carbon Surfaces for Adsorption of Dibenzothiophene," *Lungmuir*, vol. 21, pp. 7752–7759, 2005.

[69] Y. N. Prajapati, B. Bhaduri, H. C. Joshi, A. Srivastava, and N. Verma, "Chemosphere Aqueous phase adsorption of different sized molecules on activated carbon fi bers : Effect of textural properties," *Chemo*, vol. 155, pp. 62–69, 2016, doi: 10.1016/j.chemosphere.2016.04.040.

[70] Y. Nath and N. Verma, "Adsorptive desulfurization of diesel oil using nickel nanoparticle-doped activated carbon beads with / without carbon nanofibers : Effects of adsorbate size and adsorbent texture," *Fuel*, vol. 189, pp. 186–194, 2017, doi: 10.1016/j.fuel.2016.10.044.

[71] M. S. Shafeeyan, W. Mohd, A. Wan, A. Houshmand, and A. Shamiri, "A review on surface modification of activated carbon for carbon dioxide adsorption," *J. Anal. Appl. Pyrolysis*, vol. 89, pp. 143–151, 2010, doi: 10.1016/j.jaap.2010.07.006.

[72] H. Liang, L. Chen, G. Liu, and H. Zheng, "Surface morphology properties of biochars produced from different feedstocks," *International Conference of Civil, Transportation and Environment*, pp. 1205–1208, 2016.

[73] S. Gavalda, K. E. Gubbins, Y. Hanzawa, K. Kaneko, and K. T. Thomson, "Nitrogen Adsorption in Carbon Aerogels: A Molecular simulation study," *Langmuir*, vol. 18, pp. 2141–2151, 2002.

[74] J. Yue, Z. Wang, and J. Chen, "Investigation of pore structure characteristics and adsorption characteristics of coals with different destruction types," *Adsorption*, vol. 37 pp. 623–648, 2019, doi: 10.1177/0263617419868076.

[75] N. Yoshizawa, K. Maruyama, and Y. Yamada, "XRD evaluation of CO_2 activation process of coal and coconut shell-based carbons," *Fuel*, vol. 79, pp. 1461–1466, 2000.

[76] Z. Guo, L. Zhang, P. Wang, H. Liu, J. Jia, X. Fu, S. Li, X. Wang, Z. Li, X. Shu, "Study on kinetics of coal pyrolysis at different heating rates to produce hydrogen," *Fuel Process. Technol.*, vol. 107, pp. 23–26, 2013, doi: 10.1016/j.fuproc.2012.08.021.

Chapter 7

General Conclusion

It was concluded that, in general, the unprocessed amarula waste biomass from the production of Amarula liqueur, was able to reduce the sulphur content in diesel fuel. This was because of the active functional groups present in large quantities in the biomass, as confirmed by FTIR analysis. It was also found that the crystallinity of the biomass also contributed to improved absorptivity of DBT. This was confirmed by XRD analysis. The amarula shell waste biomass had the highest adsorption capacity of DBT and a higher crystallinity than the amarula seed and fruit waste biomass samples. The TEM and EDX analysis confirmed the presence of sulphur on the surface of the biomass after adsorption; this was not seen on the amarula waste biomass before adsorption. Although the textural analysis showed the presence of micro porosity, which limited the adsorption of DBT, it was found that the entire adsorption process was controlled by the chemisorption process.

The thermally processed amarula waste biomass was found to improve the desulphurization efficiency significantly. This was because heat treatment removed all the volatiles on the surface of the biomass, which resulted in the microporosity. Steam processing also further widened the micro porosity and formed the mesoporosity. Microscopic analysis confirmed the presence of macropores, mesopores and micropores. Therefore, it was concluded that the adsorption of DBT by processed amarula waste was controlled by the speed of diffusion to the pores, which resulted in the highest absorptivity. FTIR analysis showed the reduced content of O-functional groups due to thermal cracking - hence chemisorption limited the adsorption process of DBT with processed amarula waste. It was found that the processed amarula shells waste to activated carbons had a higher adsorption capacity than the processed amarula seed and fruit waste activated carbons.

Gasification biochar was also found to be a potential adsorbent for reducing sulphur content in diesel fuel. The performance effect on desulphurization of diesel fuel was compared to that of amarula shells waste biochar. It was found that the amarula shells waste biochar performed better than gasification char from plasma and down draft gasifiers. It was concluded that, besides the raw material, the reactor design for a gasifier contributed to different properties of

biochar, which resulted in different levels of absorptivity of organo-sulphur compounds in diesel fuel. It was further found that the gasification biochar that was processed by KOH to activated carbon improved the surface area and the porosity of the biochar by two-fold. This was found to improve the desulphurization efficiency of diesel fuel. It was also found that the gasification biochar of Wood-PGBC and the AmShBC that was processed by steam improved the adsorptive desulphurization efficiency significantly, owing to the various pore sizes which were able to adsorb the large toxic molecule. The processed amarula shell waste biochar was found to perform better than the processed gasification biochar, irrespective of the activation agent type.

It was generally concluded that this study was able to deep desulphurize diesel fuel using processed and unprocessed amarula waste as low-cost adsorbents. Therefore, a possible process for mitigating land-pollution and for waste management was achieved by utilizing amarula waste biomass that was polluting the environment from the waste of Amarula liqueur production. Furthermore, sustainable, and efficient processes for converting amarula waste biomass to activated carbons was achieved through steam activation, which is a sustainable and environmentally friendly activating process. In addition, the desulphurization of diesel fuel was carried out at room temperature, which is a sustainable approach that saves on energy consumption.

The content of toxic organo-sulphur compounds in diesel fuel was reduced using sustainable processes. This in later stage will overcame the issue of air pollution and thus mitigate the climate change issues. On that note, it was concluded that the study provided valuable data to design a small-scale desulphurization plant for purifying diesel fuel.

Appendix A / Supplementary data

Adsorption of Dibenzothiophene in Model Diesel Fuel by adsorption on Amarula wastes biomass as a Low-Cost Adsorbent

Tsepiso Kabi[a] , Yali Yao[a*], Diane Hildebrandt[a], Xinying Liu[a]

a Institution for Development of Energy for African Sustainability (IDEAS), University of South Africa (UNISA),
Florida Campus, Private Bag X 6, Johannesburg 1710, South Africa.
*E-mail: yaoy@unisa.co.za**

Appendix A: Table A1 Peak temperatures from DTG of Amarula wastes biomass under Nitrogen atmosphere

Biomass Type	Peak temperature (∘C) under N2 Atmosphere										Total masss loss %	
	Moisture		Llight volatiles		Hemicellulose		Cellulose		Lignin			
	Before	After	Before	After	Before	After	Before	After	Before	After	Before	After
Raw AmSh	53	49	205	-	311	316	356	355	416	434	82	80,4
Raw AmSe	43	37	192	-	313	316	357	355	431	433	81,3	80,8
Raw AmWa	40	35	219	-	317	312	349	349	384	404	77,5	72,5

Appendix A: Table A2 Peak temperatures from DTG of Amarula wastes biomass under Air conditions

| Biomass Type | Peak temperature (°C) under Air Atmosphere | | | | | | | | | | Total masss loss % | |
| | Moisture | | Llight volatiles | | Hemicellulose | | Cellulose | | Lignin | | | |
	Before	After	Before	After	Before	After	Before	After	Before	After	Before	After
Raw AmSh	44	43	-	-	321	-	334	490	425	716	90,3	81,9
Raw AmSe	39	28	298	315	320	327	339	392	425	410	91,4	97,2
Raw AmWa	54	30,3	298	256	321	323	328	417	413	451	97	95,9
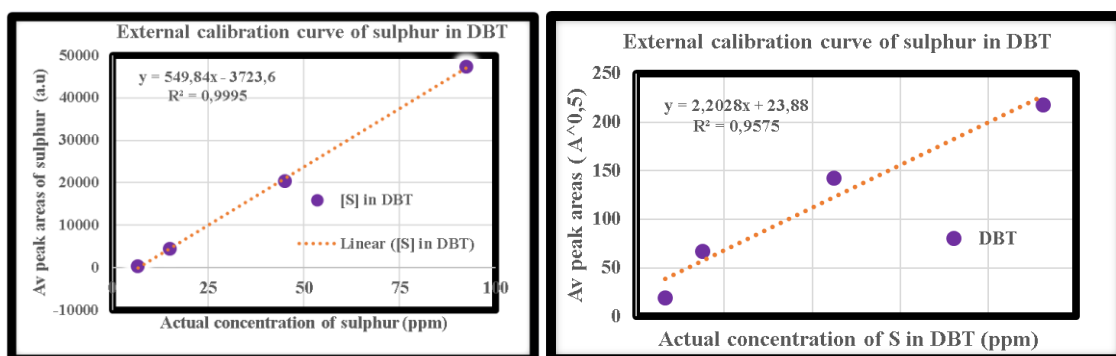
Appendix A: Fig. A1. Calibration curves for external method of analysis of Dibenzothiophene

Appendix A: Table A3 Adsorption efficiencies or effect of adsorption time on Amarula wastes biomass

| Adsorption temp (°C) | Adsorption efficiency % | | |
	Raw AmSh	Raw AmSe	Raw AmWa
20	17,5	9,3	8,1
25	30,3	19,1	9,5
35	14,8	11,1	11,7
45	14,7	6,9	9,6
55	8,9	13,7	11,9

Appendix A: Table A4 Parameters of kinetic models for the effect of temperature on Amarula shells wastes biomass

Constants and Correlation values of kinetic models for effect of temp - Raw AmSh											
Adsorption temp °C	Pseudo 1st order			Pseudo 2nd order			Intra particle diffusion				$q_{e\ exp}$
	$q_{e\ calc}$	K_1	R 2	$q_{e\ calc}$	K_2	R 2	$q_{e\ calc}$	K_i	C	R 2	
20	0,01	-0,01157	0,1373	0,16	1088,5539	0,9963	0,19	0,0011	0,09	0,3709	0,161
25	0,06	-0,0093	0,2051	0,28	256,92354	0,9956	0,32	0,0019	0,15	0,399	0,278
35	0,01	-0,015	0,2558	0,14	1213,8907	0,9968	0,16	0,0008	0,08	0,272	0,136
45	0,05	-0,0176	0,5355	0,14	3426,2618	0,9869	0,16	0,0011	0,06	0,5413	0,134
55	0,02	-0,0209	0,5028	0,09	13182,74	0,976	0,10	0,0007	0,04	0,4924	0,081

Appendix A: Table A5 Amarula Seeds Wastes Biomass-Kinetic parameters for the effect of adsorption temperature

Constants and Correlation values of kinetic models for effect of temp - Raw AmSe											
Adsorption temp °C	Pseudo 1st order			Pseudo 2nd order			Intra particle diffusion				$q_{e\ exp}$
	$q_{e\ calc}$	K_1	R 2	$q_{e\ calc}$	K_2	R 2	$q_{e\ calc}$	K_i	C	R 2	
20	0,02	-0,0131	0,1293	0,08	11,986	0,9922	0,10	0,0004	0,06	0,1258	0,08507
25	0,03	-0,0184	0,3693	0,18	5,5747	0,9983	0,20	0,0012	0,09	0,3596	0,175208
35	0,02	-0,0134	0,2589	0,10	9,6241	0,9879	0,11	0,0007	0,05	0,4459	0,101813
45	0,02	-0,0134	0,2589	0,10	9,6241	0,9971	0,11	0,0007	0,05	0,4459	0,101813
55	0,04	-0,0113	0,2651	0,13	7,5783	0,9846	0,15	0,0011	0,05	0,4768	0,125958

Appendix A: Table A6 Amarula Fruit wastes biomass: Kinetic parameters for the effect of adsorption temperature

Constants and Correlation values of kinetic models for effect of temp - Raw AmWa											
Adsorption temp °C	Pseudo 1st order			Pseudo 2nd order			Intra particle diffusion				$q_{e\ exp}$
	$q_{e\ calc}$	K_1	R 2	$q_{e\ calc}$	K_2	R 2	$q_{e\ calc}$	K_i	C	R 2	
20	0,01	-0,0192	0,5215	0,07	16306,49	0,9736	0,08	0,0004	0,04	0,2843	0,07
25	0,20	-0,0128	0,3856	0,09	1798,6866	0,9876	0,11	0,0006	0,06	0,233	0,09
35	0,16	-0,0148	0,261	0,11	3611,8021	0,997	0,13	0,0008	0,06	0,4009	0,11
45	0,02	-0,0211	0,2684	0,09	7541,9057	0,9937	0,10	0,0006	0,05	0,3816	0,09
55	0,24	-0,0116	0,2991	0,12	6310,0229	0,8727	0,14	0,0008	0,07	0,1895	0,11
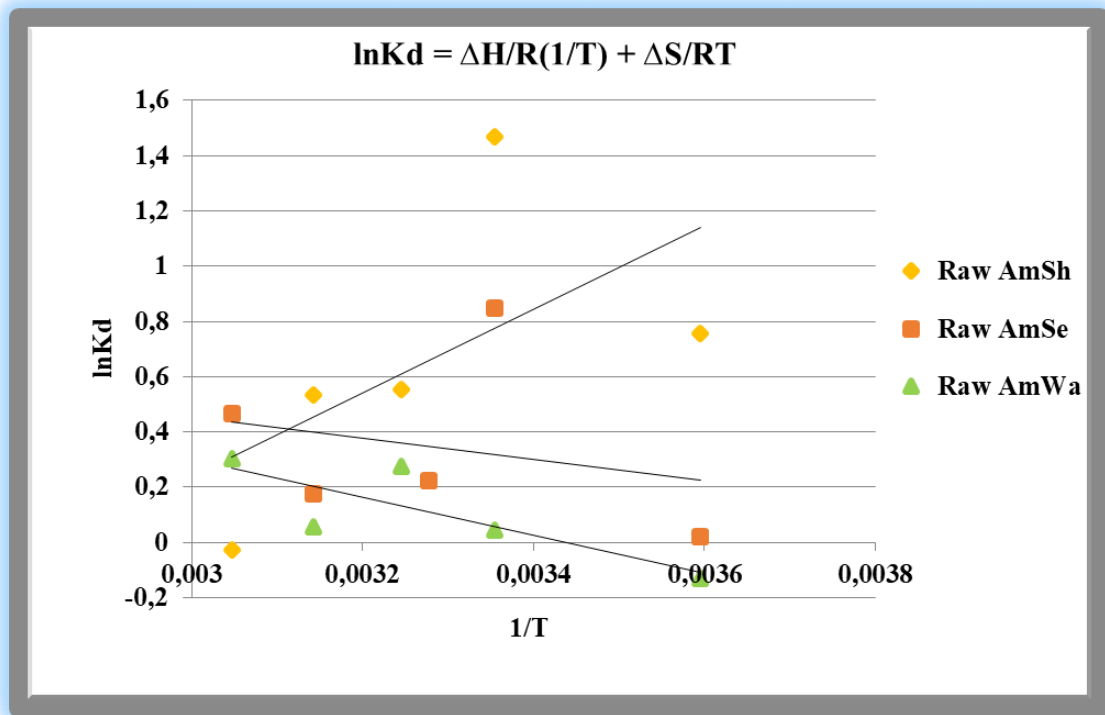
Appendix A: Fig. A2. Van Hoff plot on Amarula wastes biomass

Appendix B /Supplementary data

Deep Desulphurization of Diesel fuel by Processed Amarula wastes to activated carbon, a low-cost adsorbent

Tsepiso Kabi[a] , Yali Yao[a*], Diane Hildebrandt[a], Xinying Liu[a], Neil Coville[b]

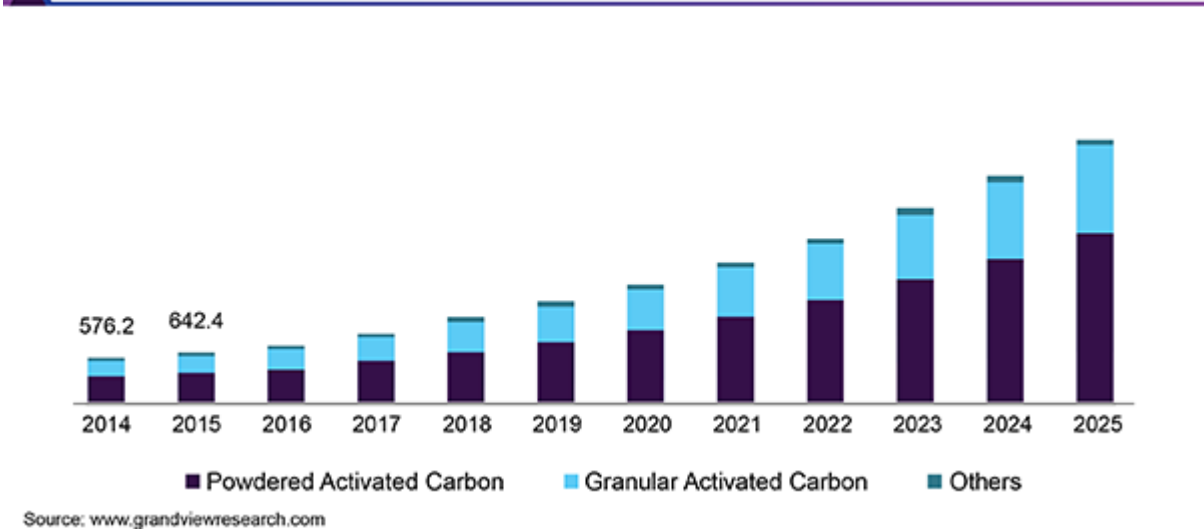*[a] Institution for Development of Energy for African Sustainability (IDEAS), University of South Africa (UNISA),*
South Africa (UNISA),
Florida Campus, Private Bag X 6, Johannesburg 1710, South Africa. E-mail:
yaoy@unisa.co.ac*.
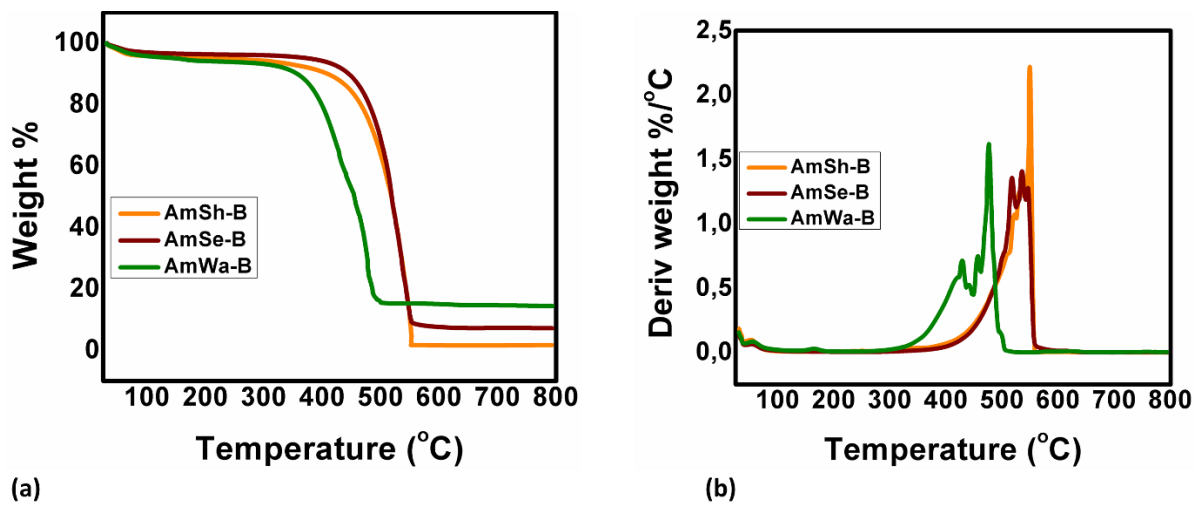*[b] Catalysis and Material (CATMAT) , University of Witwatersrand (Wits), Private bag X 3,*
Braamfontein Johannesburg South Africa

U.S. activated carbon market size, by product, 2014 - 2025 (USD Million)

576.2   642.4

2014 2015 2016 2017 2018 2019 2020 2021 2022 2023 2024 2025

■ Powdered Activated Carbon   ■ Granular Activated Carbon   ■ Others

Source: www.grandviewresearch.com

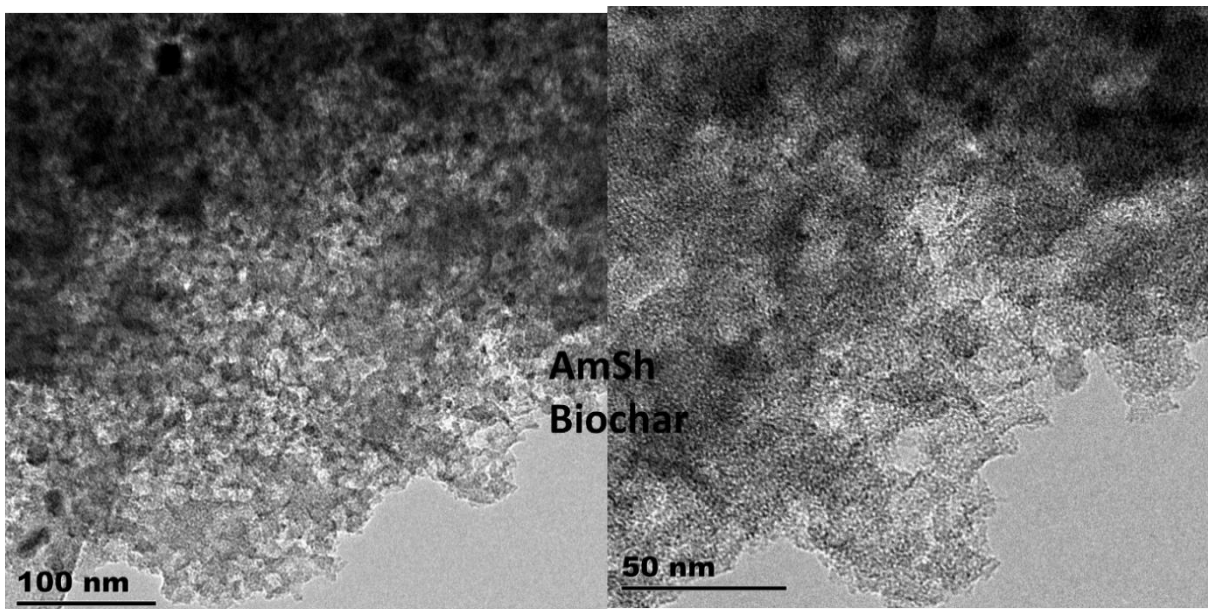**Appendix B: Fig. B1.** Market size of Activated Carbon [90]

Appendix B: Fig. B2. TGA/DTG of Amarula wastes biochar
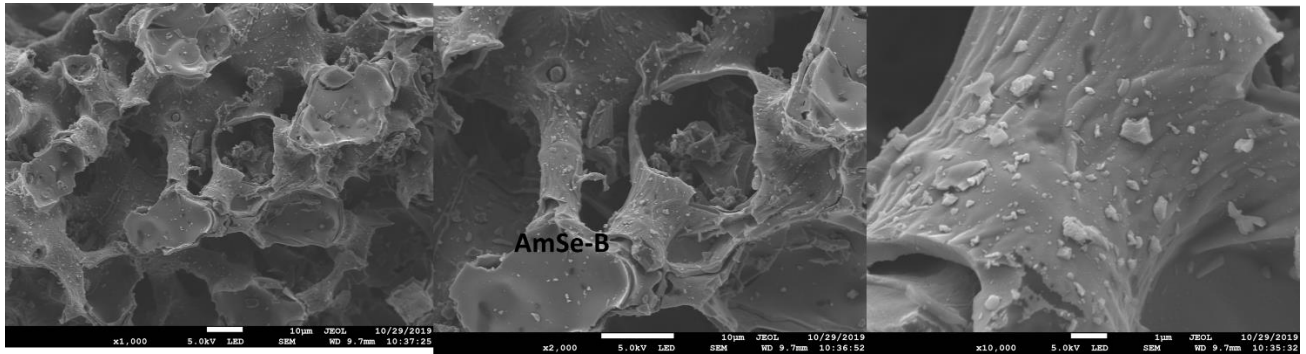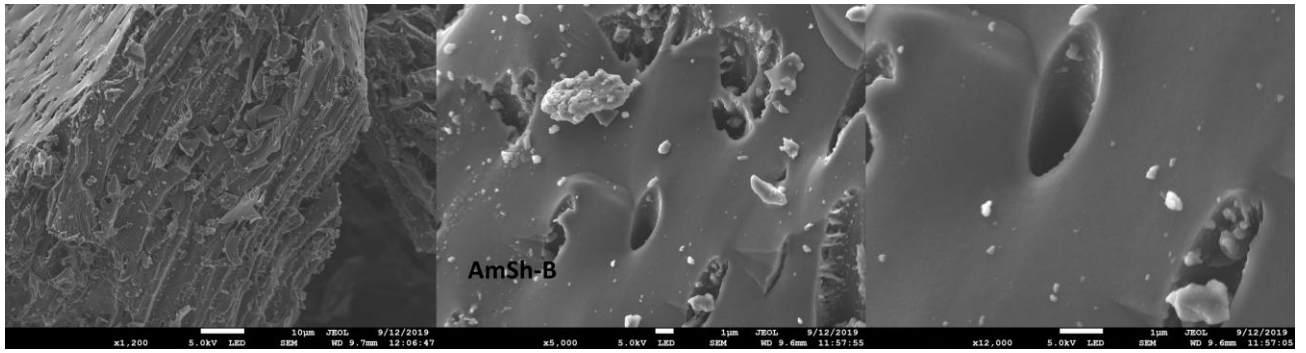
Appendix B: Fig. B3. Morphology of Amarula wastes Biochar

Appendix B: Fig. B4. TEM image of Amarula shells biochar
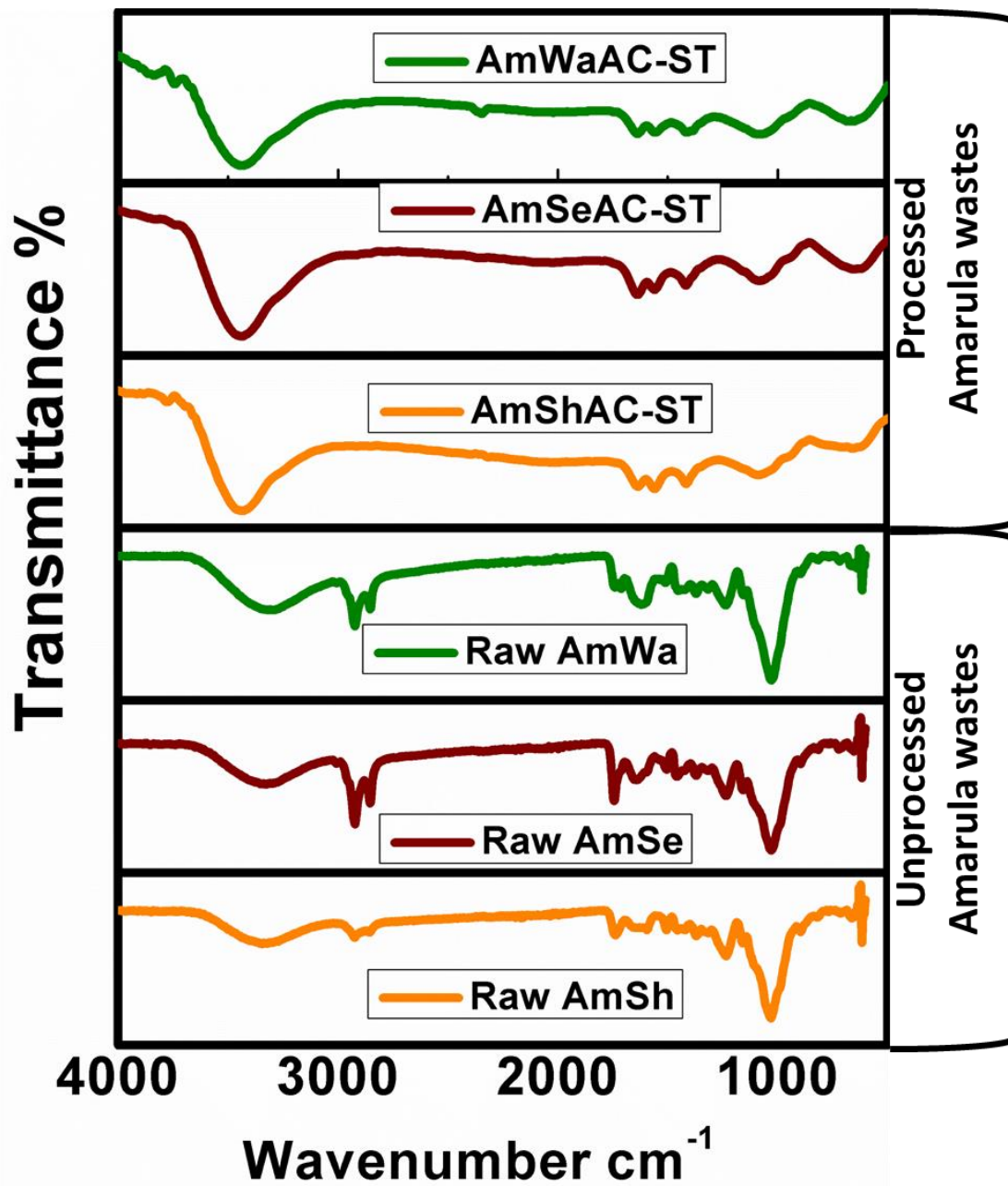
Appendix B: Fig. B5. FTIR spectra of processed and unprocessed Amarula wastes
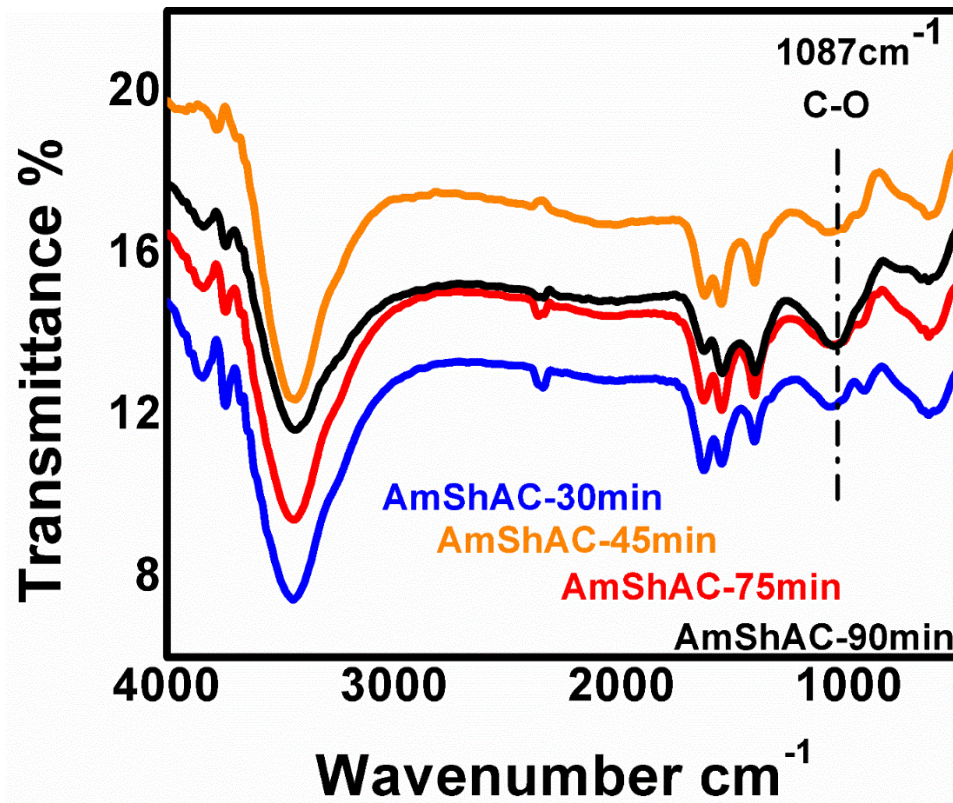
Appendix B: Fig. B6. Effect of steam residence time on C-O group of Amarula shells wastes activated carbons

Appendix B: Fig. B7. Effect of Residence time on AC in the application of Desulphurization of model diesel fuel

Appendix B: Table B1 Aromaticity from Areas of Aromatic(Ar) and Aliphatic(Al) carbons in the Amarula wastes ACs
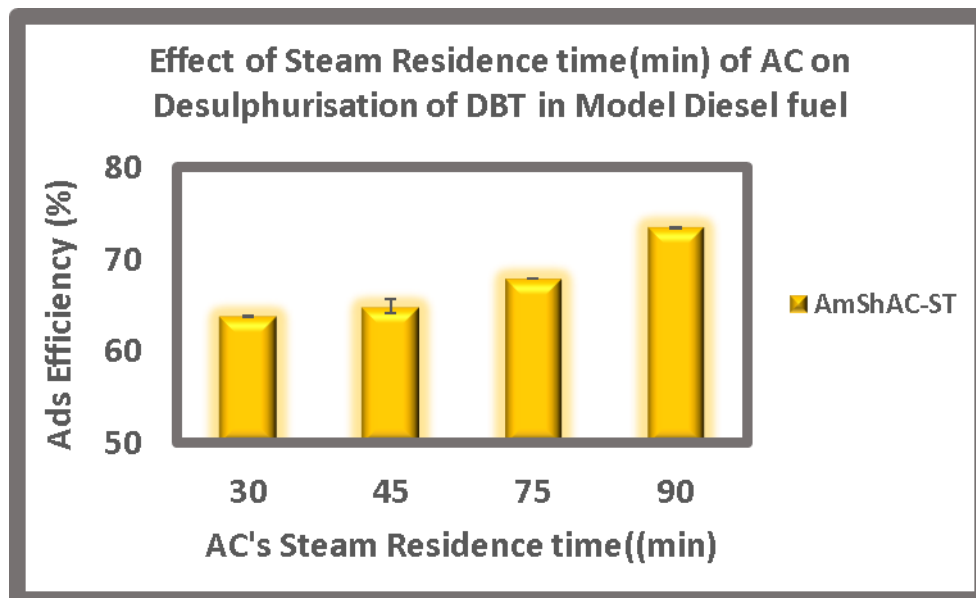
AC type	Aromaticity (fa)
AmShAC-ST	0,93
AmSeAC-ST	0,55
AmWaAC-ST	0,08

Appendix B: Table 2 BET analysis of Amarula wastes Biochar

	BET-S-Area (m^2/g)	Pore Size (Å)	Pore Volume (cm^3/g)
AmSh-B	19,69	43,31	0,021
AmSe-B	37,96	37,48	0,035
AmWa-B	28,8	40,37	0,029

Appendix B Table B3 Adsorption efficiency % of Amarula wastes Activated with adsorption time

Ads Type	Ads Efficiency % @ 25°C				
	10min	30 min	60 min	90 min	180 min
AmShAC-ST	13	28	50	55	64
AmSeAC-ST	17	19	24	27	31
AmWaAC-ST	5	21	31	42	52

Appendix B: Table B4 Effect of steam residence time during production of AmShAC in the application of desulphurization of model diesel

Effect of Seam	Ads Efficiency % @ 25°C			
Residence Time (min)	30 min	60 min	90 min	180 min
AmShAC-ST-30	30	44	53	64
AmShAC-ST-45	28	50	55	65
AmShAC-ST-75	40	60	63	68
AmShAC-ST-90	52	64	68	73

Appendix B: Table B5 Adsorption capacity of processed Amarula wastes

Adsorption capacity q_t (mg/g)				
Ads type	30 min	60 min	90 min	180 min
AmWaAC-ST-45min	0,120	0,279	0,369	0,473
AmSeAC-ST-45min	0,099	0,123	0,137	0,160
AmShAC-ST-30min	0,274	0,398	0,479	0,584
AmShAC-ST-45min	0,260	0,459	0,503	0,594
AmShAC-ST-75min	0,362	0,547	0,578	0,623
AmShAC-ST-90min	0,475	0,582	0,628	0,670

Appendix C /Supplementary data

Gasification Biochar as Potential adsorbent In Adsorptive Desulphurization of Diesel Fuel

Tsepiso Kabi[a] , Xinying Liu[a], Diane Hildebrandt[a], Neil Coville[b], Yali Yao[a*]

[a]Institution for Development of Energy for African Sustainability (IDEAS), University of South Africa (UNISA),
Florida Campus, Private Bag X 6, Johannesburg 1710, South Africa. E-mail:
yaoy@unisa.ac.za*
[b] Catalysis and Material (CATMAT), University of Witwatersrand (Wits), Private bag X 3, Braamfontein Johannesburg, South Africa

Appendix C: Table C1 EDX analysis of Biochar before activation

Before activation-EDX analysis of Gassification chars								
	Amsh-BC		Wood-DGBC		Wood PGBC		ALGC-DGBC	
Elements	element wt %	Atom %	element wt %	Atom %	element wt %	Atom %	element wt %	Atom %
C	94,9	96,6	71,3	84,2	67	86,9	-	-
O	3,9	3	12,7	11,3	7,5	7,3	-	-
Na	-	-	-	-	-	-	-	-
K	0,8	0,3	4	1,6	3,7	1,5	-	-
Mg	-	-	0,5	0,3	0,5	0,3	-	-
Ca	-	-	6,2	2,2	7,6	3	-	-
Si	0,4	0,2	-	-	-	-	-	-

Appendix C: Table C2 EDX analysis of biochar after KOH activation

	After KOH activation-EDX analysis of Gassification chars
	Amsh-BC		Wood-DGBC		Wood PGBC		ALGC-DGBC	
Elements	element wt %	Atom %	element wt %	Atom %	element wt %	Atom %	element wt %	Atom %
C	78,4	97	68	86,2	-	-	-	-
O	0,8	0,7	3,5	3,3	-	-	-	-
Na	-	-	-	-	-	-	-	-
K	0,9	0,4	1,7	0,7	-	-	-	-
Mg	0,3	0,2	7,7	8,4	-	-	-	-
Ca	1	0,4	-	-	-	-	-	-
Si	-	-	-	-	-	-	-	-

Appendix C: Table C3 EDX analysis of biochar after steam activation

| | After Steam activation-EDX analysis of Gassification chars |
|---|---|---|---|---|---|---|---|---|
| | Amsh-BC | | Wood-DGBC | | Wood PGBC | | ALGC-DGBC | |
| Elements | element wt % | Atom % | element wt % | Atom % | element wt % | Atom % | element wt % | Atom % |
| C | 78,4 | 97 | 70,7 | 90,2 | 58,8 | 78,4 | 68,3 | 84,1 |
| O | 0,8 | 0,7 | 5,3 | 5,1 | 14 | 14 | 10,5 | 9,7 |
| Na | - | - | - | - | - | | 0,5 | 0,3 |
| K | 0,9 | 0,4 | 2,2 | 0,9 | 1,3 | 0,5 | - | - |
| Mg | 0,3 | 0,2 | 0,4 | 0,3 | 1,4 | 0,9 | - | - |
| Ca | 1 | 0,4 | 6,4 | 2,4 | 13,2 | 5,3 | 1,6 | 0,6 |
| Si | - | - | - | - | - | - | 4,7 | 2,5 |
| Al | - | - | - | - | - | - | 3,3 | 1,8 |

Appendix D / Supplementary data

Commercial activated carbon (Com-AC) was used as Reference Standard Material (RSM) to determine some parameters effects on ADS of ≈ 100ppm DBT model diesel fuel
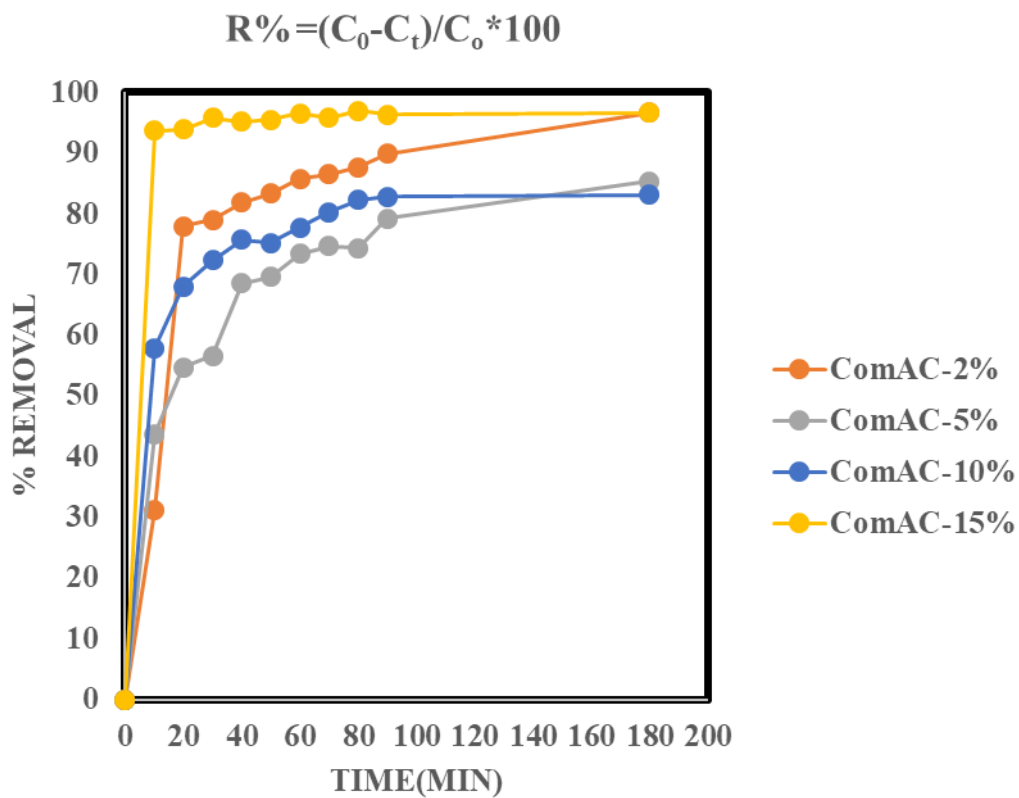

DBT model diesel fuel on 10wt % ComAC	
Ads Time (min)	Ads Eff %
0	0
10	57,84
20	67,99
30	72,38
40	75,69
50	75,23
60	77,76
70	80,24
80	82,27
90	82,81
180	83,17
1444	83,23
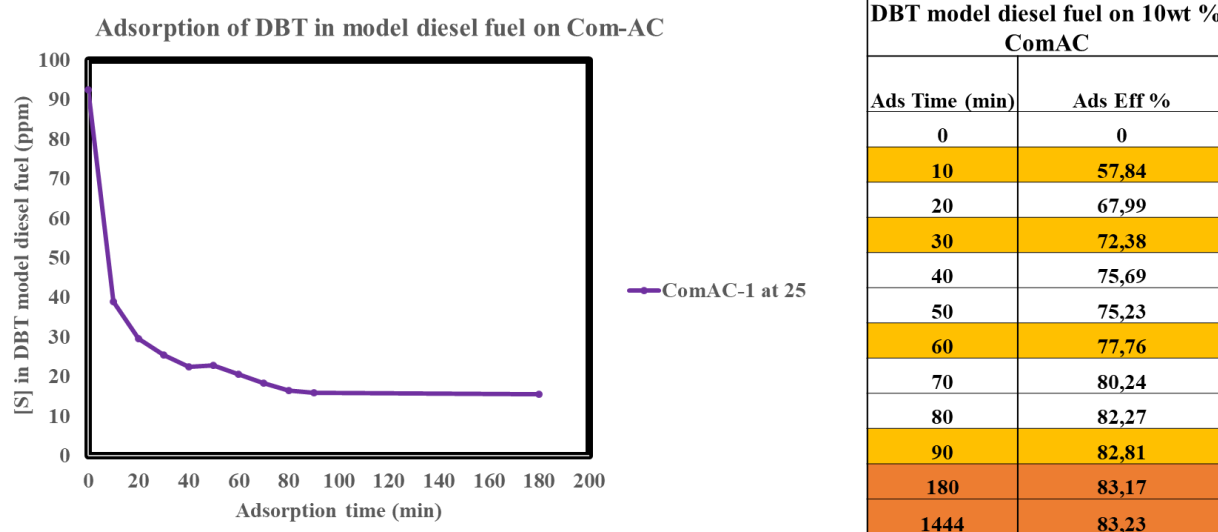
Appendix D Fig. D1. Effect of adsorption time of DBT model diesel fuel on ComAC: 10wt % ads dosage, 25 ^{0}C ads temp, 800 rpm stirring, 1 444 min ads time and 1-2 mm size particle size of ComAC

R%=(C0-Ct)/Co*100
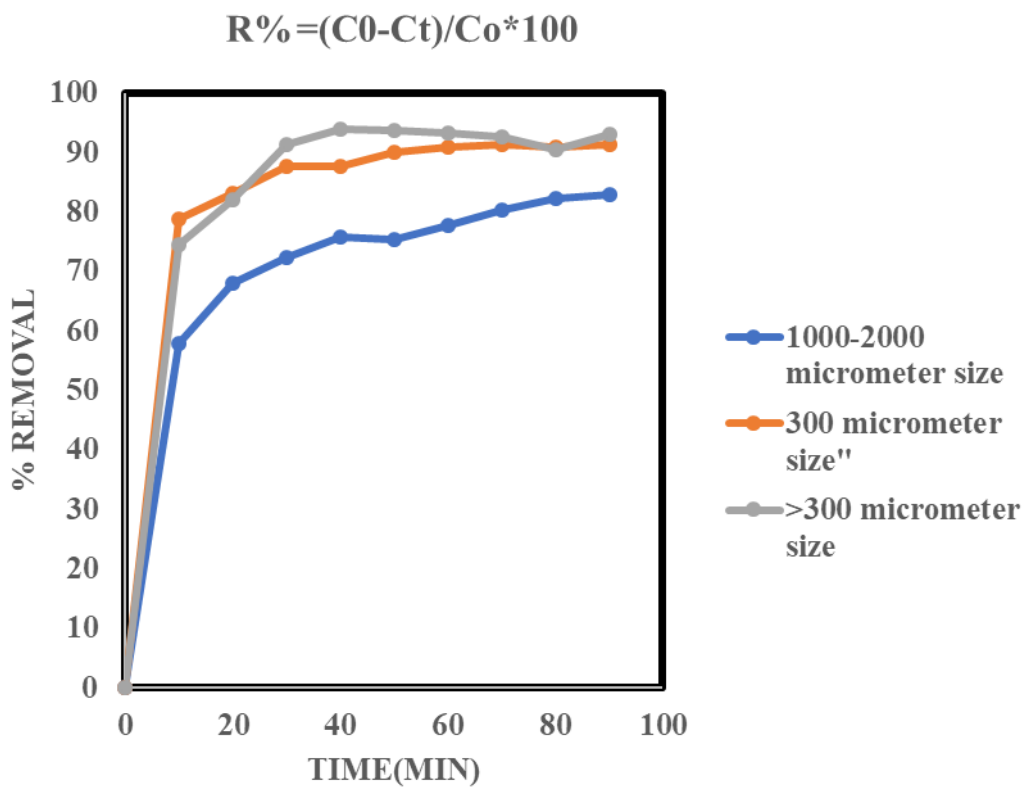
Appendix D: Fig. D2. Effect of particle size of DBT model diesel fuel on Com-AC: 10wt % ads dosage, 25 ^{0}C ads temp, 800 rpm stirring and 90 min ads time

Effect of adsorptionTemperature on DBT
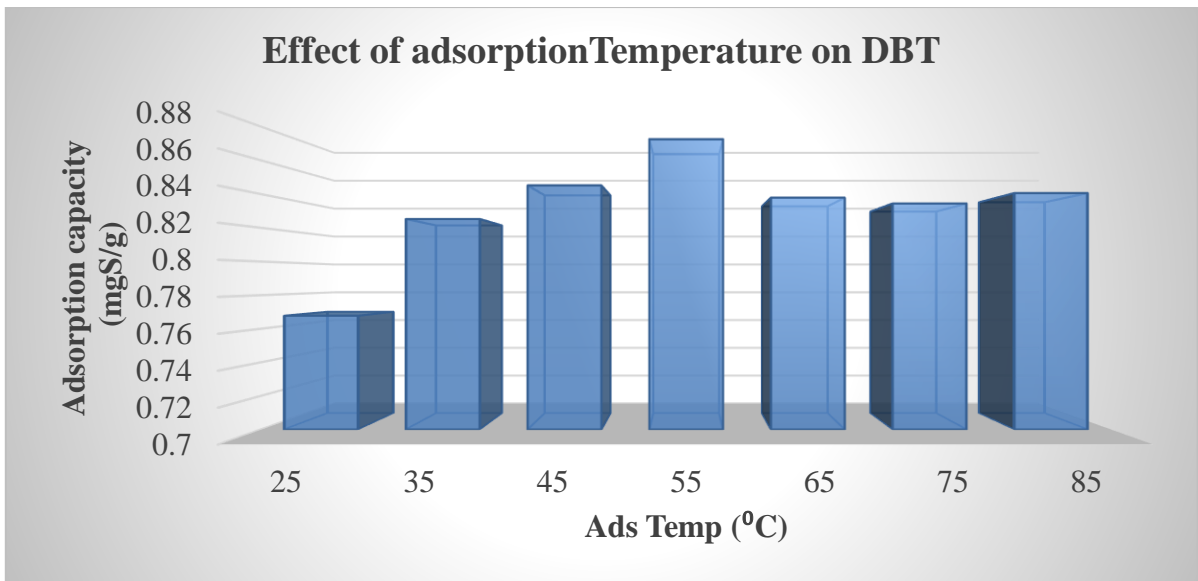
Appendix D: Fig. D3. Effect of adsorption temperature of DBT model diesel fuel on Com-
AC:10wt % ads dosage, 800 rpm stirring 180 min ads time, and 1-2 mm particle size of
ComAC

Appendix D: Fig. D4. Effect of adsorbent dosage on DBT model diesel fuel on ComAC: 25 ^{0}C ads temp, 800 rpm stirring 180 min ads time and 1-2 mm size particle size of ComAC